ON QUANTUM STATE CONVERSION IN THE CONSTRAINED TWO-QUBIT SYSTEM AND ITS APPLICATION TO A REDUCED RYDBERG-TRIMER MODEL

TECHNISCHE
UNIVERSITÄT
DARMSTADT

Vom Fachbereich Physik
der Technischen Universität Darmstadt

Zur Erlangung des Grades
Doctor rerum naturalium
(Dr. rer. nat.)
genehmigte

Dissertation
von Thorsten Haase

Erstgutachter:	Prof. Dr. Gernot Alber
Zweitgutachter:	Prof. Dr. Reinhold Walser

Darmstadt 2022

Thorsten Haase: *On quantum state conversion in the constrained two-qubit system and its application to a reduced Rydberg-trimer model*

Darmstadt, Technische Universität Darmstadt
Jahr der Veröffentlichung der Dissertation auf TUprints: 2022
URN: urn:nbn:de:tuda-tuprints-229595
URI: https://tuprints.ulb.tu-darmstadt.de/id/eprint/22959
Tag der mündlichen Prüfung: 24.10.2022

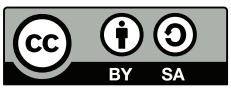

"Any serious consideration of a physical theory must take into account the distinction between the objective reality, which is independent of any theory, and the physical concepts with which the theory operates. These concepts are intended to correspond with the objective reality, and by means of these concepts we picture this reality to ourselves."

- A. Einstein, B. Podolsky, N. Rosen, [1]

"It is also important never to forget that physics is ultimately an experimental subject."

- A. R. P. Rau, [2, p. 137]

ABSTRACT

Preparing quantum states is essential for quantum information processing since any process must start at a well-defined initial state. State conversion describes techniques to transform a specific initial- into a predefined target state. This dissertation investigates quantum state conversion for two interacting qubits and its specialization to a constrained system where only adjacent levels are connected. Furthermore, it shows its applicability in a system of three qubits supposed to model interacting Rydberg atoms.

A general Lie-algebraic approach is discussed, allowing a wide range of unitary transformations of the interacting two-qubit system to be described by two independent pseudospin degrees of freedom. Although restricting the representable transformations, the approach offers a simple description of many different conversion schemes and is well-suited to discuss the mentioned constrained situation.

For this constrained Hamiltonian, a specific state conversion scheme is developed, which can be adopted in a reduced system of three qubits. These three qubits are supposed to model a Rydberg-atom trimer, and the developed conversion scheme maps onto the transformation between the three-atomic W state and the corresponding Greenberger-Horne-Zeilinger state. This mapping is achieved by reducing the eight-dimensional system to an effective four-level system. Two possible reduction schemes are presented. One depends on phase-matching conditions and the other on lifting degeneracies and employing multiple separated time scales in the eight-dimensional dynamics. The control over the atomic ensemble is established via the interaction with coherent states of the electromagnetic field.

All topics are presented in the framework of quantum optics which is the theoretical foundation of much of the developing field of quantum technologies.

The presented research shows how to design quantum state conversion protocols for two interacting qubits and apply such conversion protocols to more complex systems by employing reduction schemes. These reduction schemes allow for an effective description by lowering the dimension of the considered dynamics. The presented W to Greenberger-Horne-Zeilinger state conversion protocol in the Rydberg-trimer model outperforms previously proposed solutions for the same task.

ZUSAMMENFASSUNG

Die Präparation von Quantenzuständen ist eine grundlegende Fragestellung der Quanteninformationsverarbeitung, da jeder Prozess in einem wohldefinierten Anfangszustand beginnen muss. Zustandstransformation beschreibt Methoden der Umwandlung zwischen festgelegten Anfangs- und Endzuständen eines Quantensystems. Diese Dissertation präsentiert Untersuchungen zur Quantenzustandstransformation im System zweier miteinander wechselwirkender Qubits und spezialisiert sie auf Fälle, die der Nebenbedingung unterliegen, dass nur benachbarte Level verbunden sind. Die Anwendbarkeit der entwickelten Transformationsprotokolle auf ein System aus drei Qubits ist eine weitere Fragestellung. Dieses letztgenannte System modelliert drei miteinander in Wechselwirkung stehende Rydbergatome.

Zuerst wird ein allgemeiner Zugang diskutiert, der auf den dynamischen Symmetrien des Systems basiert. Obwohl zur Vereinfachung nur eine Teilmenge aller unitärer Transformationen betrachtet wird, kann eine Vielzahl von Zustandsumwandlungen innerhalb des Systems dargestellt werden. Auch wenn einige Transformationen ausgeschlossen werden, ist der entwickelte Ansatz besonders geeignet, die Dynamik unter den oben genannten Nebenbedingungen zu beschreiben.

Unter Berücksichtigung dieser Nebenbedingungen wird ein Verfahren für eine konkrete Quantenzustandstransformation entwickelt. Dieses kann auf ein System aus drei Qubits angewandt werden und entspricht hierin der Umwandlung vom W zum Greenberger-Horne-Zeilinger Zustand. Um das höherdimensionale System durch ein Vierniveausystem beschreiben zu können, werden Reduktionsmethoden angewendet. Zwei konkrete Beispiele werden diskutiert: eins basiert auf Phasenanpassung, das andere nutzt eine Separierung verschiedener dynamischer Zeitskalen. Die Kontrolle der Übergänge innerhalb des Quantensystems wird durch treibende optische Felder bewerkstelligt.

Die quantenmechanische Beschreibung elektromagnetischer Felder und ihrer Wechselwirkung mit Materie, bzw. im vorliegenden Fall mit Atomen, wird in der theoretische Quantenoptik untersucht. Quantenoptik bildet die Grundlage für eine Vielzahl der aktuell aufkommenden Quantentechnologien.

Die in dieser Arbeit vorgelegten Forschungsergebnisse beschreiben Möglichkeiten zur Kontrolle des Zustandes zweier miteinander Wechselwirkenden Qubits. Weiterhin zeigen sie, wie komplexere Systeme auf dieses einfachere System abgebildet werden können. Die entwickelte W zu Greenberger-Horne-Zeilinger Zustandstransformation ermöglicht eine effizientere Umwandlung beider Zustände als frühere Protokolle.

DANKSAGUNG

Die vorliegende Arbeit wäre mir nicht möglich gewesen ohne die fachliche, administrative und persönliche Unterstützung einer Vielzahl von Personen.

Zuerst möchte ich mich bei Prof. Alber für die Möglichkeit bedanken, in seiner Arbeitsgruppe und unter seiner fachlichen Betreuung promovieren zu dürfen. Seine Vorlesungen zur theoretischen Physik haben mich schon im Bachelorstudium, aber erst recht bis zum Masterabschluss davon überzeugt, mich in meiner Promotion weiter mit theoretischer Physik und im speziellen der Quantenoptik zu befassen.

Weiterhin möchte ich mich bei den Professoren Walser, Walther und Martínez-Pinedo bedanken, die sich bereit erklärt haben, als Gutachter bzw. Prüfer an der Beurteilung dieser Arbeit teilzunehmen.

Vladimir M. Stojanović gilt mein Dank für die Ideen und den Schwung, die er zur zweiten Hälfte meiner Promotionsdauer in unsere Arbeitsgruppe eingebracht hat. Er hat den Anstoß zu den Forschungsarbeiten gegeben, die ausführlich in dieser Arbeit besprochen werden.

Bei allen (ehemaligen) Kollegen am Institut für angewandte Physik möchte ich mich für fachliche Unterstützung und vor allem auch für viele Mensagänge und andere ablenkende Dinge – wie Diskussionen mit oder ohne Kaffee – bedanken, die den Arbeitsalltag aufgelockert haben. Besonders zu erwähnen ist dabei Alexander. Er hat sich mit mir die letzten Jahre ein Büro geteilt (bevor die Coronapandemie das Homeoffice eingeführt/erzwungen hat) und wir sind zusammen durch Masterarbeits- und Promotionszeit gegangen. Er hat sich nie beschwert, wenn ich ihn mit Fragen gelöchert und dabei in seiner Arbeit unterbrochen habe.

Mein Dank für administrative Unterstützung aller Art gilt Frau Kutschera und Frau Schütze, die fast immer wussten, wie etwas zu erledigen ist und wenn sie es nicht wussten, an wen man sich wenden kann. Dies gilt auch für Stefanie Kettler. Bei ihr möchte ich mich stellvertretend für das ganze CROSSING Team bedanken.

Für Unterstützung im Schreibprozess möchte ich mich bei Ute Henning vom Schreibcenter der TU Darmstadt bedanken. Sie hat mir das ein oder andere Mal aufzeigen können, worauf es bei dieser Arbeit ankommt. Florian, Tilman und Johannes haben zu Teilen dieser Arbeit konstruktives Feedback gegeben, das ich dringend benötigt habe.

Wichtiger für mich ist aber ihre Freundschaft und die vieler weiterer Personen in Darmstadt, die mich durch das Studium und die Promotion gebracht haben. Ob nun beim Laufen, Wandern, Feiern,

Kaffeetrinken, Diskutieren, Gärtnern, Reisen oder vielen weiteren Aktivitäten seid ihr zu meiner Ersatzfamilie vor Ort geworden.

Zuletzt möchte ich mich bei meinen Eltern und meinen Geschwistern bedanken, die mich auch schon vor dem Studium immer unterstützt und auch aus der Ferne damit nie aufgehört haben. Zu dieser und der oben erwähnten Ersatzfamilie gehört seit einigen Jahren auch meine Freundin Roxane, der ich zu besonderem Dank verpflichtet bin. Mit mir zusammenzuziehen bevor es in die Endphase der Promotion ging, hat ihr sicher einiges an Sorgen und Mühen bereitet. Ich für meinen Teil habe es allerdings nie bereut.

CONTENTS

1 INTRODUCTION AND OUTLINE

With all its different aspects and branches, the theory of quantum mechanics is one of the modern pillars of physics and lies at the heart of much of current [3] and future technology [4]. Since the first introduction of the quantization of black body radiation by *Max Planck* in 1900 [5, 6] and the explanation of the photoelectric effect by *Albert Einstein* in 1905 [7], the theory of quantum physics was further developed and able to explain a lot of different experimentally observed phenomena, such as atomic spectral lines of hydrogen [8, 9] and diatomic molecules [10, 11] or the alpha decay of heavy elements [12] via the tunnel effect [13].

After its first culmination into a thorough physical theory – among others by *John von Neumann* [14] and *Paul Dirac* [15] – quantum mechanics was developed in different branches to tackle different questions from fundamental physics to applied science and technology. Though many of these questions are already answered, there are still numerous unresolved issues [16, 17], and quantum physics continues to be an active field of research, maybe, today even more than ever before.

Two of these branches are quantum optics and quantum information. This dissertation deals with a particular aspect of these two: the interconversion of quantum states of two constrained qubits and the reduction of a specific quantum optical model to such a two-qubit system. It is part of the author's application for the German academic degree *Doctor rerum naturalium (Dr. rer. nat.)*.

Although the applicant is the sole author of this dissertation, the plural form is used throughout this text. We believe science and research is almost always a dedicated team effort. As such, some of the following content was already published elsewhere with several co-authors or originated from students' (under)graduate projects co-supervised by the author[1]. All such content is labeled accordingly, and contributions by others are clearly acknowledged.

1.1 INTRODUCTION

Although many contributions were already made before it, the discussion by *Richard Feynman* about how to simulate physics with computers [18] is sometimes considered the starting point of quantum information. It is one of the newest and fastest developing branches

1 Compare the list of publications and the list of co-supervised (under)graduate projects on p. 139.

of quantum physics.[2] As the bit in classical information theory, the qubit is the basic element of quantum information. It is represented by a two-level quantum system (TLS). Its most general pure[3] state is a superposition of the computational basis states $|0\rangle$ and $|1\rangle$[4], i.e.,

$$|\psi\rangle = \alpha|0\rangle + \beta|1\rangle\,, \tag{1.1}$$

where $\alpha, \beta \in \mathbb{C}$ and $|\alpha|^2 + |\beta|^2 = 1$. Preparing and manipulating strings of such qubits lies at the heart of any task in quantum information processing (QIP).

To execute a quantum algorithm, such as *Shor's* algorithm for prime factorization [21], single qubits have to interact with each other in a controlled manner. In chapter 4 of this dissertation, we present investigations for quantum state conversion in the second most basic system of QIP: the two-qubit system.

In general, quantum state conversion is the task of manipulating a quantum system, which occupies an initial state at time t_0, over time T such that at the end of the manipulation, it occupies a predefined target state. We restrict this discussion to pure states $|\psi(t)\rangle$, such that

$$|\psi(t_0)\rangle = |\psi_i\rangle \xrightarrow{\widehat{H}(t)} |\psi(t_0+T)\rangle = |\psi_t\rangle\,. \tag{1.2}$$

Due to the Schrödinger equation, the Hamiltonian $\widehat{H}(t)$ of a quantum system is the generator of its time evolution. Therefore, quantum state conversion results in finding and applying appropriate (potentially time-dependent) Hamiltonians to control the time evolution of the quantum system under consideration.

Another aspect investigated in quantum information theory is quantum entanglement.[5] It constitutes one of the main features in which QIP differs from classical information processing. In 1935, *Erwin Schrödinger* defined the (originally German) term "Verschränkung" using his famous example of a cat being in a state of superposition of dead and alive that is entangled with a radioactive particle, either disintegrated or not [23]. Earlier the same year, Einstein-Podolsky-Rosen (EPR) formulated what was later called the EPR-paradox. They found that quantum mechanics and entangled states contradict their assumptions of physical reality [1]. *John S. Bell*, reformulating their arguments, derived a set of inequalities that allow for an experimental test if physical reality is consistent with the EPR assumptions of local realism [24]. Many experiments so far confirmed the predictions of

2 For an extensive overview of most aspects of quantum information, we suggest the seminal textbook by *Nielsen & Chuang* [19].

3 With one exception, we will only consider pure states throughout this dissertation. A density operator $\hat{\rho}$ and mixed states only appear in the context of open system dynamics in section 5.6.

4 We use Dirac's notation [20] throughout this dissertation. *Ket* states $|\rangle$ represent elements of a Hilbert space, *Bra* states $\langle|$ elements of the dual space, and *BraKets* $\langle|\rangle$ the scalar product.

5 For an extensive review of quantum entanglement, see *Horodecki et al.* [22].

quantum mechanics (e.g., [25–28]), although usually, not all loopholes are simultaneously closed in such experiments. For example, the detection loophole sets bounds for the efficiencies of detectors [29, 30]. Due to the convincing experimental evidence, entanglement is nowadays considered a confirmed aspect of quantum mechanical systems. However, many of its features, especially in higher dimensions are not easy to characterize [22] and are ongoing research topics [31].

In the context of quantum state conversion, the existence of different entanglement classes and the interconversion of states representing different classes are particularly interesting. Local operations and classical communication (LOCC) define two examples of such classes. They are the setup for many protocols in quantum communication, such as quantum key distribution [32, 33] or quantum teleportation [34–36]. Prominent examples of multipartite entangled states are W states and Greenberger-Horne-Zeilinger (GHZ) states. They cannot be transformed into each other by LOCC alone [37, 38]. A W state[6] is the superposition of states of precisely one excitation, e.g., in a three-qubit system

$$|\mathrm{W}\rangle = \frac{1}{\sqrt{3}} \left(|001\rangle + |010\rangle + |001\rangle \right) . \tag{1.3}$$

It is a multipartite entangled state most robust against particle loss [40, 41]. The GHZ state [42, 43] is a superposition of maximal possible and vanishing excitation in the qubit string, e.g, in the three-qubit system

$$|\mathrm{GHZ}\rangle = \frac{1}{\sqrt{2}} \left(|000\rangle + |111\rangle \right) . \tag{1.4}$$

It is maximally entangled as a complete qubit string, but if one qubit is lost or measured, all pairwise entanglement vanishes. The GHZ state allows for testing local realism without formulating inequalities. [43–45].

Due to their LOCC inequivalency, a quantum state conversion $|\mathrm{W}\rangle \xrightarrow{\hat{\mathrm{U}}(t)} |\mathrm{GHZ}\rangle$ or vice versa is only possible if either $\hat{\mathrm{U}}(t)$ acts globally on the complete system or real quantum communication, i.e., the transmission of qubits, is performed. Chapter 5 of this dissertation discusses the first possibility for a system of three qubits interacting with the electromagnetic field. The qubits model an ensemble of pairwise interacting *Rydberg* atoms[7].

Rydberg atoms are *"atoms in states of high principal quantum number, n, [...] with exaggerated properties."* [46, p. 1] Arranged in arrays of optical tweezers, they are a promising quantum optical platform for QIP [47, 48]. Since the invention of the laser, it has been possible to control

6 According to *A. Cabello* [39], W states are named after *Wolfang Dür*. He is one of the authors describing the LOCC inequivalency [38].

7 They are named after *Johannes R. Rydberg*. *"Discoverer of the formula that bears his name for spectral lines from an atom when it changes from one energy level to another."* [2, p. 34]

quantum mechanical aspects of specific systems with ever increasing precision. Although it cannot considered as QIP, laser cooling of atom clouds [49, 50] is an early example of such a control, and it is a working tool in almost all experiments controlling single quantum emitters such as trapped atoms or ions. Such experimental techniques are now so sophisticated that experiments are not only able to trap single quantum emitters in different geometries [51] but also whole ensembles of more than a hundred single atoms [52].

All of the referenced examples of experiments use quantum optical setups to investigate QIP or fundamental physics. In general, quantum optics is the quantum theory of the electromagnetic field and its interaction with matter. Because further developing quantum technologies allow for controlling quantum systems very precisely, quantum state conversion in specific systems is on the brink of becoming experimentally feasible. In chapter 4, we present research focusing on the quantum state conversion in the second most basic element of quantum information, the two-qubit system. It is an important building block for QIP, since qubits must interact which each other. Further, we show the reduction of a quantum optical model of Rydberg atoms to an effective system of lower dimension in chapter 5. In the particular case of three Rydberg atoms, the results of the preceding chapter are then applied to achieve a W to GHZ quantum state conversion.

1.2 OUTLINE

This section presents an overview of the content of this dissertation. We start with what it does not include.

Right at the beginning, we mentioned some early achievements of the theory of quantum mechanics. Even though some of the examples [9, 11] used the formulation in terms of matrix mechanics by *Heisenberg, Born, and Jordan* [53–55], the last one [13] used the formulation in terms of the wave function by *Schrödinger* [56–59], both descriptions were soon recognized to be equivalent [60, 61]. Although it is the foundation of all following discussions, we do not thoroughly introduce quantum physics since plenty of textbooks cover the topic. Such a fundamental account would by far exceed the scope of this dissertation. For example, *Ballentine*'s book [62] offers a well-written introductory account of basic quantum mechanics. It also features some aspects of advanced topics including the basics of quantum optics. We especially want to emphasize the textbook by *Nielsen and Chuang* [19] about quantum computation and quantum information. It gives a thorough overview of most of the relevant aspects of quantum information theory. Additionally, since it is written for computer scientists and physicists alike, it gives a well-structured introduction to finite quantum systems, which are the main topic of theoretical quantum information. It explains most of the mathematical tools needed

in chapter 4, which contains the author's research on quantum state conversion in a constrained two-qubit system.

However, we do give a short introduction to some aspects of quantum theory. We focus on quantum optics, which offers the more advanced theoretical background for the research on state conversion in a model system of neutral Rydberg atoms presented in chapter 5.

The following account gives a chapter-wise overview of the remaining content. This dissertation is structured into two main parts:

- Part I gives an overview of some aspects of quantum theory important for understanding part II and, in particular, chapter 5. The covered topics are the fundamentals of quantum optics and the theory of effective Hamiltonians. We always try to reference textbooks or reviews with different foci, which offer the reader the possibility for a more extensive study of the different subjects.
  - Chapter 2 summarizes the fundamentals of quantum optics. It starts with the quantization of the electromagnetic field. In this context, we briefly discuss the topic of different modes in quantum optics. It continues by discussing special classes of quantum states of the electromagnetic field. Coherent field states form one of these classes. They well-represent classical fields. The chapter concludes by describing their interaction with discrete and finite quantum systems as the standard quantum optical model for light–atom interaction.
  - Chapter 3 summarizes the theory of effective Hamiltonians. Under well-defined circumstances, such effective Hamiltonians allow describing the dynamics of a complex system approximately by a simpler one. In section 5.3, we derive effective Hamiltonians for a discrete quantum system interacting with several classical light fields.
- Part II covers the author's research on quantum state preparation and interconversion. It presents two different topics:
  - Chapter 4 discusses a Lie-algebraic approach to quantum state conversion in a two-qubit system. It presents a specific conversion scheme for a constrained Hamiltonian, which only allows for adjacent connections between the four quantum levels of the two-qubit system. Although presented there in the more specialized context of Rydberg trimers, some of the chapter's content was already published as
    * Haase, T., Alber, G. & Stojanović, V. M. Conversion from W to Greenberger-Horne-Zeilinger states in the Rydberg-blockade regime of neutral-atom systems: Dynamical-symmetry-based approach. *Physical Review A* **103,** 032427. doi:10.1103/PhysRevA.103.032427 (Mar. 2021), [63].

- Chapter 5 discusses a model of a system proposed for QIP: neutral Rydberg atoms in the blockade regime. It presents a theoretical description of the atomic ensemble via effective Hamiltonians, which allow describing the global control of the finite-dimensional Rydberg system via laser fields, and it introduces reductions of the degenerated system to effectively non-degenerated systems of lower dimension. The particular case of three neutral Rydberg atoms, a Rydberg trimer, is used as an example to apply the quantum state conversion scheme presented in the preceding chapter. Although presented in more detail in this dissertation, the main content of this chapter was already published as
  * Haase, T., Alber, G. & Stojanović, V. M. Dynamical generation of chiral *W* and Greenberger-Horne-Zeilinger states in laser-controlled Rydberg-atom trimers. *Physical Review Research* **4,** 033087. doi:10.1103/PhysRevResearch.4.033087 (July 2022), [64].

Both chapters containing excerpts of the author's research activities feature a summary explaining which parts already have appeared in the aforementioned publications, and how the content differs from the presentation given in this dissertation.

The two main parts are followed by closing remarks, appendices, and technical aspects, such as the bibliography and declarations:

- Chapter 6 contains the conclusion of this dissertation and the presented topics. It summarizes the findings and lays down some open questions for possible further research.

- Appendices A to C depict some mathematical aspects or lengthy calculations of part II in more detail.

Part I

FUNDAMENTALS

2 FUNDAMENTALS OF QUANTUM OPTICS

The aim of this chapter is to introduce quantum optics. Primarily, we want to give a short overview of its fundamentals, on which many of the research topics presented in part II are based on. Additionally, its sections and also the following chapter introduce notation and conventions used throughout the remaining content.

Naturally, quantum optics is based on the theory of electromagnetism and classical optics in particular. As a basic theory of classical physics, the first is introduced in many textbooks (e.g., [65–67]). The seminal compendium by *Born and Wolf* [68] gives a thorough account of the latter. Elaborate and extensive overviews of quantum optics itself are given, e.g., by *Mandel and Wolf* [69], *Loudon* [70] or *Cohen-Tannoudji et al.* [71, 72]. More recent and, in some ways, more specialized presentations of quantum optics can be found, e.g., in the freely online-available lecture notes by *Steck* [73] and the textbooks by *Agarwal* [74] or *Schleich* [75]. The following discussion of the fundamentals of quantum optics is partly based on all of these references and influenced by the lecture *Theoretical Quantum Optics* hold on a regular basis at Technische Universität Darmstadt by *Prof. Dr. Gernot Alber*.

2.1 QUANTIZATION OF THE ELECTROMAGNETIC FIELD

Since quantum optics is the quantum theory of the electromagnetic field, classical electromagnetism acts as a starting point for our discussion. Already in classical optics, the notion of electromagnetic field modes is essential. These modes are then taken as individual harmonic oscillators and treated via canonical quantization. The author already gave a similar account of some of this section's content in his master's thesis [76].

2.1.1 *The free electromagnetic field*

Maxwell's equations (here given in SI-units)[1]

$$(\boldsymbol{\nabla} \cdot \boldsymbol{E})(\boldsymbol{x}, t) = \frac{\rho(\boldsymbol{x}, t)}{\epsilon_0}\,, \tag{2.1a}$$

$$(\boldsymbol{\nabla} \cdot \boldsymbol{B})(\boldsymbol{x}, t) = 0\,, \tag{2.1b}$$

1 Although many textbooks on electromagnetism use Gauß units, we use SI-units throughout this dissertation. For an overview of translations from one in the other, see, e.g., [65, App. A].

$$(\boldsymbol{\nabla} \times \boldsymbol{E})(\boldsymbol{x}, t) = -\frac{\partial \boldsymbol{B}}{\partial t}(\boldsymbol{x}, t)\,, \tag{2.1c}$$

and

$$(\boldsymbol{\nabla} \times \boldsymbol{B})(\boldsymbol{x}, t) = \frac{\boldsymbol{j}(\boldsymbol{x}, t)}{\epsilon_0 c^2} + \frac{1}{c^2}\frac{\partial \boldsymbol{E}}{\partial t}(\boldsymbol{x}, t) \tag{2.1d}$$

are the fundamental basis of electromagnetism and all of optics. They describe the dynamics of the electric field $\boldsymbol{E}$ and the magnetic induction $\boldsymbol{B}$ and their interaction with matter represented by the charge density ρ and the electric current $\boldsymbol{j}$ in space and time $(\boldsymbol{x}, t)$. ϵ_0 is the vacuum permittivity, and c is the speed of light in vacuum. With the Lorentz force acting on charged particles, Maxwell's equations allow deducing all relevant aspects of classical electrodynamics [65, ch. 16].

Introducing the vector potential $\boldsymbol{A}(\boldsymbol{x}, t)$ and the scalar potential $\Phi(\boldsymbol{x}, t)$, we can describe the electric and magnetic field as

$$\boldsymbol{E}(\boldsymbol{x}, t) = \left(-\boldsymbol{\nabla}\Phi - \frac{\partial \boldsymbol{A}}{\partial t}\right)(\boldsymbol{x}, t) \tag{2.2a}$$

and

$$\boldsymbol{B}(\boldsymbol{x}, t) = (\boldsymbol{\nabla} \times \boldsymbol{A})\,(\boldsymbol{x}, t)\,. \tag{2.2b}$$

Since both the curl of a gradient field and the gradient of a purely rotational field vanish, this description automatically incorporates eqs. (2.1b) and (2.1c).

Most of the time, quantum optics only considers the free electromagnetic field. Hence, we set $\rho(\boldsymbol{x}, t)$ and $\boldsymbol{j}(\boldsymbol{x}, t)$ to zero. Matter is often considered via models in certain ranges of approximations. The interaction of the quantized field with such a model of matter as a finite discrete quantum system is discussed in section 2.3.

In the Coulomb gauge, i.e., $\boldsymbol{\nabla} \cdot \boldsymbol{A} = 0$, eq. (2.1a) reduces to the homogeneous Laplace equation for Φ. If we choose proper boundary conditions, its solution is unique, and we do not have to consider it a dynamical degree of freedom. Therefore, we concentrate on the vector potential $\boldsymbol{A}$.

Due to Helmholtz's theorem we can describe any vector field via its transverse and its longitudinal component. The magnetic induction is always transverse since $\boldsymbol{\nabla} \cdot \boldsymbol{B} = 0$, but we can split up the electric field as

$$\boldsymbol{E}(\boldsymbol{x}, t) = \boldsymbol{E}_\perp(\boldsymbol{x}, t) + \boldsymbol{E}_\parallel(\boldsymbol{x}, t)\,, \tag{2.3a}$$

where

$$(\boldsymbol{\nabla} \cdot \boldsymbol{E}_\perp)\,(\boldsymbol{x}, t) = 0 \tag{2.3b}$$

and

$$(\boldsymbol{\nabla} \times \boldsymbol{E}_\parallel)\,(\boldsymbol{x}, t) = 0\,. \tag{2.3c}$$

In the Coulomb gauge, the vector potential completely determines the transverse component $\boldsymbol{E}_\perp$ of the electric field, while the scalar potential

determines the longitudinal component $\boldsymbol{E}_{\parallel}$. Since we do not consider the latter a dynamical variable, we only discuss the transverse field in the following discussion. As long as not stated otherwise, $\boldsymbol{E}(\boldsymbol{x},t)$ denotes the transverse component only.

With the aforementioned assumptions, eq. (2.1d) reduces to

$$\left(\frac{1}{c^2}\frac{\partial^2 \boldsymbol{A}}{\partial t^2} - \boldsymbol{\nabla}^2 \cdot \boldsymbol{A}\right)(\boldsymbol{x},t) = 0\,, \tag{2.4}$$

constituting a wave equation for the vector potential.

The product ansatz

$$\boldsymbol{A}(\boldsymbol{x},t) = \alpha(t)\boldsymbol{g}(\boldsymbol{x}) + \text{c.c.}\,, \tag{2.5}$$

ensuring a real valued vector potential, seperates temporal and spatial derivatives in eq. (2.4), such that

$$\frac{\partial^2 \alpha(t)}{\partial t^2} = -\omega^2 \alpha(t)\,. \tag{2.6}$$

The complex conjugated part fulfills an analogous equation. Hence, $\alpha(t)$ fulfills the differential equation of a harmonic oscillator. We describe its solution as $\alpha(t) = \alpha(t_0)\mathrm{e}^{-\mathrm{i}\omega(t-t_0)}$ where $\omega \geq 0$ and $\alpha(t_0) \in \mathbb{C}$. The parameters $\alpha_l(t_0)$ incorporate the initial conditions.[2]

The introduced ansatz is called mode ansatz, and the spatial mode function $\boldsymbol{g}(\boldsymbol{x})$ then fulfills the Helmholtz equation

$$\left(\frac{\omega^2}{c^2}\boldsymbol{g} + \boldsymbol{\nabla}^2 \cdot \boldsymbol{g}\right)(\boldsymbol{x}) = 0\,. \tag{2.7}$$

The mode functions are determined by boundary conditions to the Helmholtz equation. The vector potential expanded in such a set of mode function is

$$\boldsymbol{A}(\boldsymbol{x},t) = \sum_l \left(\boldsymbol{g}_l(\boldsymbol{x})\alpha_l(t_0)\mathrm{e}^{-\mathrm{i}\omega_l t} + \text{c.c.}\right)\,, \tag{2.8}$$

The electric field $\boldsymbol{E}(\boldsymbol{x},t)$ and the magnetic induction $\boldsymbol{B}(\boldsymbol{x},t)$ can be calculated from eqs. (2.2).

Different boundary conditions to the Helmholtz equation lead to different mode functions. Plane waves are one of the simplest examples. They correspond to periodic boundary conditions on a cube of size L. In this case, the wave vector $\boldsymbol{k} = 2\pi\boldsymbol{n}/L$ with $\boldsymbol{n} \in \mathbb{Z}$ and the polarization parameter λ completely determine a mode function

$$\boldsymbol{g}_{k,\lambda}(\boldsymbol{x}) = \boldsymbol{\varepsilon}_{k,\lambda}\frac{1}{L^{3/2}}\mathrm{e}^{i\boldsymbol{k}\cdot\boldsymbol{x}}\,. \tag{2.9}$$

λ differentiates two orthogonal polarization directions (either linear, circular, or more complex and $\boldsymbol{\varepsilon}_{k,\lambda} \cdot \boldsymbol{\varepsilon}_{k,\lambda'} = \delta_{\lambda\lambda'}$) fulfilling the Coulomb gauge $\boldsymbol{k} \cdot \boldsymbol{\varepsilon}_{k,\lambda} = 0$.

2 We often shift the time scale such that $t_0 = 0$.

2.1.2 *Electromagnetic modes*

Although plane-wave modes are used throughout most of this dissertation, we briefly want to discuss other types of modes. The particular set of mode functions only marginally affects the quantization discussed afterward. However, it is often one of the main aspects, in which quantum optical applications differ from each other. In the following, we briefly discuss a selection of different sets of modes and examples of their applications linked to some research topics the author was involved in[3], which are not discussed in more detail throughout this dissertation. For a thorough overview of electromagnetic modes with an extensive discussion of mode types most commonly used in quantum optics, we refer to the review by *Fabre and Treps* [77].

In principle, modes are solutions $\boldsymbol{f}(x,t)$ of the wave equation (2.4) fulfilling the Coulomb gauge $\boldsymbol{\nabla}\cdot\boldsymbol{f}(\boldsymbol{x},t)=0$, and the integral over their squared modulus $|\boldsymbol{f}(\boldsymbol{x},t)|^2$ over the whole space of interest Ω is finite. It is most convenient to work with a complete set of orthonormal modes $\{\boldsymbol{f}_i(\boldsymbol{x},t)\}$ which are all normalized and fulfill the orthogonality condition

$$\int_\Omega \mathrm{d}\Omega\, \boldsymbol{f}_i(x,t)\boldsymbol{f}_j^*(x,t)=\delta_{ij} \tag{2.10}$$

at any time t. Starting from one particular mode it is always possible to construct a complete orthogonal set [77].

Often, the space of interest is the volume containing the whole physical system under consideration. However, sometimes it is sufficient to consider one-dimensional modes, e.g., if quantum optics along a waveguide is considered [78–80]. In this case, we can reduce the equations describing the modes to scalar equations.

In such a one-dimensional scenario, a mode function is completely determined by its scalar wave number $|\boldsymbol{k}|=\omega_k/\mathrm{c}$ and its direction of propagation. Allowing the frequency and the wave number to extend to the negative real numbers offers a one-to-one correspondence of wave number and frequency, where the direction of propagation is reflected in their signs $\pm$. In this context, it is possible to define temporal modes [81, 82]. They are convenient in some quantum communication protocols, such as time-bin quantum key distribution [83] or for the characterization of the temporal response of a photon detector used in such protocols [33, 84].

In three dimensions, still, plane waves are not always the most convenient choice. If the electromagnetic field is considered inside a cavity, ideal metallic boundary conditions must be applied. It means the electric field proportional to $\boldsymbol{g}(\boldsymbol{x})$ and the magnetic flux proportional to the normal component of $\boldsymbol{\nabla}\times\boldsymbol{g}(\boldsymbol{x})$ have to vanish at the metallic surface. The geometry of the cavity plays a decisive role. Plane waves

3 Compare the list of publications on and co-supervised (under)graduate projects on p. 139

remain the ideal choice of mode functions if rectangular cavity boundaries are considered. In a spherical cavity, mode functions composed of vector spherical harmonics [85, ch. 11] fulfill the aforementioned boundary conditions [86].

Often approximations allow simplifying the considered mode functions. For example, metallic boundary conditions on the surface of an infinite parabolic mirror give rise to a set of very complex mode functions [87]. However, it is possible to use the only non-vanishing mode function of a spherical cavity at the focal point if the parabolic mirror's focal length is very large compared with the considered optical wavelength [76, 88–91].

Another example is a beam of laser light for which the amplitude of the electromagnetic field diminishes rapidly with growing distance to the beam center and the direction of propagation is predominantly aligned along an particular axis. In such a situation, the paraxial approximation reduces the problem essentially to one dimension. For example, spatial Hermite-Gauss modes are a convenient mode basis for quasi one-dimensional cavities made of spherical mirrors [77].

In the following section, we discuss the canonical quantization of the electromagnetic field.

Each mode will be seen as an independent harmonic degree of freedom of the quantum system. Although the particular choice of mode functions does not play a decisive role in the quantization, it is important to choose the appropriate mode functions for each situation. Especially, one has to take care of the range of applicability of approximations made to derive at a certain set of mode functions.

2.1.3 *The canonical quantization*

In order to quantize the electromagnetic field, we have to formulate a Hamiltonian description of it. In the following, V will denote the volume of interest, and we assume the mode functions $\boldsymbol{g}_l(\boldsymbol{x})$ to fulfill the Helmholtz equation with appropriate boundary conditions and to form a complete set of modes. The energy of the electromagnetic field can be expressed as (see, e.g., [65, ch. 16])

$$H(t) = \frac{\epsilon_0}{2} \int_V \mathrm{d}V \left(\boldsymbol{E}^2(\boldsymbol{x},t) + c^2 \boldsymbol{B}^2(\boldsymbol{x},t) \right) = 2\epsilon_0 \sum_l \omega_l^2 |\alpha_l(t)|^2 \,. \quad (2.11)$$

The integral of $\boldsymbol{E}^2(\boldsymbol{x},t)$ over space can be directly performed using the orthogonality condition eq. (2.10) fulfilled by a set of mode functions. The same argument does not apply to the integral of $c^2\boldsymbol{B}^2(\boldsymbol{x},t)$. It involves products of the form $(\boldsymbol{\nabla} \times \boldsymbol{g}_l) \cdot (\boldsymbol{\nabla} \times \boldsymbol{g}_{l'})$. For mode functions fulfilling metallic boundary conditions, it can be shown that the orthogonality condition translates to the curls of the mode functions [75, ch. 10, 62, ch. 19]. A similar orthogonality condition for the curls can be directly shown for the plane wave modes of eq. (2.9). Under these

conditions, the particular form of the mode functions $g_l(x)$ does not enter the Hamiltonian form, which leads to the quantization of the electromagnetic field.

Hence, in the following, we derive a quantum theory only for the time dependence of the electromagnetic field. The dynamical degrees of freedom are the functions $\alpha_l(t)$ of all modes. All spatial aspects are described by the mode functions $g_l(x)$.

We introduce real variables

$$q_l(t) = \alpha_l(t) + \alpha_l^*(t)\,, \tag{2.12a}$$

referring to the real part of $\alpha(t)$, and

$$p_l(t) = -\mathrm{i}\epsilon_0\omega_l\left(\alpha(t) - \alpha^*(t)\right) \tag{2.12b}$$

referring to the imaginary part of $\alpha(t)$.

These variables allow us to reformulate the field energy in Hamiltonian form

$$H(t) = \sum_l \left(\frac{p_l^2(t)}{2\epsilon_0} + \frac{1}{2}\epsilon_0\omega_l^2 q_l^2(t)\right)\,. \tag{2.13}$$

We recognize a set of harmonic oscillators of frequency ω_l. Compared with the classical harmonic oscillator describing the movement of a particle, ϵ_0 can be seen as analogous to the mass.

For the quantization of the electromagnetic field, we perform the canonical quantization for each harmonic oscillator separately. It allows us to take over all aspects well-known from this basic system of quantum mechanics, such as eigenstates, its time evolution, and the concept of ladder operators $\hat{a}$ and $\hat{a}^\dagger$[4].

We replace all pairs of variables with pairs of non-commuting operators $\hat{q}_l$ and $\hat{p}_l$ fulfilling the canonical commutation relations

$$[\hat{q}_l(t), \hat{p}_{l'}(t)] = \mathrm{i}\hbar\delta_{ll'}\,, \tag{2.14a}$$
$$[\hat{q}_l(t), \hat{q}_{l'}(t)] = 0\,, \tag{2.14b}$$

and

$$[\hat{p}_l(t), \hat{p}_{l'}(t)] = 0\,. \tag{2.14c}$$

From the canonical variables, we form dimensionless ladder operators, i.e., the annihilation or lowering operator

$$\hat{a}_l(t) = \sqrt{\frac{2\epsilon_0\omega_l}{\hbar}}\left(\hat{q} + \mathrm{i}\frac{\hat{p}}{\epsilon_0\omega_l}\right) = \sqrt{\frac{2\epsilon_0\omega_l}{\hbar}}\hat{\alpha}_l(t) \tag{2.15a}$$

and the creation or raising operator

$$\hat{a}_l^\dagger(t) = \sqrt{\frac{2\epsilon_0\omega_l}{\hbar}}\left(\hat{q} - \mathrm{i}\frac{\hat{p}}{\epsilon_0\omega_l}\right) = \sqrt{\frac{2\epsilon_0\omega_l}{\hbar}}\hat{\alpha}_l^\dagger(t) \tag{2.15b}$$

4 See, e.g., [62, ch. 6] for a fundamental discussion of the quantum harmonic oscillator

by inverting the transformations for q and p above. They are raising and lowering operators for single modes. These non-hermitian operators obey the dimensionless version of the commutation relations (2.14)

$$\left[\hat{a}_l(t), \hat{a}_{l'}^\dagger(t)\right] = \delta_{ll'} \tag{2.16a}$$

$$\left[\hat{a}_l(t), \hat{a}_{l'}(t)\right] = 0\,, \tag{2.16b}$$

and

$$\left[\hat{a}_l^\dagger(t), \hat{a}_{l'}^\dagger(t)\right] = 0\,. \tag{2.16c}$$

The time evolution of these operators is to be interpreted in terms of the Heisenberg picture. In the Schrödinger picture, the operators are constant.

Hence, we can write the Hamiltonian of the electromagnetic field by the correspondence principle as

$$\widehat{H} = \sum_l \frac{\hbar\omega_l}{2}\left(\hat{a}_l\hat{a}_l^\dagger + \hat{a}_l^\dagger\hat{a}_l\right) = \sum_l \hbar\omega_l\left(\hat{a}_l^\dagger\hat{a}_l + \frac{1}{2}\right)\,. \tag{2.17}$$

$\hat{n}_l = \hat{a}_l^\dagger\hat{a}_l$ are number operators. They measure the number of photons in the mode enumerated by l.

The second term $\hbar\omega_l/2$ for each mode is the zero-point contribution to the energy. It results in a non-vanishing ground state energy of the quantum harmonic oscillator. Although countable, the number of modes in a given system is usually infinite. This countable infinity leads the energy as sum over all these modes to diverge even if not a single mode is excited, i.e., containing no photons. Renormalization can deal with such kind of infinite values but is not always satisfactory either.

Although we will neglect the zero-point contribution in the following, it can yield real physical results. For example, comparing the different zero-point contributions of a free field and the field between two conducting surfaces leads to the *Casimir* effect [92], resulting in a force onto the two surfaces, even when there is no excitation in the electromagnetic field [75, sec. 10.4]. Such an effect has been experimentally measured, e.g., by *Lamoreaux* in 1997 [93].

We will be quite pragmatic regarding the zero-point contribution. From the viewpoint of the correspondence principle, we demand our quantum theory to agree with electrodynamics in the classical limit, i.e., when photon numbers are high. Then, we can neglect the constant part in the energy since the number of photons $\hat{n} = \hat{a}_l^\dagger\hat{a}_l$ dominates the energy per mode [69, sec. 10.3]. From this pragmatic viewpoint, we adopt as Hamiltonian of the free electromagnetic field

$$\widehat{H}_\mathrm{F} = \sum_l \hbar\omega_l\hat{a}_l^\dagger\hat{a}_l\,. \tag{2.18}$$

From the correspondence principle, we can also find operator identities of the electromagnetic vector potential, the electric field, and the magnetic induction. Exchanging $\alpha_l(t) \to \hat{a}_l$ in eq. (2.8) results into

$$\widehat{\boldsymbol{A}}(\boldsymbol{x}) = \widehat{\boldsymbol{A}}^{+}(\boldsymbol{x}) + \text{H.c.} = \sum_l \sqrt{\frac{\hbar}{2\epsilon_0 \omega_l}} \boldsymbol{g}_l(\boldsymbol{x}) \hat{a}_l + \text{H.c.} \tag{2.19a}$$

and for eqs. (2.2a) and (2.2b) into

$$\widehat{\boldsymbol{E}}(\boldsymbol{x}) = \widehat{\boldsymbol{E}}^{+}(\boldsymbol{x}) + \text{H.c.} = \sum_l \mathrm{i} \sqrt{\frac{\omega_l \hbar}{2\epsilon_0}} \boldsymbol{g}_l(\boldsymbol{x}) \hat{a}_l + \text{H.c.}\,, \tag{2.19b}$$

and

$$\widehat{\boldsymbol{B}}(\boldsymbol{x}) = \widehat{\boldsymbol{B}}^{+}(\boldsymbol{x}) + \text{H.c.} = \sum_l \sqrt{\frac{\hbar}{2\epsilon_0 \omega_l}} (\boldsymbol{\nabla} \times \boldsymbol{g}_l)(\boldsymbol{x}) \hat{a}_l + \text{H.c.}\,, \tag{2.19c}$$

respectively. Here we introduced the field operator's positive or clockwise rotating parts indicated with an upper index $+$, whereby the negative or counterclockwise rotating parts are their hermitian conjugates, and thus, e.g.,

$$\widehat{\boldsymbol{E}}^{-}(\boldsymbol{x}) = [\widehat{\boldsymbol{E}}^{+}(\boldsymbol{x})]^{\dagger}\,. \tag{2.19d}$$

The notation indicates their time dependency stemming from the solutions $\alpha(t)$ in the product ansatz for the vector potential in eq. (2.5).

For now, we have found operators describing the quantized electromagnetic field and its Hamiltonian. In quantum theory, the Hamiltonian describes the time evolution of a system according to the Schrödinger equation

$$\mathrm{i}\hbar \frac{\partial}{\partial t} |\psi(t)\rangle = \widehat{\mathrm{H}} |\psi(t)\rangle\,. \tag{2.20}$$

We have not yet discussed what kind of states $|\psi\rangle$ these operators are supposed to act on. All these states form a Hilbert space $\widehat{\mathrm{H}}_{\mathrm{F}}$. In the next section, we discuss this state space to complete our quantum theory of the electromagnetic field.

2.2 QUANTUM STATES OF THE ELECTROMAGNETIC FIELD

In the last section, we derived the Hamiltonian describing the dynamics of the electromagnetic field. To complete this quantum system, we must define on which states these operators act. In principle, we could work either in the position representation defining wave functions $\psi(\{\boldsymbol{q}_l\})$ or in the momentum representation with $\psi(\{\boldsymbol{p}_l\})$, as known from basic quantum mechanics. Here $\{\boldsymbol{q}_l\}$ and $\{\boldsymbol{p}_l\}$ are the sets of all coordinates. Such a representation allows for visualizing quantum

states via phase space functions. All physics of the electromagnetic field can be described in phase space.[5]

We choose a different representation for the electromagnetic field's Hilbert space $\mathcal{H}_\mathrm{F}$. We start from the ground state of the Hamiltonian in eq. (2.18). We call it the vacuum state $|\mathrm{vac}\rangle$ and define it as the state of photon number zero. If we neglect zero-point contributions (alternatively, we renormalize the energy), it fulfills the eigenvalue equation

$$\hat{\mathrm{H}}_\mathrm{F}|\mathrm{vac}\rangle = 0\,. \tag{2.21}$$

In this case, the Hamiltonian is up to the mode weights $\hbar\omega_l$ equivalent to the photon number operator $\hat{\mathrm{N}} = \sum_l \hat{\mathrm{a}}_l^\dagger \hat{\mathrm{a}}_l$. We assume the energy level associated with the vacuum state to be non-degenerate. A degenerate vacuum would lead to completely separated branches in the Hilbert space of the electromagnetic field.

The creation operators allow defining single-photon states

$$|f(l)\rangle = \sum_l f(l)\hat{\mathrm{a}}_l^\dagger|\mathrm{vac}\rangle\,, \tag{2.22}$$

where $\sum_l f(l) = 1$. With the help of the commutation relations from eq. (2.16), verifying that such a state has eigenvalue one regarding the number operator $\hat{\mathrm{N}}$ is easy.

Single photon states are of high interest in QIP and especially in quantum communication. For example, storage proposals for quantum information exist via their interaction with single quantum emitters [78, 94]. Also, creating entanglement between distant quantum emitters is possible using single-photon states in a waveguide [79, 80].

We want to emphasize that the term single-photon state is not synonymous with state of a single photon in a given mode. The number of exited modes depends drastically on our choice of mode functions. In fact, we can take any single-photon state, define it as as single-mode state, and can construct a complete set of orthogonal modes starting from its corresponding mode function.

As for the single-photon state, we can build the whole Hilbert space using the different creation operators. For a given set of modes, we define Fock states[6] or number states

$$|\{n_l\}\rangle = \left(\prod_l \frac{(\hat{\mathrm{a}}_l^\dagger)^{n_l}}{\sqrt{n_l!}}\right)|\mathrm{vac}\rangle\,. \tag{2.23}$$

All Fock states form an infinite orthonormal basis of the Hilbert space $\mathcal{H}_\mathrm{F}$.

5 For an extensive discussion of *quantum optics in phase space*, see [75].

6 Fock states are named after *Vladimir A. Fock*, who worked, among other topics, on the canonical quantization [95].

Coherent states are another essential class of field states. *Roy Glauber* introduced them as eigenstates of the annihilation operator [96]. An equivalent approach is to define them as displaced vacuum

$$|\{\alpha_l\}\rangle = \widehat{\mathrm{D}}(\{\alpha_l\})|\mathrm{vac}\rangle = \prod_l \widehat{\mathrm{D}}(\alpha_l)|\mathrm{vac}\rangle \tag{2.24a}$$

with the displacement operators

$$\widehat{\mathrm{D}}(\alpha_l) = \mathrm{e}^{\alpha_l \hat{\mathrm{a}}_l^\dagger - \alpha_l^* \hat{\mathrm{a}}_l} \,, \tag{2.24b}$$

where $\alpha_l \in \mathbb{C}$. [7] The displacement operators are unitary, i.e., $\widehat{\mathrm{D}}\widehat{\mathrm{D}}^\dagger = \mathbb{1}$, and transform the ladder operators as

$$\widehat{\mathrm{D}}^\dagger(\alpha_l)\hat{\mathrm{a}}_l\widehat{\mathrm{D}}(\alpha_l) = \hat{\mathrm{a}}_l + \alpha_l \tag{2.25a}$$

and

$$\widehat{\mathrm{D}}^\dagger(\alpha_l)\hat{\mathrm{a}}_l^\dagger\widehat{\mathrm{D}}(\alpha_l) = \hat{\mathrm{a}}_l^\dagger + \alpha_l^* \,. \tag{2.25b}$$

For brevity in notation, we discuss some properties of the coherent state only for a single mode of arbitrary frequency ω. They are all easily extended to the multimode case. For a more extensive discussion of coherent states and their properties, we refer to [75, sec. 11.2].

Here, we only state the most important characteristics we will need in the discussions below. A coherent state can be represented in the Fock basis as

$$|\alpha\rangle = \mathrm{e}^{-\frac{1}{2}|\alpha|^2} \sum_n \frac{\alpha^n}{\sqrt{n!}} |n\rangle \,, \tag{2.26}$$

where $|n\rangle$ is the single-mode Fock state. Therefore, its photon number statistics $\mathcal{P}(n) = |\langle n|\alpha\rangle|^2$ is a Poisson distribution with mean value or mean photon number $|\alpha|^2$. Its Fock state representation allows the time evolution of the coherent state to be deduced from the action of the creation and annihilation operators onto the number states. We find

$$|\alpha(t)\rangle = \mathrm{e}^{-\mathrm{i}\,\hat{\mathrm{H}}_\mathrm{F}\, t/\hbar}|\alpha\rangle = \mathrm{e}^{-\frac{1}{2}|\alpha|^2} \sum_n \frac{\mathrm{e}^{-\mathrm{i}\omega t n}\alpha^n}{\sqrt{n!}} |n\rangle = |\alpha \mathrm{e}^{-\mathrm{i}\omega t}\rangle \,. \tag{2.27}$$

Hence, coherent states rotate in phase but stay constant in absolute value $|\alpha|$. They are often called the most classical states of the electromagnetic field because they minimize the uncertainty relations considering the operators $\widehat{\boldsymbol{E}}$ and $\widehat{\boldsymbol{B}}$ of the electromagnetic field with symmetric uncertainties in both of these conjugated variables.

We now have completed the basic quantum theory of the electromagnetic field. We defined the field states forming the underlying

7 α_l as the coherent-state parameter must not be confused with the complex function $\alpha_l(t)$ in the product ansatz in eq. (2.5), but it should never be ambiguous because we replaced $\alpha_l(t) \to \hat{\mathrm{a}}_l$ during the canonical quantization.

Hilbert space and found an appropriate Hamiltonian describing the dynamics via the Schrödinger equation. Many interesting aspects of quantum optics can be studied only by considering the free field and its dynamic, but in many applications, its interaction with matter is vital. We discuss a model for such an interacting theory in the next section.

2.3 FIELD–MATTER INTERACTION

> *"Dirac's theory of radiation is based on a very simple idea; instead of considering an atom and the radiation field with which it interacts as two distinct systems, he treats them as a single system whose energy is the sum of three terms: one representing the energy of the atom, a second representing the electromagnetic energy of the radiation field, and a small term representing the coupling energy of the atom and the radiation field."*

- E. Fermi, [97]

In the spirit of this quote by *Enrico Fermi*, we start our discussion by developing an appropriate interaction Hamiltonian $\widehat{H}_{\text{int}}$ describing the coupling between single quantum emitters (atoms, ions, quantum dots, or other examples) and the quantized electromagnetic field. Afterward, we discuss the specific case of a coherent state of the electromagnetic field interacting with a two-level system as the most simple model of such a quantum emitter.

2.3.1 *Interaction in the dipole approximation*

Before defining the interaction between the electromagnetic field and matter, we have to describe the latter. In the previous section 2.1, we discussed the free electromagnetic field and assumed vanishing charge and current densities, but these two describe matter in the theory electromagnetism and thus, cannot vanish in an interacting theory.

We consider matter as an ensemble of charged point-like particles of charges q_i and masses m_i. Neglecting particle movement (and other aspects such as spin), we can describe it solely via its charge density[8]

$$\rho(\boldsymbol{x}) = \sum_{n=1}^{N} q_n \delta\left(\boldsymbol{x} - \boldsymbol{r}_n\right) , \tag{2.28}$$

where $\boldsymbol{r}_i$ is the position of particle i, and $\delta(\boldsymbol{x} - \boldsymbol{x}')$ is the delta distribution.

8 To start this account with a general charge distribution instead of modeling an atom is inspired by [98, sec. 2.2].

From classical electrodynamics, it is known that an appropriate Green's function $G(\boldsymbol{x}, \boldsymbol{x}')$, which solves

$$\boldsymbol{\nabla}_x^2 G(\boldsymbol{x}, \boldsymbol{x}') = \delta(\boldsymbol{x} - \boldsymbol{x}')\,, \tag{2.29}$$

constructs the electromagnetic potential for a given charge distribution as

$$\Phi(\boldsymbol{x}) = -\frac{1}{\epsilon_0} \sum_{n=1}^{N} q_n G(\boldsymbol{x}, \boldsymbol{r}_n) + \mathcal{B}\left[G(\boldsymbol{x}, \boldsymbol{x}')\right]\,. \tag{2.30}$$

$\mathcal{B}\left[G(\boldsymbol{x}, \boldsymbol{x}')\right]$ is a boundary term and does not depend on the charge distribution [66, sec. 1.10]. Hence, with an appropriate Green's function, the electric potential is still defined, and we can calculate the potential energy of the charge distribution by successively adding the point-like charges to the considered volume. With this treatment, we still can argue that we do not have to consider the scalar potential a dynamical variable. Hence, we take over our quantum theory of the transverse field from the previous section 2.1, but additionally, quantize the considered system of charged particles.

We introduce canonical operators $\hat{\boldsymbol{p}}_n$ and $\hat{\boldsymbol{r}}_n$ for each particle's position and momentum variables. Each of these operators fulfills canonical commutation relations in each spatial coordinate, and operators describing different particles commute. Analogous to the field quantization,

$$\left[(\hat{r}_i)_n\,, (\hat{p}_j)_{n'}\right] = \mathrm{i}\hbar\delta_{nn'}\delta_{ij}\,, \tag{2.31a}$$
$$\left[(\hat{r}_i)_n\,, (\hat{r}_j)_{n'}\right] = 0\,, \tag{2.31b}$$

and

$$\left[(\hat{p}_i)_n\,, (\hat{p}_j)_{n'}\right] = 0\,. \tag{2.31c}$$

All of the operators act on a Hilbert space $\mathcal{H}_\mathrm{A}$ distinct from the Hilbert space $\mathcal{H}_\mathrm{F}$ of the electromagnetic field. An interacting theory must be considered on the tensor product space

$$\mathcal{H} = \mathcal{H}_\mathrm{F} \otimes \mathcal{H}_\mathrm{A}\,. \tag{2.32}$$

All operators that only act on one part of such a product space commute with operators from another part. We have to introduce operators acting on both parts simultaneously to achieve interaction.

The minimal coupling scheme is the standard approach to couple the electromagnetic field with charged particles. It transforms all canonical momenta of the particles as

$$\hat{\boldsymbol{p}}_n \longrightarrow \hat{\boldsymbol{p}}_n - q_n \widehat{\boldsymbol{A}}(\hat{\boldsymbol{r}}_n)\,. \tag{2.33}$$

It can be deduced from a combination of gauge invariances of both electrodynamics and quantum mechanics. For a more detailed discussion of the deeper reasoning of the minimal coupling scheme and its

origin from gauge theory, we refer to the discussion by *Schleich* [75, sec. 14.2].

The resulting minimal coupling Hamiltonian is

$$\hat{H} = \hat{H}_F + \sum_{n=1}^{n} \frac{\left(\hat{\boldsymbol{p}}_n - q_n \hat{\boldsymbol{A}}(\hat{\boldsymbol{r}}_n)\right)^2}{2m_e} - \frac{1}{\epsilon_0} \sum_{n<m}^{N} q_n q_m G(\hat{\boldsymbol{r}}_n, \hat{\boldsymbol{r}}_m) \,. \quad (2.34)$$

Here, the first term is the free field Hamiltonian as deduced in section 2.1, the second describes the kinetic energy of the charged particles under the minimal coupling scheme, and the last one is the potential energy of the charge distribution. We neglected constant contributions arising from the boundary term $\mathcal{B}$ and possible self-interaction of single particles. They would shift the energy levels of the charge distribution and are comparable to zero point contributions of the electromagnetic field [71, App.3].

In the following, we will make a significant approximation to the full system Hamiltonian. Since optical wavelengths ($\lambda \gtrsim 10^{-7}$m) are much larger than the typical extent of quantum emitters ($a_0 \approx 10^{-10}$m), we can employ the so called dipole approximation and assume that the electromagnetic field does not change much between different positions $\hat{\boldsymbol{r}}_n$ and just consider its value at $\boldsymbol{r}$: the center of mass of the charge distribution. Therefore we evaluate the field operators $\hat{\boldsymbol{A}}(\hat{\boldsymbol{r}}_n) \approx \hat{\boldsymbol{A}}(\hat{\boldsymbol{r}})$ at this common position.

Further, we introduce the *Göppert-Mayer* transformation[9]

$$\hat{U} = e^{i\hat{\boldsymbol{d}}\cdot\hat{\boldsymbol{A}}(\boldsymbol{r})} \,, \quad (2.35)$$

where $\hat{\boldsymbol{d}} = \sum_{n=1}^{n} q_n \hat{\boldsymbol{r}}_n$ is the dipole-operator of the charge distribution.

It affects certain parts of the Hamiltonian in eq. (2.34). We have

$$\hat{U}^\dagger \left(\hat{p}_n - q_n \hat{\boldsymbol{A}}(\boldsymbol{r})\right) \hat{U} = \hat{p}_n \quad (2.36a)$$

and

$$\hat{U}^\dagger \hat{H}_F \hat{U} = \hat{H}^F - \hat{\boldsymbol{d}} \cdot \hat{\boldsymbol{E}}(\boldsymbol{r}) + \sum_l \frac{|\hat{\boldsymbol{d}} \cdot \boldsymbol{g}_l(\boldsymbol{r})|^2}{2\epsilon_0} \,. \quad (2.36b)$$

We neglect the last term since if we consider large volumes the mode function $\boldsymbol{g}_l(\boldsymbol{r})$ at a single point in space scarcely contributes. The third part of eq. (2.34) is not affected since it commutes with $\hat{U}$. Altogether, we find the transformed Hamiltonian

$$\hat{U}^\dagger \hat{H} \hat{U} = \hat{H}_F + \sum_{n=1}^{n} \frac{\hat{\boldsymbol{p}}_n^2}{2m_e} - \frac{1}{\epsilon_0} \sum_{n<m}^{N} q_n q_m G(\hat{\boldsymbol{r}}_n, \hat{\boldsymbol{r}}_m) - \hat{\boldsymbol{d}} \cdot \hat{\boldsymbol{E}}(\boldsymbol{r}) \,. \quad (2.37)$$

The interaction term

$$\hat{H}_{\text{int}} = -\hat{\boldsymbol{d}} \cdot \hat{\boldsymbol{E}} \quad (2.38)$$

9 The transformation is named after *Maria Göppert-Mayer*. She recognized the equivalence of the minimal and dipole coupling schemes. The latter directly postulates the interaction Hamiltonian $\hat{H}_{\text{int}}$, as deduced in this section [99, 75, secs. 14.4-6].

describes the field–matter interaction in dipole approximation. We group the two unnamed terms as $\widehat{H}_A$ anticipating that most of the time, we describe the interaction with a single atom. In conclusion, we adopt the full system Hamiltonian

$$\widehat{H} = \widehat{H}_F + \widehat{H}_A + \widehat{H}_{int} \ . \tag{2.39}$$

The resulting Hamiltonian has precisely the form indicated in the quote at the beginning of this section. We must emphasize that we made several approximations to derive this result. Most prominent is the dipole approximation itself, but we also described the particles as spinless and neglected their relative movement together with several terms appearing during the deduction of the interaction Hamiltonian. Depending on the situation, these aspects can rise in prominence and become important.

However, $\widehat{H}_{int}$ is the most commonly used interaction model in all quantum optics. It describes wide variations of light particle interactions in good agreement with experimental results. Therefore, it will serve as our primary model for all further considerations of field–matter interaction. In the following section, we will simplify it further by making additional approximations regarding the form of the atomic Hamiltonian.

2.3.2 *A two-level quantum system interacting with coherent light*

In the previous section, we derived the basic model of field–matter interaction. It resulted in the interaction Hamiltonian $\widehat{H}_{int}$ in the dipole approximation. Although it already simplifies the interaction significantly, real atoms are still very hard to describe. There exist almost no analytical solutions for atoms more complex than hydrogen-like atoms. The whole branch of atom physics is dedicated to finding suitable models and approximations to describe atoms' energy levels and other aspects. Many textbooks discuss this area of physics from introductory accounts to extensive compendiums of specific topics, e.g., Rydberg atoms [46] which will be of importance in part II of this dissertation.

Here, we only want to highlight particular aspects of the field–matter interaction. We already will find them in the most basic model imaginable: The two-level atom. Although such atoms do not exist in reality, it is often possible to approximate them as such when their internal energy level spacing (in frequency terms) is much broader than the frequency width of the considered light fields, and their center of mass motion can either be described classically via a position vector $\boldsymbol{x}(t)$ or can assumed to be constant over the considered interaction time. The last assumption of constant position $\boldsymbol{x}$ is sometimes called frozen dynamics and will be adopted in the following discussion.

To be more precise, we describe the atom (or ion, molecule, quantum emitter) by its energy levels: Its ground state $|g\rangle$ of energy E_g, a

distinguished excited level $|r\rangle$[10] with energy E_r and other levels $|s\rangle$ with energies E_s. If we set the energy origin such that $E_g \to 0$, we can write $E_r = \hbar\omega_A$ with the two-level resonance frequency ω_A. The light field is assumed to populate only modes of frequencies ω_l around a center frequency $\overline{\omega}$, such that $|\omega_l - \overline{\omega}| \ll \Delta\omega$, where $2\Delta\omega$ is the considered bandwidth. Assuming $\omega_A \in [\overline{\omega} - \Delta\omega, \overline{\omega} + \Delta\omega]$ and $|E_s - E_{s'}|/\hbar \notin [\overline{\omega} - \Delta\omega, \overline{\omega} + \Delta\omega]$ for all $s, s' \neq g, r$, we can ignore all other states and simplify the atomic Hamiltonian as

$$\widehat{\mathrm{H}}_\mathrm{A} = \hbar\omega_A |r\rangle\langle r| \,. \tag{2.40a}$$

The dipole operator of the two level system is

$$\widehat{\boldsymbol{d}} = \boldsymbol{d}|r\rangle\langle g| + \mathrm{H.c.}\,, \tag{2.40b}$$

where $\boldsymbol{d} = \langle r|\widehat{\boldsymbol{d}}|g\rangle$.

To be able to concentrate on the interaction between field and two-level system, we transform the system Hamiltonian in dipole approximation in eq. (2.39) according to the unitary transformation $\widehat{\mathrm{U}} = \mathrm{e}^{-\mathrm{i}(\widehat{\mathrm{H}}_\mathrm{F} + \widehat{\mathrm{H}}_\mathrm{A})t/\hbar}$. Hence, we consider the interaction picture for which the interaction Hamiltonian transforms as

$$\widehat{\mathrm{U}}^\dagger \widehat{\mathrm{H}}_\mathrm{int} \widehat{\mathrm{U}} = -\left(\boldsymbol{d}\,\mathrm{e}^{\mathrm{i}\omega_A t}|r\rangle\langle g| + \mathrm{H.c.}\right) \cdot \left(\widehat{\boldsymbol{E}}^+(\boldsymbol{x}, t) + \mathrm{H.c.}\right)\,, \tag{2.41a}$$

where,

$$\widehat{\boldsymbol{E}}^+(\boldsymbol{x}, t) = \sum_l \mathrm{i}\sqrt{\frac{\omega_l \hbar}{2\epsilon_0}}\boldsymbol{g}_l(\boldsymbol{x})\hat{\mathrm{a}}_l\,\mathrm{e}^{-\mathrm{i}\omega_l t} \tag{2.41b}$$

is the electromagnetic field's part rotating positive or clockwise in time. We observe four different frequencies per mode. Two near-resonant terms rotate with low frequencies $\pm\Delta = \pm(\omega_l - \omega_A)$, and two far off-resonant terms rotate with a high frequencies $\pm(\omega_l + \omega_A)$. Applying the so-called rotating wave approximation (RWA) allows neglecting the fast rotating terms. It is an argument of the separation of time scales, where fast oscillations are considered to be averaged over time and not observable on the time scale of the slower oscillations. The RWA is usually well satisfied in optical systems, where the transition frequency ω_A, and thus the central frequency $\overline{\omega}$ is much larger than all other typical frequencies. Transforming back into the Schrödinger picture results in the system Hamiltonian

$$\widehat{\mathrm{H}} = \widehat{\mathrm{H}}_\mathrm{F} + \widehat{\mathrm{H}}_\mathrm{A} - \left(|r\rangle\langle g|\boldsymbol{d} \cdot \widehat{\boldsymbol{E}}^+(\boldsymbol{x}) + \mathrm{H.c.}\right) \tag{2.42}$$

with the interaction Hamiltonian in RWA and dipole approximation. Since in the RWA we only consider combinations of atomic excitation

10 The notation $|r\rangle$ already anticipates its usage in part II where we model Rydberg atoms as two-level systems.

operator $|r\rangle\langle g|$ and annihilation operators $\hat{a}_l$ or of the atomic de-excitation operator $|g\rangle\langle r|$ and creation operators $\hat{a}_l^\dagger$, the dynamics induced by this system Hamiltonian conserves the total number of excitations.

Now, we want to discuss the special case of a classical field driving the two-level atom. As discussed in the previous section, a coherent state $|\alpha\rangle$ of high mean photon number $|\alpha|^2$ well-presents a classical field. Although the following arguments also hold for a multi-mode coherent state, we want to avoid terms considering the sum over all modes. In essence, we tighten the former approximations to $\Delta\omega \ll \overline{\omega}$ so that $\omega_l \approx \overline{\omega} = \omega$ holds for all considered modes.

Due to the conversation of the total excitation number, we expect the change in the coherent states' photon number to be negligible compared to its high mean value. As a result, we assume the coherent state is not affected by the interaction, and its time evolution is described by $|\alpha(t)\rangle$ from eq. (2.27). Tracing over the field's degrees of freedom results in the dynamics of the two-level system. For the single mode case,

$$\mathrm{Tr}_\mathrm{F}\,\hat{H} = \langle\alpha|\,\hat{H}|\alpha\rangle = \hbar\omega|\alpha|^2 + \hat{H}_\mathrm{A} - (\hbar\Omega(\boldsymbol{x},t)|g\rangle\langle r| + \mathrm{H.c.})\ , \tag{2.43a}$$

where due to the eigenvalue relation for the coherent state

$$\Omega(\boldsymbol{x},t) = \mathrm{i}\alpha\sqrt{\frac{\omega}{2\epsilon_0\hbar}}\boldsymbol{d}\cdot\boldsymbol{g}(\boldsymbol{x})\mathrm{e}^{-\mathrm{i}\omega t} = \Omega(\boldsymbol{x})\mathrm{e}^{-\mathrm{i}\omega t}\,. \tag{2.43b}$$

Here and throughout all following considerations, we call the coefficient corresponding to a jump operator in a Hamiltonian from some atomic state to another the Rabi frequency Ω[11] of the transition $|g\rangle \leftrightarrow |r\rangle$.[12]

Subtracting (i.e., renormalizing) the constant field energy from the result and transforming it into a rotating frame via the unitary transformation $\hat{U}(t) = \mathrm{e}^{\mathrm{i}\omega t|r\rangle\langle r|}$, we find the basic Rabi Hamiltonian

$$\hat{H}_\mathrm{A}^\mathrm{Rabi} = -\hbar\Delta|r\rangle\langle r| + (\Omega|g\rangle\langle r| + \mathrm{H.c.})\ , \tag{2.44}$$

where we have omitted the spatial variable for the Rabi frequency. Its eigenenergies are

$$E_\pm = -\frac{\hbar\Delta}{2} \pm \frac{\hbar\sqrt{\Delta^2 + 4|\Omega|^2}}{2}\,. \tag{2.45}$$

Assuming the atom is in the ground state at some starting point $t = t_0$, the possibility of finding it in the excited state at time $t > t_0$ is

$$|\langle r|\mathrm{e}^{-\mathrm{i}\hat{H}_\mathrm{A}^\mathrm{Rabi}t/\hbar}|g\rangle|^2 = \frac{4|\Omega|^2}{\omega_R^2}\sin^2\left(\frac{\omega_R}{2}t\right)\,. \tag{2.46}$$

11 It is named after *Isidor I. Rabi*, who won the Nobel Prize in physics *"for his resonance method for recording the magnetic properties of atomic nuclei"* [100].

12 Note that an additional factor of two is often included in the definition of the Rabi frequency (see, e.g., [73, sec. 5.1]), such that it equals the generalized Rabi frequency on resonance. We avoid this factor for later convenience.

Hence, we see Rabi oscillations of amplitude $4|\Omega|^2/\omega_R^2$. The frequency $\omega_R = \sqrt{\Delta^2 + 4|\Omega|^2}$ is called generalized Rabi frequency[12]. Although we neglected many aspects of real atoms, already this simple model allows discussing the magnitude of the interaction with classical fields. On resonance, i.e., $\Delta \to 0$, the amplitude is unity; thus, the atom is excited at times $t = (2n+1)\pi/\omega_R$ with $n \in \mathbb{N}_0$. Off resonance, i.e., $|\Delta| \neq 0$, the amplitude is less than unity, but a higher Rabi frequency can partly compensate for it, resulting in faster Rabi oscillations. The magnitude of the oscillations and their different frequencies will be of importance when we discuss effective Hamiltonians of more complicated systems.

Rabi oscillations are one of the most common phenomena in quantum optics. Many others can be discussed if the interaction with other states as coherent states of high photon number is discussed. For example, the vacuum state is the coherent state with $\alpha = 0$, and its interaction with an initially excited atom allows for a simple theory of spontaneous decay, as shown by *Weisskopf and Wigner* already at the beginning of quantum theory [101]. Spontaneous decay is also crucial if the back-action onto the field is not entirely neglected. An extensive discussion of effects such as damping and saturation in the excitation probability or photon scattering was discussed by *Mollow* [102]. Considering the center of mass motion of the atom leads to mechanical effects of light onto atoms, and, e.g., used to cool down and trap atoms with light fields [76, 91, 103]. As we discussed only the most basic version of light–matter interaction, we refer to extensive descriptions in the literature, e.g., in [71, 73, 75]. They discuss the mentioned phenomena and many other aspects of light–matter interaction in more detail.

3

EFFECTIVE HAMILTONIANS

This chapter briefly introduces the theory of effective Hamiltonians via an expansion of the resolvent operator. It is based on a private lecture by *Prof. Dr. Gernot Alber*. Also, the textbook by *Galindo and Pascual* [104, sec. 10.7] presents an overview of it. *Steck* [73, ch. 15] discusses the resolvent with a focus on its applications in quantum optics. Here, we do not claim any mathematical rigorousness, and only want to motivate how to deduce effective Hamiltonians. For a mathematical sound discussion of the properties of the resolvent operator, see, e.g., the textbook by *Richtmyer* on advanced mathematics in physics [105, ch. 8].

To derive effective Hamiltonians we use the resolvent operator of the system Hamiltonian. For a Hermitian operator $\widehat{\mathrm{H}}$, the resolvent $\widehat{\mathrm{G}}(z)$ fulfills the defining equation

$$\mathbb{1} = (z - \widehat{\mathrm{H}})\widehat{\mathrm{G}}(z)\,, \tag{3.1}$$

where $z \in \mathbb{C}$. For simplicity, we assume $\widehat{\mathrm{H}}$ features a discrete and countable spectrum, but we allow for degenerate eigenvalues.

Using the defining property of the resolvent, we find for a projection operator $\widehat{\mathrm{P}}$ ($\widehat{\mathrm{P}}^2 = \widehat{\mathrm{P}}$) and its complementary projection $\widehat{\mathrm{Q}}$ ($\widehat{\mathrm{P}} + \widehat{\mathrm{Q}} = \mathbb{1}$)

$$\begin{aligned}\widehat{\mathrm{P}} &= \widehat{\mathrm{P}}(z - \widehat{\mathrm{H}})(\widehat{\mathrm{P}} + \widehat{\mathrm{Q}})\widehat{\mathrm{G}}(z)\widehat{\mathrm{P}} \\ &= (z - \widehat{\mathrm{P}}\,\widehat{\mathrm{H}}\,\widehat{\mathrm{P}})\widehat{\mathrm{P}}\widehat{\mathrm{G}}(z)\widehat{\mathrm{P}} - \widehat{\mathrm{P}}\,\widehat{\mathrm{H}}\,\widehat{\mathrm{Q}}\,\widehat{\mathrm{Q}}\widehat{\mathrm{G}}(z)\widehat{\mathrm{P}}\end{aligned} \tag{3.2a}$$

and

$$\begin{aligned}0 &= \widehat{\mathrm{Q}}(z - \widehat{\mathrm{H}})(\widehat{\mathrm{P}} + \widehat{\mathrm{Q}})\widehat{\mathrm{G}}(z)\widehat{\mathrm{P}} \\ &= -\widehat{\mathrm{Q}}\,\widehat{\mathrm{H}}\,\widehat{\mathrm{P}}\widehat{\mathrm{G}}(z)\widehat{\mathrm{P}} + (z - \widehat{\mathrm{Q}}\,\widehat{\mathrm{H}}\,\widehat{\mathrm{Q}})\widehat{\mathrm{Q}}\widehat{\mathrm{G}}(z)\widehat{\mathrm{P}}\,.\end{aligned} \tag{3.2b}$$

We find $\widehat{\mathrm{Q}}\widehat{\mathrm{G}}(z)\widehat{\mathrm{P}}$ from the second equation and substitute it into the first to get

$$\begin{aligned}\widehat{\mathrm{P}} &= \left[z - \left(\widehat{\mathrm{P}}\,\widehat{\mathrm{H}}\,\widehat{\mathrm{P}} + \widehat{\mathrm{P}}\,\widehat{\mathrm{H}}\,\widehat{\mathrm{Q}}\frac{\widehat{\mathrm{Q}}\,\widehat{\mathrm{H}}\,\widehat{\mathrm{P}}}{z - \widehat{\mathrm{Q}}\,\widehat{\mathrm{H}}\,\widehat{\mathrm{Q}}}\right)\right]\widehat{\mathrm{P}}\widehat{\mathrm{G}}(z)\widehat{\mathrm{P}} \\ &= \left[z - \widehat{\Sigma}(z)\right]\widehat{\mathrm{P}}\widehat{\mathrm{G}}(z)\widehat{\mathrm{P}}\,.\end{aligned} \tag{3.2c}$$

Therefore, we find $\widehat{\Sigma}(z)$ akin to $\widehat{\mathrm{H}}$ in a defining equation for the resolvent restricted onto the subspace defined by $\widehat{\mathrm{P}}$ and call it the effective Hamiltonian in this subspace.

We define the projectors

$$\widehat{\mathrm{P}}_E = \sum_{i=1}^{m_E} |E_i\rangle\langle E_i| \tag{3.3}$$

projecting onto the subspace of $\widehat{H}$ spanned by orthogonal eigenstates $|E_i\rangle$ of equal energy E. m_E is the multiplicity of E. Using these projectors, we can rewrite the Hamiltonian as a sum over its whole spectrum as

$$\widehat{H} = \sum_{E\in\sigma(\widehat{H})} \widehat{P}_E \left(\widehat{H} + \widehat{P}_E \widehat{H} \widehat{Q}_E \frac{1}{E - \widehat{Q}_E \widehat{H} \widehat{Q}_E} \widehat{Q}_E \widehat{H} \right) \widehat{P}_E \,. \tag{3.4}$$

Rewriting alone does not allow us to investigate the Hamiltonian any further, but if we can decompose it as $\widehat{H} = \widehat{H}_0 + \lambda \widehat{H}_1$, where $\widehat{H}_1$ is supposed to be a *small* correction to $\widehat{H}_0$, we can discuss the Hamiltonian in a perturbative approach. We then expand

$$\frac{1}{E - \widehat{Q}_E \widehat{H} \widehat{Q}_E} = \frac{1}{E - \widehat{Q}_E \widehat{H}_0 \widehat{Q}_E} + \frac{\lambda \widehat{H}_1}{(E - \widehat{Q}_E \widehat{H}_0 \widehat{Q}_E)^2} + \dots \tag{3.5}$$

around $\lambda \approx 0$.

We have motivated here how to construct effective Hamiltonians via a perturbation theory. If the perturbation is small enough, i.e., the parameter λ is much smaller than all energy differences appearing in the sum over all energies, we can cut off such an expansion early on and approximate the Hamiltonian dynamics of a system by using the projectors onto the unperturbed eigenstates of the system. We will make use of this theory of effective Hamiltonians in chapter 5 to find effective descriptions of a multi-atom system interacting with several classical laser fields.

An alternative describing the interaction of the atomic ensemble with classical fields is Floquet theory [106] and for our case of multiple laser fields, many-mode Floquet theory [107]. It maps the oscillatory time dependence of the interaction onto an infinite number of Floquet modes described by a time-independent Hamiltonian. Perturbation theory gives quantities such as transition frequencies between different atomic states within this formulation. However, we prefer the resolvent formalism in our effective description for the atomic ensemble since it directly gives the effective Hamiltonian rather than only the dynamics of a specific initial state.

Part II

QUANTUM STATE CONVERSION

4

QUANTUM STATE CONVERSION IN A TWO-QUBIT SYSTEM

In this chapter, we discuss an abstract concept of quantum state conversion. Without any specific physical realization in mind, we investigate the conversion in a system of two qubits realizing a four-level quantum system. Abstract Rabi frequencies describe transition rates between different levels and represent the control over the system's dynamics.

After the qubit, the two-qubit system is the most basic system in quantum information. Besides total control over single qubits, at least one two-qubit gate is necessary to form a complete set of quantum operations to implement a general quantum logical circuit [108]. The conversion schemes developed in this chapter are later used in the context of a quantum system modeling neutral Rydberg atoms driven by external laser fields.

We begin with defining the two-qubit system and developing a Lie-algebraic approach to describe quantum state conversion within it in sections 4.1 to 4.3. Sections 4.4 and 4.5 present some examples using the developed approach and discuss some limitations. Section 4.6 then discusses quantum state conversion in a constrained two-qubit system. The specific constraints on the Hamiltonian will be reflected in dimensional reduction of quantum systems discussed in chapter 5, where we present a quantum optical model to implement the specific state conversion scheme developed in section 4.7.

Some content of this chapter was already published as a W to GHZ state conversion scheme for a quantum system of three neutral Rydberg atoms in the blockade regime [63]. To apply the aforementioned scheme, we used a reduction of the eight-level quantum system to an effective four-level system, which was first presented by *Zheng et al.* [109]. However, sections 4.6 and 4.7 of this chapter present the developed conversion scheme in the generalized context of a generic two-qubit system. A discussion of the Rydberg-atom system is deferred to chapter 5. A more detailed description of how some of the content already appeared in other publications can be found in the summary (section 4.8.2).

4.1 THE FOUR-LEVEL QUANTUM SYSTEM

We consider a system of two qubits, i.e., two two-level quantum systems, each described in a two-dimensional Hilbert space $\mathcal{H}_i$. The Hilbert space describing two qubits is the tensor product of the Hilbert spaces of the two individual qubits, i.e., $\mathcal{H}_1 \otimes \mathcal{H}_2$. It has dimension

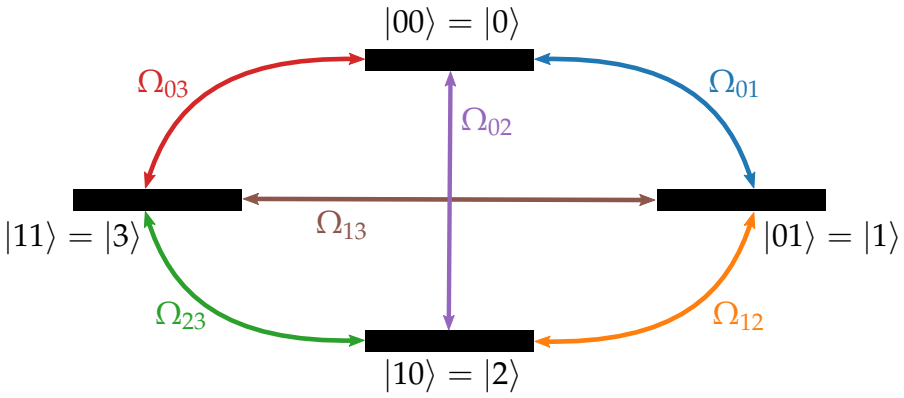

Figure 4.1: Schematic drawing of the four-level quantum system. All depicted levels are eigenlevels of the Hamiltonian, fulfilling the eigenvalue relation $\widehat{H}^{4LS}|i\rangle = E_i|i\rangle$ $(i \in 0,1,2,3)$ [cf. eq. (4.2)]. Rabi frequencies Ω_{ij} $(i < j \in 0,1,2,3)$ are the off-diagonal elements of the Hamiltonian driving transitions between levels i and j.

four. We use the computational basis and identify each of the first four binary numbers with one four-dimensional unit vector as

$$|0\rangle_1 \otimes |0\rangle_2 = |00\rangle = |0\rangle \rightarrow \begin{pmatrix} 1 & 0 & 0 & 0 \end{pmatrix}^T , \tag{4.1a}$$

$$|0\rangle_1 \otimes |1\rangle_2 = |01\rangle = |1\rangle \rightarrow \begin{pmatrix} 0 & 1 & 0 & 0 \end{pmatrix}^T , \tag{4.1b}$$

$$|1\rangle_1 \otimes |0\rangle_2 = |10\rangle = |2\rangle \rightarrow \begin{pmatrix} 0 & 0 & 1 & 0 \end{pmatrix}^T , \tag{4.1c}$$

and

$$|1\rangle_1 \otimes |1\rangle_2 = |11\rangle = |3\rangle \rightarrow \begin{pmatrix} 0 & 0 & 0 & 1 \end{pmatrix}^T . \tag{4.1d}$$

Most of the time, we will use the binary notation $(00, 01, 10, 11)$ for quantum states of the two-qubit system, but especially in definitions of operators, it is often easier to count the basis states and refer to them as $|i\rangle$, where $i \in \{0,1,2,3\}$.[1] Hence, in definitions we often use the decimal notation.

In quantum mechanics, the Hamiltonian governs the dynamics of a quantum system. For the four-level quantum system (4LS), the most general Hamiltonian in terms of the computational basis is

$$\widehat{H}^{4LS}(t)/\hbar = \sum_{i=0}^{3} e_i |i\rangle\langle i| + \sum_{i<j=0}^{3} \left(\Omega_{ij}(t)|i\rangle\langle j| + \text{H.c.}\right) , \tag{4.2}$$

where the parameters $e_i = E_i/\hbar$ describe the energies of the four levels and $\Omega_{ij}(t)$ are the abstract Rabi frequencies of the quantum transitions $|i\rangle \leftrightarrow |j\rangle$. Figure 4.1 shows a schematic drawing of the considered system.

1 Of course, it is possible to count in binary notation, but we are far more used to the decimal number system.

In this chapter's discussion, we will neglect the energy differences between the four levels, and we set $E_i = 0$ for all i. An equivalent approach is a transformation into the interaction picture regarding the diagonal part of $\widehat{H}^{4\mathrm{LS}}(t)$. In real quantum systems, such as atoms, the energy differences of the energy levels play a crucial role but can often considered to induce dynamics on a different time scale than the dynamics introduced by the Rabi frequencies. Such a hierarchy of different time scales will be used in chapter 5 when we discuss quantum state conversion in a system of neutral Rydberg atoms.

In the following, we discuss quantum state conversion in the introduced quantum system. In general, quantum state conversion describes the controlled transition from an initial quantum state $|\psi(t_0)\rangle$ at time $t_0 = 0$ to a final or target quantum state $|\psi(T)\rangle$ at time $t = T$. We present an approach describing such a transition via curves in a Lie algebra and connecting it to time-dependent Hamiltonians of the form of $\widehat{H}^{4\mathrm{LS}}(t)$.

4.2 DYNAMICAL SYMMETRY

We utilize its dynamical symmetries to find suitable state conversion schemes in the system under consideration. Symmetries are an essential concept of modern physics as they often simplify theoretical descriptions of the considered system. *Noether's*[2] theorem connects each symmetry with a conservation law. The resulting invariants can be exploited to find solutions to time-dependent problems. For example, using such invariants *Lewis & Riesenfelds* constructed solutions for the time-dependent quantum harmonic oscillator [110]. Together with the dynamical algebra of the considered system, it is possible to find time-dependent Hamiltonians which implement a specific state conversion [109, 111]. For an extensive discussion of the group theoretical background of dynamical symmetries, Lie groups, and Lie algebras, we refer to the textbook by *Barut and Rączka* [112]. Aspects of it, which we will apply in the following can also be found in, e.g., in the textbooks by *Richtmyer* or *Hall* [113, 114].

The Lie algebra $\mathrm{su}(4)$ describes the complete dynamical symmetry of two qubits and is described by 16 elements. There are many possibilities for choosing a set of 16 linearly independent matrices as a set of generators of the dynamics of the two qubits [115]. *Rau & Alber* thoroughly discussed this system's symmetries, possible subalgebras, and analogies to other quantum systems [116]. In addition, the first of these authors gave a general review of *Symmetries and Geometries of Qubits, and their Uses* [117]. Here, we concentrate on applying these dynamical symmetries to describe quantum state conversion.

2 *"Emmy Noether, 1882-1935, [...] Many major physicists described her as the most important woman in the history of mathematics" [2, p. 118]*

In the following, we will restrict all discussions to the Lie algebra so(4), i.e., a subalgebra of su(4). It corresponds to the group of rotations in R^4. This restriction reduces the number of generators to six. The smaller dimension of the subalgebra simplifies the following approach significantly. Although we cannot describe all unitary transformations of the four-level quantum system, we can still find solutions for interesting state-conversion problems. Furthermore, the smaller Lie algebra perfectly suits the Hamiltonian constraints we will impose onto the system later in sections 4.6 and 4.7.

First, we have to choose a representation for the considered Lie algebra. The six matrices

$$\widehat{\mathrm{S}}_1 = \frac{1}{2}\begin{pmatrix} 0 & 1 & 0 & 0 \\ 1 & 0 & 0 & 0 \\ 0 & 0 & 0 & 1 \\ 0 & 0 & 1 & 0 \end{pmatrix}, \qquad \widehat{\mathrm{T}}_1 = \frac{1}{2}\begin{pmatrix} 0 & 1 & 0 & 0 \\ 1 & 0 & 0 & 0 \\ 0 & 0 & 0 & -1 \\ 0 & 0 & -1 & 0 \end{pmatrix}, \tag{4.3a}$$

$$\widehat{\mathrm{S}}_2 = \frac{1}{2}\begin{pmatrix} 0 & 0 & 0 & -1 \\ 0 & 0 & 1 & 0 \\ 0 & 1 & 0 & 0 \\ -1 & 0 & 0 & 0 \end{pmatrix}, \quad \widehat{\mathrm{T}}_2 = \frac{1}{2}\begin{pmatrix} 0 & 0 & 0 & 1 \\ 0 & 0 & 1 & 0 \\ 0 & 1 & 0 & 0 \\ 1 & 0 & 0 & 0 \end{pmatrix}, \tag{4.3b}$$

$$\widehat{\mathrm{S}}_3 = \frac{1}{2}\begin{pmatrix} 0 & 0 & -\mathrm{i} & 0 \\ 0 & 0 & 0 & \mathrm{i} \\ \mathrm{i} & 0 & 0 & 0 \\ 0 & -\mathrm{i} & 0 & 0 \end{pmatrix}, \quad \widehat{\mathrm{T}}_3 = \begin{pmatrix} 0 & 0 & -\mathrm{i} & 0 \\ 0 & 0 & 0 & -\mathrm{i} \\ \mathrm{i} & 0 & 0 & 0 \\ 0 & \mathrm{i} & 0 & 0 \end{pmatrix}. \tag{4.3c}$$

constitute a four-dimensional representation of the Lie algebra so(4). In the following, we subsume these matrices into two three-dimensional vectors, $\widehat{\boldsymbol{S}}$ and $\widehat{\boldsymbol{T}}$, in which $\widehat{\mathrm{S}}_i$ and $\widehat{\mathrm{T}}_i$ constitute respective Cartesian components. We build the two independent invariant operators,

$$\widehat{\mathrm{I}} = \sum_{i=1}^{3} \left(\widehat{\mathrm{S}}_i^2 + \widehat{\mathrm{T}}_i^2\right) = \frac{3}{2} \tag{4.4a}$$

and

$$\widehat{\mathrm{J}} = \sum_{i=1}^{3} \left(\widehat{\mathrm{S}}_i^2 - \widehat{\mathrm{T}}_i^2\right) = 0\,. \tag{4.4b}$$

Hence, each set $\widehat{\boldsymbol{S}}$ and $\widehat{\boldsymbol{T}}$ fulfills

$$\sum_{i}^{3} \widehat{\mathrm{S}}_i^2 = \sum_{i}^{3} \widehat{\mathrm{T}}_i^3 = \frac{1}{2}(1 + \frac{1}{2})\,. \tag{4.4c}$$

Further, the two sets of matrices fulfill the Lie bracket or commutation relations

$$[\widehat{\mathrm{S}}_i, \widehat{\mathrm{S}}_j] = \mathrm{i}\epsilon_{ijk}\widehat{\mathrm{S}}_k\,, \tag{4.5a}$$

$$[\widehat{\mathrm{T}}_i, \widehat{\mathrm{T}}_j] = \mathrm{i}\epsilon_{ijk}\widehat{\mathrm{T}}_k\,, \tag{4.5b}$$

and

$$[\widehat{S}_i, \widehat{T}_j] = 0\,. \tag{4.5c}$$

The properties in eqs. (4.4) and (4.5) of our chosen representation explicitly show that a subspace of the dynamical symmetry of our system is $\mathrm{su}(2) \oplus \mathrm{su}(2) \cong \mathrm{so}(4)$. Here, the Lie algebra $\mathrm{so}(4)$ represents a combination of two independent pseudospin-$1/2$–degrees of freedom. It is not a surprising fact since we describe two two-level systems. However, we will see in the following that one of the pseudospin-$1/2$–degrees of freedom cannot be identified with an individual qubit. Changing the representation in eqs. (4.3) to the six Pauli operators of the individual qubits (three per qubit) does allow for such an identification.

We construct a suitable eigenbasis for the two independent pseudospins in analogy to a system of arbitrary angular momentum. We start from the state of highest eigenvalue for the operator $\widehat{S}_3 + \widehat{T}_3$, i.e.

$$|\uparrow\uparrow\rangle \to \frac{1}{\sqrt{2}} \begin{pmatrix} -\mathrm{i} & 0 & 1 & 0 \end{pmatrix}^{\mathrm{T}}. \tag{4.6a}$$

The state of highest pseudospin is not identical to state $|11\rangle$, which, considering each qubit as a spin-$1/2$–particle, represents the state of highest total spin.

We apply the individual lowering operators $\widehat{S}_1 - \mathrm{i}\widehat{S}_2$ and $\widehat{T}_1 - \mathrm{i}\widehat{T}_2$ onto $|\uparrow\uparrow\rangle$ o obtain the remaining orthonormal basis states of the combined pseudospins. We get

$$\widehat{T}_1 - \mathrm{i}\widehat{T}_2|\uparrow\uparrow\rangle = |\uparrow\downarrow\rangle \to \frac{1}{\sqrt{2}} \begin{pmatrix} 0 & -\mathrm{i} & 0 & -1 \end{pmatrix}^{\mathrm{T}}, \tag{4.6b}$$

$$\widehat{S}_1 - \mathrm{i}\widehat{S}_2|\uparrow\uparrow\rangle = |\downarrow\uparrow\rangle \to \frac{1}{\sqrt{2}} \begin{pmatrix} 0 & -\mathrm{i} & 0 & 1 \end{pmatrix}^{\mathrm{T}}, \tag{4.6c}$$

and

$$\widehat{S}_1 - \mathrm{i}\widehat{S}_2|\uparrow\downarrow\rangle = |\downarrow\downarrow\rangle \to \frac{1}{\sqrt{2}} \begin{pmatrix} -\mathrm{i} & 0 & -1 & 0 \end{pmatrix}^{\mathrm{T}}. \tag{4.6d}$$

We decompose any unitary transformation acting independently on the first and second pseudospin, respectively, and write such a transformation using vectors $\boldsymbol{\alpha}$ and $\boldsymbol{\beta}$ in the Lie-parameter space as

$$\widehat{U}(\boldsymbol{\alpha}, \boldsymbol{\beta}) = \mathrm{e}^{-\mathrm{i}\boldsymbol{\alpha}\cdot\widehat{\boldsymbol{S}}} \mathrm{e}^{-\mathrm{i}\boldsymbol{\beta}\cdot\widehat{\boldsymbol{T}}}\,. \tag{4.7}$$

In the following, we will use the transformed eigenstates $\widehat{U}(\boldsymbol{\alpha}, \boldsymbol{\beta})|\psi\rangle$, where $|\psi\rangle \in \{|\uparrow\uparrow\rangle, |\uparrow\downarrow\rangle, |\downarrow\uparrow\rangle, |\downarrow\downarrow\rangle\}$, to describe unitary transformations onto the considered four-level system via time-dependent Hamiltonians.

The chosen representation of the Lie algebra [cf. eqs.(4.3)] fulfills

$$(2\widehat{R}_i)(2\widehat{R}_j) = \mathrm{i}\epsilon_{ijk}(2\widehat{R}_k) + \delta_{ij}\,, \tag{4.8}$$

where $i,j,k \in \{1,2,3\}$ and $\widehat{\mathrm{R}}$ stands for $\widehat{\mathrm{S}}$ or $\widehat{\mathrm{T}}$, respectively. This property allows to simplify each of the two individual exponentials in eq. (4.7) as

$$e^{-\mathrm{i}\gamma\cdot\boldsymbol{R}} = \cos\frac{|\gamma|}{2} - 2\mathrm{i}\frac{\gamma\cdot\boldsymbol{R}}{|\gamma|}\sin\frac{|\gamma|}{2}\,, \tag{4.9}$$

where $\boldsymbol{R}$ is either $\widehat{\boldsymbol{S}}$ or $\widehat{\boldsymbol{T}}$. Recalling the pseudospin-$^1/_2$–properties, the action of the exponential including $\boldsymbol{\alpha}\cdot\widehat{\boldsymbol{S}}$ onto the first pseudospin is

$$e^{-\mathrm{i}\boldsymbol{\alpha}\cdot\widehat{\boldsymbol{S}}}|{\uparrow}\,\nu\rangle = M_{++}(\boldsymbol{\alpha})|{\uparrow}\,\nu\rangle + M_{+-}(\boldsymbol{\alpha})|{\downarrow}\,\nu\rangle\,, \tag{4.10a}$$

$$e^{-\mathrm{i}\boldsymbol{\alpha}\cdot\widehat{\boldsymbol{S}}}|{\downarrow}\,\nu\rangle = -M^*_{+-}(\boldsymbol{\alpha})|{\uparrow}\,\nu\rangle + M^*_{++}(\boldsymbol{\alpha})|{\downarrow}\,\nu\rangle\,, \tag{4.10b}$$

where $\nu \in \{\uparrow,\downarrow\}$ and

$$M_{++}(\boldsymbol{\alpha}) = \cos\frac{|\boldsymbol{\alpha}|}{2} - \mathrm{i}\frac{\alpha_3}{|\boldsymbol{\alpha}|}\sin\frac{|\boldsymbol{\alpha}|}{2}\,, \tag{4.10c}$$

$$M_{+-}(\boldsymbol{\alpha}) = \frac{(-\mathrm{i}\alpha_1+\alpha_2)}{|\boldsymbol{\alpha}|}\sin\frac{|\boldsymbol{\alpha}|}{2}. \tag{4.10d}$$

The action of the exponential including $\boldsymbol{\beta}\cdot\widehat{\boldsymbol{T}}$ onto the second pseudospin ($|\nu\uparrow\rangle$ and $|\nu\downarrow\rangle$) is analogous. Since it involves some extended expressions with several different combinations of the functions M_{++} and M_{+-}, we relegate the explicit presentation of the four transformed pseudospin eigenvectors to appendix A.1.

The unitary transformation in eq. (4.7) describes an arbitrary unitary transformation on the system of two independent pseudospin-$^1/_2$–degrees of freedom. With our restrictions to the Lie algebra $\mathrm{so}(4)$, we set aside all possible unitary transformations in which the action onto one pseudospin depends on the other. We discuss some examples of operations which are non-representable in our chosen description in section 4.5.

In quantum mechanics, the system's dynamics are described via the unitary time-evolution operator $\widehat{\mathrm{U}}(t)$, and the Schrödinger equation connects $\widehat{\mathrm{U}}(t)$ with the Hamiltonian of the system. The following section concentrates on reverse engineering a time-dependent Hamiltonian $\widehat{\mathrm{H}}(t)$ given an arbitrary unitary transformation $\widehat{\mathrm{U}}(\boldsymbol{\alpha},\beta)$.

4.3 TIME-DEPENDENT HAMILTONIANS

This section will connect arbitrary unitary transformation of the system of two independent pseudospin-$^1/_2$–degrees of freedom as described in eq. (4.7) to a unitary time evolution induced by a time-dependent Hamiltonian acting onto the four-level quantum system.

To do so, we consider one-dimensional curves $\gamma(t) \mapsto (\boldsymbol{\alpha}(t),\boldsymbol{\beta}(t))$ in the six-dimensional real parameter space of the Lie algebra $\mathrm{so}(4)$. In the following, we call this space Lie-parameter space. For each curve $\gamma(t)$, we identify the corresponding unitary transformation

$\widehat{\mathrm{U}}[\boldsymbol{\alpha}(t), \boldsymbol{\beta}(t)]$ with the time-evolution operator of the four-level quantum system. The relation between the time-evolution operator and Hamiltonian is given by the Schrödinger equation

$$\mathrm{i}\hbar \frac{\mathrm{d}}{\mathrm{d}t} \widehat{\mathrm{U}}[\boldsymbol{\alpha}(t), \boldsymbol{\beta}(t)] = \widehat{\mathrm{H}}(t)\, \widehat{\mathrm{U}}[\boldsymbol{\alpha}(t), \boldsymbol{\beta}(t)] \,. \tag{4.10}$$

Since $[\widehat{\mathrm{S}}_i, \widehat{\mathrm{T}}_j] = 0$, we can decompose $\widehat{\mathrm{U}}(\boldsymbol{\alpha}, \boldsymbol{\beta})$ into two commuting exponential maps. We use the derivative of the exponential map [114, ch. 5] to find the relation between the time derivative of the curve in the Lie-parameter space and the Hamiltonian.

The following statement holds for any differentiable curve $\gamma(t)$ in any Lie (sub)algebra[3]

$$\mathrm{e}^{-\lambda(t)} \frac{\mathrm{d}}{\mathrm{d}t} \mathrm{e}^{\lambda(t)} = f\left([\lambda(t), \cdot]\right) \frac{\mathrm{d}\lambda(t)}{\mathrm{d}t} \tag{4.11}$$

with

$$f(z) = \frac{1 - \mathrm{e}^{-z}}{z} = 1 - \sum_{n=2}^{\infty} \frac{-1^n z^{n-1}}{n!} \,. \tag{4.11a}$$

For our purpose, the curves are $-\mathrm{i}\boldsymbol{\alpha}(t) \cdot \widehat{\boldsymbol{S}}$ and $-\mathrm{i}\boldsymbol{\beta}(t) \cdot \widehat{\boldsymbol{T}}$, respectively, and we will use the time derivative of the exponential map to manipulate the left-hand side of the Schrödinger equation (4.10).

Here and in the following, we often have to use iterated commutators of the form

$$\left[-\mathrm{i}\boldsymbol{\alpha}(t) \cdot \widehat{\boldsymbol{S}}, \boldsymbol{\gamma}(t) \cdot \widehat{\boldsymbol{S}}\right]_n = \underbrace{\Big[-\mathrm{i}\boldsymbol{\alpha}(t) \cdot \widehat{\boldsymbol{S}}, \big[\ldots, [-\mathrm{i}\boldsymbol{\alpha}(t) \cdot \widehat{\boldsymbol{S}}, \boldsymbol{\gamma} \cdot \widehat{\boldsymbol{S}}] \ldots \big] \Big]}_{n-\text{times}} \,. \tag{4.12}$$

Due to the property (4.8), we can split up infinitive sums of such iterated commutators into series of even and odd iteration steps. Such split-ups result in simplified expressions including sin- and cos-functions of the absolute values $|\boldsymbol{\alpha}(t)|$ and $|\boldsymbol{\beta}(t)|$ of the two vectors forming the curve $\gamma(t)$. A detailed discussion of the specific iterated commutator and the split-up into even and odd terms is presented in appendix A.2.

Using eq. (4.11), we find for a curve in our chosen Lie-algebra representation

$$\mathrm{e}^{\mathrm{i}\boldsymbol{\alpha}(t)\cdot\widehat{\boldsymbol{S}}} \mathrm{e}^{\mathrm{i}\boldsymbol{\beta}(t)\cdot\widehat{\boldsymbol{T}}} \frac{\mathrm{d}}{\mathrm{d}t} \mathrm{e}^{-\mathrm{i}\boldsymbol{\beta}(t)\cdot\widehat{\boldsymbol{T}}} \mathrm{e}^{-\mathrm{i}\boldsymbol{\alpha}(t)\cdot\widehat{\boldsymbol{S}}} = \tilde{\boldsymbol{\omega}}\left[\boldsymbol{\alpha}(t)\right] \cdot \widehat{\boldsymbol{S}} + \tilde{\boldsymbol{\omega}}\left[\boldsymbol{\beta}(t)\right] \cdot \widehat{\boldsymbol{T}} \tag{4.13}$$

with

$$\begin{aligned} \tilde{\boldsymbol{\omega}}\left[\boldsymbol{\gamma}(t)\right] = & -\mathrm{i}\dot{\boldsymbol{\gamma}}(t) - \frac{1 - \cos(|\boldsymbol{\gamma}(t)|)}{|\boldsymbol{\gamma}(t)|^2} \boldsymbol{\gamma}(t) \times \dot{\boldsymbol{\gamma}}(t) \\ & + \frac{|\boldsymbol{\gamma}(t)| - \sin(|\boldsymbol{\gamma}(t)|)}{|\boldsymbol{\gamma}(t)|^3} \boldsymbol{\gamma}(t) \times \left(\boldsymbol{\gamma}(t) \times \dot{\boldsymbol{\gamma}}(t)\right) , \end{aligned} \tag{4.13a}$$

3 For a proof, see, e.g., [114, Theorem 5.4] or [113, Lemma 25.9].

where $\dot{\gamma}(t)$ stands for the time derivative of the vector $\gamma(t)$. Here, we have used the evaluation of the iterated commutator in eq. (4.12) as mentioned above. We transform this result as[4]

$$e^{-i\gamma\cdot R}\tilde{\omega}[\gamma(t)]\cdot R e^{i\gamma\cdot R} = \sum_{n=0}^{\infty}\frac{[-i\gamma\cdot R,\tilde{\omega}[\gamma(t)]\cdot R]_n}{n!}, \tag{4.14}$$

to find the relation between the curve in the Lie-parameter space and the Hamiltonian to be

$$\widehat{H}(t)/\hbar = \omega[\alpha(t)]\cdot\widehat{S} + \omega[\beta(t)]\cdot\widehat{T}, \tag{4.15}$$

where

$$\begin{aligned}\omega[\alpha(t)] = {}& \frac{\sin|\alpha(t)|}{|\alpha(t)|}\dot{\alpha}(t) + \frac{1-\cos|\alpha(t)|}{|\alpha(t)|^2}[\alpha(t)\times\dot{\alpha}(t)] \\ & + \frac{|\alpha(t)|-\sin|\alpha(t)|}{|\alpha(t)|^3}[\alpha(t)\cdot\dot{\alpha}(t)]\alpha(t).\end{aligned} \tag{4.15a}$$

$\omega[\beta(t)]$ is analogously defined. We call $\omega[\alpha(t)]$ and $\omega[\beta(t)]$ vectorial Rabi frequencies. To evaluate the relation (4.14), we again used the iterated commutator (4.12).

Each time-dependent and continuous curve $\gamma(t) = (\alpha(t),\beta(t))$ induces a time-dependent Hamiltonian $\widehat{H}(t)$. The reversed conclusion is not valid. There are Hamiltonians $\widehat{H}$ of the four-level quantum system for which

$$\widehat{H}(t) \neq \sum_{i=1}^{3}\mathrm{Tr}\left(\widehat{H}\widehat{S}_i\right)\widehat{S}_i + \mathrm{Tr}\left(\widehat{H}\widehat{T}_i\right)\widehat{T}_i. \tag{4.16}$$

Hence, the trace with all generators $\widehat{S}_i$ and $\widehat{T}_i$ vanishes, at least for some part of $\widehat{H}$. Such a Hamiltonian cannot be represented by a real linear combination of our representation $\widehat{S}$ and $\widehat{T}$, which is a consequence of the restriction to a $su(4)$-subalgebra. By only using the generators of $so(4)$, we cannot describe an arbitrary transformation onto the four-level quantum system. We give some examples of such non-representable transformations in section 4.5.

However, the Hamiltonian in eq. (4.15) implements a quantum state conversion in the considered four-level system. It connects the initial state

$$\widehat{U}[\alpha(0),\beta(0)]|\psi(0)\rangle = e^{i\Phi_0}|\psi(0)\rangle \tag{4.17a}$$

at $t = 0$ with the target state

$$\widehat{U}[\alpha(T),\beta(T)]|\psi(0)\rangle = e^{i\Phi_T}|\psi(t)\rangle \tag{4.17b}$$

at time $t = T$. T is the conversion time in which the target state is reached. The global phases Φ_t take into account that specific quantum

4 For a proof of the following general relation, see, e.g., [114, Proposition 3.35].

states correspond to rays in the Hilbert space rather than to specific elements of it. There are many different curves and, therefore, many different state conversions with different time-dependent Hamiltonians connecting specific initial- and target states.

In the subsequent section, we discuss some examples of quantum state conversions in the four-level quantum system, employing of the approach developed from this section.

4.4 EXAMPLES OF STATE CONVERSIONS

This section presents state conversion schemes in the four-level quantum system applying the Lie-algebraic approach depicted in the preceding section. We discuss some simple examples of state conversion using the chosen representation of the Lie algebra so(4) in eqs. (4.3). First, we show how a given Hamiltonian translates into a curve in the parameter space of the Lie algebra. We discuss the π pulse as an example for which the effect on a system is well understood. Second, we reverse engineer a Hamiltonian by describing the state conversion in terms of the Lie algebra. Whereas the first example only illustrates the formalism, the second is the primary interest for developing this approach but really becomes of interest later on when additional constraints to the Hamiltonian are considered.

4.4.1 *Known Hamiltonians*

For a given Hamiltonian, we need its representation in terms of the basis elements of the Lie algebra. Since our chosen representation is traceless and fulfills eq. (4.8), we can calculate the representation of the Hamiltonian by projecting it onto the elements of the Lie-algebra representation, i.e.,

$$\omega_i[\alpha(t)] = \mathrm{Tr}\left(\widehat{\mathrm{H}}(t)\widehat{\mathrm{S}}_i\right) \tag{4.18}$$

and analogous for $\boldsymbol{\beta}(t)$ and $\widehat{\mathrm{T}}_i$. We must be cautious that the Hamiltonian in question lies in the linear span of our generating elements. Otherwise, eq. (4.15) does not hold true. Substituting these time-dependent vectorial Rabi frequencies as input into (4.15) gives a system of differential equations describing $\boldsymbol{\alpha}(t)$ and $\boldsymbol{\beta}(t)$. This system can be (numerically) solved assuming appropriate initial conditions.

For example, we consider the simplest state transfer known in quantum optics or even quantum mechanics in general. Applying a π pulse in the form of the Hamiltonian

$$\widehat{\mathrm{H}}^{\pi\text{ pulse}}_{|\psi(0)\rangle \leftrightarrow |\psi(T)\rangle} /\hbar = \frac{\pi}{2T}|\psi(T)\rangle\langle\psi(0)| + \mathrm{H.c.} \tag{4.19}$$

drives a quantum system initialized in state $|\psi(0)\rangle$ at time $t = 0$ into state $|\psi(T)\rangle$ at time T. In eq. (4.19), we have chosen an appropriate

orthogonal basis for the four-level quantum system containing both the initial and the target state. Such a basis allows for the description of this Hamiltonian by the single Rabi frequency $\Omega_\pi = \pi/(2T)$, which is constant in time. The Hamiltonian induces Rabi oscillations (cf. eq. (2.46) in section 2.3.2). Starting in the initial state, T is the first time the system occupies the target state.

To demonstrate a simple time evolution, we consider the initial state $|\psi(0)\rangle = |00\rangle = |0\rangle$ and a π-pulse cascade induced by the Hamiltonian

$$\widehat{\mathrm{H}}^{\pi\text{ cascade}}_{|00\rangle \leftrightarrow |11\rangle}(t)/\hbar = \frac{3\pi}{2T} \sum_{n=1}^{2} \chi_{\left[\frac{T(n-1)}{3}, \frac{Tn}{3}\right]}(t) |i-1\rangle\langle i| + \text{H.c.}\,, \tag{4.20}$$

where $\chi_{[a,b]}(t) = 1$ if $1 \in [a,b]$, and $\chi_{[a,b]}(t) = 0$, otherwise. We solve the resulting system of differential equations for the initial conditions $\boldsymbol{\alpha}(0) = \boldsymbol{\beta}(0) = \mathbf{0}$ numerically[5]. Figure 4.2 shows the time evolution of the Lie-parameter vectors $\boldsymbol{\alpha}(t)$ and $\boldsymbol{\beta}(t)$. Since the piecewise-defined Hamiltonian from eq. (4.20) induces the dynamics, the solutions show the same piecewise behavior in time. To visualize the time evolution of the quantum state

$$|\psi(t)\rangle = \mathrm{e}^{-\mathrm{i}\boldsymbol{\alpha}(t)\cdot\widehat{\mathbf{S}}} \mathrm{e}^{-\mathrm{i}\boldsymbol{\beta}(t)\cdot\widehat{\boldsymbol{T}}} |00\rangle\,, \tag{4.21}$$

fig. 4.3 shows the fidelities[6]

$$\mathcal{F}_{|\phi\rangle}(t) = |\langle\phi|\psi(t)\rangle|^2\,, \tag{4.22}$$

where $|\phi\rangle$ is either the initial state $|00\rangle$, one of the intermediate states $|01\rangle$ and $|10\rangle$, or the target state $|11\rangle$. If not stated otherwise, the fidelity is always considered towards the state $|\psi(t)\rangle$ of the system under consideration. As to be expected from the cascade of π pulses, the initial state $|00\rangle$ at time $t = 0$ is transformed via $|01\rangle$ at time $t = T/3$ and $|10\rangle$ at $t = 2T/3$ into the state $|11\rangle$ at $t = T$.

4.4.2 *Reverse Hamiltonian engineering*

The first examples illustrated how to represent a given Hamiltonian in our Lie-algebraic approach. To reverse-engineer a Hamiltonian inducing a specific state conversion, we have to find Lie parameters $(\boldsymbol{\alpha}, \boldsymbol{\beta})(t)$ describing the target state in terms of the transformed initial state. Anticipating the state conversion problem of section 4.7, we choose as an example the initial state $|01\rangle$ and a GHZ state as target state. Using the representation of the initial state in terms of the

5 We employed Wolfram Mathematica 12 for the numerical calculations in this chapter (cf. declarations on 141)

6 *Nielsen & Chuang* introduce the fidelity as a distance measure of quantum information as square root of our definition [19, ch. 9], which was also used in some of the author's publications [63, 64]. However, the definition used throughout this dissertation corresponds directly to occupation probabilities.

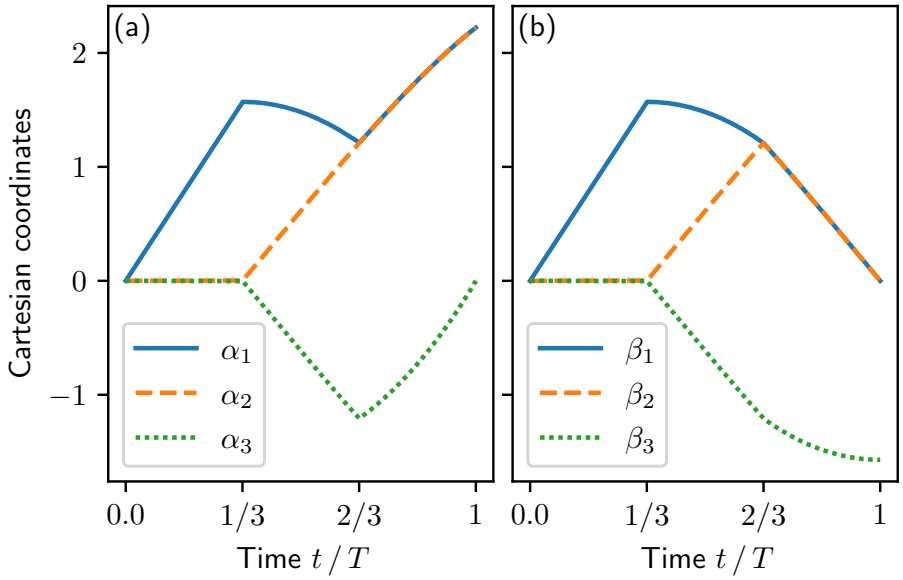

Figure 4.2: Numerical solutions for the Cartesian coordinates $\alpha_i(t)$ (a) and $\beta_i(t)$ (b) for the system of differential equations in eq. (4.15) with the π-cascade Hamiltonian in eq. (4.20) as input. The initial conditions are $\alpha_i(0) = \beta_i(0) = 0$ and T is the conversion time.

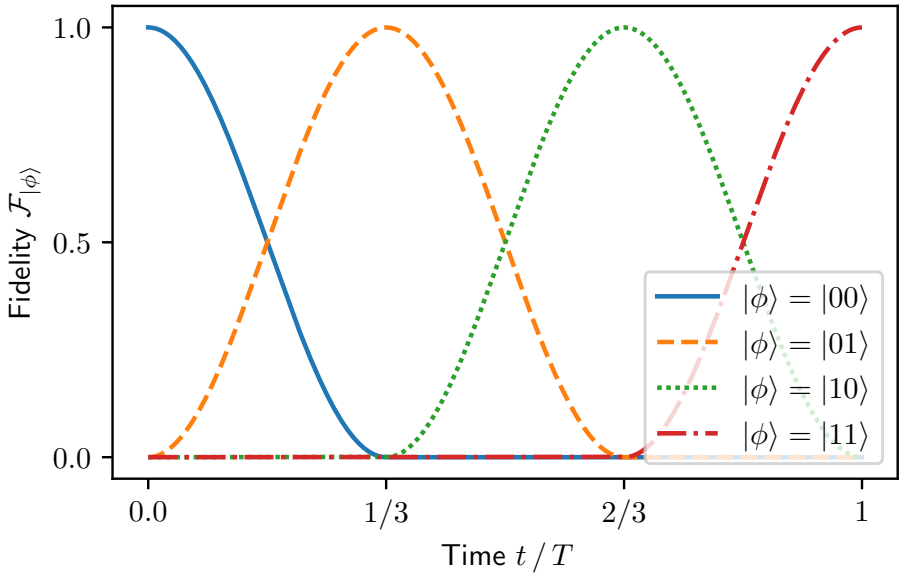

Figure 4.3: Fidelites $\mathcal{F}_{|\phi\rangle}(t) = |\langle\phi|\psi(t)\rangle|^2$ of the quantum state $|\psi(t)\rangle$ [cf. eq. (4.21)] over time for the quantum state conversion induced by the π-cascade Hamiltonian in eq. (4.20). $|\phi\rangle \in \{|00\rangle, |01\rangle, |10\rangle, |11\rangle\}$ and T is the conversion time.

pseudospin eigenbasis [cf. eqs. (4.6)] and their transformation as given in appendix A.1, we can describe the target state via

$$|\psi(T)\rangle = \frac{1}{\sqrt{2}}\left(|00\rangle - \mathrm{i}|11\rangle\right) = \mathrm{e}^{-\mathrm{i}\pi\widehat{\mathrm{S}}_3}\mathrm{e}^{-\mathrm{i}\pi\widehat{\mathrm{T}}_2/2}|01\rangle \tag{4.23}$$

(cf. appendix A.3). Note that we refer here to a GHZ state in terms of the computational basis, not in terms of the two pseudospins. The same quantum state conversion will be considered in section 4.7. With initial conditions $\boldsymbol{\alpha}(0) = \boldsymbol{\beta}(0) = \mathbf{0}$, we can describe this quantum state conversion via $\dot{\boldsymbol{\alpha}}(t) = \pi/T\boldsymbol{e}_3$ and $\dot{\boldsymbol{\beta}}(t) = \pi\boldsymbol{e}_2/2$, where $\boldsymbol{e}_i$ are Cartesian unit vectors. The vectorial Rabi frequencies eq. (4.15a) are then simplified to $\omega[\boldsymbol{\gamma}(t)] = \dot{\boldsymbol{\gamma}}(t)$, where $\boldsymbol{\gamma} = \boldsymbol{\alpha}, \boldsymbol{\beta}$, and according to eq. (4.15),

$$\widehat{\mathrm{H}}_{|01\rangle \leftrightarrow \mathrm{GHZ}}/\hbar = -\frac{\pi}{4T}\begin{pmatrix} 0 & 0 & 2\mathrm{i} & 1 \\ 0 & 0 & 1 & -2\mathrm{i} \\ -2\mathrm{i} & 1 & 0 & 0 \\ 1 & 2\mathrm{i} & 0 & 0 \end{pmatrix}. \tag{4.24}$$

The four Rabi frequencies $\Omega_{13} = -\Omega_{24} = -\pi\mathrm{i}/2T$ and $\Omega_{14} = \Omega_{23} = -\pi/4T$ describe the Hamiltonian in terms of the computational basis. We verify our reverse-engineered Hamiltonian by numerically solving the differential equation (4.15) for the vectorial Rabi frequencies as we already did for the first example. It reassures us that $|\psi(T)\rangle$ is reached at the conversion time $t = T$. Figure 4.4 shows the time evolutions for the two vectors $\boldsymbol{\alpha}(t)$ and $\boldsymbol{\beta}(t)$. They evince the linear ansatz in α_3 and β_2, as both vectors $\boldsymbol{\alpha}(t)$ and $\boldsymbol{\beta}(t)$ form straight lines connecting the initial with the target state. Figure 4.5 shows fidelities regarding the initial state $|01\rangle$ and the targeted GHZ state.

An arbitrary transformation that can be described in the chosen so(4) representation can be formulated as a straight line in terms of $(\boldsymbol{\alpha}, \boldsymbol{\beta})(t)$. The situation bedevils if additional requirements on the curves in the Lie-parameter space hinder such a simple description. We will see such a case in section 4.7, where we revise the $|01\rangle$ to GHZ state conversion under a set of Hamiltonian constraints.

4.5 NON-REPRESENTABLE TRANSFORMATIONS

When introducing the specific representation of so(4) to develop the Lie-algebraic approach to quantum state conversion, we already pointed out that not all possible unitary transformations onto the four-level quantum system can be represented in the chosen subalgebra.

Since

$$\mathrm{Tr}\left(\widehat{\mathrm{H}}^{\pi\text{ pulse}}_{|00\rangle \leftrightarrow |11\rangle}\,\widehat{\mathrm{S}}_i\right) = \mathrm{Tr}\left(\widehat{\mathrm{H}}^{\pi\text{ pulse}}_{|00\rangle \leftrightarrow |11\rangle}\,\widehat{\mathrm{T}}_i\right) = 0 \tag{4.25}$$

for all $i = 1, 2, 3$, a π pulse connecting $|00\rangle \leftrightarrow |11\rangle$ is an example of such a non-representable transformation in our chosen representation.

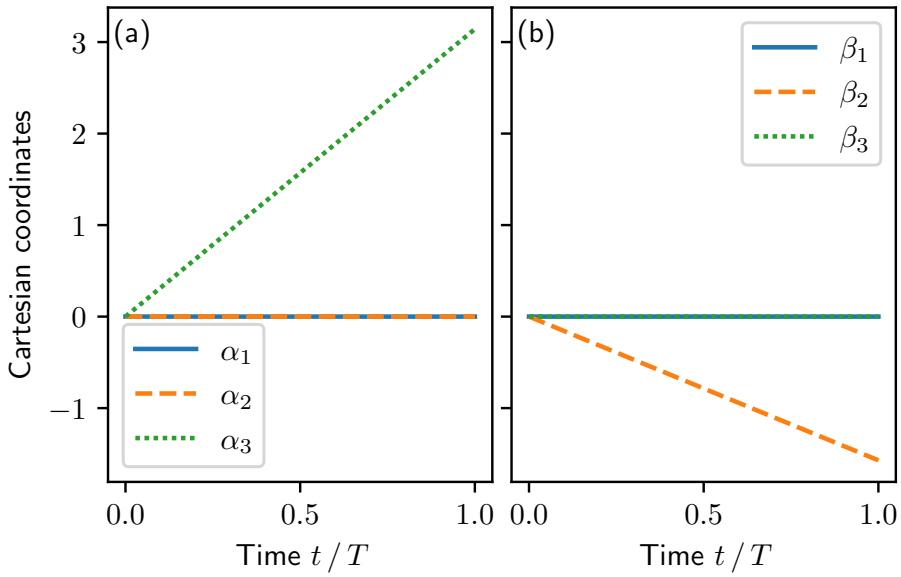

Figure 4.4: Numerical solutions for the Cartesian coordinates $\alpha_i(t)$ (a) and $\beta_i(t)$ (b) for the system of differential equations in eq. (4.15) with the reverse-engineered Hamiltonian in eq. (4.24) as input. The initial conditions are $\alpha_i(0) = \beta_i(0) = 0$ and T is the conversion time.

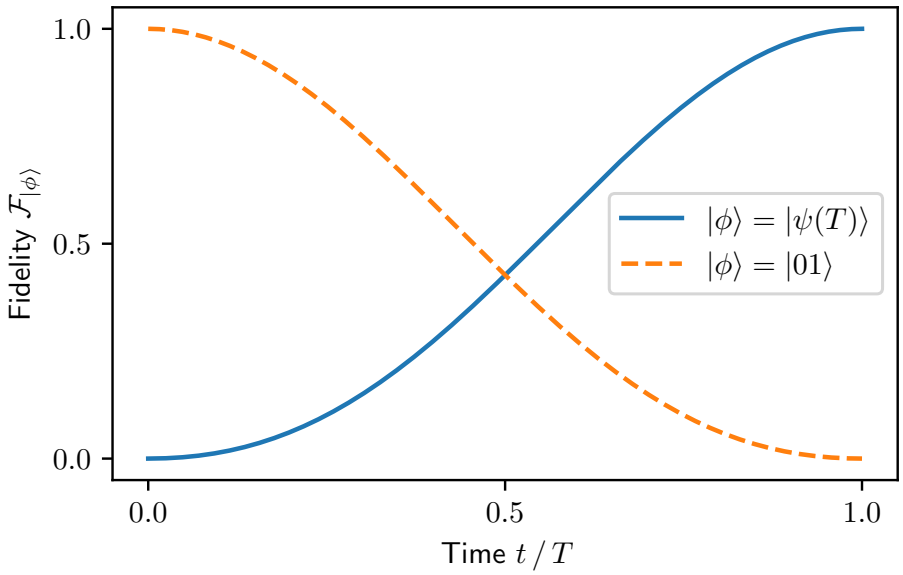

Figure 4.5: Target- and initial-state fidelites $\mathcal{F}_{|\phi\rangle}(t) = |\langle\phi|\psi(t)\rangle|^2$ of the quantum state $|\psi(t)\rangle$ [cf. eq. (4.21)] over time for the quantum state conversion induced by the reversed-engineered Hamiltonian in eq. (4.24). $|01\rangle$ is the initial state and $|\psi(T)\rangle$ the targeted GHZ state from eq. (4.23). T is the conversion time.

However, it does not matter for the underlying specific quantum state conversion problem, because a π pulse driving $|00\rangle \leftrightarrow \mathrm{i}|11\rangle$ is representable. The global phase is of no significance in this simple example, but it becomes crucial if the Hamiltonian consists, e.g., of multiple simultaneous π pulses, such that the phase of each pulse acts as a relative phase in the resulting quantum states. The constraints on the phases limit which GHZ states are reachable with a Hamiltonian similar to our example in the preceding section [cf. eq. (4.24)].

Another important class of non-representable transformations acts on both pseudospins conditionally. Since $\widehat{\mathrm{U}}(\boldsymbol{\alpha}, \boldsymbol{\beta})$ [cf. eq. (4.7)] describe only unitary transformations acting on both pseudospins independently, we cannot represent operations acting onto one pseudospin depending on the state of the other. We consider as an example the Controlled NOT operation (CNOT) in terms of the pseudospins, which is a simple example of a two-qubit gate [19, p. 21]. It interchanges the states $|\uparrow\downarrow\rangle$ and $\mathrm{e}^{\mathrm{i}\phi}|\uparrow\uparrow\rangle$, leaving the other pseudospin basis-states invariant. Hence, the π pulse

$$\widehat{\mathrm{H}}^{\pi\text{ pulse}}_{|\uparrow\downarrow\rangle \leftrightarrow \mathrm{e}^{\mathrm{i}\phi}|\uparrow\uparrow\rangle} = \frac{\pi}{2T}\,\mathrm{e}^{\mathrm{i}\phi}|\uparrow\uparrow\rangle\langle\uparrow\downarrow| + \mathrm{H.c.}\,, \tag{4.26}$$

induces the CNOT-gate over the conversion time T. No phase ϕ exists for which this Hamiltonian is representable in terms of our Lie-algebraic approach for the chosen representation.

In contrast, the CNOT-gate in terms of the computational basis is representable. It transforms $|10\rangle$ into $|11\rangle$ and vice versa while leaving $|00\rangle$ and $|01\rangle$ invariant. In fact, we already have used the corresponding π pulse as the last step in the cascade Hamiltonian in eq. (4.20).

We want to emphasize that representability obviously depends on the chosen representation. Choosing different generators $\widehat{\mathrm{S}}_i$ and $\widehat{\mathrm{T}}_i$ would allow for describing other transformations. For example, sometimes, it is enough to redefine some basis states to include a phase to allow a state of a specific phase to be reachable.

This section shows that the restriction to the Lie algebra $\mathrm{so}(4)$ limits the representable transformation. Likewise, we can apply restrictions on the Hamiltonian of the four-level quantum system. We will see in the following section that Hamiltonian constraints restrict the possible curves $(\boldsymbol{\alpha}, \boldsymbol{\beta})(t)$. Depending on the form of the constraints, it does not necessarily limits which target states are reachable from which initial states, but it complicates the reverse engineering of an appropriate Hamiltonian.

4.6 HAMILTONIAN CONSTRAINTS

As the second example in section 4.4, we discussed some examples of quantum state conversion in the system of two independent pseudospin degrees of freedom. The simple example of a reversed engi-

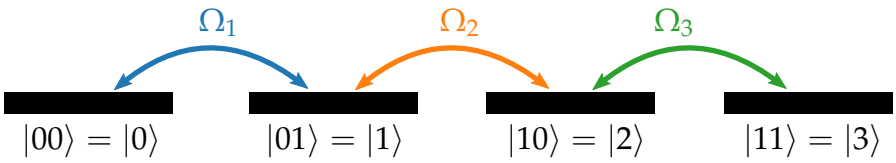

Figure 4.6: Schematic drawing of the four-level ladder Hamiltonian. All depicted levels are eigenlevels of the Hamiltonian, fulfilling the eigenvalue relation $\widehat{H}^{4\text{LS}}|i\rangle = 0|i\rangle$ for binary numbers $i = 0, 1, 2, 3$ [cf. eq. (4.27)]. The Rabi frequencies Ω_i ($i \in 1, 2, 3$) are the off-diagonal elements of the Hamiltonian driving transitions between adjacent levels.

neered Hamiltonian resulted in curves $(\boldsymbol{\alpha}, \boldsymbol{\beta})(t)$ represented by straight lines. A somewhat diminished control over the quantum system decreases the degrees of freedom of the time-dependent Hamiltonian and results in constraints on the time-dependent curves $\gamma(t)$. We concentrate on Hamiltonians which only connect adjacent quantum levels. We call such a Hamiltonian ladder Hamiltonian.

This section presents these specific constraints and their influence on the Lie-algebraic approach developed before. Further, we find a subset of curves $(\boldsymbol{\alpha}, \boldsymbol{\beta})(t)$ fulfilling the considered constraints, which will be later used to reverse-engineer a ladder Hamiltonian for specific quantum state conversions.

4.6.1 *Four-level ladder Hamiltonian*

The general Hamiltonian of the four-level quantum system contains six independent Rabi frequencies: one for each pair of levels. They are, in principle, arbitrary complex-valued functions of time. If now all levels are only connected to their respective adjacent levels in the order of the computational basis, half of the Rabi frequencies vanish. The resulting ladder Hamiltonian is represented as

$$\widehat{H}^{\text{4-ladder}}(t)/\hbar = \begin{pmatrix} 0 & \Omega_1(t) & 0 & 0 \\ \Omega_1(t) & 0 & \Omega_2(t) & 0 \\ 0 & \Omega_2(t) & 0 & \Omega_3(t) \\ 0 & 0 & \Omega_3(t) & 0 \end{pmatrix} \tag{4.27}$$

in the computational basis. By enumerating the Rabi frequencies as ladder spokes or steps 1, 2, and 3, we simplified the notation of the Rabi frequencies compared to the general four-level Hamiltonian in eq. (4.2). Additionally, the Rabi frequencies Ω_i are now real-valued functions to ensure the representability by our chosen $\mathfrak{so}(4)$-representation.

Comparing eq. (4.27) with the relationship between time-dependent Hamiltonian and the chosen Lie algebra representation in eq. (4.15), we find the following constraints

$$0 = \omega_3[\boldsymbol{\alpha}(t)]\,, \tag{4.28a}$$

$$0 = \omega_3[\boldsymbol{\beta}(t)]\,, \tag{4.28b}$$

and

$$0 = \omega_2[\boldsymbol{\alpha}(t)] - \omega_2[\boldsymbol{\beta}(t)]\,. \tag{4.28c}$$

These constraints are anholonomic boundary conditions for curves in the Lie-parameter space and ascertain the absence of Rabi frequencies connecting non-adjacent levels of the computational basis. They prohibit implementing the $|01\rangle$ to GHZ state conversion scheme as a π pulse $\widehat{\mathrm{H}}^{\pi\text{ pulse}}_{|01\rangle \leftrightarrow |\mathrm{GHZ}\rangle}$ or via a straight line in the Lie parameters as discussed in section 4.4.2. Both rely on a direct connection between the states $|01\rangle$ and $|11\rangle$, thus, featuring non-vanishing values of $\omega_3[\boldsymbol{\alpha}(t)]$ and values of $\omega_2[\boldsymbol{\beta}(t)]$ not compensated by values of $\omega_2[\boldsymbol{\alpha}(t)]$.

The relationships between Rabi frequencies connecting adjacent levels and vectorial Rabi frequencies are

$$\Omega_1(t) = \frac{\omega_1[\boldsymbol{\alpha}(t)] + \omega_1[\boldsymbol{\beta}(t)]}{2}\,, \tag{4.29a}$$

$$\Omega_2(t) = \frac{\omega_1[\boldsymbol{\alpha}(t)] - \omega_1[\boldsymbol{\beta}(t)]}{2}\,, \tag{4.29b}$$

and

$$\Omega_3(t) = \frac{\omega_2[\boldsymbol{\alpha}(t)] + \omega_2[\boldsymbol{\beta}(t)]}{2}\,. \tag{4.29c}$$

Finding adequate solutions to a desired state conversion problem is generally challenging. In the following, we constrain the possible curves $\gamma(t)$ in the Lie-parameter space even further. Under these tighter restrictions, the constrained equations have a simpler form, which allows us to find an appropriate solution.

4.6.2 *Simplified constraints*

One nonintuitive way to find solutions is to restrict the possible curves in the Lie-parameter space even further, such that the anholonomic boundary conditions are automatically fulfilled. For example, many of the examples of state conversions in section 4.4 can be considered as stretching the Lie-parameter vectors, i.e. $\boldsymbol{\alpha}(t) \parallel \dot{\boldsymbol{\alpha}}(t)$, hence $\boldsymbol{\alpha}(t) \times \dot{\boldsymbol{\alpha}}(t) = 0$ (analogous for $\boldsymbol{\beta}(t)$ and its derivative). As a result, the relations of the vectorial Rabi frequencies $\boldsymbol{\omega}[\alpha(t)]$ and $\boldsymbol{\omega}[\beta(t)]$ are significantly simplified, but such straight lines still have to fulfill the anholonomic boundary conditions. Unfortunately, the $|01\rangle$ to GHZ state conversion from section 4.4 does not fulfill the anholonomic boundary conditions. As discussed before, it induces additional Rabi frequencies not present in the ladder Hamiltonian $\widehat{\mathrm{H}}^{\text{4-ladder}}$. In the

following, we introduce another restriction to the Lie-parameter curves that simplifies the anholonomic boundary conditions and allows us to find a solution for the $|01\rangle$ to GHZ state conversion.

We restrict ourselves to curves in the Lie-parameter space with constant absolute values π for the two parameter vectors, i.e., $|\boldsymbol{\alpha}(t)| = |\boldsymbol{\beta}(t)| = \pi$. This restriction is in no way necessary and seems at first somewhat arbitrary, but it simplifies the anholonomic boundary conditions in eqs. (4.28) enough to construct a set of simple solutions for a general state conversion problem. We will see in the end that some fast conversion schemes are still possible.

With the absolute value of the two vectors fixed, it is utile to express the remaining degrees of freedom in spherical coordinates, such that the Lie parameters are described by

$$\alpha_1(t) = \pi \sin\theta_\alpha(t) \cos\phi_\alpha(t)\,, \tag{4.30a}$$
$$\alpha_2(t) = \pi \sin\theta_\alpha(t) \sin\phi_\alpha(t)\,, \tag{4.30b}$$

and

$$\alpha_3(t) = \pi \cos\theta_\alpha(t)\,, \tag{4.30c}$$

where $0 \leq \theta_\alpha \leq \pi$ and $0 \leq \phi_\alpha < 2\pi$ and a set of analogous definitions for the components of $\boldsymbol{\beta}(t)$ with $\theta_\beta(t)$ and $\phi_\beta(t)$, respectively.

Since $\sin(\pi) = 0$, $\cos(\pi) = -1$, and $(\boldsymbol{\alpha} \cdot \dot{\boldsymbol{\alpha}})(t) = 0$ for vectors of constant absolute value $|\boldsymbol{\alpha}(t)|$, only the term including the cross product in the expression for the vectorial Rabi frequency in eq. (4.15a) does not vanish. Consequently, the anholonomic boundary conditions (4.28) in terms of the just-introduced spherical coordinates simplify to

$$0 = \dot{\phi}_\alpha(t) \sin^2\theta_\alpha(t)\,, \tag{4.31a}$$
$$0 = \dot{\phi}_\beta(t) \sin^2\theta_\beta(t)\,, \tag{4.31b}$$

and

$$0 = \dot{\theta}_\alpha(t) \cos\phi_\alpha(t) - \dot{\theta}_\beta(t) \cos\phi_\beta(t)\,. \tag{4.31c}$$

The first two are easy to fulfill by choosing constant azimuthal angles ϕ_α and ϕ_β, i.e., $\dot{\phi}_\alpha(t) = \dot{\phi}_\beta(t) = 0$. The constant azimuthal angles allow us to integrate the third condition. Hence,

$$\theta_\beta(t) = \theta_\beta(0) + \frac{\cos\phi_\alpha}{\cos\phi_\beta} \int_0^t \mathrm{d}t'\, \dot{\theta}_\alpha(t')\,. \tag{4.32}$$

Any integrable function $\dot{\theta}_\alpha(t)$ and two fixed azimuthal angles ϕ_α and ϕ_β induce a time-dependent ladder Hamiltonian as in eq. (4.27), whereby the Rabi frequencies [cf. eqs. (4.29)] in terms of the spherical coordinates are

$$\Omega_1(t) = -\dot{\theta}_\alpha(t) \left(\sin\phi_\alpha + \cos\phi_\alpha \tan\phi_\beta\right)\,, \tag{4.33a}$$
$$\Omega_2(t) = 2\dot{\theta}_\alpha(t) \cos\phi_\alpha\,, \tag{4.33b}$$

and

$$\Omega_3(t) = -\dot{\theta}_\alpha(t)\left(\sin\phi_\alpha - \cos\phi_\alpha \tan\phi_\beta\right) . \tag{4.33c}$$

To describe a specific state conversion with these Rabi frequencies, we have to describe the initial- and the target state as superpositions of the rotated basis vectors from appendix A.1. The vectors must fulfill $|\boldsymbol{\alpha}(t)| = |\boldsymbol{\beta}(t)| = \pi$ for all times, and the azimuthal angles must be constant in time. Initial- and target state then must be connectable by time dependent polar angles fulfilling eq. (4.32).

In the following section 4.7, we present a $|01\rangle$ to GHZ state-conversion scheme fulfilling the simplified constraint in this section. Thus, it is realizable in a system of four adjacently connected quantum states. Further, we compare our solution to other published schemes of the same restricted conversion problem, which not necessarily fulfill the same simplified version of the constraints.

4.7 01 TO GHZ STATE CONVERSION

This section presents the possibility to implement the $|01\rangle$ to GHZ state conversion in a constrained four-level quantum system as described by the ladder Hamiltonian in eq. (4.27).

The problem can be formulated as follows. We search for a continuous curve $\gamma(t) = (\boldsymbol{\alpha}, \boldsymbol{\beta})(t)$ such that the Hamiltonian $\hat{H}^{\text{4-ladder}}(t)$ induces a time evolution over the time T connecting

$$|\psi(t=0)\rangle = |01\rangle = \frac{\mathrm{i}}{\sqrt{2}}\left(|{\downarrow\uparrow}\rangle + |{\downarrow\uparrow}\rangle\right) \tag{4.34a}$$

and

$$\begin{aligned} |\psi(t=T)\rangle &= \frac{1}{\sqrt{2}}\left(|00\rangle + \mathrm{e}^{\mathrm{i}\phi}|11\rangle\right) \\ &= \frac{1}{2}\left(\mathrm{i}|{\uparrow\uparrow}\rangle + \mathrm{i}|{\downarrow\downarrow}\rangle - \mathrm{e}^{\mathrm{i}\phi}|{\uparrow\downarrow}\rangle + \mathrm{e}^{\mathrm{i}\phi}|{\downarrow\uparrow}\rangle\right) , \end{aligned} \tag{4.34b}$$

where $\phi \in [0, 2\pi)$. $|\psi(T)\rangle$ describes the family of two-qubit GHZ states with the relative phase ϕ as a free parameter. Again, we consider a GHZ state in terms of the computational basis and not the pseudospins.

Whereas we use here the simplified curves of constant absolute value $|\boldsymbol{\alpha}(t)| = |\boldsymbol{\beta}(t)| = \pi$ as induced by Rabi frequencies of the form of eqs. (4.33) there are other solutions to the same problem. For example, *Kang et al.* [118] employed a dynamical symmetry-based approach similar to the one introduced in this work but with a different Lie-algebra representation. An alternative approach based on Lewis-Riesenfeld invariants [110] was employed by *Zheng et al.* [109]. We compare our solution to these alternatives at the end of this section (cf. section 4.7.4).

To find an appropriate curve in the Lie-parameter space connecting the initial state $|01\rangle$ with the GHZ state, we have to express the latter via an expansion of the transformed version of the former one. Since we

want to use the simplified constraints from section 4.6.2, the curve has to fulfill the anholonomic boundary conditions from equations (4.31) and $|\boldsymbol{\alpha}(t)| = |\boldsymbol{\beta}(t)| = \pi$ for all times t.

We split up the task into three steps: First, we describe appropriate initial values in the Lie-parameter spaces. Second, we find possible transformations of the initial state describing the target state. Third, we search for a curve $\gamma(t)$ connecting both states and fulfilling all imposed constraints.

4.7.1 *Initial state*

The first step is to describe the initial state. The easiest way to represent the initial state in terms of the rotated pseudospin basis is to start at the origin and represent it in terms of the unrotated pseudospin eigenbasis. Hence,

$$\boldsymbol{\alpha}(0) = \boldsymbol{\beta}(0) = \mathbf{0}\,. \tag{4.35}$$

We parameterized the initial states in all examples in section 4.4 in such a way. Unfortunately, such initial conditions do not fulfill the simplified constraints $|\boldsymbol{\alpha}(t)| = |\boldsymbol{\beta}(t)| = \pi$.

However, we can use the fact that $|01\rangle$ lies in the kernel of the operator $\widehat{S}_3 + \widehat{T}_3$. Therefore, a time evolution generated by this operator does not affect our initial state, and $|01\rangle$ especially fulfills

$$\mathrm{e}^{\mp \mathrm{i}\pi\widehat{S}_3}\mathrm{e}^{\mp \mathrm{i}\pi\widehat{T}_3}|01\rangle = |01\rangle\,. \tag{4.36}$$

Thus, we can set as initial Lie-parameter vectors

$$\boldsymbol{\alpha}(0) = \boldsymbol{\beta}(0) = \begin{pmatrix} 0 & 0 & \pm\pi \end{pmatrix}^T\,. \tag{4.37}$$

These vectors are obviously of absolute value π as required.

The next step is to find all possible solutions $(\boldsymbol{\alpha}(T), \boldsymbol{\beta}(T))$ describing the targeted GHZ state.

4.7.2 *Target state*

In the second step, we describe the target state as a general transformation of the initial state. Hence,

$$|\psi(T)\rangle = \frac{\mathrm{i}}{\sqrt{2}}\mathrm{e}^{-\mathrm{i}\boldsymbol{\alpha}(T)\cdot\widehat{\boldsymbol{S}}}\mathrm{e}^{-\mathrm{i}\boldsymbol{\beta}(T)\cdot\widehat{\boldsymbol{T}}}\left(|{\downarrow\uparrow}\rangle + |{\downarrow\uparrow}\rangle\right)\,, \tag{4.38}$$

where $|\psi(T)\rangle$ is the GHZ state [cf. eq. (4.34b)]. Using the transformed pseudospin basis-states from appendix A.1, it is possible to formulate necessary conditions to transform the state $|01\rangle$ into a GHZ state. We relegate a detailed discussion of the general conditions to appendix A.3 and just state the specialized version we will use. Under the restriction

of constant absolute values $|\boldsymbol{\alpha}(T)| = |\boldsymbol{\beta}(T)| = \pi$, these conditions [cf. eqs. (A.6)] reduce to

$$\frac{\pi^2}{\sqrt{2}} = |\alpha_3(T)\beta_2(T) + \alpha_2(T)\beta_3(T)| \,, \tag{4.39a}$$

$$0 = \alpha_1(T)\beta_1(T) + \alpha_2(T)\beta_2(T) - \alpha_3(T)\beta_3(T) \,, \tag{4.39b}$$

$$0 = \alpha_1(T)\beta_3(T) + \alpha_3(T)\beta_1(T) \,, \tag{4.39c}$$

and

$$\frac{\pi^2}{\sqrt{2}} = |\alpha_2(T)\beta_1(T) - \alpha_1(T)\beta_2(T)| \,. \tag{4.39d}$$

Their general solutions can be given up to one free parameter. As functions of $\alpha_3(T)$, these solutions are

$$\boldsymbol{\alpha}(T) \longrightarrow \begin{pmatrix} q_1\alpha_3(T) \\ q_2\sqrt{\pi^2 - 2\alpha_3^2(T)} \\ \alpha_3(T) \end{pmatrix} \tag{4.40a}$$

and

$$\boldsymbol{\beta}(T) \longrightarrow \frac{1}{\sqrt{2}} \begin{pmatrix} -q_1q_2q_3\sqrt{\pi^2 - 2\alpha_3^2(T)} \\ 2q_3\alpha_3(T) \\ q_2q_3\sqrt{\pi^2 - 2\alpha_3^2(T)} \end{pmatrix} \tag{4.40b}$$

with $-\pi/\sqrt{2} \leq \alpha_3(T) \leq \pi/\sqrt{2}$ and $q_1, q_2, q_3 \in \{-1, +1\}$. The parameters q_i describe sign relations between different coordinates.

We used $\alpha_3(T)$ as free parameter since $\dot{\theta}_\alpha(t)$ was left as an arbitrary integrable function in eq. (4.32), and $\theta_\alpha(t)$ is completely determined by $\alpha_3(t)$. In terms of spherical coordinates, the limits on $\alpha_3(T)$ impose $\pi/4 \leq \theta_\alpha(T) \leq 3\pi/4$, and the general solutions fulfill

$$\cos\phi_\alpha(T) - q_1 \cot\theta_\alpha(T) = 0 \,, \tag{4.41a}$$

$$\cos\phi_\beta(T) + q_1 \cot\theta_\beta(T) = 0 \,, \tag{4.41b}$$

and

$$\cos^2\theta_\alpha(T) + \cos^2\theta_\beta(T) = \frac{1}{2} \,. \tag{4.41c}$$

The first two relate $\alpha_1(T)$ to $\alpha_3(T)$ and $\beta_1(T)$ to $\beta_3(T)$, respectively. The third relates $\alpha_3(t)$ to $\beta_3(t)$. The parameters q_i determine unique solutions, but we do not explicitly state the corresponding spherical coordinates of the solutions (4.40) here. They are straightforward to deduce from the inversion of the definition of spherical coordinates in eqs. (4.30) under consideration of the sign relations defined by q_1, q_2, and q_3.

Figure 4.7 visualizes on a double sphere all possible transformations which realize a GHZ state starting from $|01\rangle$ as initial state under the constraints $|\boldsymbol{\alpha}| = |\beta| = \pi$. Each sphere represents one of the vectors $\boldsymbol{\alpha}(T)$ and $\boldsymbol{\beta}(T)$, which together describe the GHZ state as represented in eq. (4.38).

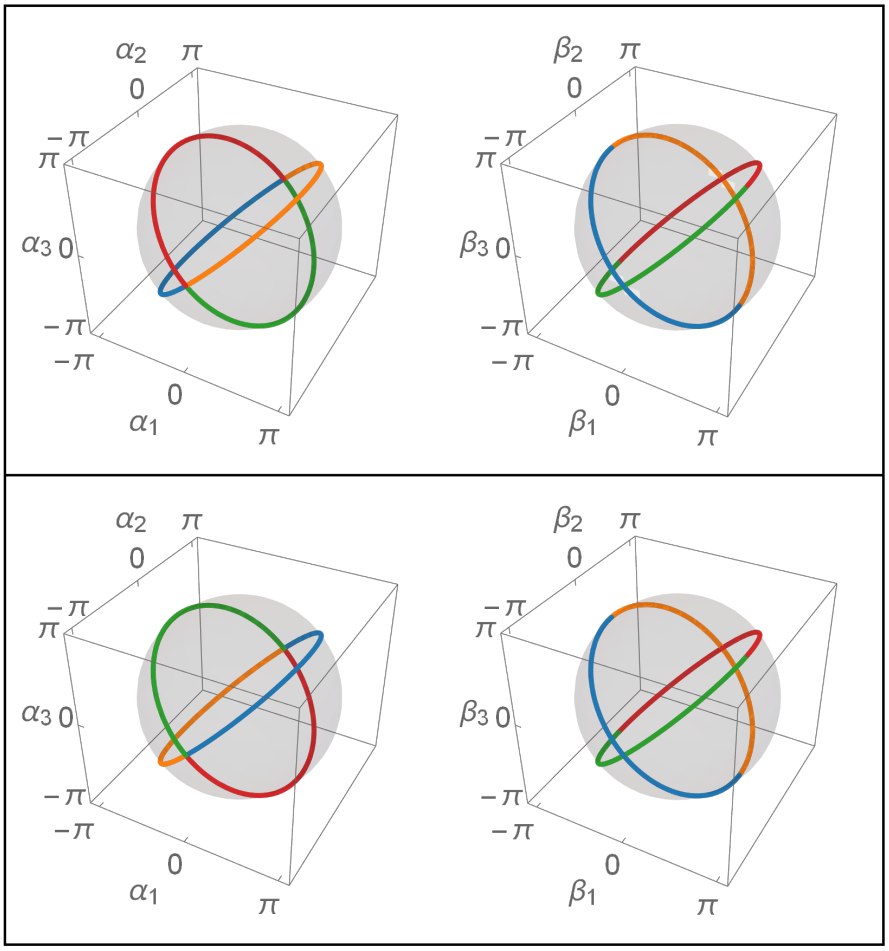

Figure 4.7: Lie-parameter vectors $\boldsymbol{\alpha}$ and $\boldsymbol{\beta}$ transforming the initial state $|10\rangle = \mathrm{i}\left(|{\downarrow\uparrow}\rangle + |{\downarrow\uparrow}\rangle\right)/\sqrt{2}$ into a GHZ state [cf. eq. (4.34b)]. In each row one color corresponds to one family of solutions $\{q_1, q_2, q_3\}$ of eqs. (4.40).
Upper row: $\{-,-,-\}$ (blue), $\{-,+,-\}$ (orange), $\{+,-,-\}$ (green), and $\{+,+,-\}$ (red)
Lower row: $\{-,-,+\}$ (blue), $\{-,+,+\}$ (orange), $\{+,-,+\}$ (green), and $\{+,+,+\}$ (red).

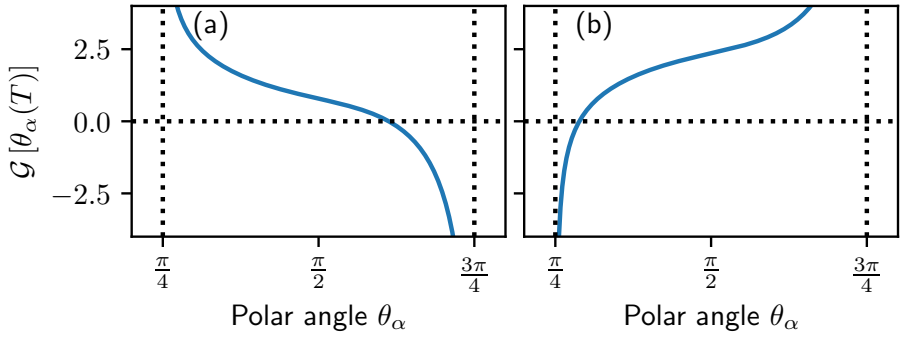

Figure 4.8: Graphs $\mathcal{G}[\theta_\alpha(T)] = \theta_\beta(T) - m[\theta_\alpha(T)]\theta_\alpha(T)$ [cf. eq. (4.42)] for the families of GHZ state solutions in eqs. (4.41) ($\pi/4 \leq \theta_\alpha \leq 3\pi/4$). Four sets $\{q_1, q_2, q_3\}$ share one graph.
(a) $\{-,-,-\}$, $\{-,+,+\}$, $\{+,-,-\}$, and $\{+,+,+\}$
(b) $\{-,-,+\}$, $\{-,+,-\}$, $\{+,-,+\}$, and $\{+,+,-\}$.

4.7.3 *Curves in the Lie algebra*

In the last step, we have to find time-dependent curves in the Lie-parameter space connecting the initial state described in the first step with a GHZ state described in the second step while additionally fulfilling the simplified anholonomic boundary conditions from eqs. (4.31). These conditions state that the azimuthal angles ϕ_α and ϕ_β are constant in time and that the polar angles are related via the integral in eq. (4.32).

Since we set the initial Lie-parameter vectors at the poles of a sphere, e.g., $\theta_\alpha(0) = \theta_\beta(0) = 0$, we can select arbitrary constant ϕ_α and ϕ_β and concentrate on solving the integral equation (4.32) to match the conditions (4.41c) describing the target state. Due to our initial conditions, both polar angles $\theta_\alpha, \theta_\beta$ vanish at $t = 0$, and in terms of the spherical coordinates, we get the linear relation

$$\theta_\beta[\theta_\alpha(T)] = m[\theta_\alpha(T)]\theta_\alpha(T)\,, \tag{4.42}$$

where the incline

$$m[\theta_\alpha(T)] = \frac{\cos\phi_\alpha[\theta_\alpha(T)]}{\cos\phi_\beta[\theta_\alpha(T)]} \tag{4.42a}$$

is defined by the azimuthal angles. The equation is not as simple as implied by the notation.

The graphs of eq. (4.42) (see fig. 4.8; four sets $\{q_1, q_2, q_3\}$ coincide per graph) show exactly one real root for each of our families of GHZ-state solutions [cf. eq. (4.40)].

Hence, for each combination $\{q_1, q_2, q_3\}$, there is a single set of spherical coordinates $\{\theta_\alpha, \phi_\alpha, \theta_\beta, \phi_\beta\}$ describing a GHZ state, and this set of coordinates is reachable from our initial conditions by a curve in the Lie-parameter space fulfilling the tighten constraints of section 4.6. Table 4.1 presents these solutions, whereby the root of eq. (4.42), i.e., the result for $\theta_\alpha(T)$ was calculated numerically. Substituting these

Table 4.1: Approximate spherical coordinates of the Lie-parameter vectors for each family of solutions defined by $\{q_1, q_2, q_3\}$ [cf. eqs. (4.41)] and corresponding constant Rabi frequencies [cf. eqs. (4.33)] for $\dot{\theta}_\alpha = 1/T$. T is the conversion time. The coordinates describe GHZ states as in eq. (4.44) that are reachable by curves $(\boldsymbol{\alpha}, \boldsymbol{\beta})(t)$ fulfilling the anholonomic boundary conditions of eqs. (4.31).

q_1	q_2	q_3	$\theta_\alpha(T)$	$\theta_\beta(T)$	$\phi_\alpha(T)$	$\phi_\beta(T)$	$\Omega_1 T$	$\Omega_2 T$	$\Omega_3 T$
$-$	$-$	$-$	1.92	0.91	5.09	0.67	1.22	1.42	2.35
$-$	$-$	$+$	0.91	1.92	3.81	1.95	-1.22	-1.42	2.35
$-$	$+$	$-$	0.91	1.92	2.47	4.33	1.22	-1.42	-2.35
$-$	$+$	$+$	1.92	0.90	1.19	5.61	-1.22	1.42	-2.35
$+$	$-$	$-$	1.92	0.91	4.33	2.47	1.22	-1.42	2.35
$+$	$-$	$+$	0.91	1.92	5.61	1.19	-1.22	1.42	2.35
$+$	$+$	$-$	0.91	1.92	0.67	5.09	1.22	1.42	-2.35
$+$	$+$	$+$	1.92	0.91	1.95	3.81	-1.22	-1.42	-2.35

coordinates in eq. (4.33) delivers the Rabi frequencies inducing such a state conversion, whereas the time derivative of $\theta_\alpha(t)$ is almost arbitrary, because only its integral enters the constraint in eq. (4.32).

The easiest possibility is a linear time dependency for $\theta_\alpha(t)$, i.e.,

$$\theta_\alpha(t) = \theta_\alpha(0) + \frac{\theta_\alpha(T)}{T} t \tag{4.43}$$

resulting in constant Rabi frequencies over the conversion time. These constant Rabi frequencies (cf. table 4.1) comprise the main result of this section. When we apply the state conversion scheme in the following, we will always use one of these sets of Rabi frequencies.

Since only the target value $\theta_\alpha(T)$ is of importance, other function $\theta_\alpha(t)$ reaching the same value at $t = T$ induce the same state conversion, but with different Rabi frequencies and different curves $(\boldsymbol{\alpha}, \boldsymbol{\beta})(t)$. Hence, the dynamic during the conversion changes.

Evaluating the target state [cf. eq. (4.34b)] for each of our solutions $\{q_1, q_2, q_3\}$ shows that two orthogonal GHZ states are reachable with the presented scheme. These states are

$$|\psi(T)\rangle = \frac{1}{\sqrt{2}} \left(|00\rangle + q_1 \mathrm{i} |11\rangle \right) . \tag{4.44}$$

Which of these two is realized by the state conversion depends on the parameter q_1.

To visualize the solutions, we present the Lie-parameter curves for constant Rabi frequencies in fig. 4.10 and show target state fidelities over the conversion time in fig. 4.9.

Despite the constraints imposed by the ladder Hamiltonian in eq. (4.27) and the tightening of these constraints by restricting us to curves of constant absolute value π, we have found sets of Rabi

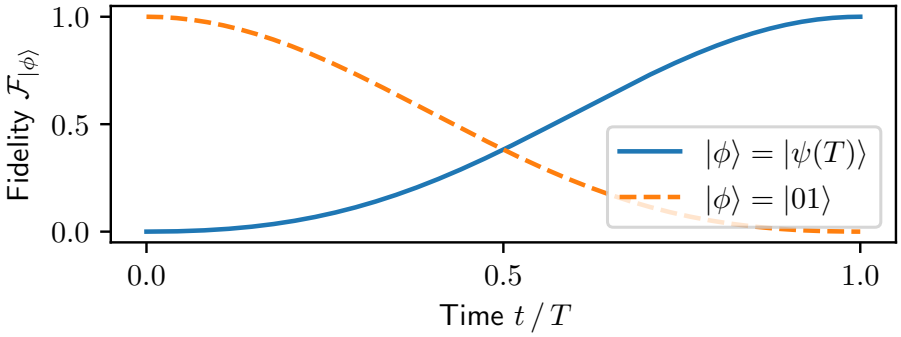

Figure 4.9: Initial state fidelity fidelity $\mathcal{F}_{|01\rangle} = |\langle 01|\psi(t)\rangle|^2$ (blue line) and target state fidelity $\mathcal{F}_{|\psi(T)\rangle} = |\langle \psi(T)|\psi(t)\rangle|^2$ (orange line) for the quantum state conversion with constant Rabi frequencies. The solution parameters q_i are not specified because the fidelities' time evolution towards the corresponding $|\psi(T)\rangle$ [cf. eq. (4.44)] is the same for all solutions.

frequencies implementing the state conversion scheme from the initial state $|01\rangle$ to a GHZ state. The resulting curves in the Lie-parameter space end up being relatively simple as they describe circular movements of constant azimuthal angle. In terms of Rabi frequencies, they are as simple as they can be by allowing a conversion with constant Rabi frequencies.

Having found these sets of Rabi frequencies, we can lift the constraints $|\boldsymbol{\alpha}(t)| = |\boldsymbol{\beta}(t)| = \pi$ and start with both vectors at the origin at the initial time $t = 0$. The Rabi frequencies induce the considered state conversion independent from its description in the Lie-parameter space. We only used the constraints in the Lie-parameter space as a tool to simplify the underlying equations to aid us in finding solutions.

In the following section, we will compare our developed conversion scheme to a direct π pulse, as shown in section 4.4, and with another conversion scheme abiding by the same constraints of the ladder Hamiltonian.

In chapter 5, we will employ the conversion scheme presented here for an abstract four-level quantum system in a quantum state conversion for a Rydberg-atom trimer. Although it is an eight-dimensional system, it can be reduced to four levels and the scheme becomes applicable. In this context, $|01\rangle$ will be interpreted as the W state of the Rydberg trimer.

Before that discussion, we will assess the efficiency of our developed scheme according to an appropriate figure of merit and compare it with other schemes as mentioned above.

4.7.4 *Comparison with other schemes*

In the last section, we found different sets of Rabi frequencies for the ladder Hamiltonian in eq. (4.27) inducing the $|01\rangle$ to GHZ state

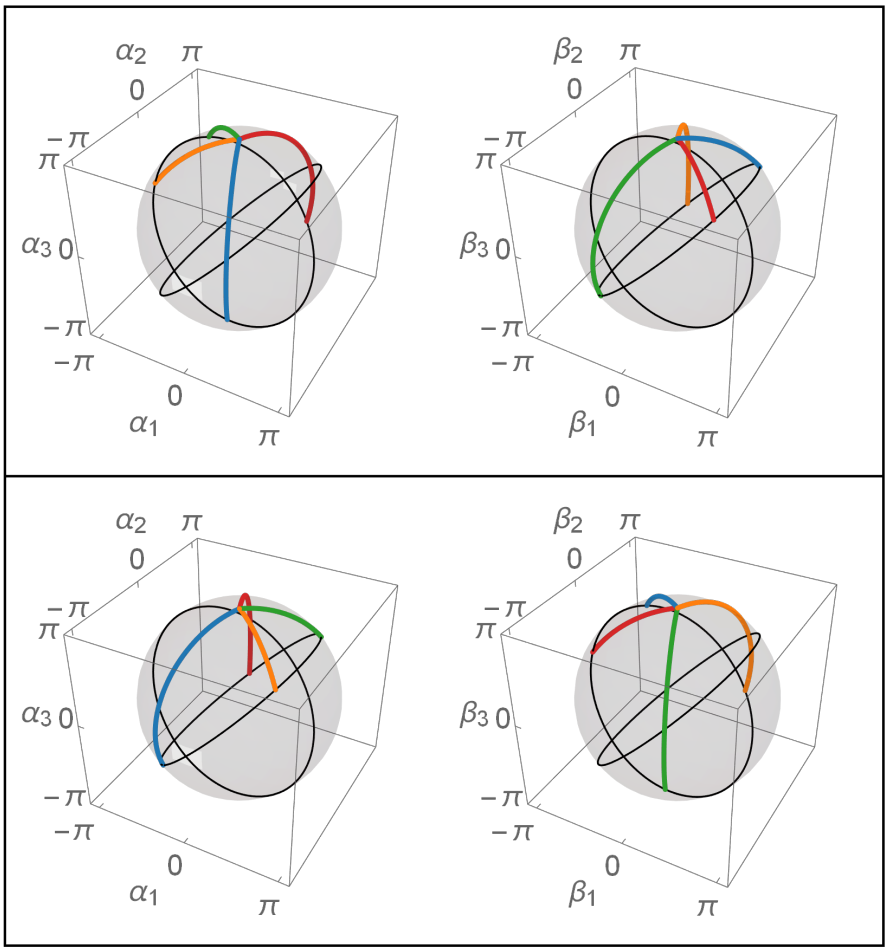

Figure 4.10: Curves from the Lie-parameter vectors $\boldsymbol{\alpha}(t)$ and $\boldsymbol{\beta}(t)$ for $t \in [0, T]$ for the $|01\rangle$ to GHZ state conversion. T is the conversion time. All solution start at $\boldsymbol{\alpha}(0) = \boldsymbol{\beta}(0) = \pi \boldsymbol{e}_3$. The black circles indicate the targeted GHZ-state solutions as in fig. 4.7. In each row one color corresponds to one solution $\{q_1, q_2, q_3\}$ of eqs. (4.41).
Upper row: $\{-,-,-\}$ (blue), $\{-,-,+\}$ (orange), $\{-,+,-\}$ (green), and $\{-,+,+\}$ (red)
Lower row: $\{+,-,-\}$ (blue), $\{+,-,+\}$ (orange), $\{+,+,-\}$ (green), and $\{+,+,+\}$ (red).

conversion. As already mentioned, there exist different proposals for the same task. For example, *Kang et al.* [118] and *Zheng et al.* [109] presented proposals in two distinct physical systems. While the first investigated spin qubits, the second considered a system of Rydberg atoms in the blockade regime. In both examples, the respective physical systems were reduced to a four-level quantum system governed by a ladder Hamiltonian, i.e., the same abstract system we are considering. To assess the quality of our solution for the specific quantum state conversion problem, we compare it to these different proposals. In section 4.4, we presented other examples of $|01\rangle$ to GHZ state conversions, but for unconstrained Hamiltonians. We also include these examples in the comparison to assess how much the restrictions to the ladder Hamiltonian affect the ability to transform the state conversion efficiently. An unrestricted π pulse as in eq. (4.19) connecting the initial- and target state will be taken as benchmark.

First, we shortly summarize the two different proposals from the literature. We refer to the respective publications [109, 118] for a more detailed discussion of these solutions. Second, we introduce a figure of merit which allows the comparison of all solutions to the $|01\rangle$ to GHZ state-conversion problem.

Kang et al. published their proposal in 2019 [118]. They realized the W to GHZ state conversion in spin qubits by reducing the full Hamiltonian first to the ladder Hamiltonian by appropriate coupling conditions and then reverse-engineer a Hamiltonian based on Lie-transforms [119]. In their reduced description, the W state corresponds to the state $|01\rangle$ of our description in this chapter. Their approach is similar to ours presented in the preceding sections. They represent the Hamiltonian via elements of a Lie algebra and relate the unitary time evolution to a curve in the corresponding parameter space. Due to the constrained Hamiltonian, they get three equations describing the Rabi frequencies in terms of the curve parameters and their time derivatives and three equations constraining some of these time derivatives. As the starting point for a Lie-algebra representation, they use the elements

$$\widehat{G}_i = |i+1\rangle\langle i| + \text{H.c.} \tag{4.45}$$

with $i = 1, 2, 3$. Each of these elements is associated with one of the Rabi frequencies $\Omega_i(t)$ of the ladder Hamiltonian. Subsequently, they complete the Lie algebra with additional three elements fulfilling the respective commutator relations.

Zheng et al. published their proposal in 2020 [109]. They used a permuted version of the same representation as *Kang et al.* [118] and constructed solutions employing invariants of the dynamical algebra [110, 111]. They also find three equations describing the Rabi frequencies and three constraints.

In the end, both alternative approaches deliver essentially the same time-depending Rabi frequencies $\Omega_i(t)$ (cf. [109, 118]). The striking

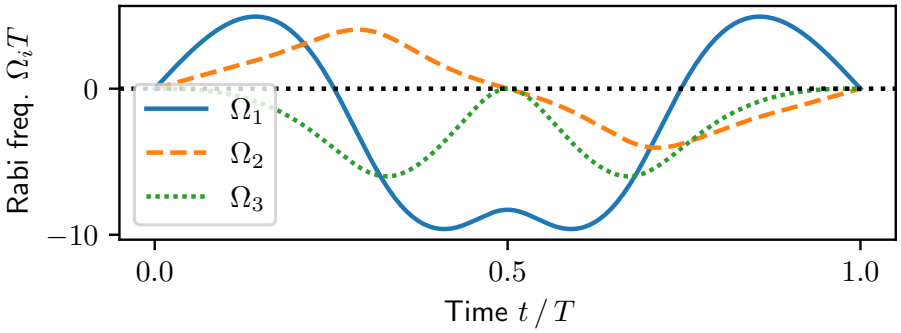

Figure 4.11: Exemplary Rabi frequencies from *Zheng et al.* [109] inducing the desired state conversion via the ladder Hamiltonian in eq. (4.27). In comparison to the Rabi frequencies as presented within [109], the signs are changed to match the relative phase of the target state in eq. (4.47).

difference compared to our approach in both cases is the different representation of the Lie algebra so(4). Their representations do not imply independent pseudospin-1/2–degrees of freedom.

In the following, we compare an exemplary set of Rabi frequencies from [109], shown in fig. 4.11, to one of our solutions of constant Rabi frequencies from the preceding section. We choose the solution described by the signs $q_1 = q_3 = -1$ and $q_2 = +1$ (cf. table 4.1), but the only difference to other solutions would be the phase of the target state and the signs of the Rabi frequencies. The corresponding set of constant Rabi frequencies from eq. (4.33) is approximately

$$\Omega_1 \approx 1.22/T\,, \tag{4.46a}$$

$$\Omega_2 \approx -1.42/T\,, \tag{4.46b}$$

and

$$\Omega_3 \approx -2.35/T\,. \tag{4.46c}$$

Both sets of Rabi frequencies Ω_i from eqs. (4.46) and shown in fig. 4.11 induce the state conversion

$$|\psi(0)\rangle = |01\rangle \longrightarrow |\psi(T)\rangle = \frac{1}{\sqrt{2}}\left(|00\rangle - \mathrm{i}|11\rangle\right)\,, \tag{4.47}$$

via the corresponding ladder Hamiltonian $\widehat{H}^{\text{4-ladder}}(t)$ from eq. (4.27). Additionally, we also compare these solutions for the ladder Hamiltonian with more unrestricted state conversion schemes from section 4.4. The first example is a simple π pulse as in eq. (4.19), and the second is the reverse-engineered Hamiltonian from eq. (4.24).

For the four different Hamiltonians, we numerically solve the system of differential equations for the vectorial Rabi frequencies [cf. eq. (4.15)] with initial conditions $\boldsymbol{\alpha}(0) = \boldsymbol{\alpha}(0) = 0$. Each of the different solutions $(\boldsymbol{\alpha}, \boldsymbol{\beta})(t)$ describes a time-dependent quantum state

$$|\psi(t)\rangle = \mathrm{e}^{-\mathrm{i}\boldsymbol{\alpha}(t)\cdot\widehat{\boldsymbol{S}}}\mathrm{e}^{-\mathrm{i}\boldsymbol{\beta}(t)\cdot\widehat{\boldsymbol{T}}}|01\rangle \tag{4.48}$$

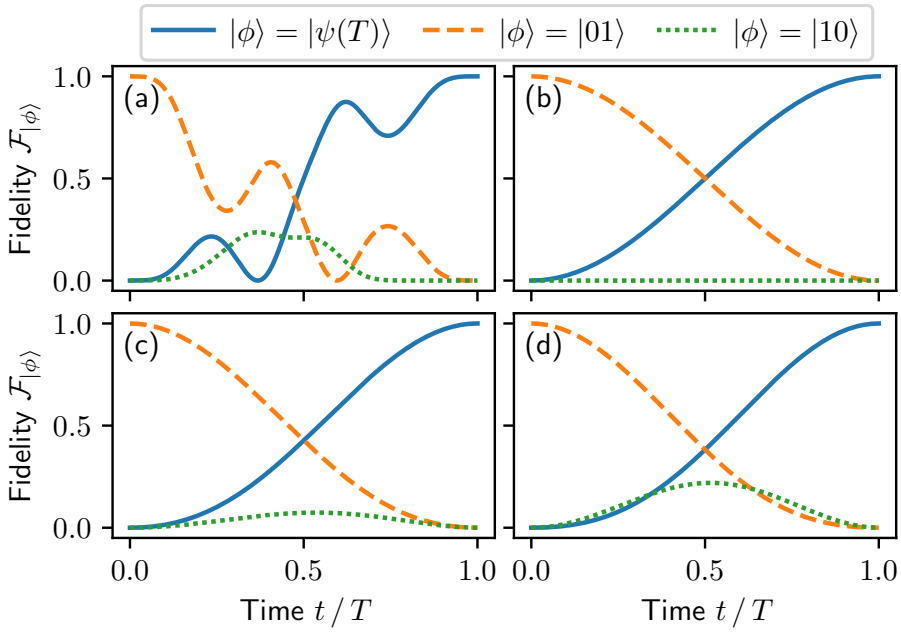

Figure 4.12: Target-, initial-, and intermediate state fidelities $\mathcal{F}_{|\phi\rangle}(t) = |\langle\phi|\psi(t)\rangle|^2$ over time for different state conversion schemes (cf. table 4.2). $|\phi\rangle \in \{|01\rangle, |10\rangle, |\psi(T)\rangle\}$ [cf. eq. (4.47)]. T is the conversion time. (a) ladder Hamiltonian with Rabi frequencies $\Omega_i(t)$ adopted from [109] (cf. 4.11) (b) π pulse [cf. eq. (4.19)] (c) reversed engineered Hamiltonian (cf. section 4.4.2) (d) ladder Hamiltonian with constant Rabi frequencies corresponding to $\{q_1, q_2, q_3\} = \{+, -, +\}$ (cf. table 4.1)

over the conversion time $t \in [0, T]$. Figure 4.12 shows initial- and target-state fidelities over time t. The additionally displayed fidelity $\mathcal{F}_{|10\rangle}(t) = |\langle 10|\psi(t)\rangle|^2$ visualizes that the four schemes differ in the amount of intermediate state occupation. With the exception of the π pulse, all quantum state conversions show a varying population of the state $|10\rangle$, which is orthogonal to both the initial- and target state. In this sense, the π pulse is the most direct state conversion. Its conversion path does not include orthogonal states. But since the ladder Hamiltonian does not allow a direct connection between $|01\rangle$ and $|11\rangle$, it is not surprising that the state $|10\rangle$ appears as an intermediate state for conversion schemes constrained by it.

To compare the different schemes quantitatively, we have to define an appropriate figure of merit. T is a free parameter in all schemes, and we can consistently achieve shorter conversion times with higher Rabi frequencies and rescaling the time t. Therefore, T cannot serve as figure of merit, but we can compare different conversion schemes via their pulse area. To do so, we introduce the total squared pulse

Table 4.2: References and relative TSPA of the four different quantum state conversion Hamiltonians. All realize the quantum state transfer defined in eq. (4.47) with the conversion time T, but differ in their Hamiltonian description and the applied Rabi frequencies. The TSPA are displayed relative to the TSPA_π of the π pulse with $A(T) = \pi^2/4T^2$.

Scheme	Hamiltonian	$\frac{\text{TSPA}}{\text{TSPA}_\pi}$	see and cf.
π pulse	$\widehat{\text{H}}^{\pi\text{ pulse}}_{\lvert 01\rangle \leftrightarrow \lvert\psi(T)\rangle}$	1	section 4.4.1; eq. (4.19)
time-dep. Rabi frequencies	$\widehat{\text{H}}^{\text{4-ladder}}$	21.03	[109, 118]; fig. 4.11
constant Rabi frequencies	$\widehat{\text{H}}^{\text{4-ladder}}$	3.67	section 4.7; eq. (4.46)
rev.-engineered	$\widehat{\text{H}}_{\lvert 01\rangle \leftrightarrow \text{GHZ}}$	2.5	section 4.4.2; eq. (4.24)

area (TSPA) $A(T)$, where T is the conversion time when the target state is reached. The squared pulse area (SPA) is defined as

$$A(t) = \int_0^t \sum_{i<j=0}^{3} |\langle i|\, \widehat{\text{H}}^{\text{4LS}}(t')|j\rangle|^2 \text{d}t' \,. \tag{4.49}$$

The number of non-vanishing matrix elements depends on the considered scheme. For the ladder Hamiltonian, they correspond to the three Rabi frequencies $\Omega_i(t)$. The squared absolute value of the Rabi frequency is strongly related to the energy consumption of the state conversion for many physical systems. For example, if the Rabi frequencies are induced by laser fields driving transitions between atomic energy levels, $|\Omega(t)|^2$ is proportional to the laser intensity, and the laser intensity is related to the energy consumption of the laser. A given conversion scheme is efficient if its TSPA is small. The π pulse sets a lower limit with $A(T) = \pi^2/4T^2$ and is, as the most efficient one in our comparison, taken as benchmark. Table 4.2 summarizes the four different conversion schemes. It also shows their corresponding TSPA.

Although it has a higher TSPA than the unconstrained Hamiltonians, our solution is over five times as efficient as the time-dependent one.

Accordingly, if we normalize all conversion schemes such that they have the same energy consumption, the constant Rabi frequencies of our scheme realize the state conversion in a significantly shorter time than the time-dependent Rabi frequencies. Figure 4.13 shows the target state fidelities for the compared conversion schemes, all normalized to the TSPA of the π pulse.

In such a normalized scenario, our solution is faster than the solution from [109, 118]. Its TSPA is more comparable with the unrestricted π pulse. Hence, we have found simple sets of Rabi frequencies for the

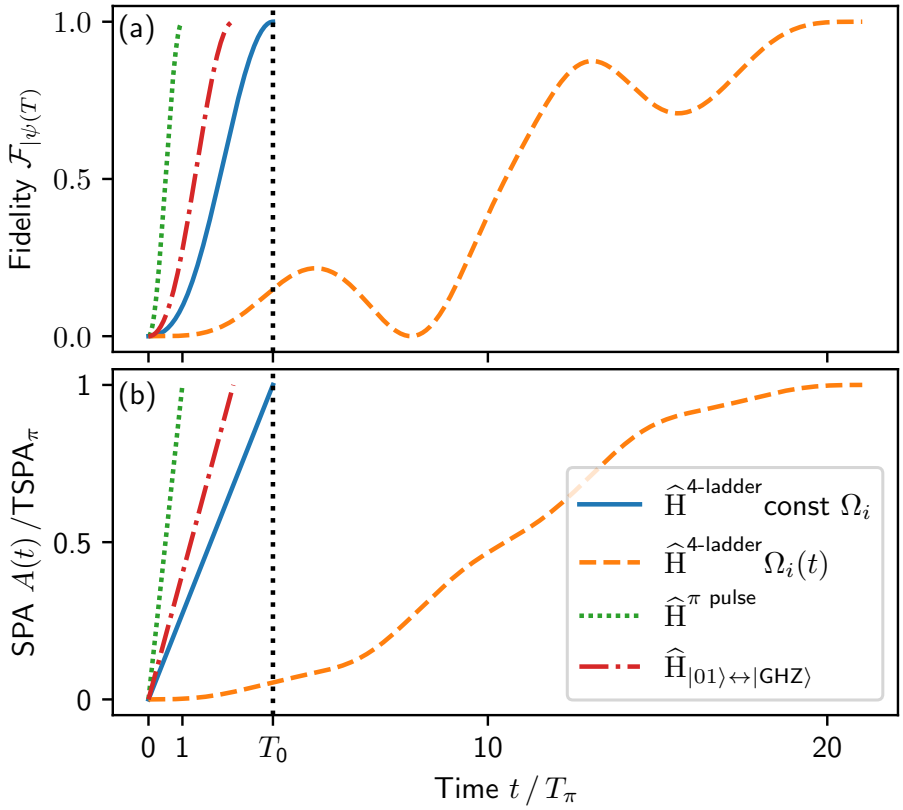

Figure 4.13: Target state fidelities $\mathcal{F}_{|\psi(T)\rangle} = |\langle\psi(T)|\psi(t)\rangle|^2$ (a) and squared pulse area $A(t)$ (b) for the adjusted conversion schemes table 4.2. All Rabi frequencies were rescaled such that the TSPA=TSPA$_\pi$, where TSPA$_\pi = \pi^2/(4T_\pi^2)$. T_π is the conversion time corresponding to the π pulse.

ladder-Hamiltonian, which are constant in time, and induce the $|01\rangle$ to GHZ state conversion almost as efficiently as an unrestricted π pulse.

4.8 CONCLUSION AND SUMMARY

4.8.1 *Conclusion*

In this chapter, we discussed quantum state conversion in the two-qubit system. We developed a simplified Lie-algebraic approach that relies on the restriction to a subalgebra of the full dynamical symmetry of the system. Although this leads to non-representable transformations, it significantly simplifies the description of specific quantum state conversion schemes. Choosing a slightly different representation of the so(4)-Lie algebra would allow to include different phases in the transformations. We did not completely characterize the underlying state space's geometry and its connectivity offered by our approach, but we gave some examples of non-representable transformations. Such a complete characterization could be a question for ongoing re-

search. Another possible research direction is generalizations to higher dimensions. However, many properties of the Lie algebra $so(4)$ do not necessarily translate to dynamical symmetries of a system of more than two qubits.

As the presented approach to quantum state conversion is rather abstract, it can be applied to many different real physical systems. Spin systems [118] or reduced Rydberg systems [63, 109] are only some examples. As two-qubit interactions are essential for a complete set of computational gates in quantum computing [108], the presented approach offers a form of investigating such interactions in terms of quantum state conversion.

For the constrained problem, represented by the ladder Hamiltonian, we found appropriate solutions for the specific quantum state conversion from $|01\rangle$ to a GHZ state. Our solutions offer a far more efficient conversion scheme as presented before [109, 118], although it still requires over three times the conversion time of an unrestricted π pulse of same TSPA.

We did not address the question if we have found the optimal solution given the constraints of the ladder Hamiltonian. Recently, *Nauth & Stojanović* [120] addressed this issue by applying an quantum-brachistochrone approach [121]. They found that an optimal solution to the discussed conversion problem can be more efficient than our solutions (in terms of the TSPA), but their discussed Rabi frequencies feature complex time-dependencies. In contrast, although not as efficient, our conversion scheme offers additional freedom in choosing the time-dependency as our solution only has to fulfill an integral relation. This last fact even allows for the most simple time dependency, i.e., the constant Rabi frequencies we utilized in the presented examples.

The following chapter presents a model system of higher dimension and its reduction to ladder Hamiltonians. For a special case, the state conversion developed in this chapter is applicable and will be used to transform W- into GHZ states.

4.8.2 *Summary*

This chapter contains a Lie-algebraic approach to quantum state conversion in the two-qubit system employing a restricted dynamical symmetry. It discusses several examples and non-representable transformations. In addition, section 4.6 presents a constrained system in which a ladder Hamiltonian induces the time evolution. This ladder Hamiltonian only connects adjacent levels of the computational basis. Under these constraints, we found solutions for the $|01\rangle$ to GHZ state conversion by restricting the dynamics even further. Finally, a comparison of the found scheme with other proposals discussing the same quantum state conversion problem is presented.

Some of the presented content is a more detailed version of a similar discussion published by the author, *Gernot Alber*, and *Vladimir Stojanović* in *Physical Review A* [63]. In what follows, we give a short description of how content presented in this chapter relates to content in the mentioned publication. The general description of the system and the Lie-algebraic approach in sections 4.1 to 4.3 and appendix A.1 is related to sections I.-IV. in [63] but presented here in far more detail. The examples for unrestricted quantum state conversion and the discussion of non-representable transformations in sections 4.4 and 4.5 have not yet appeared in any former publication. Sections 4.6 and 4.7 and appendix A.3 are also enlarged versions of already published content. They correspond to section V. in [63]. Although a discussion comparing the found conversion scheme with the scheme by *Zheng et al.* [109] has already been presented within [63], section 4.7.4 of this dissertation additionally features a comparison with unrestricted conversion schemes and considers the π pulse as a benchmark.

5

REDUCED RYDBERG-TRIMER MODEL

This chapter discusses state preparation and interconversion in a multi-qubit system featuring pairwise interaction. The qubits are supposed to model neutral Rydberg atoms arranged by lattices of optical tweezers, i.e., optical traps formed by focused light fields. We especially emphasize the case of three qubits modeling a Rydberg trimer.

Such systems of neutral atoms are envisioned to be of high importance in QIP due to their sound scalability and controllability via laser fields [47] and are an emerging platform for quantum simulation [122–124] and computing [48, 125]. Rydberg atoms are atoms in a state of high principal quantum number n [46]. Due to this high excitation, they feature large atom radii and strong interparticle interaction [47].

Many experiments are conducted on this particular platform for QIP. For example, it is nowadays possible to ensemble defect-free arrays of more than one hundred single Rydberg atoms in such optical setups [52, 126–128]. Also, experiments based on optical tweezers continue to achieve higher precision in the individual positioning of single atoms [129, 130].

As this is a theoretical account, we do not describe any experimental setup in detail or consider a particular excitation scheme of real Rydberg-atom species.

We are interested in reducing a simple model for an array of neutral atoms to lower dimensions and finding an effective Hamiltonian that allows for implementing state conversion schemes as, e.g., developed in the preceding chapter.

We describe each Rydberg atom as a two-level quantum system (TLS), its Hamiltonian, and some basic notation in section 5.1. Section 5.2 introduces special sets of states important for the following discussion. As a special concept it introduces twisting and twisted states of the atomic ensemble. Section 5.3 discusses the interaction of the atomic ensemble with laser fields via effective Hamiltonians using the resolvent formalism (cf. chapter 3). Having these effective descriptions at hand, we present a quantum state preparation scheme for twisted W states in section 5.4 and several reduction schemes in section 5.5. The latter reduce the descriptions of a three qubit system to lower dimension and allow the dynamics to be described by ladder Hamiltonians as discussed in section 4.6. To validate the presented reduction schemes, we conducted numerical calculations implementing the $|01\rangle$ to GHZ state conversion from section 4.7 of the preceding chapter. These calculations are presented in section 5.6. In the context of a Rydberg trimer the $|01\rangle$ corresponds to the W state. Therefore,

we present an example of a W to GHZ state conversion using global system interactions.

Much of this chapter's content was already published as article in *Physical Review Research* [64]. A more detailed description of how some of the content already appeared in other publications can be found in the summary (section 5.7.2).

5.1 SYSTEM AND SYSTEM HAMILTONIAN

We consider a system of several neutral Rydberg atoms positioned in individual traps formed by tweezer arrays. For an extensive discussion of how experiments in such arrays are setup and conducted, see, e.g., [126]. We will not discuss the complete internal structure of the Rydberg atoms and only describe them as two-level quantum systems. The atomic ensemble formed by the neutral atoms interacts with several laser fields driving the individual Rydberg transitions. We do not consider the addressability of individual atoms but rather a global interaction of the atomic ensemble as a whole.

First, we give the basic theoretical description of the considered system in the form of the system Hamiltonian. Afterward, we introduce generic basis states and some notation, which we will use throughout the remaining chapter.

5.1.1 *System Hamiltonian*

The system under consideration consists of N identical neutral Rydberg atoms (enumerated with n). Each of these atoms is located at $\boldsymbol{x}_n$, a specific position in space. We assume no time dependence of the position vectors for all our following considerations and model the internal atomic structure as a TLS. Therefore, each of the N identical two-level systems consists of a ground state $|g\rangle_n$ with energy E_g and a Rydberg state $|r\rangle_n$ with energy E_r.

We assume the atomic interaction is completely described via $V(d_{pq})$ that is the dipole-dipole (Van der Waals) interaction potential between atoms enumerated p and q. It depends on the distance $d_{pq} = |\boldsymbol{x}_p - \boldsymbol{x}_q|$ between two Rydberg atoms and scales roughly as $1/d_{pq}^6$ [47]. Therefore, the energy spectrum of the atomic ensemble depends not only on the number of excited atoms but also on all pairwise distances d_{pq}.

If all atom positions are equidistantly apart, the blockade potential becomes a constant, hence $V(d_{pq}) \to V$. This is only possible for up to $N = 4$ particles. $N = 2$ trivially fulfills the equidistance condition since there is only one pair of atoms. For $N = 3$, the atoms have to form an equilateral triangle. It will be the case for which we discuss most of the following results in more detail, and Figure 5.1 shows a sketch of the considered atomic ensemble and its energy scheme.

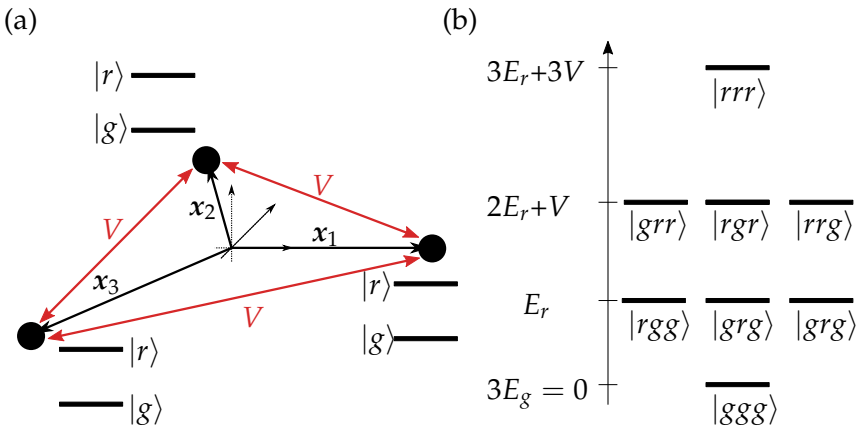

Figure 5.1: (a) Schematic drawing of a Rydberg trimer modeled by three qubits in an equilateral triangle.
(b) Energy scheme corresponding to a Rydberg trimer composed of three atoms forming an equilateral triangle. V is the dipole-dipole interaction potential.
Adopted from FIG. 1. [64], which is licensed under Attribution 4.0 International (CC BY 4.0).

For $N = 4$, the atoms must form a regular tetrahedron. Although, for $N > 4$, no geometrical object in three spacial dimensions exists that features all vertices, hence atoms, equidistantly apart, we still assume a constant blockade potential V for a general number of N atoms. This assumption allows us to give general expressions and deal with all cases of low N simultaneously. Afterward, we can specialize our results to $N = 3, 4$. Furthermore, all our following derivations are not strictly restricted to Rydberg-atom systems. In essence, we describe a theoretical qubit model with pairwise constant qubit interaction. In principle, it is possible to design other QIP systems described by the same model Hamiltonian as discussed below. All our following results would apply to such systems.

With all the mentioned assumptions, we can write down the Hamiltonian describing the atomic ensemble as

$$\widehat{\mathrm{H}}_{\mathrm{A}} = \sum_{n=1}^{N} \left(E_g |g\rangle_{nn}\langle n| + E_r |r\rangle_{nn}\langle r| \right) + \sum_{p<q}^{N} V |r\rangle_p |r\rangle_{qq} \langle r|_p \langle r| \,. \quad (5.1)$$

Here and in the following $\sum_{p<q}^{N}$ means a sum over all $\binom{N}{2}$ subsets $\{p, q\}$ of two distinct atoms. The first sum describes the internal energies of the N two-level systems, whereas the second sum describes the pairwise atomic interactions. The energy levels of the atomic ensemble are

$$E_a = N E_g + a\hbar\omega_{\mathrm{A}} E_r + \binom{N}{a} V \,, \quad (5.2)$$

where a is the number of excited atoms and $\omega_{\mathrm{A}} = (E_r - E_g)/\hbar$ is the atomic resonance- or Rydberg frequency. Further, the energy gaps

between adjacent levels with succeeding numbers of excited atoms are

$$\Delta E_a = E_a - E_{a-1} = \hbar\omega_\mathrm{A} + V(a-1)\,. \tag{5.3}$$

We assume the atomic ensemble interacts with several different plane-wave laser fields (enumerated with $j \leq J$ and starting with $j = 0$ for later convenience). All these light fields are completely determined by their respective wave vector $\boldsymbol{k}_j$, frequency ω_j, and their field state. Hence, each laser field is described by a distinct electromagnetic field mode. The free-field Hamiltonian of this ensemble of considered modes is

$$\widehat{\mathrm{H}}_\mathrm{F} = \sum_{j=0}^{J} \hbar\omega_j \hat{\mathrm{a}}_j^\dagger \hat{\mathrm{a}}_j\,. \tag{5.4}$$

We omit here the ground-state energies $\hbar\omega_j/2$ because, in the following, we assume all fields to resemble classical fields of high mean photon number, and the small amount of each ground-state energy does not contribute significantly to the total energy of each mode (cf. section 2.1).

We describe the interaction of atomic ensemble and electromagnetic field in the dipole- and RWA. To shorten our notation in the following, we introduce the coupling constants d_j which are essentially determined by the atomic dipole operators $\hat{\boldsymbol{d}}_j$ (cf. section 2.3), such that the interaction Hamiltonian can be written as

$$\widehat{\mathrm{H}}_\mathrm{int} = \sum_{n=1}^{N}\sum_{j=1}^{J} \left(|g\rangle_{nn}\langle r| d_j^* \hat{\mathrm{a}}_j^\dagger \mathrm{e}^{-\mathrm{i}\boldsymbol{k}_j\cdot\boldsymbol{x}_n} + \mathrm{H.c.} \right)\,. \tag{5.5}$$

The exponential function in each addend describes phases $\boldsymbol{k}_j \cdot \boldsymbol{x}_n$ due to the different positions of each atom relative to the wavefronts of the respective field. By introducing the unitary transformation

$$\widehat{\mathrm{U}}(\boldsymbol{k}) = \bigotimes_{n=1}^{N} \left(\mathrm{e}^{\mathrm{i}\boldsymbol{k}\cdot\boldsymbol{x}_n} |r\rangle_{nn}\langle r| + |g\rangle_{nn}\langle g| \right)\,, \tag{5.6}$$

we can rewrite the interaction Hamiltonian (5.5) into

$$\widehat{\mathrm{H}}_\mathrm{int} = \sum_{n=1}^{N}\sum_{j=1}^{J} \left(\widehat{\mathrm{U}}(\boldsymbol{k}_j)|g\rangle\langle r|\,\widehat{\mathrm{U}}^\dagger(\boldsymbol{k}_j) d_j^* \hat{\mathrm{a}}_j^\dagger + \mathrm{H.c.} \right)\,. \tag{5.7}$$

The transformations $\widehat{\mathrm{U}}(\boldsymbol{k})$ allow in the following calculations to reduce all cases of particular site-dependent phases to the case of vanishing phases, and we will use them repeatedly to simplify calculations.

The three introduced Hamiltonians form the full system Hamiltonian

$$\widehat{\mathrm{H}} = \widehat{\mathrm{H}}_\mathrm{A} + \widehat{\mathrm{H}}_\mathrm{F} + \widehat{\mathrm{H}}_\mathrm{int}\,. \tag{5.8}$$

In the given description of the system, we omit deleterious effects such as spontaneous decay from the excited atomic state to the ground state or dephasing. The first reduces the lifetime of atomic ensemble states with higher excitation numbers, whereby the latter diminishes the control and addressability of certain states by the laser fields. To some extent, we will reintroduce and discuss these effects via an open system approach in section 5.6 to investigate their impact on the applications presented later in this chapter.

5.1.2 *Notation and generic basis states*

To discuss the considered system's dynamics, we introduce a specific notation that we use throughout this chapter.

First, we define the general basis states describing the atomic ensemble. Since the atomic ensemble consists of N two-level systems, we need 2^N basis states. Instead of writing down all individual atoms, we will use a set-based notation, where $\{n_1, \ldots, n_a\}$ is a lexicographically ordered subset, i.e., $n_1 < n_2 < \ldots < n_a$, of all atom labels $\{1, \ldots, N\}$. A set $\{n_1, \ldots, n_a\}$ displays a atoms which are exited, such that

$$|\{n_1, \ldots, n_a\}\rangle = \bigotimes_{i=1}^{a} |r\rangle_{n_i} \otimes \bigotimes_{i=1}^{N-a} |g\rangle_{n'_i} \tag{5.9}$$

is the corresponding state.

$$\{n'_1, \ldots, n'_{N-a}\} = \{1, \ldots, N\} \setminus \{n_1, \ldots, n_a\} \tag{5.9a}$$

describes the complement set of all atoms in the ground state. We will refer to these states as lexicographic states.

All lexicographic states with the same number of atoms in the excited state form a subspace of the atomic-ensemble Hilbert space $\mathcal{H}_\mathrm{A}$. We write an orthogonal projection onto such a subspace as

$$\widehat{\mathrm{P}}_a = \sum_{n_1 < \ldots < n_a}^{N} |\{n_1, \ldots, n_a\}\rangle\langle\{n_1, \ldots, n_a\}| \,, \tag{5.10}$$

where the sum runs over all $\binom{N}{a}$ possible states with precisely a excited atoms. As in the definition of the atomic-ensemble Hamiltonian in eq. (5.1) with the two indices p, q describing different atoms, we use here the notation $n_1 < \ldots < n_a$ with a variables to indicate lexicographic order of all addends and the upper limit N for all of the a summation variables to ensure that none possible combination is left out. These states are a complete basis of the atomic-ensemble Hilbert space, hence

$$\sum_{a=0}^{N} \widehat{\mathrm{P}}_a = \mathbb{1}_\mathrm{A} \,. \tag{5.11}$$

As an exception, we notate the ground state and the state of highest excitation number $a = N$ more generic most of the time. Instead of using the empty set $\emptyset$ or the whole set $\{1, \ldots, N\}$, we write $|g \ldots g\rangle$ and $|r \ldots r\rangle$ indicating all atoms in the ground or excited state, respectively.

We introduce a slightly different set-based notation for the electromagnetic field. Most of the time, we use Fock states $|m_j\rangle$ (cf. section 2.2) for each mode to describe its quantum state. The number of considered modes differs from situation to situation but is always finite. A generic basis state of the field is

$$|\{m_j\}\rangle = \bigotimes_{m_j} |m_j\rangle \,, \tag{5.12}$$

where $\{m_j\}$ is a set of photon numbers, one for each mode. We use this slightly different notation for the electromagnetic field because the indices j will not always run from 0 or 1 to some finite value, but the indices indicate a specific purpose for each field. Furthermore, the notation of the field states is much shorter this way and is rarely used, such that it should not stir confusion at any point.

Combining atomic ensemble and electromagnetic field, a generic basis state of the full system of atoms and field is therefore

$$|\{n_1, \ldots, n_a\}, \{m_j, \ldots, m_{j'}\}\rangle = |\{n_1, \ldots, n_a\}\rangle \otimes |\{m_j\}\rangle \,. \tag{5.13}$$

With the lexicographic states as a generic basis, we will describe other special sets of states in the following section. We will introduce states that are especially useful regarding the global interaction of the atomic ensemble with the different electromagnetic field modes. Furthermore, we introduce the concept of twisting and twisted states.

5.2 SPECIAL STATES OF THE ATOMIC ENSEMBLE

This section discusses some special states of the atomic ensemble, which are of interest for the application discussed later in this chapter. Especially, we want to introduce the concept of twisted states. At last, we specialize the discussed states for the case $N = 3$. In this context, we discuss chiral states, which are at the center of the applications in sections 5.4 and 5.5.

5.2.1 *W, GHZ, and Dicke states*

We start with two sets of states which are essential when discussing multipartite quantum entanglement. These are W- and GHZ states representing two distinct classes of multipartite entangled states, as already mentioned in the introduction 1.1.

If we superpose all possible states of one excited atom, we recognize the W state

$$|\mathrm{W}_N(\{\phi_1, \ldots, \phi_N\})\rangle = \frac{1}{\sqrt{N}} \sum_n^N \mathrm{e}^{\mathrm{i}\phi_n} |\{n\}\rangle \tag{5.14}$$

of N atoms and phases $\{\phi_1, \ldots, \phi_N\}$. We can always take one of the phases as a reference resulting in $N-1$ relative phases, e.g., $\phi_n' = \phi_1 - \phi_n$. The W states span an N-dimensional subspace of the atomic ensemble. If all relative phases are zero, we recall the *ordinary* W state $|\mathrm{W}_N\rangle$. Furthermore, the atomic ensemble can form a N-party GHZ state, i.e.,

$$|\mathrm{GHZ}_N(\phi)\rangle = \frac{1}{\sqrt{2}}\left(|g\ldots g\rangle + \mathrm{e}^{\mathrm{i}\phi}|r\ldots r\rangle\right) . \tag{5.15}$$

Since the GHZ states form a two-dimensional subspace, one relative phase is sufficient to identify a specific state.

More than one atom can be in its excited state in the atomic ensemble. Therefore, we introduce Dicke states [131, 132][1] via

$$|\mathrm{D}_N^{(0)}\rangle = |g\ldots g\rangle \tag{5.16a}$$

and

$$|\mathrm{D}_N^{(a)}\rangle = \binom{N}{a}^{-1/2} \sum_{n_1<\ldots<n_a}^{N} |\{n_1, \ldots, n_a\}\rangle , \tag{5.16b}$$

where a again is the number of excited atoms. Dicke states generalize the ordinary W state since $|\mathrm{W}_N\rangle = |\mathrm{D}_N^{(1)}\rangle$.

Dicke states were first investigated by *R.H. Dicke* in the context of collective effects in the radiation from a molecular or atomic cloud [134] and are an essential class of entangled states. They show beneficial characteristics in many areas, such as quantum metrology [135, 136] or quantum mechanical game theory [137].

Since the interaction in our considered model is global, Dicke states and collective excitations play a crucial role in our following discussion, but to incorporate the site-dependent phases described by the unitary transformations $\widehat{\mathrm{U}}(\boldsymbol{k}_j)$, we have to relax the symmetry of the Dicke states. We can generalize Dicke states to arbitrary phases as we already did with the W states before. Hence,

$$\begin{aligned} &|\mathrm{D}_N^{(a)}(\{\phi_{1\ldots a}, \ldots, \phi_{(N-a+1)\ldots N}\})\rangle \\ &\quad = \binom{N}{a}^{-1/2} \sum_{n_1<\cdots<n_a}^{N} \mathrm{e}^{\mathrm{i}\phi_{n_1\ldots n_a}} |\{n_1, \ldots, n_a\}\rangle , \end{aligned} \tag{5.17}$$

where $\{\phi_{1\ldots a}, \ldots, \phi_{(N-a+1)\ldots N}\}$ is a set of $\binom{N}{a}$ phases, one for each (lexicographic) basis state $|\{a_1, \ldots, n_a\}\rangle$. Relative phases degrade the permutation invariance of the Dicke states. In the following, we will specialize this notation of generalized Dicke states by taking the underlying structure of the atomic ensemble into account.

1 Sometimes, the states $|\mathrm{D}_N^{(a)}\rangle$ are called symmetric Dicke states and are considered a special subclass of more general Dicke states [133] as in eq. (5.17), which are not necessarily permutation invariant.

5.2.2 *Twisted states*

At the end of the last section, we introduced generalized Dicke states defined by relative phases. These phases break the permutation invariance of Dicke states and can be, in principle, arbitrary. However, due to the structure of the considered interaction with the electromagnetic field [cf. eq. (5.5)], the laser fields introduce unique site-dependent phases described by the unitary transformations $\widehat{U}(\boldsymbol{k}_j)$ in eq. (5.6). It is reasonable to define *twisted* Dicke states of the form

$$|D_N^{(a)}(\boldsymbol{k})\rangle = \widehat{U}(\boldsymbol{k})|D_N^{(a)}\rangle = \binom{N}{a}^{-1/2} \sum_{n_1<\cdots<n_a}^{N} e^{i\boldsymbol{k}\sum_{l=1}^{a}\boldsymbol{x}_{n_l}} |\{n_1,\ldots,n_a\}\rangle \tag{5.18}$$

accounting for the field-induced phases. The term twisted means that the relative phases distort the original symmetry of the state, but the single-site phases $\boldsymbol{k}\cdot\boldsymbol{x}_n$ are well defined through the optical lattices formed by the wave vector $\boldsymbol{k}$ of the considered field.

The term twisted is chosen in analogy to states of well-defined phases in the *Kuramoto* model [138] of a sequence of interacting oscillators in non-linear physics. States of this system with well-defined phases are called twisted states [139–141]. Another analogy refers to *Bloch* states of electrons in crystal lattices, where $\boldsymbol{k}$ is the reciprocal vector of the underlying atomic structure [142].

The overlap of two twisted Dicke states defined by two different wave vectors $\boldsymbol{k}$ and $\boldsymbol{k}'$ but constant atomic positions $\boldsymbol{x}_n$ is

$$\langle D_N^{(a)}(\boldsymbol{k})|\, D_N^{(a)}(\boldsymbol{k}')\rangle = \frac{1}{\binom{N}{a}} \sum_{n_1<\ldots<n_a}^{N} e^{i(\boldsymbol{k}'-\boldsymbol{k})\sum_{i=1}^{a}\boldsymbol{x}_{n_i}}\,. \tag{5.19}$$

Both states are equal if all $\binom{N}{a}$ contributions are in phase (up to a global phase). There are several ways to achieve this. Either $\boldsymbol{k} = \boldsymbol{k}'$ mod 2π or both wave vectors are perpendicular to the position vectors of all atoms, i.e., $\boldsymbol{k}\cdot\boldsymbol{x}_n = 0$.

Twisted Dicke states will play a crucial role in representing the effective Hamiltonians in section 5.3. Their overlaps are of major importance for the applications presentend in sections 5.5.1 and 5.5.2. Since we mainly restrict these applications to three atoms, we discuss the twisted states for $N = 3$ in more detail in the following section.

5.2.3 *Chiral states*

In our applications in sections 5.4, 5.5.1 and 5.5.2, we mainly concentrate on the case $N = 3$. Therefore, we introduce another basis for the atomic ensemble with three atoms, which will be more appropriate as the generic basis of lexicographic states $|\{n_1,\ldots,n_a\}\rangle$ when dealing with global interactions.

For $N = 3$, the Hilbert space is eight-dimensional, whereby the energy levels E_1 and E_2 are threefold degenerate. Therefore, another operator, commuting with the atomic Hamiltonian $\widehat{H}_A$, is needed to obtain a complete set of quantum numbers and to differentiate each basis state. One possibility is the chirality operator [143]

$$\hat{\chi} = \frac{1}{2\sqrt{3}} \sum_{i,j,k=1}^{3} \epsilon_{ijk} \hat{\sigma}_{1i} \hat{\sigma}_{2j} \hat{\sigma}_{3k} \,, \tag{5.20}$$

where $\hat{\sigma}_{ij}$ is the j-th Pauli operator acting onto the i-th qubit. Its eigenvalues are $\chi = -1, 0, +1$. Due to their permutation invariance, the Dicke states $|D_3^{(a)}\rangle$ correspond to $\chi = 0$ and are called non-chiral. To complete the basis, we define four chiral states $|\chi_{a\pm}\rangle$, two for each degenerate energy subspace with $a = 1, 2$. The complete basis $\{|\chi_{a\chi}\rangle\}$ consists of four Dicke states, the non-chiral states

$$|\chi_{00}\rangle = |D_3^{(0)}\rangle = |ggg\rangle \,, \tag{5.21a}$$

$$|\chi_{10}\rangle = |D_3^{(1)}\rangle = \left(|rgg\rangle + |grg\rangle + |ggr\rangle\right)/\sqrt{3} \,, \tag{5.21b}$$

$$|\chi_{20}\rangle = |D_3^{(2)}\rangle = \left(|rrg\rangle + |rgr\rangle + |grr\rangle\right)/\sqrt{3} \,, \tag{5.21c}$$

and

$$|\chi_{30}\rangle = |D_3^{(3)}\rangle = |rrr\rangle \tag{5.21d}$$

and four chiral states

$$\begin{aligned} |\chi_{1-}\rangle &= |D_3^{(1)}(\{0, \phi, -\phi\})\rangle \\ &= \left(|rgg\rangle + e^{i\phi}|grg\rangle + e^{-i\phi}|ggr\rangle\right)/\sqrt{3} \,, \end{aligned} \tag{5.21e}$$

$$\begin{aligned} |\chi_{1+}\rangle &= |D_3^{(1)}(\{0, -\phi, \phi\})\rangle \\ &= \left(|rgg\rangle + e^{-i\phi}|grg\rangle + e^{i\phi}|ggr\rangle\right)/\sqrt{3} \,, \end{aligned} \tag{5.21f}$$

$$\begin{aligned} |\chi_{2-}\rangle &= |D_3^{(2)}(\{-\phi, 0, \phi\})\rangle \\ &= \left(e^{-i\phi}|rrg\rangle + |rgr\rangle + e^{i\phi}|grr\rangle\right)/\sqrt{3} \,, \end{aligned} \tag{5.21g}$$

and

$$\begin{aligned} |\chi_{2+}\rangle &= |D_3^{(2)}(\{\phi, 0, -\phi\})\rangle \\ &= \left(e^{i\phi}|rrg\rangle + |rgr\rangle + e^{-i\phi}|grr\rangle\right)/\sqrt{3} \end{aligned} \tag{5.21h}$$

with $\phi = 2\pi/3$.

In quantum information, chiral states can be used to construct logical qubits from physical qubits [144]. Such logical qubits are more fault-tolerant and less affected by noise. This is called noiseless subsystem encoding [145]. In section 5.4, we present a scheme to prepare twisted W states in Rydberg systems, including chiral states in the case of $N = 3$. In section 5.5.1 the orthogonality of the chiral states is used to select specific transitions in the atomic ensemble by means of selection rules.

5.3 EFFECTIVE ATOMIC-ENSEMBLE HAMILTONIANS

In this section, we derive effective Hamiltonians of the idealized neutral Rydberg-atom system discussed in section 5.1. We consider different sets of laser fields enumerated by j. All fields resemble classical fields. Thus, they are in a single-mode coherent state [96] with a high mean photon number M_j[2]. All assumptions are equivalent to the case of simple TLS Rabi oscillations in section 2.3.2. The difference is that we now consider not a TLS and a single mode, but a multilevel atomic ensemble and several modes. Further, we do not solve the model analytically, but employ the resolvent formalism to first order as introduced in chapter 3. Tracing over the field's degrees of freedom delivers effective Hamiltonians describing the atomic ensemble's dynamic.

We write the effective Hamiltonian as a sum over all (degenerate) energy levels E of the dominant part of $\widehat{\mathrm{H}}$, i.e. the Hamiltonian without interaction between atomic ensemble and field. Hence, the sum runs over the whole spectrum $\sigma(\widehat{\mathrm{H}}_0)$, where $\widehat{\mathrm{H}}_0 = \widehat{\mathrm{H}}_\mathrm{A} + \widehat{\mathrm{H}}_\mathrm{F}$ [cf. eqs. (5.1) and (5.4)]. It also can approximates the denominator of the resolvent, such that the effective Hamiltonian is

$$\widehat{\mathrm{H}}_\mathrm{eff} = \sum_{E\in\sigma(H_0)} \widehat{\mathrm{P}}_E \left(\widehat{\mathrm{H}} + \widehat{\mathrm{H}}\,\widehat{\mathrm{Q}}_E \frac{1}{E - \widehat{\mathrm{Q}}_E \widehat{\mathrm{H}}_0 \widehat{\mathrm{Q}}_E} \widehat{\mathrm{Q}}_E H \right) \widehat{\mathrm{P}}_E \,. \tag{5.22}$$

$\widehat{\mathrm{P}}_E = \mathbb{1} - \widehat{\mathrm{Q}}_E$ is the orthogonal projector onto the eigenspace corresponding to energy E. We distinguish two different cases: First, we discuss the interaction with an off-resonant laser field with a frequency far of resonance from any transition of the atomic-ensemble Hamiltonian. Second, we consider laser fields with a frequency in resonance with a specific transition of the atomic-ensemble Hamiltonian.

Our derivations only consider single laser fields, but a combination of several fields is always possible as long as the energy levels of the atomic ensemble combined with different fields do not overlap. If this condition is fulfilled, we can superpose the effective dynamic induced by several fields. We use such a combination of fields in the state conversion schemes, where different fields address different atomic-ensemble transitions.

5.3.1 *Off-resonant case*

In this section, we derive an effective Hamiltonian that describes the dynamics of the atomic ensemble in interaction with an off-resonant coherent laser field. We assume the laser field to be described by a plane wave with wave vector $\boldsymbol{k}_0$ and frequency ω_0. Off-resonant means the field's energy quantum $\hbar\omega_0$ is far from resonance with all of the

2 We changed here the notation of photon number from N (cf. section 2.2) to M to avoid any confusion with the number of considered Rydberg atoms

atomic ensemble's energy transitions. First, we will derive a general effective Hamiltonian for N Rydberg atoms and then specialize the result to the cases $N = 3, 4$. These are the first non-trivial cases but are also easily realized via simple geometric arrangements of the atoms.

5.3.1.1 *Derivation*

Since the field is far from resonance with all of the transitions in the atomic ensemble, the number of excited atoms a and the photon number m_0 distinguish different energy levels of the full system. The operators

$$\hat{\mathrm{P}}_a^{m_0} = \hat{\mathrm{P}}_a \otimes |m_0\rangle\langle m_0| \tag{5.23}$$

are projectors onto the corresponding eigenspaces of energy

$$E_a^{m_0} = E_a + m_0 \hbar \omega_0 \,. \tag{5.24}$$

With these projectors, the system Hamiltonian as defined in section 5.1, and the corresponding energies, we can evaluate equation (5.22) to determine the effective Hamiltonian. First, we notice that the subspaces are not affected by the interaction. Thus,

$$\hat{\mathrm{P}}_a^{m_0} \hat{\mathrm{H}}_{\mathrm{int}} \hat{\mathrm{P}}_a^{m_0} = 0 \,. \tag{5.25}$$

Further, the sum over all projectors acting on the system Hamiltonian describes the system without interaction, i.e.,

$$H_0 = \sum_{m_0=0}^{\infty} \sum_{a=0}^{N} P_a^{m_0} H P_a^{m_0} \,. \tag{5.26}$$

Therefore, we can write the effective Hamiltonian as

$$\hat{\mathrm{H}}_{\mathrm{eff}} = \hat{\mathrm{H}}_0 + \sum_{m_0=0}^{\infty} \sum_{a=0}^{N} \hat{\mathrm{P}}_a^{m_0} \hat{\mathrm{H}}_{\mathrm{int}} \hat{\mathrm{Q}}_a^{m_0} \frac{1}{E_a^{m_0} - \hat{\mathrm{Q}}_a^{m_0} \hat{\mathrm{H}}_0 \hat{\mathrm{Q}}_a^{m_0}} \hat{\mathrm{Q}}_a^{m_0} \hat{\mathrm{H}}_{\mathrm{int}} \hat{\mathrm{P}}_a^{m_0} \,. \tag{5.27}$$

Considering the form of $\hat{\mathrm{H}}_{\mathrm{int}}$ from equation (5.5), we can evaluate

$$\hat{\mathrm{P}}_a^{m_0} \hat{\mathrm{H}}_{\mathrm{int}} \hat{\mathrm{Q}}_a^{m_0} = \hat{\mathrm{P}}_a^{m_0} \hat{\mathrm{H}}_{\mathrm{int}} \hat{\mathrm{P}}_{a-1}^{m_0+1} + \hat{\mathrm{P}}_a^{m_0} \hat{\mathrm{H}}_{\mathrm{int}} \hat{\mathrm{P}}_{a+1}^{m_0-1} \tag{5.28}$$

since the interaction Hamiltonian directly connects only states that differ in the number of atomic excitations and photon number by one, whereas the total number of excitations $a + m_0$ stays the same. This is a result of the RWA where terms violating the conversion of the total number of excitations are neglected. As a result, we can replace all $\hat{\mathrm{Q}}_a^{m_0}$ in the sum of the effective Hamiltonian and expand the resolvent in our standard basis. Thus, we identify the denominators as the energy differences

$$E_a^{m_0} - E_{a\mp1}^{m_\pm 1} = \begin{cases} -\hbar\Delta_0 + (a-1)V \\ +\hbar\Delta_0 - aV \end{cases} \tag{5.29}$$

with the detuning $\Delta_0 = \omega_0 - \omega_A$.

The operators in each addend of the first order effective Hamiltonian in eq. (5.27) do not introduce any level transitions in the atomic ensemble. However, they cause energy shifts and mix the degenerate energy levels, and we can factorize them into projectors for the two subsystems as

$$\begin{aligned}\hat{P}_a^{m_0}\,\hat{H}_{\text{int}}\,\hat{P}_{a\mp1}^{m_0\pm1}\,\hat{H}_{\text{int}}\,\hat{P}_a^{m_0} \\ = \left\{\begin{array}{l} |d_0|^2(m_0+1)\hat{P}_a\left[\widehat{Hd}_{2,N}(\boldsymbol{k}_0)+a\right]\hat{P}_a \\ |d_0|^2 m_0\hat{P}_a\left[\widehat{Hd}_{2,N}(\boldsymbol{k}_0)+(N-a)\right]\hat{P}_a \end{array}\right\} \otimes |m_0\rangle\langle m_0|\,.\end{aligned} \tag{5.30}$$

Here, we introduce the operator

$$\begin{aligned}\widehat{Hd}_{2,N}(\boldsymbol{k}) &= \hat{U}(\boldsymbol{k})\,\widehat{Hd}_{2,N}\,\hat{U}^\dagger(\boldsymbol{k}) \\ &= \hat{U}(\boldsymbol{k})\sum_{n_1,n_2=1}^{N}\left[(1-\delta_{n_1n_2})|r\rangle_{n_1n_1}\langle g|\otimes|g\rangle_{n_2n_2}\langle r|\right]\hat{U}^\dagger(\boldsymbol{k})\,.\end{aligned} \tag{5.31}$$

It projects a state of the atomic ensemble onto an equal superposition of all other states reachable by one combination of excitation and deexcitation of distinct atoms. These are all states with the same hamming weight but a Hamming distance (Hd)[3] of two. Additionally, the $\widehat{Hd}_{2,N}(\boldsymbol{k})$-operator includes the phase factors due to the different positions of the atoms via the unitary transformation $\hat{U}(\boldsymbol{k})$ or rather the wave vector $\boldsymbol{k}$ as its argument. In the following, when we leave out the argument $\boldsymbol{k}$ and write simply $\widehat{Hd}_{2,N}$, we assume all site-dependent phases to vanish, equivalent to setting $\boldsymbol{k} = 0$. A more detailed derivation of eq. (5.30), including some tedious intermediate steps, can be found in appendix B.1.

Using the results from the last two paragraphs, we can rewrite the effective Hamiltonian from equation (5.27) into

$$\begin{aligned}\hat{H}_{\text{eff},N}^{\text{off}}(\boldsymbol{k}_0) = \hat{H}_0 + \sum_{a=0}^{N}\sum_{m_0=0}^{\infty}|d_0|^2\hat{P}_a^{m_0}\Bigg[m_0\frac{\widehat{Hd}_{2,N}(\boldsymbol{k}_0)+N-a}{\hbar\Delta_0-aV} \\ -(m+1)\frac{\widehat{Hd}_{2,N}(\boldsymbol{k}_0)+a}{\hbar\Delta_0-(a-1)V}\Bigg]\hat{P}_a^{m_0}\,,\end{aligned} \tag{5.32}$$

where for each addend the two possible operators of equation (5.30) with the corresponding energy difference (5.2) as denominator appear. The resulting effective Hamiltonian describes the dynamic of the

3 The hamming weight is the number of digits 1 in a given bit string. The Hd is the number of binary digits on which two given bit strings differ.

whole system – atomic ensemble and electromagnetic field – up to the leading order of the resolvent formalism.

A single-mode coherent state $|\alpha_0\rangle$ (cf. section 2.2) of relatively high mean photon number M_0 describes a classical laser field exceptionally well. Tracing over the field's degrees of freedom, we can define

$$\begin{aligned}\widehat{\mathrm{H}}_N^{\mathrm{off}}(\boldsymbol{k}_0) &= \mathrm{Tr}_{\mathrm{F}}\left[\widehat{\mathrm{H}}_{\mathrm{eff},N}^{\mathrm{off}}(\boldsymbol{k}_0)(\mathbb{1}_A \otimes |\alpha_0\rangle\langle\alpha_0|)\right] - \widehat{\mathrm{H}}_0 \\ &= \sum_{a=0}^{N} \widehat{\mathrm{P}}_a \left[s_a\left(\widehat{\mathrm{Hd}}_{2,\mathrm{N}}(\boldsymbol{k}_0) + N - a\right) - s_{a-1}\left(\widehat{\mathrm{Hd}}_{2,\mathrm{N}}(\boldsymbol{k}_0) + a\right)\right]\end{aligned} \tag{5.33}$$

as the lowest-order corrections to the atomic ensemble Hamiltonian. The resulting effective Hamiltonian $\widehat{\mathrm{H}}_{\mathrm{eff}} = \widehat{\mathrm{H}}_{\mathrm{A}} + \widehat{\mathrm{H}}_N^{\mathrm{off}}(\boldsymbol{k}_0)$ describes the dynamic of the atomic ensemble alone. The main coefficients of the effective Hamiltonian completely incorporate the effect of the off-resonant laser field. These main coefficients are the Stark shifts

$$s_a = \frac{\hbar^2|\Omega_0|^2}{\hbar\Delta_0 - aV}\,. \tag{5.34}$$

They describe shifts of the energetic levels of the atomic ensemble and are determined – among atomic properties – by the single atom Rabi frequency Ω_0 and the laser field's detuning Δ_0 from the atomic resonance frequency.

In the following, we emphasize some special cases of the effective Hamiltonian derived in this section. We aim especially to simplify the cases $N = 3$ and $N = 4$ since the corresponding atomic ensemble Hamiltonians (5.1) can be realized simply by suitable geometrical positioning of the individual atoms.

5.3.1.2 *Atom numbers N=3,4*

The effective Hamiltonian of the last section describes the dynamic of the whole atomic ensemble for all $\binom{N}{a}$ different states of all possible numbers of excitations, i.e., $0 \leq a \leq N$. For some cases, we can simplify the addends appearing in equation (5.33) by evaluating the $\widehat{\mathrm{Hd}}_{2,\mathrm{N}}$-operator explicitly. Since only one state exists for $a = 0$ and $a = N$ excitations, the $\widehat{\mathrm{Hd}}_{2,\mathrm{N}}$-operator vanishes in the corresponding subspaces. Hence,

$$\widehat{\mathrm{P}}_0\,\widehat{\mathrm{Hd}}_{2,\mathrm{N}}\,\widehat{\mathrm{P}}_0 = \widehat{\mathrm{P}}_N\,\widehat{\mathrm{Hd}}_{2,\mathrm{N}}\,\widehat{\mathrm{P}}_N = 0\,. \tag{5.35}$$

For the following, respectively preceding, number of excitations (i.e., $a = 1, N-1$), all states of the same Hamming weight are connected via precisely one excitation and deexcitation at distinct atoms. This fact allows us to write the $\widehat{\mathrm{Hd}}_{2,\mathrm{N}}$-operator in terms of projectors onto the Dicke states $|\mathrm{D}_N^{(1)}\rangle$ and $|\mathrm{D}_N^{(N-1)}\rangle$, respectively, and we only have to correct for the term connecting each state with itself. Therefore,

$$\widehat{\mathrm{P}}_1\,\widehat{\mathrm{Hd}}_{2,\mathrm{N}}\,\widehat{\mathrm{P}}_1 = N|\mathrm{D}_N^{(1)}\rangle\langle\mathrm{D}_N^{(1)}| - \widehat{\mathrm{P}}_1 \tag{5.36}$$

and

$$\widehat{\mathrm{P}}_{N-1}\,\widehat{\mathrm{Hd}}_{2,\mathrm{N}}\,\widehat{\mathrm{P}}_{N-1} = N|\mathrm{D}_N^{(N-1)}\rangle\langle\mathrm{D}_N^{(N-1)}| - \widehat{\mathrm{P}}_{N-1}\,, \tag{5.37}$$

respectively. The factor N stems from the N possibilities to excite precisely one atom or leave precisely one unexcited. For other values of a, we have to correct additional terms that do not appear in $\widehat{\mathrm{Hd}}_{2,\mathrm{N}}$ but in the projector of the Dicke state. With the generalized operators $\widehat{\mathrm{Hd}}_{2m,N}$ connecting states of equal Hamming weight but with Hamming distances of $2m$ (analogous to the definition in eq. (5.31)), we can rewrite

$$\widehat{\mathrm{P}}_a\,\widehat{\mathrm{Hd}}_{2,\mathrm{N}}\,\widehat{\mathrm{P}}_a = \binom{N}{a}|\mathrm{D}_N^{(a)}\rangle\langle\mathrm{D}_N^{(a)}| - \widehat{\mathrm{P}}_a - \sum_{m=2}^{\lfloor N/2\rfloor}\widehat{\mathrm{P}}_a\widehat{\mathrm{Hd}}_{2m,N}\widehat{\mathrm{P}}_a\,. \tag{5.38}$$

In the case of $N = 3$, we only need the simple eqs. (5.35) to (5.37) to rewrite the effective Hamiltonian as

$$\begin{aligned}\widehat{\mathrm{H}}_3^{\mathrm{off}}(\boldsymbol{k}_0) = {}& 3s_0|ggg\rangle\langle ggg| - 3s_2|rrr\rangle\langle rrr| \\ &+ (-3s_0+3s_1)|\mathrm{D}_3^{(1)}(\boldsymbol{k}_0)\rangle\langle\mathrm{D}_3^{(1)}(\boldsymbol{k}_0)| + s_1\widehat{\mathrm{P}}_1 \\ &+ (-3s_1+3s_2)|\mathrm{D}_3^{(2)}(\boldsymbol{k}_0)\rangle\langle\mathrm{D}_3^{(2)}(\boldsymbol{k}_0)| - s_1\widehat{\mathrm{P}}_2\,.\end{aligned} \tag{5.39}$$

We can see here that the off-resonant laser field lifts degeneracies. The energies of the Dicke states for $a = 1$ and $a = 2$ differ from the energies of orthogonal state of the same a by $(-3s_0 + 3s_1)$ and $(-3s_1 + 3s_2)$, respectively. These lifts can be used to address special transitions via a fine detuning of laser fields almost resonant to a certain transition of the original atomic Hamiltonian. *Zheng et al.* [109] used the shifts to reduce the Hamiltonian to an effective four-level Hamiltonian for a state conversion from W- to GHZ state and vice versa. Motivated by their work, we present such a reduction to an effective four-level Hamiltonian generalizing it to twisted states of the atomic ensemble in section 5.5.2.

In the case of $N = 4$, we need an additional term as in eq. (5.38) for the excitation number $a = 2$. It will correct the terms involving jump operators from states that differ precisely by two excitations and deexcitations at distinct atom positions, and we can rewrite the lowest-order corrections as

$$\begin{aligned}\widehat{\mathrm{H}}_4^{\mathrm{off}}(\boldsymbol{k}_0) = {}& 4s_0|gggg\rangle\langle gggg| - 4s_3|rrrr\rangle\langle rrrr| \\ &+ (-4s_0+4s_1)|\mathrm{D}_4^{(1)}(\boldsymbol{k}_0)\rangle\langle\mathrm{D}_4^{(1)}(\boldsymbol{k}_0)| + 2s_1\widehat{\mathrm{P}}_1 \\ &+ (-6s_1+6s_2)|\mathrm{D}_4^{(2)}(\boldsymbol{k}_0)\rangle\langle\mathrm{D}_4^{(2)}(\boldsymbol{k}_0)| \\ &+ (-s_1+s_2)\widehat{\mathrm{P}}_2 - \widehat{\mathrm{U}}(\boldsymbol{k}_0)\widehat{\mathrm{P}}_2\widehat{\mathrm{Hd}}_{4,4}\widehat{\mathrm{P}}_2\,\widehat{\mathrm{U}}^\dagger(\boldsymbol{k}_0) \\ &+ (-4s_2+4s_3)|\mathrm{D}_4^{(3)}(\boldsymbol{k}_0)\rangle\langle\mathrm{D}_4^{(3)}(\boldsymbol{k}_0)| - 2s_3\widehat{\mathrm{P}}_3\,.\end{aligned} \tag{5.40}$$

Zheng et al. [109] used the effective Hamiltonians in eqs. (5.39) and (5.40) with vanishing site-dependent phases for state conversion from $N = 3, 4$-qubit W to GHZ states. Here, we presented a

generalized version of both cases, including site-dependent phases. Additionally, we generalized the derivation to arbitrary atom numbers N with our result in eq. (5.33).

In the following section, we discuss the case of a resonant laser field interacting with the atomic ensemble. In contrast to the off-resonant case, such a field is able to drive transitions in the atomic ensemble, which is necessary for quantum state preparation and interconversion.

5.3.2 *Resonant cases*

In contrast to the preceding section, we now describe the interaction of the atomic ensemble with laser fields that are in resonance with a specific energy transition in the atomic-ensemble Hamiltonian $\widehat{\mathrm{H}}_{\mathrm{A}}$. In this case, some energy levels of the combined system including atomic ensemble and field become energetically degenerate, despite having distinct photon- and excitation numbers. Hence,

$$E_a^{m_j} = E_a + \hbar\omega_j m_j = E_{a'} + \hbar\omega_{j'} m_{j'} = E_{a'}^{m_{j'}} \tag{5.41}$$

for some atomic excitation numbers a, a' and mode numbers j, j'. Here, we want to concentrate on adjacent atomic levels. Resonances bridging several energy gaps can be treated equally, but, in the context of the conversion schemes developed for a ladder Hamiltonian connecting adjacent levels in chapter 4, are of lesser interest to us.

The particular level structure of the atomic-ensemble Hamiltonian $\widehat{\mathrm{H}}_{\mathrm{A}}$ with increasing energy gap ΔE_a [cf. eq. (5.3)] allows addressing each transition separately. This assumption holds as long as the Rydberg-blockade potential V is high enough.

In the following, we derive the effective Hamiltonian of leading order for laser fields in resonance with adjacent energy levels with excitation numbers $a-1$ and a. The discussion of some special cases follows this derivation. First, the well-known effect of enhanced Rabi oscillations is described by setting $a = 1$. This case is the foundation for the preparation scheme for chiral states in section 5.4. Second, we introduce a ladder Hamiltonian, which connects all the levels of our atomic ensemble succeedingly and, thus, is of the form as discussed in section 4.6. This Hamiltonian is the foundation for the reduction schemes presented in sections 5.5.1 and 5.5.2.

5.3.2.1 *Derivation*

If the energy quantum $\hbar\omega_j$ of a laser field precisely fills one of the energy gaps Δ_a [cf. eq. (5.3)], the atomic states with energy E_a combined with the field state $|m_a\rangle$ and atomic states with energy E_{a-1} combined with the field state $|m_a + 1\rangle$ form a degenerate subspace. By equating $E_a^{m_0}$ and $E_{a-1}^{m_a+1}$, we get

$$\hbar\Delta_a = \hbar(\omega_a - \omega_A) = (a-1)V \tag{5.42}$$

for the detuning of the laser field in question. We call this resonance condition detuning, although it is in resonance with the transition $a \leftrightarrow a-1$. We always describe detuning relative to the single-atom Rydberg transition. Δ_a vanishes for $a = 1$ since, in this case, the considered transition is precisely the Rydberg transition. Note, we choose to parameterize the resonance via a and $a-1$, such that the enumeration of the fields starts with $j = a = 1$ since we already used $j = 0$ for the off-resonant case in section 5.3.1. We call the fields with $j > 0$ resonance or driving fields in the following.

We again apply the resolvent formalism to derive the effective Hamiltonian for the atomic ensemble interacting with a resonant laser field. Due to the additional degeneracy in the energy levels, we have to join the projectors onto subspaces of the same energy. Hence, we use the projectors

$$\hat{\mathrm{P}}_{a,a-1}^{m_a,m_a+1} = \hat{\mathrm{P}}_a^{m_a} + \hat{\mathrm{P}}_{a-1}^{m_a+1} = \mathbb{1} - \hat{\mathrm{Q}}_{a,a-1}^{m_a,m_a+1} \tag{5.43}$$

in the sum over all energy levels in eq. (5.22) instead of separate addends for each $\hat{\mathrm{P}}_a^{m_a}$ and $\hat{\mathrm{P}}_{a-1}^{m_a+1}$. The joined subspaces are directly affected by the interaction Hamiltonian since

$$\begin{aligned}\hat{\mathrm{P}}_{a,a-1}^{m_a,m_a+1}\,\hat{\mathrm{H}}_{\mathrm{int}}\,\hat{\mathrm{P}}_{a,a-1}^{m_a,m_a+1} = \hat{\mathrm{P}}_{a,a-1}^{m_a,m_a+1}\,\hat{\mathrm{H}}_0\,\hat{\mathrm{P}}_{a,a-1}^{m_a,m_a+1} \\ + \left(\hat{\mathrm{P}}_a^{m_a}\,\hat{\mathrm{H}}_{\mathrm{int}}\,\hat{\mathrm{P}}_{a-1}^{m_a+1} + \mathrm{H.c.}\right).\end{aligned} \tag{5.44}$$

In contrast, the term containing $\hat{\mathrm{H}}_{\mathrm{int}}$ does not appear for single projectors $\hat{\mathrm{P}}_a^{m_a}$ in the off-resonant case [cf. eq. (5.25)]. The additional term contains jump operators between atomic-ensemble levels with a and $a-1$ atomic excitations, resulting in

$$\hat{\mathrm{P}}_a^{m_a}\,\hat{\mathrm{H}}_{\mathrm{int}}\,\hat{\mathrm{P}}_{a-1}^{m_a+1} = d_a\sqrt{m_a+1}\,\hat{\mathrm{U}}(\boldsymbol{k}_a)\hat{\sigma}_{a-1}^{+}\,\hat{\mathrm{U}}^{\dagger}(\boldsymbol{k}_a) \otimes |m_a\rangle\langle m_a+1|\,. \tag{5.45}$$

Here, we introduced the atomic-ensemble raising operator $\hat{\sigma}_a^+$. It connects atomic-ensemble subspaces of succeeding excitation numbers and is defined as

$$\hat{\sigma}_a^{+} = \sum_{n_1<\ldots<n_a}^{N}\sum_{n=1}^{N} |r\rangle_{nn}\langle g|\{n_1,\ldots,n_a\}\rangle\langle\{n_1,\ldots,n_a\}|\,. \tag{5.46a}$$

Equivalently,

$$\hat{\sigma}_a^{-} = \sum_{n_1<\cdots<n_a}^{N}\sum_{n=1}^{N} |g\rangle_{nn}\langle r|\{n_1,\ldots,n_a\}\rangle\langle\{n_1,\ldots,n_a\}| \tag{5.46b}$$

is the atomic-ensemble lowering operator. They are related via $(\hat{\sigma}_a^+)^\dagger = \hat{\sigma}_{a+1}^-$ and act onto Dicke states as

$$\hat{\sigma}_a^{+}|\mathrm{D}_N^{(a)}\rangle = \sqrt{(N-a)(a+1)}|\mathrm{D}_N^{(a+1)}\rangle\,, \tag{5.47a}$$

$$\hat{\sigma}_a^{-}|\mathrm{D}_N^{(a)}\rangle = \sqrt{a(N-a+1)}|\mathrm{D}_N^{(a-1)}\rangle\,. \tag{5.47b}$$

We relegate a more detailed derivation of eq. (5.45) to appendix B.2.1. It is again a straightforward but rather tedious calculation.

For all energy subspaces, both the joined ones with projectors $\widehat{\mathrm{P}}_{a,a-1}^{m_a,m_a+1}$ and the off-resonant ones with projectors $\widehat{\mathrm{P}}_{a'}^{m_a}$, we still have to calculate the term containing the resolvent. In the second case, we can use the result already produced in the previous section 5.3.1 [cf. eqs. (5.28) to (5.30)] since the field is off-resonant towards transitions different from the considered one. Likewise, we can reduce the term containing the resolvent in the addend corresponding to the energy of the resonant subspaces in eq. (5.22) to

$$\widehat{\mathrm{P}}_{a,a-1}^{m_a,m_a+1}\,\widehat{\mathrm{H}}\,\widehat{\mathrm{Q}}_{a,a-1}^{m_a,m_a+1} = \widehat{\mathrm{P}}_{a}^{m_a}\,\widehat{\mathrm{H}}_{\mathrm{int}}\,\widehat{\mathrm{P}}_{a+1}^{m_a-1} + \widehat{\mathrm{P}}_{a-1}^{m_a+1}\,\widehat{\mathrm{H}}_{\mathrm{int}}\,\widehat{\mathrm{P}}_{a-2}^{m_a+2}\,. \tag{5.48}$$

As in section 5.3.1, we used that $\widehat{\mathrm{H}}_0$ does not connect different energy subspaces and $\widehat{\mathrm{H}}_{\mathrm{int}}$ only adjacent ones. Except for different indices, the last equation resembles eq. (5.28), and we can use the same line of arguing as in the off-resonant case in section 5.3.1 [cf. eqs. (5.28) to (5.32)]. We just have to introduce index shifts $a \leftrightarrow a-1$ and $m_a \leftrightarrow m_a+1$ in the second term of eq. (5.48). The corresponding energy differences in the denominator are

$$E_a^{m_a} - E_{a+1}^{m_a-1} = E_{a-1}^{m_a+1} - E_{a-2}^{m_a+2} = -V \tag{5.49}$$

since $\hbar\Delta_a = (a-1)V$. Thus, all terms of the effective Hamiltonian in eq. (5.22) containing the resolvent either scale like $|d_a|^2 m_a$, $|d_a|^2(m_a+1)$, or $|d_a|^2(m_a+2)$ divided by the corresponding energy difference. We can neglect these terms if we assume

$$V, \Delta_a - a'V \gg |d_a m_{a'}| \tag{5.50}$$

for all $a' \neq a, a-1$ up to a maximal relevant photon number $\max m_a$. This assumption leaves the result from eq. (5.45) and its hermitian conjugate as leading order corrections to $\widehat{\mathrm{H}}_0$ in the effective Hamiltonian.

Tracing over the field's degrees of freedom and assuming a coherent state $|\alpha_a\rangle$ of high mean photon number M_a for the resonant mode $j = a$ result in an effective atomic-ensemble Hamiltonian of the form

$$\widehat{\mathrm{H}}_{\mathrm{eff}} = \widehat{\mathrm{H}}_{\mathrm{A}} + \widehat{\mathrm{H}}_N^{a \leftrightarrow a\text{-}1} \tag{5.51}$$

with

$$\widehat{\mathrm{H}}_N^{a \leftrightarrow a\text{-}1}(\boldsymbol{k}_a) = \hbar\Omega_a^*\,\widehat{\mathrm{U}}(\boldsymbol{k}_a)\hat{\sigma}_a^-\,\widehat{\mathrm{U}}^\dagger(\boldsymbol{k}_a) + \mathrm{H.c.}\,. \tag{5.52}$$

The leading order corrections describe Rabi oscillations between atomic states with excitation numbers a and $a-1$. Ω_a is the single atom Rabi frequency. We relegate a more detailed discussion of the neglected terms and more instructive intermediate steps to derive eq. (5.52) to appendix B.2.2.

It is noteworthy to mention that the frequency of the Rabi oscillation is not $|\Omega_a|$ but depends on the transitions involved. The different dimensions of the adjacent subspaces of different numbers of atomic excitations a play a decisive role in the structure of the atomic-ensemble lowering and raising operators.

In the following, we want to discuss some special cases and some peculiarities appearing due to the site-dependent phase shifts encoded into the unitary transformation $\widehat{\mathrm{U}}$. Further, we discuss how to use the single field result to build effective Hamiltonians that describe the interaction of the atomic ensemble with several laser fields.

5.3.2.2 *Collective Rabi oscillations*

A laser field resonant to the Rydberg transition drives Rabi oscillations between the ground and the Rydberg state (cf. section 2.3). Due to the blockade potential V in the atomic-ensemble Hamiltonian, none of the atoms can oscillate independently since the blockade potential suppresses the simultaneous excitation of two or more atoms. Since $\Delta_1 = 0$, the laser field is far detuned from the other transitions $a = 0, 1 \leftrightarrow a = 2$ or even higher a. However, the whole ensemble oscillates coherently. This effect is called collective Rabi oscillations [146]. We immediately recognize this effect in our result for a resonant field interacting with the atomic ensemble. With $a = 1$ in eq. (5.52), the effective Hamiltonian for the atomic ensemble is

$$\widehat{\mathrm{H}}_{\mathrm{eff}} = \widehat{\mathrm{H}}_{\mathrm{A}} + \left(\hbar\Omega_1^* \sqrt{N} |g \ldots g\rangle\langle \mathrm{D}_N^{(1)}(\boldsymbol{k}_1)| + \mathrm{H.c.}\right) . \tag{5.53}$$

The ground state is not affected by the unitary transformation since $\widehat{\mathrm{U}}(\boldsymbol{k}_0)$ only shifts the phases of excited atoms. This Hamiltonian describes Rabi oscillations with the enhanced Rabi frequency $\sqrt{N}\Omega_1$ between the ground and the twisted Dicke state. The effect has been experimentally observed in large cold-atom clouds [147, 148] and also for two [149] and three individual atoms [126, 150].

There are other ways than the Rydberg blockade to inhibit the population of a second atom of the ensemble. The same enhanced Rabi frequency appears in the population of the field state in an N-atom Jaynes-Cummings (JC) (sometimes called Tavis-Cummings) model with a single excited atom and no field excitation as initial conditions [151]. Note, in the last case, the regime of the electromagnetic field is a an entirely different one than for our considerations since it involves vacuum Rabi oscillations [152]. Furthermore, the atomic excitation gets trapped and hardly vanishes for a high number of atoms N [153]. In this case, the conservation of the total number of excitations prevents more than one atom from being excited simultaneously.

The site-dependent phases determine the superposition of atomic-ensemble basis states that make up the quantum state in eq. (5.53) participating in the Rabi oscillation. Especially in the $N = 3$–case, they determine the chirality of the state. Therefore, to control the

site-dependent phases lies at the heart of the preparation scheme for chiral states in section 5.4.

5.3.2.3 *Rydberg ladder*

In the previous section, we only considered a single resonant field. It is straightforward to describe the interaction with several fields by introducing several modes and combining their respective transition corrections in the effective Hamiltonian. It leads to a possible experimental setup where N laser fields with detunings $\Delta_a = (a-1)V$ interact with the atomic ensemble. If all laser fields fulfill the Rydberg-blockade regime, hence $\hbar|\Omega_a| \ll V$ for all a, we can ignore all non-linear terms in any Ω_a as we already have done to derive the effective Hamiltonian for a single resonant field in eq. (5.52). Hence, the effective Hamiltonian is

$$\widehat{\mathrm{H}}_{\mathrm{eff}} = \widehat{\mathrm{H}}_{\mathrm{A}} + \widehat{\mathrm{H}}_N^{\mathrm{ladder}} \tag{5.54}$$

with leading corrections

$$\widehat{\mathrm{H}}_N^{\mathrm{ladder}} = \sum_{a=1}^{N} \left(\hbar\Omega_a^* \, \widehat{\mathrm{U}}(\boldsymbol{k}_a) \hat{\sigma}_a^- \, \widehat{\mathrm{U}}^\dagger(\boldsymbol{k}_a) + \mathrm{H.c.} \right) \tag{5.54a}$$

connecting adjacent atomic-ensemble energy levels. All subspaces are connected succeedingly via the resonant fields $j = 1, \ldots, N$, which bridge the respective energy gap ΔE_a in the atomic-ensemble Hamiltonian step by step from $a = 0$ to $a = N$.

We can rewrite eq. (5.54a) as

$$\begin{aligned} \widehat{\mathrm{H}}_N^{\mathrm{ladder}} = \sum_{a=1}^{N} \hbar\Omega_a^* \Bigg[& \sqrt{a(N-a+1)} |\mathrm{D}_N^{(a-1)}(\boldsymbol{k}_a)\rangle\langle \mathrm{D}_N^{(a)}(\boldsymbol{k}_a)| \\ & + \widehat{\mathrm{U}}(\boldsymbol{k}_a) \hat{\sigma}_a^- \left(\widehat{\mathrm{P}}_a - |\mathrm{D}_N^{(a)}\rangle\langle \mathrm{D}_N^{(a)}| \right) \widehat{\mathrm{U}}^\dagger(\boldsymbol{k}_a) \Bigg] \\ & + \mathrm{H.c.}\,, \end{aligned} \tag{5.55}$$

using the twisted Dicke states $|\mathrm{D}_N^{(a)}(\boldsymbol{k}_a)\rangle$ and the known action of the atomic-ensemble lowering and raising operators onto these states [cf. eqs. (5.47a) and (5.47b)]

Even though we call this Hamiltonian a ladder, it does not precisely generalize $\widehat{\mathrm{H}}^{4\text{-ladder}}$ in section 4.6 and eq. (4.27) which describes a four-level quantum system adjacently connected via three Rabi frequencies. $\widehat{\mathrm{H}}_N^{\mathrm{ladder}}$ resemble a slightly different structure. Here, we do not deal with an $N+1$ level system connected via N resonant laser fields but instead with a 2^N-level system due to the $\binom{N}{a}$-fold degeneracy of each atomic-ensemble energy E_a. As with the single field in the previous section, the unitary transformations $\widehat{\mathrm{U}}(\boldsymbol{k}_a)$ describe site-dependent phases on each atom in the multi-level scenario, but now, we have up to N different unitary transformations $\widehat{\mathrm{U}}$, since $\boldsymbol{k}_{a'} \neq \boldsymbol{k}_a$ in general. If

the overlaps $\langle \mathrm{D}_N^{(a)}(\boldsymbol{k}_a)| \mathrm{D}_N^{(a)}(\boldsymbol{k}_{a+1})\rangle$ for succeeding wave vectors are smaller than unity, the ladder spokes in the effective Hamiltonian in eq. (5.54a) do not match. If succeedingly numbered fields fulfill the phase-matching condition $\langle \mathrm{D}_N^{(a)}(\boldsymbol{k}_a)| \mathrm{D}_N^{(a)}(\boldsymbol{k}_{a+1})\rangle = 1$, the effective Hamiltonian describes Rabi oscillations between the twisted Dicke states $|\mathrm{D}_N^{(a-1)}(\boldsymbol{k}_a)\rangle$ and $|\mathrm{D}_N^{(a)}(\boldsymbol{k}_a)\rangle$. Since the time evolution induced by a Hamiltonian is unitary, the time evolution of these twisted Dicke states decouples from orthogonal states of the same excitation number, respectively. If all $N-1$ phase-matching conditions are fulfilled, we can identify the ground state $|g\ldots g\rangle$ and the N twisted Dicke states $|\mathrm{D}_N^{(a)}(\boldsymbol{k}_a)\rangle$, one for each $a = 0,\ldots,N$, forming an $N+1$-level system connected via N Rabi frequencies. The time evolution of the remaining $2^N-(N+1)$ orthogonal states decouples from this subsystem, such that

$$\begin{aligned}\widehat{\mathrm{P}}_D(\{\boldsymbol{k}_a\})\,\widehat{\mathrm{H}}_N^{\text{ladder}}\,\widehat{\mathrm{P}}_D(\{\boldsymbol{k}_a\}) \\ = \sum_{a=1}^{N}\Omega_a^*\sqrt{a(N-a+1)}|\mathrm{D}_N^{(a-1)}(\boldsymbol{k}_a)\rangle\langle\mathrm{D}_N^{(a)}(\boldsymbol{k}_a)| + \text{H.c.}\,,\end{aligned} \tag{5.56}$$

where

$$\widehat{\mathrm{P}}_D(\{\boldsymbol{k}_a\}) = \sum_{a=0}^{N}|\mathrm{D}_N^{(a)}(\boldsymbol{k}_a)\rangle\langle\mathrm{D}_N^{(a)}(\boldsymbol{k}_a)|\,, \tag{5.56a}$$

projects onto the subspace spanned by all considered twisted Dicke states.

This Hamiltonian induces a restricted time evolution only on the spanned subspace. It resembles the structure of $N+1$ levels succeedingly connected by N Rabi frequencies. Hence, if all matching conditions are fulfilled the projection of the $\widehat{\mathrm{H}}_N^{\text{ladder}}$ in the subspace $\widehat{\mathrm{P}}_D$ really generalizes $\widehat{\mathrm{H}}^{\text{4-ladder}}$ to $N+1$ levels.

An obvious solution for the phase matching is $\boldsymbol{k}_a\cdot\boldsymbol{x}_n = 0 \mod 2\pi$ for all combinations of a and n, such that $\widehat{\mathrm{U}}(\boldsymbol{k}_a) = \mathbb{1}$. In this case, the ladder Hamiltonian connects all ordinary Dicke states without any twisting.

For $N=3$, the ladder Hamiltonian in eq. (5.56) resembles the same structure as the Hamiltonian discussed in chapter 4. Aligning all laser fields perpendicular to the plane spanned by the three atoms achieves the phase-matching conditions $\boldsymbol{k}_a\cdot\boldsymbol{x}_n = 0$. In this case, we can write the leading corrections as

$$\begin{aligned}\widehat{\mathrm{P}}_D\,\widehat{\mathrm{H}}_3^{\text{ladder}}(\{\boldsymbol{k}_a\})\widehat{\mathrm{P}}_D = \sqrt{3}\Omega_1^*|ggg\rangle\langle\mathrm{D}_N^{(1)}| + 2\Omega_2^*|\mathrm{D}_3^{(1)}\rangle\langle\mathrm{D}_3^{(2)}| \\ + \sqrt{3}\Omega_3^*|\mathrm{D}_2^{(1)}\rangle\langle\mathrm{D}_3^{(3)}| + \text{H.c.}\,.\end{aligned} \tag{5.57}$$

If precise positioning of the atoms and alignment of the laser fields in three dimensions is possible, the phase-matching condition can hold even for $N = 4$. In this case, we get

$$\begin{aligned}\widehat{\mathrm{P}}_D\,\widehat{\mathrm{H}}_4^{\text{ladder}}(\{\boldsymbol{k}_a\})\widehat{\mathrm{P}}_D = {} & 2\Omega_1^*|gggg\rangle\langle \mathrm{D}_4^{(1)}| + \sqrt{6}\Omega_2^*|\mathrm{D}_4^{(1)}\rangle\langle \mathrm{D}_4^{(2)}| \\ & + \sqrt{6}\Omega_3^*|\mathrm{D}_4^{(2)}\rangle\langle \mathrm{D}_4^{(3)}| + 2\Omega_4^*|\mathrm{D}_4^{(3)}\rangle\langle \mathrm{D}_4^{(4)}| \\ & + \text{H.c.}\,.\end{aligned} \tag{5.58}$$

Zheng et al. [109] also derived these two effective Hamiltonians by introducing an additional strong off-resonant laser field (cf. section 5.3.1) and fine detunings to the N resonant laser fields. Furthermore, they implicitly assumed the phase-matching condition to be fulfilled. Here, we showed that the strong off-resonant field is not necessary to derive the ladder Hamiltonian, and we emphasized the importance of the phase-matching condition.

In section 5.5.1, we use the result for $N = 3$ to reduce the corresponding eight-dimensional system to an effective four-level ladder Hamiltonian for different sets of states. Selection rules determine which states form this set, and the selection rules depend on the chosen phase-matching conditions. Effective Hamiltonians formed by these selection rules can be seen as an extension of the preparation scheme for chiral states in section 5.4, since it allows to convert each of the chiral states into a GHZ state.

In section 5.5.2, we use an additional strong off-resonant laser field to lift the degeneracies in the system Hamiltonian to some extent. Particular transitions can then be addressed using fine detunings of the resonant laser fields.

In both cases, we realize a four-level ladder Hamiltonian, thus, we can use our quantum state conversion scheme from section 4.7.

5.4 PREPARATION OF CHIRAL W STATES

In this and the following section, we want to discuss applications of the effective Hamiltonians derived in sections 5.3.1 and 5.3.2. We start with a preparation scheme for twisted W states for the $N = 3$–case. The scheme includes the preparation of chiral states as discussed in section 5.2.3.

Section 5.3.2.2 shows that a single resonant plane-wave laser field with vanishing detuning $\Delta_1 = 0$ and wave vector $\boldsymbol{k}_1$ drives collective Rabi oscillations between the ground state $|g\ldots g\rangle$ and the twisted W state $|\mathrm{D}_N^{(1)}(\boldsymbol{k}_1)\rangle$ [cf. eq. (5.53)]. Therefore, a simple π pulse [cf. eq. (4.19)] of the laser field prepares the twisted W state from the initially occupied ground state.

To choose which twisted state is prepared by the π pulse, we have to control the site-dependent phases $\boldsymbol{k}_1 \cdot \boldsymbol{x}_n$ describing the twisting. In the $N = 3$–case, this control can be understood purely via geometrical

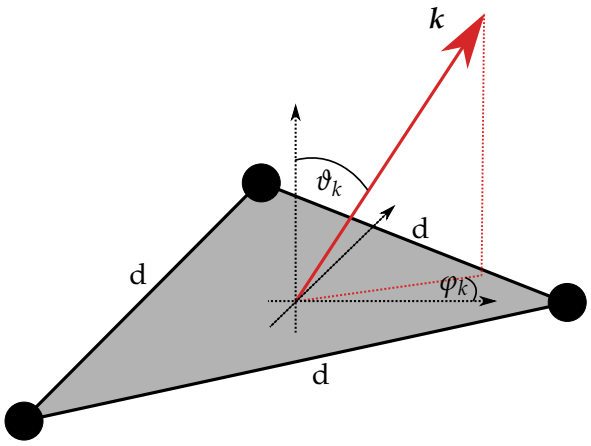

Figure 5.2: Schematic drawing of the orientation of the laser field and the atomic plane for the $N = 3$ case. The atoms form an equilateral triangle with interatomic distance d. The orientation of a plane laser field with wave vector $\boldsymbol{k}$ is defined through the angles ϑ_k and φ_k.
Adopted from FIG. 2. [64], which is licensed under Attribution 4.0 International (CC BY 4.0).

arguments, thus, specific positioning of the atoms and alignment of the laser field towards the atomic ensemble. We can realize the atomic Hamiltonian in eq. (5.1) by positioning all atoms pairwise equidistantly to ensure a constant interaction potential V. Hence, they form an equilateral triangle of some interatomic distance d. We describe the three individual relative atom positions via the radial coordinate $r = d\sqrt{3}$ and three equally distributed azimuthal angles φ_1, $\varphi_2 = \varphi_1 + 2\pi/3$, and $\varphi_3 = \varphi_1 + 4\pi/3$. Relative to the plane spanned by the three atoms, we can describe the laser field's direction of propagation via the angles ϑ_k and φ_k, whereby ϑ_k describes the angle between the direction of propagation $\boldsymbol{k}/|\boldsymbol{k}|$ and the normal of the atomic plane. φ_k is the corresponding azimuthal angle of the laser field. Figure 5.2 shows a schematic drawing of the geometrical arrangement of atomic ensemble and laser field.

Considering all this and the RWA, we can write the site-dependent phases as

$$\boldsymbol{k}_1 \cdot \boldsymbol{x}_n = \frac{\omega_{\mathbf{A}}}{\mathrm{c}} \frac{d}{\sqrt{3}} \sin(\vartheta_k) \cos(\varphi_k - \varphi_n) \,. \tag{5.59}$$

In the equilateral triangle, we have $\sum_{n=1}^{N} \cos(\varphi - \varphi_n) = 0$ for any angle φ. Therefore, we can only prepare symmetrically twisted W states, where all site-dependent phases add up to zero, i.e., $\sum_{n=1}^{N} \boldsymbol{k}_1 \cdot \boldsymbol{x}_n = 0$.

A basic example of such a geometrical arrangement is an interatomic distance of twice the wavelength of the laser field, i.e., $d = 4\pi c/\omega_A$,

and laser alignment such that $\varphi_k - \varphi_2 = \pi/2$. This geometrical arrangement leads to $\cos(\varphi_k - \varphi_n) = -\sqrt{3}/2, 0, \sqrt{3}/2$ and relative site-dependent phases

$$\boldsymbol{k}_1 \cdot (\boldsymbol{x}_{1,3} - \boldsymbol{x}_2) = \mp\Phi\,, \tag{5.60}$$

where Φ can vary over the whole range $0 \leq \Phi \leq 2\pi$ by tilting the laser field with respect to the atomic plane, such that $0 \leq \vartheta_k \leq \pi/2$. Note, that other multiples of the wavelength are possible choices for d, as well, but they result in in different laser field alignments as described in the following to set specific phases.

In this exemplary arrangement, a π pulse of the resonant laser field drives the ground state into the symmetrically twisted state

$$|\mathrm{W}(\{-\Phi, 0, \Phi\})\rangle = \frac{1}{\sqrt{3}}\left(\mathrm{e}^{-i\Phi}|rgg\rangle + |grg\rangle + \mathrm{e}^{i\Phi}|ggr\rangle\right)\,, \tag{5.61}$$

where the tilt of the laser field determines the phase $\Phi = 2\pi\sin(\vartheta_k)$. In particular, this allows preparing the chiral states $|\chi_{1+}\rangle$ and $|\chi_{1-}\rangle$ with laser orientations described by $\vartheta_k = \arcsin(1/3)$ and $\arcsin(2/3)$, respectively. With the ordinary W state, which corresponds to an orthogonal orientation of the laser field ($\vartheta_k = 0$), we are able to prepare a complete set of the atomic-ensemble states with a single excitation.

Figure 5.3 shows the fidelity of the basis states $|\chi_{10}\rangle$, $|\chi_{1+}\rangle$, and $|\chi_{1-}\rangle$ towards the prepared state $|\mathrm{W}(-\Phi, 0, \Phi)\rangle$, which depends on the angle $\vartheta_k = \arcsin(\Phi/2\pi)$. In principle, since the three aforementioned states form an orthonormal basis of the subspace of a single excitation, an arbitrary twisted W state can be prepared if three laser fields drive the system and each field matches the phases for one of the basis states.

As already mentioned in section 5.2.3, chiral states can be of significant importance in QIP since they allow the implementation of noiseless-subsystem qubit encoding [144, 145]. There exist already preparation schemes for different QIP-platforms, e.g., trapped ion systems [154]. Here, we presented a simple preparation scheme in neutral atom systems, which is purely described by the geometry or arrangement of the atomic ensemble and the driving field. The crucial aspect for an experimental realization in Rydberg systems is the possibility to position the atoms with a precision lower than the wavelength of the laser field. Such precision requires the cooling of the atoms to their motional ground states. Although it is experimentally very demanding, there are experiments localizing Rydberg atoms already on a subwavelength scale, e.g., alkaline-earth atoms [129, 155, 156] or recently also alkali atoms [130]. Taking this recent advances in motional ground state cooling into account, a precision as required here seems in reach in the not to distant future. This exclusive preparation of a state of specific relative phases $\pm\Phi$ by the field depicts a selection rule. The ground state, which has chirality 0, is only connected to the

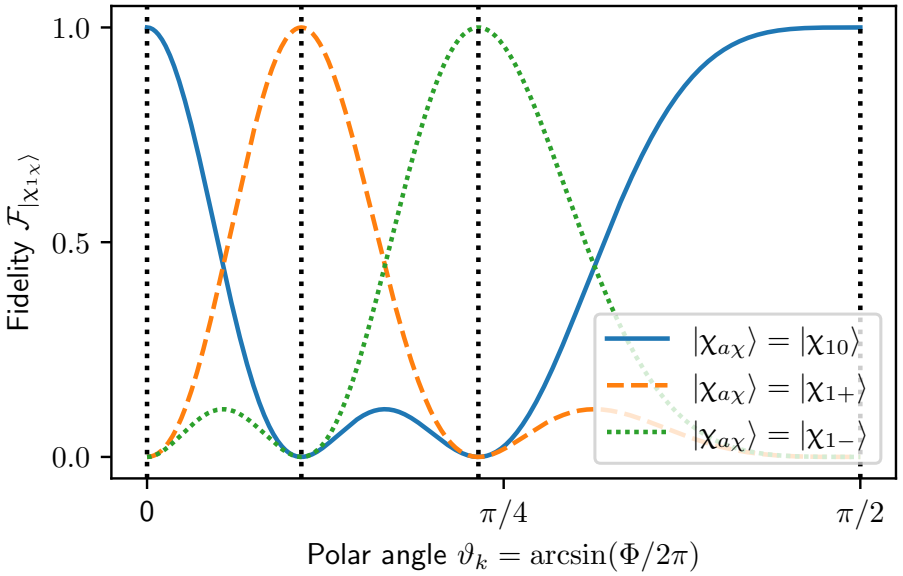

Figure 5.3: Chiral basis state fidelities $\mathcal{F}_{|\chi_{1\chi}\rangle} = |\langle\chi_{1\chi}|W(\Phi)\rangle|^2$ of the twisted W state $|W(\Phi)\rangle$ prepared via a π pulse of the collective Rabi Hamiltonian in eq. (5.53) for different polar angles $\vartheta_k = \arcsin(\Phi/2\pi)$ of the laser field. Its azimuthal angle fulfills $\varphi_k - \varphi_2 = \pi/2$, where φ_2 is the azimuthal angle of atom $n = 2$. All atoms form an equilateral triangle (cf. fig. 5.2). The vertical dotted lines indicate the configurations achieving the preparation of the atomic eigenstates $|\chi_{1\chi}\rangle$ of the chirality operator.

twisted W state corresponding to the twisting or chirality introduced by the laser field. This kind of selection rule applies to states of all possible excitation numbers a will play a crucial role in the first of the following schemes to reduce the atomic-ensemble Hamiltonian for $N = 3$ to an effective four-level-system.

5.5 EFFECTIVE FOUR-LEVEL SYSTEMS

This section presents different possibilities to reduce the effective Hamiltonian of the Rydberg-atom trimer, i.e., the special case of $N = 3$ atoms of the atomic ensemble described before, to a four-level ladder Hamiltonian. These reductions then allow to apply the conversion schemes for the constrained dynamics of the four-level quantum system developed in sections 4.6 and 4.7.

The starting point is the Rydberg-ladder Hamiltonian in eq. (5.54a). Rabi frequencies induced by several laser fields connect adjacent levels of the atomic ensemble, but the Hamiltonian only describes a decoupled dynamic for $N + 1$ distinct quantum states if specific phase-matching conditions are fulfilled.

In the following, we describe two possibilities to reduce the ladder Hamiltonian for a Rydberg-atom trimer with $N = 3$ to an effective system of four quantum states. In the first presented reduction, we use

the same kind of selection rules as we already did to prepare chiral states in the preceding section. Suitable alignments of the laser fields involved allow for the fulfillment of the matching conditions. Second, we discuss a reduction employing an additional far off-resonant laser field, which partially lifts the degeneracies of the atomic-ensemble energy levels, such that fine detunings of the ladder fields can single out specific transitions decoupled from unwanted transitions by a hierarchy of timescales. This second approach is motivated by the derivation of the effective Hamiltonian by *Zheng et al.*[109], but since we included site-dependent phases, we generalize it to almost arbitrary twisted states.

Since we concentrate here on the special case of Rydberg trimers, the resulting effective Hamiltonians describe four-level quantum systems, and we can use the $|01\rangle$ to GHZ state conversion scheme developed in chapter 4, where $|01\rangle$ represents the (twisted) W state in the Rydberg-trimer system.

In both cases, we present numerical simulations for the time evolution of the considered quantum system in the subsequent section 5.6 to validate the reduction schemes. These numerical investigations also include discussions of deleterious effects, such as dephasing and spontaneous decay via an open system approach or possible uncertain atom positions.

5.5.1 *Employing selection rules*

The ladder Hamiltonian in eq. (5.56) already reduces the full ladder Hamiltonian to an $N+1$-level system. The ordinary Dicke states span the decoupled subspace. Here, we want to explore the possibility of different phase-matching conditions to achieve a decoupled dynamic for different sets of states in the special case of Rydberg trimers, thus $N = 3$.

In contrast to the preceding section where a single laser field was considered, we assume three laser fields (enumerated $j = 1, 2, 3$) to interact with the atomic ensemble. Each of them is in resonance with one of the energetic transitions in the atomic Hamiltonian $\widehat{H}_A$.

Section 5.4 shows that collective Rabi oscillations connect the ground state with the twisted Dicke state $|D_3^{(1)}(\boldsymbol{k}_1)\rangle$. Orthogonal states of $a = 1$ excitations are decoupled from the dynamics of the ground state. If we want to include the ground state into the effective dynamics, we must include this particular twisted Dicke state, as well. In this sense, the twisting introduced by the first ladder field ($j = 1$) sets a reference frame such that we can rewrite the ladder Hamiltonian eq. (5.54a) as

$$\begin{aligned}\widehat{U}^\dagger(\boldsymbol{k}_1)\,\widehat{H}_3^{\text{ladder}}\,\widehat{U}(\boldsymbol{k}_1) = &\sum_{a=1}^{3} \hbar\Omega_a^*\,\widehat{U}(\boldsymbol{k}_a-\boldsymbol{k}_1)\hat{\sigma}_a^-\,\widehat{U}^\dagger(\boldsymbol{k}_a-\boldsymbol{k}_1)\\ &+\text{H.c.}\,.\end{aligned} \tag{5.62}$$

In the following, we set our phase reference to simplify the notation such that $\boldsymbol{k}_1 \cdot \boldsymbol{x}_n = 0$ for all n. Equivalently, we could redefine the atomic basis states to include the phases induced by the first field. Hence,

$$|\{n_1, \ldots, n_a\}\rangle \to \widehat{\mathrm{U}}(\boldsymbol{k}_1)|\{n_1, \ldots, n_a\}\rangle \tag{5.63a}$$

and

$$\boldsymbol{k}_a \to \boldsymbol{k}_a - \boldsymbol{k}_1 \,. \tag{5.63b}$$

When discussing the ladder Hamiltonian in section 5.3.2.3, we already selected the Dicke states to rewrite it slightly [cf. eq. (5.55)]. We can rewrite it again using the eigenstates of the chirality operator $|\chi_{a\chi}\rangle$ as basis for the atomic ensemble. The Hamiltonian represented in this basis is

$$\begin{aligned}\widehat{\mathrm{H}}_3^{\text{ladder}}/\hbar = {} & \Omega_1^* \sqrt{3} |ggg\rangle\langle\chi_{10}| + \Omega_3^* \sqrt{3}\, \widehat{\mathrm{U}}(\boldsymbol{k}_3)|\chi_{20}\rangle\langle rrr|\, \widehat{\mathrm{U}}^\dagger(\boldsymbol{k}_3) \\ & + \Omega_2^*\, \widehat{\mathrm{U}}(\boldsymbol{k}_2) \Big(2|\chi_{10}\rangle\langle\chi_{20}| - |\chi_{1+}\rangle\langle\chi_{2+}| \\ & \qquad - |\chi_{1-}\rangle\langle\chi_{2-}| \Big)\, \widehat{\mathrm{U}}^\dagger(\boldsymbol{k}_2) \\ & + \text{H.c.}\,.\end{aligned} \tag{5.64}$$

To reduce this Hamiltonian to an effective four-level system, we have to single out four states via some matching conditions. When introducing the Rydberg ladder, we already introduced matching conditions of vanishing side-dependent phases of the form[4]

$$\widehat{\mathrm{U}}(\boldsymbol{k}_2)|\chi_{10}\rangle = |\chi_{10}\rangle \tag{5.65a}$$

and

$$\widehat{\mathrm{U}}(\boldsymbol{k}_2)|\chi_{20}\rangle = \widehat{\mathrm{U}}(\boldsymbol{k}_3)|\chi_{20}\rangle \,. \tag{5.65b}$$

Alternative matching conditions are

$$\widehat{\mathrm{U}}(\boldsymbol{k}_2)|\chi_{1\pm}\rangle = |\chi_{10}\rangle \tag{5.65c}$$

and

$$\widehat{\mathrm{U}}(\boldsymbol{k}_2)|\chi_{2\pm}\rangle = \widehat{\mathrm{U}}(\boldsymbol{k}_3)|\chi_{20}\rangle \,. \tag{5.65d}$$

In the $\pm$ case, the ladder Hamiltonian would decouple the dynamic of a subspace spanned by the four states $\{|ggg\rangle, |\chi_{10}\rangle, |\chi_{2-}\rangle, |rrr\rangle\}$ in the upper-sign case or $\{|ggg\rangle, |\chi_{10}\rangle, |\chi_{2+}\rangle, |rrr\rangle\}$ in the lower sign case, respectively[5]. Projecting onto the decoupled subspace delivers an effective Hamiltonian of the same structure as the ladder Hamiltonian for the Dicke states in eq. (5.57) but involves a different state of $a = 2$ excited atoms and slightly adjusted Rabi frequencies as

$$\begin{aligned}\widehat{\mathrm{P}}_\pm\, \widehat{\mathrm{H}}_3^{\text{ladder}}(\{\boldsymbol{k}_a\})\widehat{\mathrm{P}}_\pm/\hbar = {} & \sqrt{3}\Omega_1^* |ggg\rangle\langle\chi_{10}| + \Omega_2^* |\chi_{10}\rangle\langle\chi_{2\pm}| \\ & + \sqrt{3}\Omega_3^* |\chi_{2\pm}\rangle\langle rrr| + \text{H.c.}\,.\end{aligned} \tag{5.66}$$

4 Now, with $\widehat{\mathrm{U}}(\boldsymbol{k}_1) \to \mathbb{1}$ taken as reference

5 Note, in these cases $\widehat{\mathrm{U}}(\boldsymbol{k}_2)|\chi_{2\pm}\rangle = |\chi_{2\mp}\rangle$, respectively.

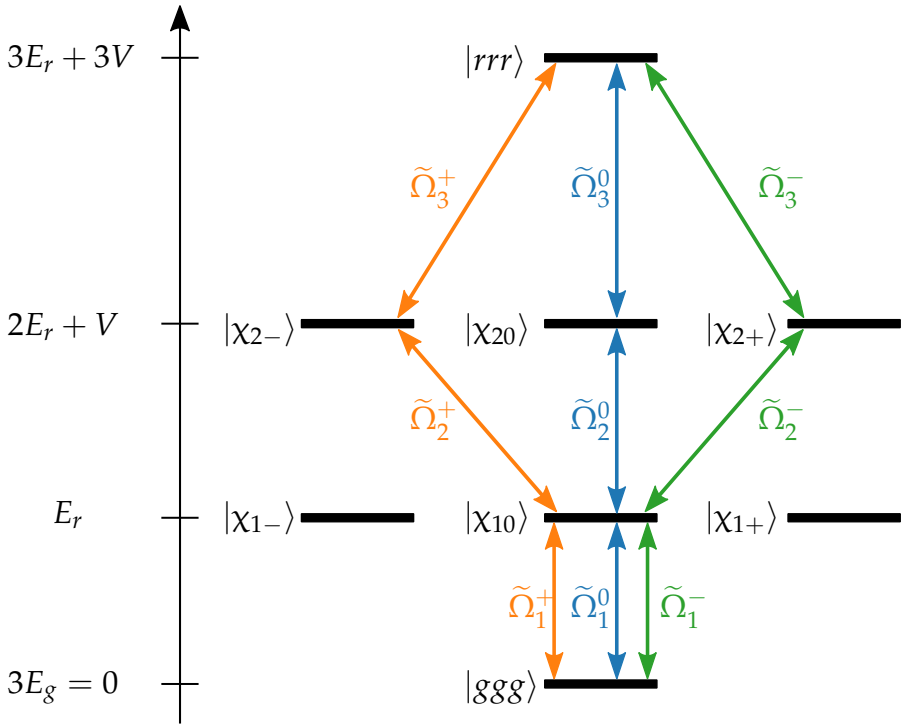

Figure 5.4: Energie scheme of the atomic ensemble with $N = 3$ in the chiral basis $|\chi_{as}\rangle$ [cf. Eqs. (5.21)]. The arrows indicate driven transitions to establish an effective 4LS depending on the matching conditions in eq. (5.65).

$\widehat{P}_\pm$ describes the orthogonal projection on either the set containing the positive or negative chiral state with $a = 2$. Note, that all schemes include $|\chi_{10}\rangle$ since we have chosen the first field as a reference and redefined the atomic basis states to include the phases introduced by this field.

For the different effective Hamiltonians to resemble the ladder Hamiltonian $\widehat{H}^{\text{4-ladder}}$ from section 4.6, we have to adjust the Rabi frequencies slightly to compensate for the different factors accompanying the Rabi frequencies Ω_j in eq. (5.64). Hence, we define effective Rabi frequencies $\widetilde{\Omega}_i$ accounting for the factors associated with a transition operator in the reduced effective Hamiltonian. In contrast to the matching conditions with vanishing side-dependent phases in eq. (5.56), the second resulting Rabi frequencies $\widetilde{\Omega}_2 = \Omega_2^*$ are diminished by a factor of two in the $\pm$ cases. Figure 5.4 shows an illustration of the connectivities implemented in different ladder Hamiltonians and summarizes the three discussed effective systems and the corresponding effective Rabi frequencies.

In section 5.6, we numerical investigate the reduction to the effective four-level system via a numerical calculation for the complete Rydberg trimer system. These investigation visualize the different intermediate states for different matching-conditions and show how robust the schemes is against deleterious effects such as dephasing and spontaneous decay.

Dephasing plays an especially crucial role, since the reduction to an effective four-level quantum system is based on setting appropriate matching conditions realized by control over the site-dependent phases. As for the scheme for the preparation of chiral W states, this requires a high precision over the positioning of the atoms on a subwavelength scale. Although this seems not to far from current experimental possibilities, subwavelength scale positioning [129, 130, 155, 156] is still technologically very demanding. Furthermore, to fulfill the matching conditions, the laser fields have to be precisely aligned. In the subsequent section, we present an alternative scheme to reduce the Rydberg-trimer Hamiltonian to an effective four-level quantum system, which allows to loosen the amount of precision in laser alignment somehow in a trade off with higher laser power of the driving fields.

5.5.2 *Employing lifted degeneracies*

Phase matching, as employed in the last section, reduces the effective Hamiltonian of the atomic ensemble to a matching Rydberg ladder and allows to employ state conversion schemes designed for succeedingly connected $N+1$-level systems. Another possibility is to lift the degeneracies to reduce the transitions in resonance with the driving laser fields. An off-resonant laser field can achieve this reduction by inducing energy shifts in the atomic ensemble. Adjusting the detuning of the driving fields can then address specific states by differentiating wanted and unwanted transitions by time scale hierarchies.

Zheng et al. [109] used this procedure to reduce the effective Hamiltonians of $N = 3$ and $N = 4$ Rydberg atoms to a matching ladder Hamiltonians of $N+1$ levels but did not consider site-dependent phases. They implicitly assumed all laser fields to fulfill the same phase-matching conditions as the strong off-resonant laser field. Inspired by their derivation of the effective Hamiltonian, we give a generalized version including site-dependent phases, hence including twisted states.

The same procedure is possible for more atoms, but we explicitly calculate it in the Rydberg trimer case, i.e., $N = 3$. We combine the Rydberg ladder of three laser fields ($j = 1, 2, 3$, cf. section 5.3.2.3) with stronger off-resonant laser field ($j = 0$, cf. section 5.3.1) to achieve the first leading order corrections in the effective Hamiltonian

$$\widehat{\mathrm{H}}_3^1 = \widehat{\mathrm{H}}_3^{\mathrm{off}}(\boldsymbol{k}_0) + \widehat{\mathrm{H}}_3^{\mathrm{ladder}}(\{\boldsymbol{k}_a\}) \,. \tag{5.67}$$

Stronger means that the Rabi frequency of the off-resonant laser field or dressing drive is much higher than the Rabi frequencies induced by the driving fields, hence $\Omega_0 \gg \Omega_a$. A consequence is that dynamics induced by the dressing drive happen on a much shorter time scale than dynamics induced by the driving fields. Furthermore, possible transitions between atomic-ensemble states happening on this short time scale are only of very limited amplitude due to the strong detuning of the dressing field (cf. section 2.3.2).

For three atoms the ladder Hamiltonian in eq. (5.54a) can be written down as

$$\begin{aligned}\widehat{H}_3^{\text{ladder}}(\{\boldsymbol{k}_a\})/\hbar = {}& \Omega_1^*\sqrt{3}|ggg\rangle\langle \mathrm{D}_3^{(1)}(\boldsymbol{k}_1)| \\ & + \Omega_2^*\Big(3|\mathrm{D}_3^{(1)}(\boldsymbol{k}_2)\rangle\langle \mathrm{D}_3^{(2)}(\boldsymbol{k}_2)| \\ & \qquad - \Phi^*(\boldsymbol{k}_2)\sum_{n=1}^{3} \mathrm{e}^{2\mathrm{i}\boldsymbol{k}_2\cdot\boldsymbol{x}_n}|gg\rangle|r\rangle_{nn}\langle g|\langle rr|\Big) \\ & + \Omega_3^*\sqrt{3}|\mathrm{D}_3^{(2)}(\boldsymbol{k}_3)\rangle\langle rrr|\Phi^*(\boldsymbol{k}_3) + \text{H.c.}\,,\end{aligned} \tag{5.68}$$

where $\Phi(\boldsymbol{k}) = \mathrm{e}^{\mathrm{i}\boldsymbol{k}\sum_{n=1}^{N}\boldsymbol{x}_n}$. Here, we have explicitly displayed the phases caused by the different laser fields. The overlaps of twisted Dicke states defined by succeeding fields describe the phase matching of the driving fields ($j = 1, 2, 3$) as in the conversion scheme in the preceding section. Hence,

$$\langle \mathrm{D}_3^{(1)}(\boldsymbol{k}_1)|\,\mathrm{D}_3^{(1)}(\boldsymbol{k}_2)\rangle = \frac{1}{3}\Sigma_{\boldsymbol{k}_2-\boldsymbol{k}_1} \tag{5.69a}$$

and

$$\langle \mathrm{D}_3^{(2)}(\boldsymbol{k}_2)|\,\mathrm{D}_3^{(2)}(\boldsymbol{k}_3)\rangle = \frac{\Phi(\boldsymbol{k}_3-\boldsymbol{k}_2)}{3}\Sigma_{\boldsymbol{k}_3-\boldsymbol{k}_2}\,, \tag{5.69b}$$

where $\Sigma_{\boldsymbol{k}} = \sum_{n=1}^{3}\mathrm{e}^{\mathrm{i}\boldsymbol{k}\cdot\boldsymbol{x}_n}$ and in general $0 \leq |\Sigma_{\boldsymbol{k}} = \sum_{n=1}^{3}| \leq 3$.

Instead of adjusting the laser fields in alignment and phase such that the overlaps reach unity, as it was done in the preceding section, the strong off-resonant field sets energy shifts that lift degeneracies, and then specific transitions can be addressed via a fine detuning of the ladder fields. To show this, we first transform the effective Hamiltonian into an interaction picture regarding the dressing field.

This transformation does not affect the atomic ensemble Hamiltonian since $[\widehat{H}_{\mathrm{A}}, \widehat{H}_3^{\text{off}}] = 0$, but the ladder Hamiltonian transforms as

$$\begin{aligned}&\mathrm{e}^{\mathrm{i}\widehat{H}_3^{\text{off}}(\boldsymbol{k}_0)t/\hbar}\,\widehat{H}_3^{\text{ladder}}(\{\boldsymbol{k}_a\})\mathrm{e}^{-\mathrm{i}\widehat{H}_3^{\text{off}}(\boldsymbol{k}_0)t/\hbar}/\hbar \\ &\quad = \widehat{U}(\boldsymbol{k}_0)\mathrm{e}^{\mathrm{i}\widehat{H}_3^{\text{off}}t/\hbar}\sum_{a=1}^{3}\Big(\Omega_a^*\,\widehat{U}(\boldsymbol{k}_a-\boldsymbol{k}_0)\hat{\sigma}_a^-\,\widehat{U}^\dagger(\boldsymbol{k}_a-\boldsymbol{k}_0) \\ &\qquad\qquad + \text{H.c.}\Big)\mathrm{e}^{-\mathrm{i}\widehat{H}_3^{\text{off}}t/\hbar}\,\widehat{U}^\dagger(\boldsymbol{k}_0)\,.\end{aligned} \tag{5.70}$$

Since the ladder Hamiltonian does not commute with $\hat{H}_3^{\text{off}}$, the left-hand side is not as easy to calculate and represents many different terms oscillating with different frequencies. The energies of atomic levels and the driving laser fields determine these frequencies. Introducing small fine detunings δ_j, such that the total detunings of the driving fields are $\Delta_j^{\text{total}} = \Delta_j + \delta_j$, allows matching the driving fields to specific transitions shifted by the dressing field enumerated with j. Note, as long as $|\delta_j| \ll |\Delta_j|$, the fine detunings never contribute significantly to any considered term in the derivation of the effective Hamiltonian in section 5.3.2, but it results in a complex phase of the Rabi frequencies as

$$\Omega_j \longrightarrow \Omega_j e^{-i\delta_j t} \tag{5.71}$$

in an interaction picture with respect to the total system Hamiltonian $\hat{H}_0 = \hat{H}_A + \hat{H}_F$. The phases in eq. (5.71) arise due to the slight change in the time dependencies of the field operators $\hat{a}_j$ and $\hat{a}_j^\dagger$ in the mentioned interaction picture, whereby Ω_j corresponds to the combination of atomic raising operator with $\hat{a}_j$ and Ω_j^* to its hermitian conjugate. Each driving field can then be brought into resonance with one of the terms in eq. (5.70), such that its oscillatory behavior vanishes, while other terms still oscillate with residual frequencies ω_R. If all residual frequencies are large compared to the inverse time scale of interest T^{-1}, we can neglect the corresponding terms in the effective Hamiltonian as fast oscillating.

The applied conversion time to complete the considered state conversion is the time scale of interest, which roughly scales with the inverse Rabi frequencies of the driving fields. This scaling can be seen as another kind of RWA with the condition $\min\{\omega_R\} \gg T^{-1}$.

The fine detunings

$$\delta_1 = (-6s_0 + 4s_1)/\hbar\,, \tag{5.72a}$$

$$\delta_2 = (3s_0 - 8s_1 + 3s_2)/\hbar \tag{5.72b}$$

and

$$\delta_3 = (4s_1 - 6s_2)/\hbar \tag{5.72c}$$

result in the twisted ladder Hamiltonian

$$\begin{aligned}\hat{H}_3^{\text{twisted ladder}}/\hbar = {} & \sqrt{3}\Omega_1 \frac{\Sigma_{k_0-k_1}}{3} |ggg\rangle\langle D_3^{(1)}(k_0)| \\ & + 2\Omega_2 \frac{\Sigma_{k_0-k_2}}{3} |D_3^{(1)}(k_0)\rangle\langle D_3^{(2)}(k_0)| \\ & \sqrt{3}\Omega_3 \frac{\Sigma_{k_0-k_3}}{3} |D_3^{(2)}(k_0)\rangle\langle rrr| + \text{H.c.}\,.\end{aligned} \tag{5.72}$$

This effective Hamiltonian realizes a Rydberg ladder for the twisted Dicke states $|D_3^{(a)}(k_0)\rangle$ connected via driven transitions with effective Rabi frequencies

$$\widetilde{\Omega}_1 = \sqrt{3}\Omega_1 \frac{\Sigma_{k_0-k_1}}{3}\,, \tag{5.72d}$$

$$\widetilde{\Omega}_2 = 2\Omega_2 \frac{\Sigma_{k_0-k_2}}{3}\,, \tag{5.72e}$$

and

$$\widetilde{\Omega}_3 = \sqrt{3}\Omega_3 \frac{\Sigma_{k_0-k_3}}{3}\,. \tag{5.72f}$$

We relegate a more detailed derivation of the twisted ladder Hamiltonian starting from eq. (5.70), a discussion of the chosen fine detunings, and a list of the corresponding residual frequencies to appendix C, since it features some lengthy and tedious calculations. Different fine detunings δ_a would allow to single out other transitions, e.g., orthogonal states to $|\mathrm{D}_3^{(a)}(\boldsymbol{k}_0)\rangle$, but not necessarily result in a four-level ladder Hamiltonian because the chiral states are still energetically degenerate with respect to $\widehat{\mathrm{H}}_3^{\mathrm{off}}(\boldsymbol{k}_0)$.

Since $\Sigma_{\boldsymbol{k}}$ is, in general, a complex number, the effective Rabi frequencies are also complex-valued. Complex phases can always be adsorbed into the states involved in the Hamiltonian as global phases, assuring real-valued Rabi frequencies as required for the state conversion scheme from section 4.7. The relative twisting, induced by laser fields towards the states $|\mathrm{D}_3^{(a)}(\boldsymbol{k}_0)\rangle$ and the single-atom Rabi frequencies, determines the absolute value of the effective Rabi frequencies. If $|\Sigma_{\boldsymbol{k}_0-\boldsymbol{k}_a}| < 3$, a constant effective Rabi frequency $\widetilde{\Omega}_a$ can be achieved by adjusting the single atom Rabi frequency Ω_a. Such an adjustment is possible as long as the Rabi frequencies and the underlying field interaction still fulfill the conditions for the RWA. Hence, compensation is impossible if a driving field addresses orthogonal states, since then $\Sigma_{\boldsymbol{k}_0-\boldsymbol{k}_a} = 0$. Figure 5.5 shows the level scheme for twisted states induce by the strong dressing field and indicates the induced effective four-level quantum system.

The advantage in comparison with the reduction scheme based on matching-conditions is the possibility to compensate site-dependent phases. The dressing field always induces a four-level quantum system. The Rabi frequencies only have to be adjusted for the differences induced by ladder fields and dressing fields. The precise position of the atoms is not of importance, as long as we can assume frozen dynamics, i.e. the interaction time of laser fields and fields is short in comparison to the frequency of the atomic motions in the tweezer array.

If one wants to control which twisted states compile the effective four-level quantum system, the same precision requirements as in the preceding section have to be fulfilled.

In section 5.6, we validate the reduction to the effective four-level system via numerical calculations for the complete Rydberg-trimer system. These investigation visualize the different adjustment of Rabi frequencies due to different relative alignments of the dressing field and the driving fields, which have to be taken into account if a quantum state conversion protocol is to implemented in the effective four-level system.

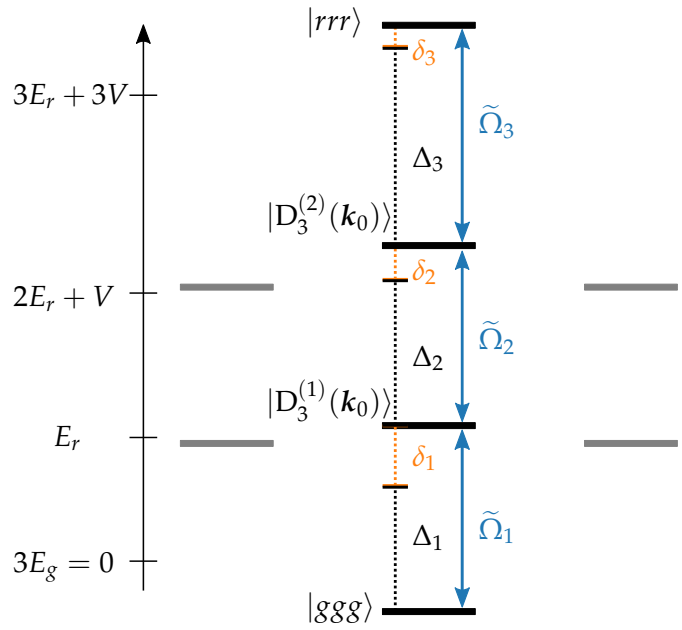

Figure 5.5: Sketch of the energy-level scheme corresponding to Rydberg-atom trimer driven by a strong and far-detuned dressing field and resulting in energy shifts. The arrows indicate the transitions driven by weaker laser fields with detunings $\Delta_i + \delta_i$ [cf. eqs.(5.72)] forming an effective 4LS. Energy shifts are not drawn to scale.

5.6 NUMERICAL VALIDATION OF REDUCTION SCHEMES

The preceding section presents two possibilities to reduce the eight-dimensional Rydberg-trimer Hamiltonian to an effective four-level quantum system. To validate these reduction schemes and to assess possible sources of error, we conduct numerical calculations of the time evolution of the eight-dimensional Rydberg-trimer system to show that it behaves like a 4LS under the proposed conditions.

We implemented the Rydberg trimer system with the help of the Python[6] package QuTiP[6]. We only concentrated on effective Hamiltonians describing the finite atomic ensemble and did not consider the infinite-dimensional Hilbert space of the electromagnetic field. The field and its different modes are incorporated into the dynamics via an effective treatment and resulting single-atom Rabi frequencies.

Additionally to the unitary Hamiltonian time evolution of the system, the QuTiP package allows for easy implementation of open system dynamics.[7] Since we necessarily have to consider mixed quantum states in the context of open quantum systems, we switch the only time throughout this thesis to a description in terms of mixed

6 Compare declarations on p. 141

7 For a detailed description, see, e.g., the textbooks by *Gardiner and Zoller* [157] or *Breuer and Petruccione* [158]. See *Weimer et al.* [159] for a review of numerical methods to solve such open system problems.

states and the density matrix $\widehat{\rho}(t)$. However, all presented simulations started with a pure state as initial state described by the density matrix $\widehat{\rho}(0) = |\psi(0)\rangle\langle\psi(0)|$. We numerically solved the Lindblad master equation [160][8]

$$\frac{\mathrm{d}\widehat{\rho}(t)}{\mathrm{d}t} = -\frac{i}{\hbar}[\widehat{\mathrm{H}}_{\mathrm{I}}(t), \widehat{\rho}(t)] + \sum_{l=1}^{2} \frac{1}{2}\left([\widehat{\mathrm{L}}_l, \widehat{\rho}(t)\widehat{\mathrm{L}}_l^{\dagger}] + [\widehat{\mathrm{L}}_l\widehat{\rho}(t), \widehat{\mathrm{L}}_l^{\dagger}]\right) , \quad (5.73)$$

where

$$\widehat{\mathrm{H}}_{\mathrm{I}} = \mathrm{e}^{i\widehat{\mathrm{H}}_0 t/\hbar}\, \widehat{\mathrm{H}}_{\mathrm{eff}}\, \mathrm{e}^{-i\widehat{\mathrm{H}}_0 t/\hbar} \quad (5.74)$$

is the respectively considered effective Hamiltonian $\widehat{\mathrm{H}}_{\mathrm{eff}}$ in an interaction picture regarding an appropriately chosen atomic Hamiltonian $\widehat{\mathrm{H}}_0$.

$$\widehat{\mathrm{L}}_1 = \sqrt{\Gamma} \sum_{n=1}^{3} |g\rangle_{nn}\langle r| \quad (5.75a)$$

and

$$\widehat{\mathrm{L}}_2 = \sqrt{\gamma} \sum_{n=1}^{3} \left(|g\rangle_{nn}\langle g| - |r\rangle_{nn}\langle r|\right) \quad (5.75b)$$

are Lindblad operators describing spontaneous decay and dephasing, respectively. Γ and γ are the corresponding decay- and dephasing rates. For a short but instructive introduction to the Lindblad equation as the most general generator of Markovian dynamics, we refer to the tutorial by *Manzano* [163].

$\widehat{\mathrm{H}}_{\mathrm{I}}$ will differ depending on which of the reduction schemes we are considering. If no Lindblad operators are specified, i.e., $\Gamma = \gamma = 0$, the dynamics reduce to the unitary time evolution.

Open system dynamics take interaction with the environment into account, but, in addition, experimental setups are never perfect. If an experimental realization of the proposed conversion schemes for Rydberg trimers in tweezer arrays is considered, variations in the position of the atoms will affect the phases $\boldsymbol{k} \cdot \boldsymbol{x}_n$ and the interatomic potential V. Since the latter depends on the interatomic distance, it cannot be assumed as constant anymore since the arrangement of the Rydberg trimer differs from the ideal equilateral triangle. Variations of the atomic positions are exemplarily investigated for the case without additional strong dressing field.

The following sections show numerical results for the two reduction schemes developed in section 5.5. They illustrate features of the resulting effective four-level systems via closed system dynamics ($\Gamma = \gamma = 0$).

We begin with the reduction scheme from section 5.5.1. For this simpler case exploiting selection rules, deleterious effects are incorporated

8 employing the *mesolve* routine in QuTiP [161, 162].

by the described Lindblad operators in eqs. (5.75) with non-vanishing open system parameters Γ and γ. Additionally, we conducted a simulation investigating the influence of uncertainties in the atomic positions on the target state fidelity for the W to GHZ state conversion.

Afterward, we shortly discuss features of the second reduction scheme from section 5.5.1.

5.6.1 *Reduction via selection rules*

Section 5.5.1 shows the possibility of reducing the eight-level quantum system of the Rydberg trimer to different effective four-level quantum systems featuring a ladder Hamiltonian by setting appropriate matching conditions of the involved laser fields with corresponding Rabi frequencies Ω_i. Each of the fields introduces transitions from states of $a = i - 1$ to a state of $a' = i$ atomic excitations. Since we take the twisting defined by the first ladder field Ω_i as phase reference, we set $|\mathrm{D}_3^{(1)}(\boldsymbol{k}_1)\rangle \to |\chi_{10}\rangle$, i.e., $\widehat{\mathrm{U}}(\boldsymbol{k}_1) = \mathbb{1}$. We simulated the eight-dimensional Rydberg-trimer system with the interaction Hamiltonian

$$\widehat{\mathrm{H}}_\mathrm{I}(t) = \sum_{j,n=1}^{3} \left(\hbar\Omega_j \mathrm{e}^{\mathrm{i}\left(\boldsymbol{k}_j\cdot\boldsymbol{x}_n - \Delta_j t\right)} |r\rangle_{nn}\langle g| + \mathrm{H.c.}\right) + \sum_{p<q} V_{pq} |rr\rangle_{pq}\langle rr| \,, \tag{5.76}$$

where $\Delta_j = (j-1)V$ are the detunings of the laser fields towards the Rydberg transition and V_{pq} is the Rydberg-blockade potential between the atoms p and q. The ideal case is $V_{pq} = V$ for all combinations of p and q.

This interaction Hamiltonian is in regard to the non-interacting part $\widehat{\mathrm{H}}_\mathrm{A} + \widehat{\mathrm{H}}_\mathrm{F}$ of eq. (5.8) assuming the field to be in a state of high mean photon number. It considers the time dependency induced by the energy differences of the atomic ground state $|g\rangle$ and the Rydberg state $|r\rangle$ of each of the three atoms as part of the atomic states, such that we do not have to take care of the fast oscillating evolution of relative phases due to the non-interacting part of the two-level systems in our numerical calculations.

Assuming the positions of the atoms to form an equilateral triangle as discussed in section 5.4, we can set the phases $\boldsymbol{k}_j \cdot \boldsymbol{x}_n$ by setting the polar angles ϑ_k of each laser field as in eq. (5.59) to match the three different sets of selection rules or matching conditions from eqs. (5.65). Taking the different corrections from eqs. (5.64) and (5.66) for effective Rabi frequencies into account, we can use solutions from the four-level quantum system in chapter 4 to implement a $|\chi_{10}\rangle$ to GHZ state conversion in the entire eight-dimensional quantum system.

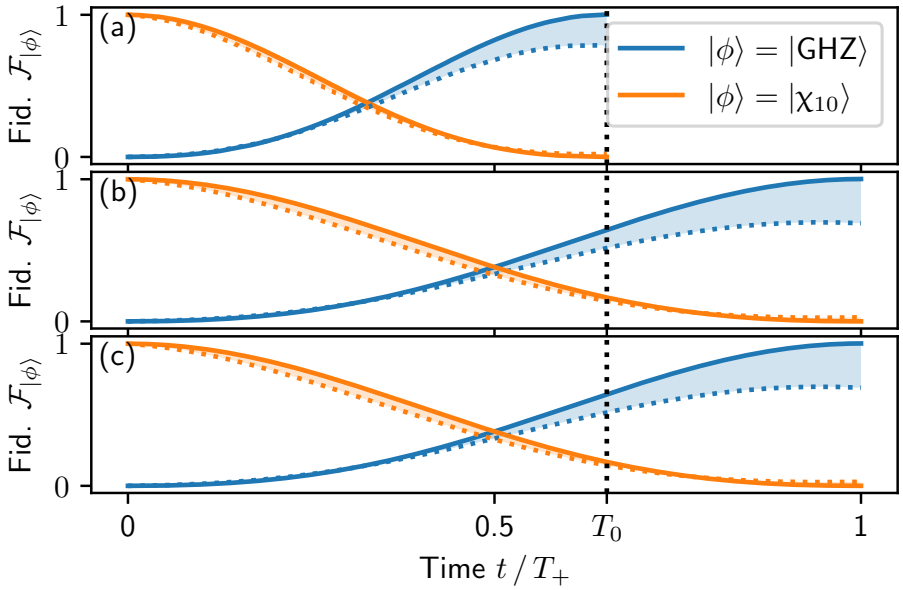

Figure 5.6: Target- and initial-state fidelities $\mathcal{F}_{|\phi\rangle}(t) = |\langle\phi|\psi(t)\rangle|^2$ for the W to GHZ state conversion under varying matching conditions [cf. eq. (5.65)]: (a) no phase differences (0 case, intermediate state $|\chi_{20}\rangle$), (b) + case (intermediate state $|\chi_{2-}\rangle$), and (c) − case (intermediate state $|\chi_{2+}\rangle$). All conversion schemes have equal TSPA [cf. eq. (4.49)]. Shaded areas indicate open system dynamics with up to $\Gamma = \gamma = 0.1/T_+$ (dotted lines), where T_+ is the conversion time for the conversion scheme with matching conditions as in the + case. $|\phi\rangle \in \{|\chi_{10}\rangle, |\mathrm{GHZ}\rangle\}$ [cf. eq. (5.77)].

The initial W state $|\chi_{10}\rangle$ corresponds to the $|01\rangle$ state from section 4.7, and

$$|\mathrm{GHZ}\rangle = \frac{1}{\sqrt{2}}\left(|ggg\rangle + \mathrm{e}^{\mathrm{i}\phi}|rrr\rangle\right) \tag{5.77}$$

is the targeted Rydberg-trimer GHZ state. The phase ϕ depends on which specific combination of Rabi frequencies is applied (cf. eq. (4.44) and table 4.1). All Rabi frequencies are rescaled such that the TSPA is equal for each of the three cases of matching conditions.

We solved the time-evolution according to eq. (5.73) with $\Gamma = \gamma = 0$ and the Hamiltonian in eq. (5.76) for $VT_\pm/\hbar = 3000$ where $T_\pm$ is the conversion time for the matching conditions in eqs. (5.65c) and (5.65d). Figure 5.6 shows target state and initial state fidelitites over the conversion time for the three different sets of matching conditions. We see that all three cases achieve the state conversion but that the conversion time T_0 for the case of vanishing site-dependent phases is smaller than the conversion time $T_\pm$ belonging to the other two matching conditions. It is not a surprising result since we know from the discussion of the effective four-level system in eq. (5.66) including the chiral states $|\chi_{2\pm}\rangle$ that the effective Rabi frequency $\widetilde{\Omega}_2$ is only half the effective Rabi frequency in the case of vanishing site-dependent phases.

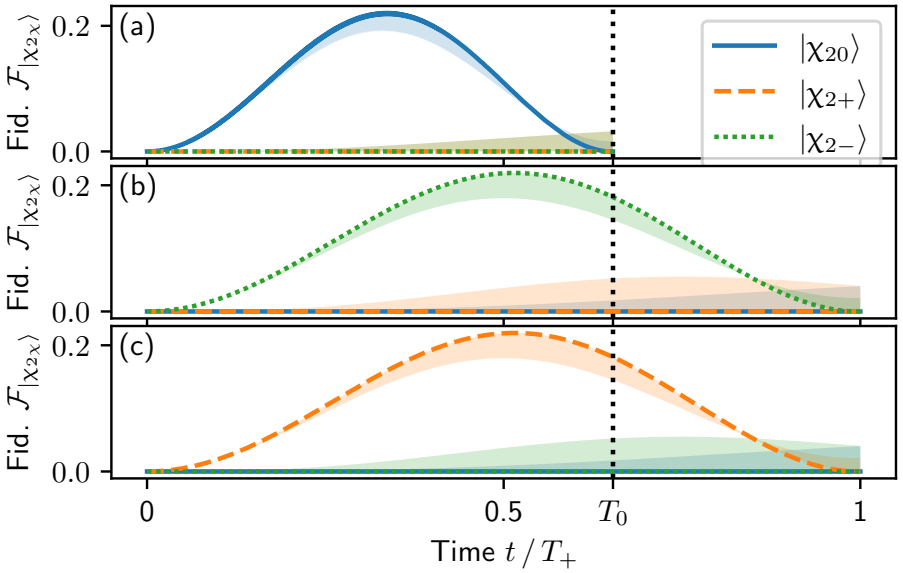

Figure 5.7: Intermediate-state fidelities $\mathcal{F}_{|\chi_{2\chi}\rangle} = |\langle\chi_{2\chi}|\psi(t)\rangle|^2$ with $\chi \in \{0, +, -\}$ for the W to GHZ state conversion under varying matching conditions [cf. eq. (5.65)]: (a) no phase differences (0 case, intermediate state $|\chi_{20}\rangle$), (b) $+$ case (intermediate state $|\chi_{2-}\rangle$), and (c) $-$ case (intermediate state $|\chi_{2+}\rangle$). All conversion schemes have equal TSPA [cf. eq. (4.49)]. Shaded areas indicate open system dynamics with up to $\Gamma = \gamma = 0.1/T_+$ (not explicitly shown), where T_+ is the conversion time for the conversion scheme with matching conditions as in the $+$ case.

Figure 5.7 shows fidelities towards the different intermediate states $|\chi_{2\chi}\rangle$.

All three cases just populate one specific state of $a = 2$ excitations during the conversion time, while orthogonal states of $a = 2$ are never occupied. Hence, the eight-dimensional system acts as an effective four-level system composed of $|ggg\rangle, |rrr\rangle, |\chi_{10}\rangle$ and $|\chi_{2\chi}\rangle$ for $\chi = 0, +$ or $-$. Which state of $a = 2$ excitations is part of the effective system depends on the matching conditions.

To investigate deleterious effects, we additionally solved the time-evolution with non-vanishing rates Γ, describing spontaneous decay of individual atoms, and γ, describing dephasing of individual atoms.

The dotted lines in fig. 5.6 show results of target state- and intermediate state fidelities under rather high decay rates $\Gamma = \gamma = 0.1/T_+$, where T_+ is the conversion time for the scheme via $|\chi_{2+}\rangle$. Of course, the target state fidelities are reduced compared to the closed system dynamics as spontaneous decay introduces quantum jumps from $|r\rangle_n \to |g\rangle_n$ at individual atoms. Consequently, neither the state $|rrr\rangle$ nor the GHZ state is stable. Since these deleterious effects depend on decay rates and the introduced error accumulates over time, the faster conversion scheme via $|\chi_{20}\rangle$ is less affected. Hence, the faster conversion scheme is, in general, to be preferred.

Figure 5.7 visualizes another aspect of the open system dynamics. Other states not part of the effective four-level system selected by the respective matching conditions show non-zero fidelities over the conversion time; thus, their occupation does not vanish anymore. Since dephasing and spontaneous decay are local errors considered at each atom individually, they connect the decoupled effective four-level system with the remaining part. For high rates Γ and γ, the description via an effective four-level system breaks down.

Experimental uncertainties are another possible source of errors. The precision demanded by the proposed scheme is very high since the atoms have to be positioned at length scales compared with the Rydberg transition wavelength to control the local phases at individual atoms. It is of no interest for the faster conversion scheme via $|\chi_{20}\rangle$. Since, in this case, all laser fields are aligned, all induced phases $\boldsymbol{k}_j \cdot \boldsymbol{x}_n = \boldsymbol{k}_1 \cdot \boldsymbol{x}_n$. As mentioned before, the phases induced by the first laser field connecting the ground state to the twisted W state $\widehat{\mathrm{U}}(\boldsymbol{k}_1)|\chi_{10}\rangle$ can be taken as phase reference. Hence, random positions do not affect the conversion scheme via $|\chi_{20}\rangle$.

Unfortunately, the site-dependent phases are not the only parameter depending on the positions of the atoms. The interaction potential V scales for real pairs of Rydberg systems strongly with the interatomic distance as $V(d) \sim C_6/d^6$, where C_6 is the van der Waals interaction coefficient [47]. Hence, if we investigate erroneous positions, we have erroneous interatomic distances, and the ensemble of three atoms differs from the assumed equilateral triangle.

To account for such experimental positioning errors, we calculated the time evolution of the eight-dimensional system according to eq. (5.76) with random errors on the atomic positions resulting in individual and varying interatomic potentials V_{pq}.

For each position, we drew random errors such that the atomic positions changed $\boldsymbol{x}_n \to \boldsymbol{x}_n + \boldsymbol{\varepsilon}_n$. The nine individual errors – one for each atomic coordinate – were independently drawn from a normal distribution of mean zero and standard deviation σ. From these random positions, the interatomic distances d_{pq} and the resulting interatomic potential were calculated as $V(d_{pq}) = Vd^6/d_{pq}^6$. V and d are the ideally aspired values without any positioning errors. We sampled the time evolution for different values of the standard deviation σ and a sample size S. Since the interatomic potential depends on the interatomic distances d_{pq} rather than independent atomic coordinates, we compiled all $3S$ distances d_{pq} per sample and calculated a standard deviation according to

$$\sigma_d = \sqrt{\overline{\left(d_{pq} - \overline{d_{pq}}\right)^2}} \,. \tag{5.78}$$

$\overline{d_{pq}}$ is the mean value of all $3S$ interatomic distances d_{pq}. Results displayed over this value rather than the standard deviation σ for

each coordinate better suit the intuition of how strong the interatomic potential is affected.

For the simulation, we tried to adopt reasonable parameters corresponding roughly to the $n = 50$ Rydberg state of Rubidium, interatomic distance of an ideal interatomic distance of 4μm and a for a conversion time of the scheme of $T_0 = 1\mu$s. Rubidium atoms are often used in real experiments with tweezer arrays and such experimental parameters are not out of reach [47].

Figure 5.8 shows result for such a simulation for standard deviations $\sigma \in [0, 0.1\lambda_0]$ and a sample size of $S = 1000$ where λ_0 is the wavelength of the Rydberg transition. The other parameter values for the presented calculations are $VT/\hbar \approx 30.86$, where T_0 is the conversion time, and $d = 40\lambda_0$.

Figure 5.8 shows obtained mean target state fidelities $\overline{\mathcal{F}}_{|\mathrm{GHZ}\rangle}(T_0)$ and corresponding standard deviations

$$\sigma_{\mathcal{F}} = \sqrt{\overline{\left(\mathcal{F}_{|\mathrm{GHZ}\rangle} - \overline{\mathcal{F}}_{|\mathrm{GHZ}\rangle}\right)^2}} \tag{5.79}$$

of all S calculated fidelities per sample at the end of the quantum state conversion.

We infer that the fidelity stays relatively high for low variations in the interatomic distance. It speaks for the experimentally feasibility if such accurate precision in positioning of the atoms can be achieved.

In conclusion, we numerically validated the reduction scheme employing selection rules and phase-matching conditions. We investigated some sources of error and concluded that the conversion scheme stays relatively robust even under small interatomic distance variations. However, Rydberg transitions mainly lie in the ultraviolet part of the electromagnetic spectrum; thus, their wavelengths are the smallest in the optical regime. Despite recent advances in Rydberg experiments in tweezer arrays [129, 130], it is still very demanding to achieve such high precision in atom localization as assumed in our simulations. However, it may be experimentally feasible with further improvements in the future.

5.6.2 *Reduction via lifted degeneracies*

Section 5.5.2 presents the possibility of reducing the eight-level quantum system of the Rydberg trimer to an effective four-level system by lifting degeneracies by applying an additional off-resonant laser field. This dressing field with Rabi frequency Ω_0 shifts the energy levels depending on their chirality towards its phase reference. Then, the weaker ladder fields can address specific non-degenerate transitions between the four twisted states $|\mathrm{D}_3^{(a)}(\boldsymbol{k}_0)\rangle$ by taking the small energy shifts via fine detunings into account. The effective Rabi frequencies in the four-level system depend on the relative alignments of the ladder

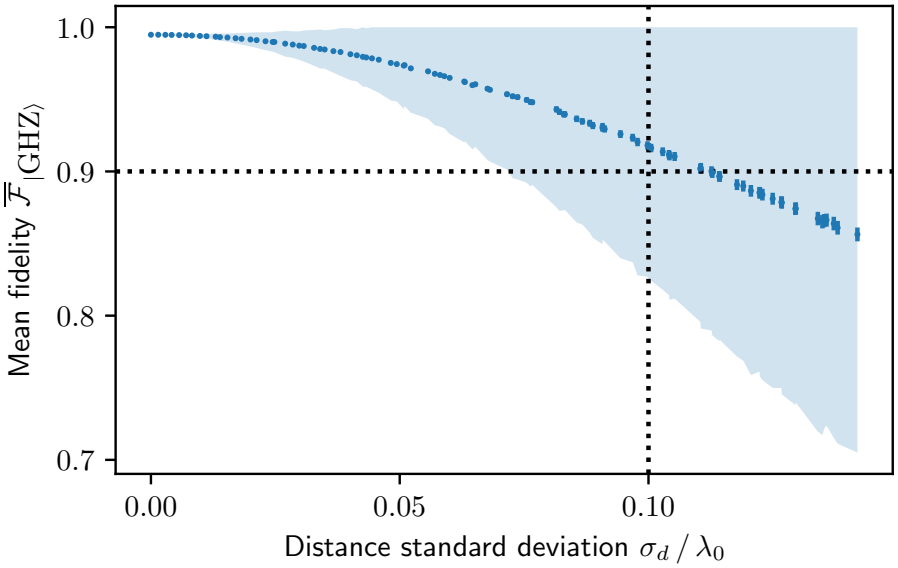

Figure 5.8: Mean values of the target-state fidelity $\mathcal{F}_{|\mathrm{GHZ}\rangle}(T_0) = |\langle \mathrm{GHZ}|\psi(T_0)\rangle|^2$ [cf. eq. (5.77)] at the conversion time T_0. The W to GHZ state conversion via $|\chi_{20}\rangle$ (o-case) was calculated with random positioning errors ϵ_n drawn component-wise from a standard normal distribution with standard deviations $\sigma^2/\lambda 0 \in [0, 0.1]$ and a sample size $S = 1000$. σ_d^2 is the standard deviation for all $3S$ calculated values of d_{pq} per sample. $VT_0/\hbar \approx 30.86$ and $d = 40\lambda_0$. λ_0 is the resonance wavelength, and T_0 is the considered conversion time. The shaded areas indicates the standard deviation $\sigma_{\mathcal{F}}$ of the target-state fidelity, and the error bars the standard error $\sigma_{\mathcal{F}}/\sqrt{S}$.

fields towards the strong dressing field. In the presented simulations, we take the twisting induced by the strong field as phase reference by setting $\boldsymbol{k}_0 \cdot \boldsymbol{x}_n = 0$, i.e., $\widehat{\mathrm{U}}(\boldsymbol{k}_0) = \mathbb{1}$.

We simulated the eight-dimensional Rydberg trimer system with the interaction Hamiltonian

$$\widehat{\mathrm{H}}_{\mathrm{I}} = \widehat{\mathrm{H}}_3^{\mathrm{off}}(\boldsymbol{k}_0) + \sum_{j=1}^{3}\sum_{n=1}^{3} \hbar\Omega_j(t) \mathrm{e}^{\mathrm{i}(\boldsymbol{k}_j\cdot\boldsymbol{x}_n - \delta_j t)} |r\rangle_{nn}\langle g| \,. \tag{5.80}$$

In contrast to the interaction Hamiltonian in eq. (5.76) of the preceding section, we include the interaction part due to V in $\widehat{\mathrm{H}}_0$ to calculate the interaction picture. As before, we disregarded the fast dynamics due to $\widehat{\mathrm{H}}_{\mathrm{A}}$. Additionally, we neglected fast Rabi oscillations induced by the dressing field. Instead, we only consider it via off-resonant leading corrections $\widehat{\mathrm{H}}_3^{\mathrm{off}}(\boldsymbol{k}_0)$. Hence, we neglected fast oscillatory behavior on the time scale of the generalized Rabi frequency induced by strong dressing drive to concentrate on the slower dynamics induced by the driving fields enumerated $j = 1, 2, 3$ instead.

We numerically solved the time-evolution according to eq. (5.73) with $\Gamma = \gamma = 0$ and the interaction Hamiltonian in eq. (5.80) using the

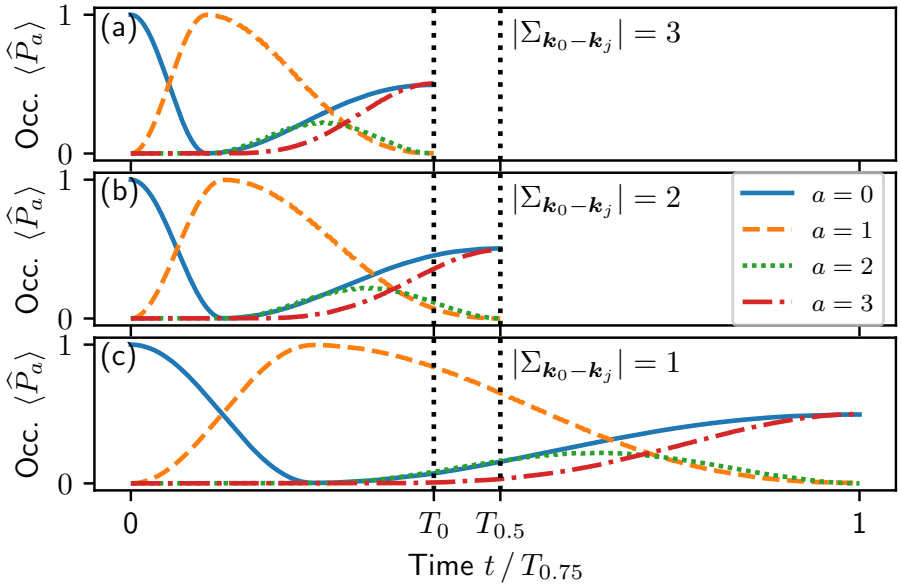

Figure 5.9: Expectation values $\langle P_a \rangle = \langle \psi(t)|P_a|\psi(t)\rangle$ for the occupation of atomic subspace with a excitations over time for a series of conversion schemes $|ggg\rangle \xrightarrow{\pi\text{-pulse}} |D_1^3(\boldsymbol{k}_0)\rangle \xrightarrow{\textit{section 4.7}} |\mathrm{GHZ}\rangle$. Each panel shows a different amount of relative twisting $|\Sigma_{\boldsymbol{k}_0-\boldsymbol{k}_j}| = 3, 2, 1$ (a-c). $T_{0,0.5,0.75}$ is the respective conversion time under the assumption of equal TSPA [cf. eq. (4.49)].

Python package QuTiP [161, 162]. We applied effective Rabi frequencies realizing the W to GHZ state conversion established in section 4.7. Before the mentioned state conversion occurred, a π pulse transferred the system from the ground state into the $|\mathrm{D}_3^{(1)}(\boldsymbol{k}_0)\rangle$. The effective Rabi frequencies were adopted to different relative alignments of the laser fields described by the parameters $\Sigma_{\boldsymbol{k}_0-\boldsymbol{k}_j}$, i.e., the relative twisting between the strong dressing field and the ladder fields [cf. eqs. (5.69a) and (5.72)].

Additionally, the Rabi frequencies were normalized to have the same TSPA [cf. eq. (4.49)] resulting in different conversion times. Higher relative twisting, i.e., lower $\Sigma_{(\boldsymbol{k}_0-\boldsymbol{k}_j)}$, leads to lower effective Rabi frequencies $\widetilde{\Omega}_j$ and longer conversion times. Further simulation parameters are $\Omega_0/\Delta_0 = -0.03$ and $\hbar\Delta_0/V = -0.7$. These parameters ensure that the assumptions to derive the twisted ladder Hamiltonian in eq. (5.72) are satisfied.

Figure 5.9 shows the populations of the effective four-level system during the conversion time for three different values of $\Sigma_{\boldsymbol{k}_0-\boldsymbol{k}_j} = 3, 2, 1$ (the same for all j). The fastest conversion time appears if all laser fields are aligned, i.e. $\Sigma_{\boldsymbol{k}_0-\boldsymbol{k}_j} = 3$ for all j. The π pulse transfers the population from the initially occupied ground state into the W state, and the subspace $a = 1$ reaches full occupation. The following state conversion prepared a GHZ state, as can be seen by the populations

of ground and fully excited states being one-half while all other populations vanish.

Because even more assumptions are involved in achieving the reduction by employing lifted degeneracies, we do not further investigate this reduction scheme or address deleterious effects for now. For open system dynamics, the effects will be comparable to the last section: diminish target state fidelity and reconnect the decoupled subspace. On the one hand, an investigation of varying V is more demanding than in the previous case since the degeneracy of atomic states of equal excitation number was assumed throughout the whole derivation of the twisted ladder Hamiltonian. On the other hand, the shift parameters s_a depend on the atomic interaction and the detuning Δ_0. Small changes in V due to distance variation should not lead to devastating effects when the latter Δ_0 dominates the energy shifts.

5.7 CONCLUSION AND SUMMARY

5.7.1 *Conclusion*

As already mentioned, systems of neutral Rydberg atoms are envisioned to be of high importance in QIP. Here, we discussed a simple interacting N-qubit system to model such Rydberg systems. *Zheng et al.* discussed a reduction of the same system for $N = 3, 4$ and reduced it to an effective 4LS [109]. We generalized their discussion by deriving effective Hamiltonians for arbitrary atom number N and site-dependent phases into the description resulting in the adaption of twisting and twisted states.

Furthermore, we showed that a strong dressing field is not strictly necessary, but also phase matching conditions can be exploited to reduce the system to an effective ladder Hamiltonians of lower dimension.

We utilized the derived effective Hamiltonians to describe several applications. We showed a straightforward preparation scheme for twisted W states representing chiral states in the particular case of three atoms. These chiral states allow for implementing noiseless-subsystem encoding [144, 145]. To the best of our knowledge and although implemented in other types of QIP systems [154], there exists so far no implementation in neutral atoms.

In the Hamiltonians for $N = 3$, it is possible to implement the state conversion scheme from chapter 4. In the context of the Rydberg trimer, it transforms the W state into the GHZ state. We investigated the feasibility of our proposed scheme based on matching conditions numerically, showing that it is relatively robust against minor deviations if a high precision in atom positioning can be achieved in general.

An investigation of the second lifted degeneracy-based scheme to the same detail is a possible future research direction. Especially if there is any advantage in comparison to the matching condition-based scheme in terms of efficiency or robustness is an interesting open question. Also, comparisons to other preparation and conversion schemes in neutral Rydberg atoms describing different models for the system, e.g., via chirped laser pulses [164], can be conducted.

From an experimental viewpoint, the strongest assumption is the high accuracy necessary for the discussed preparation and conversion schemes. Despite recent advances in subwavelength positioning of Rydberg atoms in tweezer arrays [129, 130], achieving such high precision is still experimentally challenging. With improving technical capabilities, we hope our proposed quantum state preparation and conversion schemes may be experimentally feasible in upcoming setups for neutral Rydberg atoms, and we keenly hope for the implementation of one of our proposed schemes in an actual experimental setup.

5.7.2 *Summary*

This chapter contains the discussion of a system of N pairwise interacting qubits and their interaction with several modes of the electromagnetic field. The system is supposed to model an ensemble of neutral Rydberg atoms interacting via their pairwise dipole-dipole interaction and controlled by external laser fields.

The general system properties with special emphasis on systems of equidistant atoms are discussed in section 5.1. Section 5.2 introduces special states of the atomic ensemble and different appropriate bases which are used in the following chapters. It introduces Dicke states as generalization of W states to higher excitation numbers and the concept of twisting and twisted states. In section 5.3, we deduced effective Hamiltonians employing the resolvent formalism and assuming the considered electromagnetic fields to resemble classical laser fields, either far off-resonant to all energy transitions of the atomic ensemble or resonant to a specific one. An immediate application of one of the latter cases, is an preparation scheme for chiral states presented in section 5.4. Section 5.5 presents two possibilities to reduce a Rydberg-atom trimer, modeled by a three qubit system, to an effective four-level quantum system controllable by various laser fields. The effective descriptions result in ladder Hamiltonians as discussed in section 4.6. Section 5.6 presents numerical implementation of the considered trimer model and shows that the reduction schemes from the preceding section result in effective 4LS dynamics. As an example, the state conversion scheme from section 4.7 is implemented, which realizes a W to GHZ state conversion in the context of the Rydberg trimer model.

Much of the presented content is a more detailed version of a similar discussion published by the author, *Gernot Alber*, and *Vladimir Stojanović* in *Physical Review Research* [64]. In what follows, we give a short description of how content presented in this chapter relates to content in the mentioned publication.

The general description of the system and the discussion of the relevant states of the atomic ensemble in sections 5.1 and 5.2 is related to sections II. and III. in [64]. Section 5.3 and appendix B describe the derivation of the effective Hamiltonian more extensively than the corresponding section IV. in [64]. The preparation scheme for chiral states in section 5.4 corresponds to section V. in [64]. The reduction schemes from section 5.5 and the numerical validations in section 5.6 were presented in a condensed version in section VI. of [64]. The numerical calculations presented here in section 5.6 are calculated anew and are showing different data, although mostly the same simulation parameters were used. Figures 5.1, 5.2 and 5.9 are reprinted from [64] with only slight changes, e.g., in notation.

6 CONCLUSION

Controlling quantum systems from whole ensembles down to single qubits is essential to implementations of QIP. Even when single-qubit operations are well under control, two-qubit operations often remain challenging. As quantum technologies rapidly evolve, new possibilities to apply theoretical proposals on new or updated QIP platforms will appear in the future.

Quantum state conversion protocols offer a tool case applicable to a wide range of different systems. They can be used to prepare well-defined quantum states. With the Lie-algebraic approach developed in chapter 4 of this dissertation, we give a general description of conversion schemes for two qubits. Although we simplified the discussion by restricting the conversions to a subspace of all possible unitary two-qubit operations, a wide variety of transformations is representable and, therefore, can be described, investigated, and optimized in this approach.

An open question is how to generalize it to systems of more than two qubits. All general mathematical aspects remain similar, but the complexity increases swiftly with additional qubits due to the higher dimension of the Hilbert space and possible representations of the corresponding dynamical symmetry. As we already simplified the description from fifteen to six generators in the presented case of two-qubit state conversion, considering more qubits is challenging due to the exponential growth of the Hilbert-space dimension.

However, in the two-qubit case, we presented a specific state conversion scheme under a constrained Hamiltonian, which can be applied in any four-level quantum system of adjacently connected energy levels. Although it is not the optimal solution, it offers greater flexibility than other conversion schemes due to relative freedom in the form of the applied Rabi frequencies. In addition, it is not vastly outperformed by the optimal solution for the constrained Hamiltonian with specific time-dependent Rabi frequencies or even by unrestricted solutions such as a π pulse directly inducing the desired state conversion. Furthermore, our proposal significantly outperforms previously published schemes addressing the same problem.

In the context of three interacting Rydberg atoms forming a Rydberg trimer, our proposed conversion scheme implements a W to GHZ state conversion. We presented two possible reduction methods to describe the eight-dimensional quantum system as an effective 4LS of adjacently connected energy levels. The two reduction schemes differ in complexity and the set of states participating in the effective four-level

dynamics. Both emphasize the role of phase differences induced by different laser fields in the system. These phase differences correspond to the position of atoms relative to each other and the fields. They led to the concept of twisting and twisted states proposed as viable tools to implement QIP tasks. In addition to the mentioned (twisted) W to GHZ state conversion schemes, we presented a straightforward proposal for the quantum state preparation of such twisted W states, including the preparation of chiral states in the three-qubit case.

All applications presented in chapter 5 for the Rydberg-trimer model rely heavily on model assumptions that the system must fulfill. Although we roughly estimated possible errors via numerical validations of our reduction schemes and the implemented conversion protocols, the level of accuracy necessary to implement our proposals is still challenging. A more specific investigation of the experimental feasibility of all our proposed schemes is keenly desired and opens up a future research direction, ideally, closely connected to an actual experimental realization. Recent and ongoing advances in experimental techniques for neutral Rydberg atom systems spark the hope that our theoretical considerations may be applicable in the not-to-distant future.

Furthermore, as inferable from mapping the abstract quantum conversion scheme of chapter 4 to the more specific model of interacting Rydberg atoms in chapter 5, there might be different systems on which solutions made in the process of the presented research can find an application, as theoretical models often show high flexibility on which concrete systems they are implemented.

APPENDIX

A

DETAILS REGARDING TWO-QUBIT QUANTUM STATE CONVERSION

This appendix gives some more details of the calculations in chapter 4 regarding the two-spin quantum state conversion and the presented Lie-algebraic approach. We omit most of the definitions here, but always reference the according equations and other references in the main text.

A.1 TRANSFORMATIONS OF PSEUDOSPIN STATES

The action of the unitary transformation $\widehat{\mathrm{U}}(\boldsymbol{\alpha},\boldsymbol{\beta})$ in eq. (4.7) onto the pseudospin eigenbasis of eqs. (4.6) in the computational basis [cf. eqs. (4.1)] is

$$\widehat{\mathrm{U}}(\boldsymbol{\alpha},\boldsymbol{\beta})|{\uparrow\uparrow}\rangle \to \frac{1}{\sqrt{2}}\begin{pmatrix} -\mathrm{i}M_{++}(\boldsymbol{\alpha})M_{++}(\boldsymbol{\beta}) - \mathrm{i}M_{+-}(\boldsymbol{\alpha})M_{+-}(\boldsymbol{\beta}) \\ -\mathrm{i}M_{++}(\boldsymbol{\alpha})M_{+-}(\boldsymbol{\beta}) - \mathrm{i}M_{+-}(\boldsymbol{\alpha})M_{++}(\boldsymbol{\beta}) \\ M_{++}(\boldsymbol{\alpha})M_{++}(\boldsymbol{\beta}) - M_{+-}(\boldsymbol{\alpha})M_{+-}(\boldsymbol{\beta}) \\ -M_{++}(\boldsymbol{\alpha})M_{+-}(\boldsymbol{\beta}) + M_{+-}(\boldsymbol{\alpha})M_{++}(\boldsymbol{\beta}) \end{pmatrix}, \tag{A.1a}$$

$$\widehat{\mathrm{U}}(\boldsymbol{\alpha},\boldsymbol{\beta})|{\uparrow\downarrow}\rangle \to \frac{1}{\sqrt{2}}\begin{pmatrix} \mathrm{i}M_{++}(\boldsymbol{\alpha})M^*_{+-}(\boldsymbol{\beta}) - \mathrm{i}M_{+-}(\boldsymbol{\alpha})M^*_{++}(\boldsymbol{\beta}) \\ -\mathrm{i}M_{++}(\boldsymbol{\alpha})M^*_{++}(\boldsymbol{\beta}) + \mathrm{i}M_{+-}(\boldsymbol{\alpha})M^*_{+-}(\boldsymbol{\beta}) \\ -M_{++}(\boldsymbol{\alpha})M^*_{+-}(\boldsymbol{\beta}) - M_{+-}(\boldsymbol{\alpha})M^*_{++}(\boldsymbol{\beta}) \\ -M_{++}(\boldsymbol{\alpha})M^*_{++}(\boldsymbol{\beta}) - M_{+-}(\boldsymbol{\alpha})M^*_{+-}(\boldsymbol{\beta}) \end{pmatrix}, \tag{A.1b}$$

$$\widehat{\mathrm{U}}(\boldsymbol{\alpha},\boldsymbol{\beta})|{\downarrow\uparrow}\rangle \to \frac{1}{\sqrt{2}}\begin{pmatrix} -\mathrm{i}M^*_{++}(\boldsymbol{\alpha})M_{+-}(\boldsymbol{\beta}) + \mathrm{i}M^*_{+-}(\boldsymbol{\alpha})M_{++}(\boldsymbol{\beta}) \\ -\mathrm{i}M^*_{++}(\boldsymbol{\alpha})M_{++}(\boldsymbol{\beta}) + \mathrm{i}M^*_{+-}(\boldsymbol{\alpha})M_{+-}(\boldsymbol{\beta}) \\ -M^*_{++}(\boldsymbol{\alpha})M_{+-}(\boldsymbol{\beta}) - M^*_{+-}(\boldsymbol{\alpha})M_{++}(\boldsymbol{\beta}) \\ M^*_{++}(\boldsymbol{\alpha})M_{++}(\boldsymbol{\beta}) + M^*_{+-}(\boldsymbol{\alpha})M_{+-}(\boldsymbol{\beta}) \end{pmatrix}, \tag{A.1c}$$

and

$$\widehat{\mathrm{U}}(\boldsymbol{\alpha},\boldsymbol{\beta})|{\downarrow\downarrow}\rangle \to \frac{1}{\sqrt{2}}\begin{pmatrix} -\mathrm{i}M^*_{++}(\boldsymbol{\alpha})M^*_{++}(\boldsymbol{\beta}) - \mathrm{i}M^*_{+-}(\boldsymbol{\alpha})M^*_{+-}(\boldsymbol{\beta}) \\ +\mathrm{i}M^*_{++}(\boldsymbol{\alpha})M^*_{+-}(\boldsymbol{\beta}) + \mathrm{i}M^*_{+-}(\boldsymbol{\alpha})M^*_{++}(\boldsymbol{\beta}) \\ -M^*_{++}(\boldsymbol{\alpha})M^*_{++}(\boldsymbol{\beta}) + M^*_{+-}(\boldsymbol{\alpha})M^*_{+-}(\boldsymbol{\beta}) \\ -M^*_{++}(\boldsymbol{\alpha})M^*_{+-}(\boldsymbol{\beta}) + M^*_{+-}(\boldsymbol{\alpha})M^*_{++}(\boldsymbol{\beta}) \end{pmatrix}. \tag{A.1d}$$

The functions M_{++} and M_{+-} are defined in eqs. (4.10c) and (4.10d).

A.2 ITERATED COMMUTATORS

To evaluate the iterated commutator in eq. (4.12), we distinguish odd and even values of n and discuss the resulting power series independently. All the following considerations for $\boldsymbol{\alpha}\cdot\widehat{\boldsymbol{S}}$ hold analogous for $\boldsymbol{\beta}\cdot\widehat{\boldsymbol{T}}$. Starting with

$n = 1$, we calculate using Einstein summation convention (i.e., implying a summation over indices appearing twice)

$$[\boldsymbol{\alpha}\cdot\widehat{\mathbf{S}},\boldsymbol{\gamma}\cdot\widehat{\mathbf{S}}] = \alpha_i\gamma_j[\widehat{\mathrm{S}}_i,\widehat{\mathrm{S}}_j] = \alpha_i\gamma_j\mathrm{i}\epsilon_{ijk}\widehat{\mathrm{S}}_k = \mathrm{i}(\boldsymbol{\alpha}\times\boldsymbol{\gamma})\cdot\widehat{\mathbf{S}}\,, \tag{A.2}$$

where we have used the su(2)-commutation relations from eqs. (4.5) and $\boldsymbol{\gamma}$ is some three-dimensional vector. The following results can be shown via induction. The odd terms are

$$[\boldsymbol{\alpha}\cdot\widehat{\mathbf{S}},\boldsymbol{\gamma}\cdot\widehat{\mathbf{S}}]_{2n+1} = \mathrm{i}\frac{(\sqrt{\boldsymbol{\alpha}\cdot\boldsymbol{\alpha}})^{2n+1}}{\sqrt{\boldsymbol{\alpha}\cdot\boldsymbol{\alpha}}}(\boldsymbol{\alpha}\times\boldsymbol{\gamma})\cdot\widehat{\mathbf{S}}\,, \tag{A.3a}$$

such that

$$\sum_{n=0}^{\infty}\frac{[\boldsymbol{\alpha}\cdot\widehat{\mathbf{S}},\boldsymbol{\gamma}\cdot\widehat{\mathbf{S}}]_{2n+1}}{(2n+1)!} = \frac{\mathrm{i}\sinh(\sqrt{\boldsymbol{\alpha}\cdot\boldsymbol{\alpha}})}{\sqrt{\boldsymbol{\alpha}\cdot\boldsymbol{\alpha}}}(\boldsymbol{\alpha}\times\boldsymbol{\gamma})\cdot\widehat{\mathbf{S}}\,. \tag{A.3b}$$

The even terms are

$$[\boldsymbol{\alpha}\cdot\widehat{\mathbf{S}},\boldsymbol{\gamma}\cdot\widehat{\mathbf{S}}]_{2n} = -\frac{(\sqrt{\boldsymbol{\alpha}\cdot\boldsymbol{\alpha}})^{2n}}{\boldsymbol{\alpha}\cdot\boldsymbol{\alpha}}\big(\boldsymbol{\alpha}\times(\boldsymbol{\alpha}\times\boldsymbol{\gamma})\big)\cdot\widehat{\mathbf{S}}\,, \tag{A.4a}$$

such that

$$\sum_{n=1}^{\infty}\frac{[\boldsymbol{\alpha}\cdot\widehat{\mathbf{S}},\boldsymbol{\gamma}\cdot\widehat{\mathbf{S}}]_{2n}}{(2n)!} = \frac{1-\cosh(\sqrt{\boldsymbol{\alpha}\cdot\boldsymbol{\alpha}})}{\boldsymbol{\alpha}\cdot\boldsymbol{\alpha}}\big(\boldsymbol{\alpha}\times(\boldsymbol{\alpha}\times\boldsymbol{\gamma})\big)\cdot\widehat{\mathbf{S}}\,. \tag{A.4b}$$

We explicitly wrote here $\sqrt{\boldsymbol{\alpha}\cdot\boldsymbol{\alpha}}$ instead of $|\boldsymbol{\alpha}|^2$ to be able to discuss a vector of the form $\mathrm{i}\boldsymbol{\alpha}$. If now $\boldsymbol{\alpha}\to\mathrm{i}\boldsymbol{\alpha}$, we have $\sqrt{\boldsymbol{\alpha}\cdot\boldsymbol{\alpha}}\to\mathrm{i}|\boldsymbol{\alpha}|$. With $\sinh(\mathrm{i}x) = \mathrm{i}\sin(x)$ and $\cosh(\mathrm{i}x) = \cos(x)$ [165], we get the terms used repeatedly in the context of eq. (4.12).

A.3 PARAMETERS DESCRIBING A GHZ-STATES

In this appendix, we describe in more detail how to derive the simplified conditions in eqs. (4.39) to realize a GHZ states from the initial state $|01\rangle$, as it is the task in section 4.7. We have to describe the target state [cf. eq. (4.34b)] in terms of the rotated version of the initial state [cf. eq. (4.34a)]. Hence,

$$\begin{aligned}|\psi(t=T)\rangle &= \frac{1}{\sqrt{2}}\Big(|00\rangle + \mathrm{e}^{\mathrm{i}\phi}|11\rangle\Big) &\text{(A.5a)}\\ &= \frac{1}{2}\Big(\mathrm{i}|\uparrow\uparrow\rangle + \mathrm{i}|\downarrow\downarrow\rangle - \mathrm{e}^{\mathrm{i}\phi}|\uparrow\downarrow\rangle + \mathrm{e}^{\mathrm{i}\phi}|\downarrow\uparrow\rangle\Big)\\ &= \mathrm{e}^{-\mathrm{i}\boldsymbol{\alpha}(T)\cdot\widehat{\mathbf{S}}}\mathrm{e}^{-\mathrm{i}\boldsymbol{\beta}(T)\cdot\widehat{\boldsymbol{T}}}\frac{\mathrm{i}}{\sqrt{2}}\left(|\downarrow\uparrow\rangle + |\downarrow\uparrow\rangle\right)\,. &\text{(A.5b)}\end{aligned}$$

Using the equations (A.1) for the rotated pseudospin eigenvectors we obtain the following set of equations. Each equation stands for the absolute value of the projection of a GHZ state onto the computational basis, i.e. $|\langle i|\psi(T)\rangle|$. We use the absolute value, since we do not want to predetermine the relative phase ϕ. It follows that a curve $(\boldsymbol{\alpha},\boldsymbol{\beta})(t)$ with initial state $|\psi(t=0)\rangle = |01\rangle$ to realize a GHZ state at time $t = T$ has necessarily to fulfill

$$\frac{1}{\sqrt{2}} = \left|\mathrm{Im}\left[M_{+-}(\boldsymbol{\alpha}(T))M^*_{++}(\boldsymbol{\beta}(T)) - M_{++}(\boldsymbol{\alpha}(T))M^*_{+-}(\boldsymbol{\beta}(T))\right]\right|\,, \tag{A.6a}$$

$$0 = \mathrm{Re}\left[M_{++}(\boldsymbol{\alpha}(T))M^*_{++}(\boldsymbol{\beta}(T)) - M_{+-}(\boldsymbol{\alpha}(T))M^*_{+-}(\boldsymbol{\beta}(T))\right], \tag{A.6b}$$

$$0 = \mathrm{Re}\left[M_{++}(\boldsymbol{\alpha}(T))M^*_{+-}(\boldsymbol{\beta}(T)) + M_{+-}(\boldsymbol{\alpha}(T))M^*_{++}(\boldsymbol{\beta}(T))\right], \tag{A.6c}$$

and

$$\frac{1}{\sqrt{2}} = \left|\,\mathrm{Im}\left[M_{++}(\boldsymbol{\alpha}(T))M^*_{++}(\boldsymbol{\beta}(T)) + M_{+-}(\boldsymbol{\alpha}(T))M^*_{+-}(\boldsymbol{\beta}(T))\right]\,\right|, \tag{A.6d}$$

where Re and Im stand for the real and imaginary part of the functions M_{++} and M_{+-} as defined in eqs. (4.10c) and (4.10d). These conditions are relatively complex functions of the vectors $\boldsymbol{\alpha}$ and $\boldsymbol{\beta}$. Setting $|\boldsymbol{\alpha}| = |\boldsymbol{\beta}| = \pi$ for all t simplifies them significantly. The result is given in eqs. (4.39). This simplification results in equations linear in the vector coordinates.

B

DETAILED DERIVATIONS OF EFFECTIVE RYDBERG HAMILTONIANS

In this appendix, we give some intermediate steps for the derivations of the effective Hamiltonians in section 5.3 in more detail. We start with the off-resonant case of section 5.3.1. Afterward, reusing some results for the off-resonant case, we give more details on the derivation of the effective Hamiltonian resulting from a resonant laser field.

B.1 OFF-RESONANT CASE

To derive eq. (5.30), we have to evaluate the following combination of operators

$$\widehat{\mathrm{P}}_a^{m_0}\,\widehat{\mathrm{H}}_{\mathrm{int}}\,\widehat{\mathrm{P}}_{a\mp1}^{m_0\pm1}\,\widehat{\mathrm{H}}_{\mathrm{int}}\,\widehat{\mathrm{P}}_a^{m_0} \tag{B.1}$$

making up the addends in the sum of eq. (5.27). To simplify the derivation, we compensate the site-dependent phases in $\widehat{\mathrm{H}}_{\mathrm{int}}$ with additional unitary transformations. This simplification is possible since $\widehat{\mathrm{U}}(\boldsymbol{k}_0)$ commutes with the projection operators $\widehat{\mathrm{P}}_a^{m_0}$, i.e.,

$$\left[\widehat{\mathrm{P}}_a^{m_0}, \widehat{\mathrm{U}}(\boldsymbol{k}_0)\otimes\mathbb{1}_{\mathrm{F}}\right] = 0\,. \tag{B.2}$$

With the convention $\widehat{\mathrm{P}}_{a<0}^{m_0} = \widehat{\mathrm{P}}_{a>N}^{m_0} = \widehat{\mathrm{P}}_a^{m_0<0} = 0$, we can write the addends with compensated phases as

$$\widehat{\mathcal{C}}_a^{m_0}(\boldsymbol{k}_0) = \widehat{\mathrm{U}}^\dagger(\boldsymbol{k}_0)\widehat{\mathrm{P}}_a^{m_0}\,\widehat{\mathrm{H}}_{\mathrm{int}}\,P_{a\mp1}^{m\pm1}\,\widehat{\mathrm{H}}_{\mathrm{int}}\,\widehat{\mathrm{P}}_a^{m_0}\,\widehat{\mathrm{U}}(\boldsymbol{k}_0)\,. \tag{B.3}$$

We evaluate this operator in multiple steps to be

$$\begin{aligned}
&\widehat{\mathcal{C}}_a^{m_0}(\boldsymbol{k}_0)\\
&= \widehat{\mathrm{U}}^\dagger(\boldsymbol{k}_0)\widehat{\mathrm{P}}_a^{m_0}\,\widehat{\mathrm{H}}_{\mathrm{int}} && \text{(B.3a)}\\
&\quad\times\sum_{n_1<\ldots<n_{a\mp1}}^{N}|\{n_1,\ldots,n_{a\mp1}\}\rangle\langle\{n_1,\ldots,n_{a\mp1}\}|\otimes|m_0\pm1\rangle\langle m_0\pm1|\\
&\quad\times\left(\sum_{n'=1}^{N}d_0^*|g\rangle_{n'n'}\langle r|\hat{\mathrm{a}}_0^\dagger+\mathrm{H.c.}\right)\widehat{\mathrm{P}}_a^{m_0}\\
&= \widehat{\mathrm{U}}^\dagger(\boldsymbol{k}_0)\widehat{\mathrm{P}}_a^{m_0}\,\widehat{\mathrm{H}}_{\mathrm{int}} && \text{(B.3b)}\\
&\quad\times\sum_{n'=1}^{N}\sum_{n_1<\ldots<n_{a\mp1}}^{N}\Bigg[(1-\chi_{\{n_1,\ldots,n_{a\mp1}\}}^{\{n'\}})d_0^*\sqrt{m\pm1}\\
&\qquad\times|\{n_1,\ldots,n_{a\mp1}\}\rangle\langle\{n_1,\ldots,n_{a\mp1}\}\cup\{n'\}|\\
&\qquad\otimes|m_0\pm1\rangle\langle m_0\pm1-1|\\
&\qquad+\chi_{\{n_1,\ldots,n_{a\mp1}\}}^{\{n'\}}d_0\sqrt{m\pm1+1}\\
&\qquad\times|\{n_1,\ldots,n_{a\mp1}\}\rangle\langle\{n_1,\ldots,n_{a\mp1}\}\setminus\{n'\}|\\
&\qquad\otimes|m_0\pm1\rangle\langle m_0\pm1+1|\Bigg]\widehat{\mathrm{P}}_a^{m_0}\,.
\end{aligned}$$

After the first equality sign, we just have written down $\widehat{\mathrm{P}}_{a\mp1}^{m_0\pm1}$ [cf. eq. (5.23)] and $\widehat{\mathrm{H}}_{\mathrm{int}}$ [cf. eq. (5.7)] explicitly. By doing so, we dropped the sum over all modes j since here we only deal with a single-mode enumerated $j = 0$. After the second equality sign, we used the well-known actions of $\hat{\mathrm{a}}_0$ and $\hat{\mathrm{a}}_0^\dagger$ onto Fock states and the relations for the atomic rising and lowering operator

$$\begin{aligned}&\langle\{n_1,\ldots,n_{a\mp1}\}|g\rangle_{n'n'}\langle r|\\&\quad=(1-\chi^{\{n'\}}_{\{n_1,\ldots,n_{a\mp1}\}})\langle\{n_1,\ldots,n_{a\mp1}\}\cup\{n'\}|\end{aligned}\tag{B.4a}$$

and

$$\begin{aligned}&\langle\{n_1,\ldots,n_{a\mp1}\}|g\rangle_{n'n'}\langle g|\\&\quad=\chi^{\{n'\}}_{\{n_1,\ldots,n_{a\mp1}\}}\langle\{n_1,\ldots,n_{a\mp1}\}\setminus\{n'\}|\,,\end{aligned}\tag{B.4b}$$

respectively. χ is the characteristic function with $\chi^A_B = 1$ if $A \subseteq B$ and 0 otherwise, and it encodes the effect of the atomic rising and lowering operators onto states that already have the n'-th atoms excited or not. In the last line of eq. (B.3a), the action of $\widehat{\mathrm{H}}_{\mathrm{int}}$ (with summation index n) from the left produces four terms –one for each combination of $\{n_1,\ldots,n_a\}$, n' and n. Now, we can partially evaluate the projection $\widehat{\mathrm{P}}_a^{m_0}$. It projects onto subspace containing m_0 photons and exactly a atomic excitations. Therefore, only one term per sign $\pm$ does not vanish, and we get

$$\widehat{\mathcal{C}}_a^{m_0}(\boldsymbol{k}) = \sum_{n_1<\ldots<n_{a\mp1}}^{N}\begin{cases}|d_0|^2(m+1)\sum_{n=1}^N\sum_{n'=1}^N\\\times(1-\chi^{\{n\}}_{\{n_1,\ldots,n_{a-1}\}})|\{n_1,\ldots,n_{a-1}\}\cup\{n\}\rangle\\\times(1-\chi^{\{n'\}}_{\{n_1,\ldots,n_{a-1}\}})\langle\{n_1,\ldots,n_{a-1}\}\cup\{n'\}|\\\quad\otimes|m\rangle\langle m|\\\\|d_0|^2 m\sum_{n=1}^N\sum_{n'=1}^N\\\times\chi^{\{n\}}_{\{n_1,\ldots,n_{a+1}\}}|\{n_1,\ldots,n_{a+1}\}\setminus\{n\}\rangle\\\times\chi^{\{n'\}}_{\{n_1,\ldots,n_{a+1}\}}\langle\{n_1,\ldots,n_{a+1}\}\setminus\{n'\}|\\\quad\otimes|m\rangle\langle m|\,,\end{cases}\tag{B.5}$$

where we have distinguished upper and lower sign cases. Each of the $\binom{N}{a}$ diagonal elements $|\{n_1,\ldots,n_a\}\rangle\langle\{n_1,\ldots,n_a\}|$ in the upper sign case appears a times since there are a different possible values for which $n = n' = n_a \neq n_1,\ldots,n_{a-1}$, while in the lower-sign case, each of these diagonal elements appears $N-a$ times since there are $N-a$ possible values for $n = n' = n_{a+1}$ such that $\{n_1,\ldots,n_{a+1}\}\setminus\{n\} = \{n_1,\ldots,n_a\}$. All off-diagonal elements with $n \neq n'$ appear just once in both cases. The off-diagonal elements are all possible jump-operators between states with Hamming weight a but a Hamming distance of two. Thus, together they form the operator $\widehat{\mathrm{Hd}}_{2,\mathrm{N}}$ as defined in eq. (5.31). Reintroducing the site-dependent phases, we get

$$\begin{aligned}&\widehat{\mathrm{P}}_a^{m_0}\,\widehat{\mathrm{H}}_{\mathrm{int}}\,P_{a\mp1}^{m\pm1}\,\widehat{\mathrm{H}}_{\mathrm{int}}\,\widehat{\mathrm{P}}_a^{m_0} = \widehat{\mathrm{U}}(\boldsymbol{k}_0)\widehat{\mathcal{C}}_a^{m_0}(\boldsymbol{k}_0)\,\widehat{\mathrm{U}}^\dagger(\boldsymbol{k}_0)\\&\quad=\left\{\begin{array}{l}|d_0|^2(m_0+1)\widehat{\mathrm{P}}_a\left[\widehat{\mathrm{Hd}}_{2,\mathrm{N}}(\boldsymbol{k}_0)+a\right]\widehat{\mathrm{P}}_a\\|d_0|^2 m_0\widehat{\mathrm{P}}_a\left[\widehat{\mathrm{Hd}}_{2,\mathrm{N}}(\boldsymbol{k}_0)+(N-a)\right]\widehat{\mathrm{P}}_a\end{array}\right\}\otimes|m_0\rangle\langle m_0|\,.\end{aligned}\tag{B.6}$$

In contrast with the off-diagonal elements, diagonal ones commute with $\widehat{\mathrm{U}}(\boldsymbol{k}_0)$, and thus, they are not affected by the unitary transformation. Equation (B.6) is the result shown in eq. (5.30).

B.2 RESONANT CASE

B.2.1 *Linear terms*

To derive eq. (5.45), we calculate the action of $\widehat{\mathrm{H}}_{\mathrm{int}}$ onto the projectors $\widehat{\mathrm{P}}_a^{m_a}$. As in appendix B.1, we compensate site-dependent phases via the unitary transformation $\widehat{\mathrm{U}}(\boldsymbol{k}_a)$. We calculate the right-hand side of

$$\widehat{\mathcal{C}}_{a,a-1}^{m_a,m_a+1} = \widehat{\mathrm{U}}^\dagger(\boldsymbol{k}_a)\widehat{\mathrm{P}}_a^{m_a}\,\widehat{\mathrm{H}}_{\mathrm{int}}\,\widehat{\mathrm{P}}_{a-1}^{m_a+1}\,\widehat{\mathrm{U}}(\boldsymbol{k}_a) \tag{B.7}$$

to be

$$\begin{aligned}
&\sum_{n_1<\ldots<n_a}^{N} |\{n_1,\ldots,n_a\}\rangle\langle\{n_1,\ldots,n_a\}| \otimes |m_a\rangle\langle m_a| \\
&\times \left(\sum_{n=1}^{N} d_0 |r\rangle_{nn}\langle g|\hat{\mathrm{a}}_0 + \mathrm{H.c.}\right) \\
&\times \sum_{n_1'<\cdots<n_{a-1}'}^{N} |\{n_1',\ldots,n_{a-1}'\}\rangle\langle\{n_1',\ldots,n_{a-1}'\}| \otimes |m_a+1\rangle\langle m_a+1| \\
=& d_a\sqrt{m+1} \sum_{n_1<\ldots<n_a}^{N} \sum_{n_1'<\ldots<n_{a-1}'}^{N} \sum_{n=1}^{N} \chi_{\{n_1',\ldots,n_{a-1}'\}\cup\{n\}}^{\{n_1,\ldots,n_a\}} \left(1-\chi_{\{n_1',\ldots,n_{a-1}'\}}^{\{n\}}\right) \\
&\times |\{n_1,\ldots,n_a\}\rangle\langle\{n_1',\ldots,n_{a-1}'\}| \otimes |m\rangle\langle m+1| \qquad \text{(B.7a)} \\
=& d_a\sqrt{m+1} \sum_{n_1'<\ldots<n_{a-1}'}^{N} \sum_{n=1}^{N} |r\rangle_{nn}\langle g|\{n_1',\ldots,n_{a-1}'\}\rangle\langle\{n_1',\ldots,n_{a-1}'\}| \\
&\otimes |m\rangle\langle m+1|\,. \qquad \text{(B.7b)}
\end{aligned}$$

For the second equality, we just have written down the operators explicitly. For the third equality, we have evaluated the action of $\widehat{\mathrm{H}}_{\mathrm{int}}$ to the right, where the written term excites the n-th atom if and only if it is not already excited (encoded via $1-\chi$) while lowering the photon number of the field. The Hermitian conjugate term has the contrary effect but vanishes due to the orthogonality of the field states, i.e., $\langle m_a|m_a+2\rangle = 0$. The first characteristic function results from the orthogonality of the atomic-ensemble states, and it allows executing the first summation, identifying $n_a = n$, and to rewriting

$$\left(1-\chi_{\{n_1',\ldots,n_{a-1}'\}}^{\{n\}}\right)|\{n_1,\ldots,n_a\}\rangle = |r\rangle_{nn}\langle g|\{n_1',\ldots,n_{a-1}'\}\rangle\,. \tag{B.8}$$

With the definition of the atomic-ensemble raising operator in eq. (5.46a), we get

$$\widehat{\mathrm{P}}_a^{m_a}\,\widehat{\mathrm{H}}_{\mathrm{int}}\,\widehat{\mathrm{P}}_{a-1}^{m_a+1} = \widehat{\mathrm{U}}(\boldsymbol{k}_a)\widehat{\mathcal{C}}_{a,a-1}^{m_a,m_a+1}\,\widehat{\mathrm{U}}^\dagger(\boldsymbol{k}_a)\,, \tag{B.9}$$

which we evaluate as

$$\widehat{\mathrm{P}}_a^{m_a}\,\widehat{\mathrm{H}}_{\mathrm{int}}\,\widehat{\mathrm{P}}_{a-1}^{m_a+1} = d_a\sqrt{m+1}\cdot\widehat{\mathrm{U}}(\boldsymbol{k}_a)\sigma_{a-1}^{+}\,\widehat{\mathrm{U}}^\dagger(\boldsymbol{k}_a)\otimes|m_a\rangle\langle m_a+1|\,. \tag{B.9a}$$

This is the result stated in eq. (5.45). Additional but neglected terms are discussed in what follows.

B.2.2 *Neglected terms*

In this appendix, we determine all further terms of eq. (5.22) neglected in the result of the effective Hamiltonian for a resonant field in eq. (5.52). If we assume the atomic ensemble to interact with a single laser field in resonance to the transition $a \leftrightarrow a-1$ (cf. section 5.3.2), we can separate the general term for an effective Hamiltonian in eq. (5.22) into two parts, whereby only the second contains the resolvent and the first one is

$$\sum_{E\in\sigma(H_0)} \hat{\mathrm{P}}_E \hat{\mathrm{H}} \hat{\mathrm{P}}_E = \hat{\mathrm{H}}_0 + \sum_{m_a=0}^{\infty} \left(\hat{\mathrm{P}}_a^{m_a} \hat{\mathrm{H}}_{\mathrm{int}} \hat{\mathrm{P}}_{a-1}^{m_a+1} + \mathrm{H.c.} \right) . \tag{B.10}$$

This first part contains all terms which contribute to the result in eq. (5.52). Their form and derivation are already explained in detail in the main text of section 5.3.2 and appendix B.2.1, respectively.

The terms containing the resolvent are the ones neglected in eq. (5.52). Regarding the considered transition, all projectors $\hat{\mathrm{P}}_{a'}^{m_a}$ with $a' \neq a, a-1$ are off-resonant. Therefore, eq. (5.32) in section 5.3.1, leaving out $\hat{\mathrm{H}}_0$ and the addends for a and $a-1$, already describes the corresponding terms. For the resonant projectors $\hat{\mathrm{P}}_{a,a-1}^{m_a,m_a+1}$, we evaluate the terms containing the resolvent to be

$$\begin{aligned} &\hat{\mathrm{P}}_{a,a-1}^{m_a,m_a+1} \hat{\mathrm{H}} \hat{\mathrm{Q}}_{a,a-1}^{m_a,m_a+1} \frac{1}{E_a^{m_a} - \hat{\mathrm{Q}}_{a,a-1}^{m_a,m_a+1} \hat{\mathrm{H}}_0 \hat{\mathrm{Q}}_{a,a-1}^{m_a,m_a+1}} \hat{\mathrm{Q}}_{a,a-1}^{m_a,m_a+1} \hat{\mathrm{H}} \hat{\mathrm{P}}_{a,a-1}^{m_a,m_a+1} \\ &\quad = \hat{\mathrm{P}}_a^{m_a} \hat{\mathrm{H}}_{\mathrm{int}} \frac{\hat{\mathrm{P}}_{a+1}^{m_a-1}}{E_a^{m} - E_{a+1}^{m_a-1}} \hat{\mathrm{H}}_{\mathrm{int}} \hat{\mathrm{P}}_a^{m_a} \\ &\qquad + \hat{\mathrm{P}}_{a-1}^{m_a+1} \hat{\mathrm{H}}_{\mathrm{int}} \frac{\hat{\mathrm{P}}_{a-2}^{m_a+2}}{E_{a-1}^{m_a+1} - E_{a-2}^{m_a+2}} \hat{\mathrm{H}}_{\mathrm{int}} \hat{\mathrm{P}}_{a-1}^{m_a+1} , \end{aligned} \tag{B.11}$$

where we used that $\hat{\mathrm{H}}_0$ does not connect different energy subspaces and $\hat{\mathrm{H}}_{\mathrm{int}}$ only adjacent ones [cf. eq. (5.48)]. Using ΔE_a [cf. eq. (5.2)] and the detuning Δ_a [cf. eq. (5.42)], we find the appearing energy differences to be the same since

$$E_a^{m_a} - E_{a+1}^{m_a-1} = -\Delta E_{a+1} + \hbar\omega_a = -V \tag{B.12a}$$

and

$$E_{a-1}^{m_a+1} - E_{a-2}^{m_a+2} = \Delta E_{a-1} - \hbar\omega_a = -V : , \tag{B.12b}$$

respectively. If we introduce the index shifts $a-1 \to a$ and $m_a+1 \to m_a$ in the second term, we can again use the result for the off-resonant fields in eq. (5.30) for the involved operators. With $\hat{\mathrm{H}}_0$ and the results from appendix B.2.1, we can explicitly write down the effective Hamiltonian for a resonant field as

$$\begin{aligned} &\hat{\mathrm{U}}^{\dagger}(\boldsymbol{k}_a)\, \hat{\mathrm{H}}_{\mathrm{eff},N}^{a \leftrightarrow a\text{-}1}\, \hat{\mathrm{U}}(\boldsymbol{k}_a) \\ &= \hat{\mathrm{H}}_0 + \sum_{m_a=0}^{\infty} \Bigg[\left(d^* \sqrt{m+1}\, \hat{\sigma}_a^- \otimes |m_a+1\rangle\langle m_a| + \mathrm{H.c.} \right) \\ &\quad - \frac{|d_a|^2 m_a}{V} \left(\widehat{\mathrm{Hd}}_{2,\mathrm{N}} + (N-a) \right) \hat{\mathrm{P}}_a^{m_a} \end{aligned}$$

$$
\begin{aligned}
&- \frac{|d_a|^2(m_a+2)}{V}\left(\widehat{\mathrm{Hd}}_{2,\mathrm{N}}+a-1\right)\widehat{\mathrm{P}}_{a-1}^{m+1} \\
&+ \sum_{a,a-1\neq a'=0}^{N} |d_a|^2 \\
&\times\left(m_a\frac{\widehat{\mathrm{Hd}}_{2,\mathrm{N}}+(N-a')}{\hbar\Delta_a-a'V}-(m_a+1)\frac{\widehat{\mathrm{Hd}}_{2,\mathrm{N}}+a'}{\hbar\Delta_a-(a'-1)V}\right)\widehat{\mathrm{P}}_{a'}^{m_a}\Bigg] .
\end{aligned}
\tag{B.13}
$$

Finally, assuming $|d_a|^2 m_a \ll |V|, |\Delta_a - a'|V, |\Delta_a - (a'-1)V|$, we can neglect all but the first line of the right-hand side, which leads us to the result in section 5.3.2.

C

DETAILED DERIVATION OF THE TWISTED LADDER HAMILTONIAN

This appendix presents a detailed derivation of the twisted ladder Hamiltonian in eq. (5.72).

We start from eq. (5.70) and calculate the transformation of each a-term separately using the well-known operator identity[1]

$$e^{\hat{A}}\hat{B}e^{-\hat{A}} = \sum_{m=0}^{\infty} \frac{1}{m!}\left[\hat{A},\hat{B}\right]_m , \tag{C.1}$$

where $\left[\hat{A},\hat{B}\right]_m$ is the m-th iteration of the multiple commutator, such that for $n \geq 0$

$$[\hat{A},\hat{B}]_0 = \hat{A} , \tag{C.1a}$$

and

$$[\hat{A},\hat{B}]_{n+1} = [\hat{A},[\hat{A},\hat{B}]_n] . \tag{C.1b}$$

In the following, we will shorten the notation for the unitary transformation $\hat{U}$, omitting its argument most of the time since the index a determines it completely. Further, we take the site-dependent phases induced by the strong dressing field ($j = 0$) as a reference, such that the arguments of all unitary transform as $\hat{U}(\boldsymbol{k}_a) \mapsto \hat{U}(\boldsymbol{k}_a - \boldsymbol{k}_0)$. Especially, $\hat{U}(\boldsymbol{k}_0) \mapsto \mathbb{1}$.

We begin with the $a = 1$-term and calculate the commutator

$$\left[\hat{H}_3^{\text{off}}, \hat{U}\,\hat{\sigma}_1^-\,\hat{U}^\dagger\right] = (3s_0 - s_1)\,\hat{U}\,\hat{\sigma}_1^-\,\hat{U}^\dagger + (s_0 - s_1)\Sigma_{k_0-k_1}\hat{\sigma}_1^- . \tag{C.2}$$

We see that the argument partially reproduces itself and that an additional term with vanishing site-dependent phases appears. Hence, the next iterated commutators will feature the same two operators but with coefficients piling up step by step. The iterative behavior can be formulated by a matrix exponential, such that

$$\begin{aligned} e^{i\hat{H}_3^{\text{off}}t/\hbar}\,\hat{U}\,\hat{\sigma}_1^-\,\hat{U}^\dagger\,e^{-i\hat{H}_3^{\text{off}}t/\hbar} &= \sum_{m=0}^{\infty} \frac{(it\hbar)^m}{m!}\left[\hat{H}_3^{\text{off}}, \hat{U}\,\hat{\sigma}_1^-\,\hat{U}^\dagger\right]_m \\ &= \sum_{m=0}^{\infty} \frac{(it\hbar)^m}{m!} \boldsymbol{v}_1^T \underline{\boldsymbol{A}}_1^m \boldsymbol{e}_1 = \boldsymbol{v}_1^T e^{it\underline{\boldsymbol{A}}_1/\hbar}\boldsymbol{e}_1 , \end{aligned} \tag{C.3}$$

with appropriate vectors

$$\boldsymbol{e}_1 = \begin{pmatrix} 1 \\ 0 \end{pmatrix} , \quad \boldsymbol{v}_1 = \begin{pmatrix} \hat{U}\,\hat{\sigma}_1^-\,\hat{U}^\dagger \\ \hat{\sigma}_1^- \end{pmatrix} , \tag{C.3a}$$

and a triangular matrix

$$\underline{\boldsymbol{A}}_1 = \begin{pmatrix} 3s_0 - s_1 & 0 \\ (s_0 - s_1)\Sigma_{k_0-k_1} & 6s_0 - 4s_1 \end{pmatrix} . \tag{C.3b}$$

1 For a proof of the following general relation, see, e.g., [114, Proposition 3.35].

The eigenvalue spectrum $\sigma(\underline{A}_1) = \{3s_0 - s_1, 6s_0 - 4s_1\}$ describes the additional energy gaps in the transitions $a = 0 \leftrightarrow a = 1$ due to the energy shifts induced by $\widehat{H}_3^{\text{off}}$ [cf. eq. (5.57)].

The transition $a = 2 \leftrightarrow a = 3$ has the same dimensionality and degeneracy. Hence, evaluating the commutator

$$\left[\widehat{H}_3^{\text{off}}, \widehat{U}\,\hat{\sigma}_3^-\,\widehat{U}^\dagger\right] = (-s_1 + 3s_2)\,\widehat{U}\,\hat{\sigma}_3^-\,\widehat{U}^\dagger + (-s_1 + s_2)\Sigma_{k_0-k_3}\hat{\sigma}_3^- \,, \tag{C.4}$$

we find an analogous expression featuring the vectors

$$\boldsymbol{e}_3 = \begin{pmatrix} 1 \\ 0 \end{pmatrix} \,, \quad \boldsymbol{v}_3 = \begin{pmatrix} \widehat{U}\,\hat{\sigma}_3^-\,\widehat{U}^\dagger \\ \hat{\sigma}_3^- \end{pmatrix} \,, \tag{C.5a}$$

and a matrix exponential of

$$\underline{\boldsymbol{A}}_3 = \begin{pmatrix} s_1 + 3s_2 & 0 \\ (-s_1 + s_2)\Sigma_{k_0-k_3} & -4s_1 + 6s_2 \end{pmatrix} \tag{C.5b}$$

with eigenvalue spectrum $\sigma(\underline{A}_3) = \{-s_1 + 3s_2, -4s_1 + 6s_2\}$.

For $a = 2$, we find a similar equation, but since more states are involved in the transition $a = 1 \leftrightarrow a = 2$, the calculation is more complicated. To derive the matrix $\underline{\boldsymbol{A}}_2$, we start with a more general commutator which features unitary transformations $\widehat{U}' = \widehat{U}(\boldsymbol{k}')$ and $\widehat{U} = \widehat{U}(\boldsymbol{k})$ with different wave vectors, such that

$$\begin{aligned}
\left[\widehat{H}_3^{\text{off}}, \widehat{U}'\,\hat{\sigma}_2^-\,\widehat{U}^\dagger\right] &= \Big[\widehat{H}_3^{\text{off}}, 3|\mathrm{D}_3^{(1)}(\boldsymbol{k}')\rangle\langle\mathrm{D}_3^{(2)}(\boldsymbol{k})| \\
&\qquad - \Phi(-\boldsymbol{k}) \sum_{n=1}^{3} \mathrm{e}^{\mathrm{i}(\boldsymbol{k}+\boldsymbol{k})\cdot\boldsymbol{x}_n} |gg\rangle|r\rangle_{nn}\langle g|\langle rr|\Big] \\
&= 2s_1\,\widehat{U}'\,\hat{\sigma}_2^-\,\widehat{U}^\dagger \\
&\quad + 3\Sigma_{\boldsymbol{k}'}(-s_0 + s_1)|\mathrm{D}_3^{(1)}\rangle\langle\mathrm{D}_3^{(2)}(\boldsymbol{k})| \\
&\quad + 3\Sigma_{\boldsymbol{k}}(s_1 - s_2)\Phi(-\boldsymbol{k})|\mathrm{D}_3^{(1)}(\boldsymbol{k}')\rangle\langle\mathrm{D}_3^{(2)}| \\
&\quad + 3\Phi(\boldsymbol{k}')(S_0 - s_1)|\mathrm{D}_3^{(1)}\rangle\langle\mathrm{D}_3^{(2)}(\boldsymbol{k}' + \boldsymbol{k})| \\
&\quad + 3\Phi(-\boldsymbol{k})(-s_1 + s_2)|\mathrm{D}_3^{(1)}(\boldsymbol{k}' + \boldsymbol{k})\rangle\langle\mathrm{D}_3^{(2)}| \,,
\end{aligned} \tag{C.6}$$

where $\Phi(\boldsymbol{k}) = \mathrm{e}^{\mathrm{i}\boldsymbol{k}\cdot\sum_{n=1}^{N}\boldsymbol{x}_n}$. Again, the commutator partially reproduces the operator itself but there are more additional terms. Since each term at least features either an untwisted bra or ket, the iteration would result in a term with $|\mathrm{D}_3^{(1)}\rangle\langle\mathrm{D}_3^{(2)}|$. Therefore, we find a relationship similar to eq. (C.3) with vectors

$$\boldsymbol{e}_2 = \begin{pmatrix} 1 \\ 0 \\ 0 \\ 0 \\ 0 \\ 0 \end{pmatrix} \,, \quad \boldsymbol{v}_2 = \begin{pmatrix} \widehat{U}\,\hat{\sigma}_2^-\,\widehat{U}^\dagger \\ |\mathrm{D}_3^{(1)}\rangle\langle\mathrm{D}_3^{(2)}(\boldsymbol{k})| \\ |\mathrm{D}_3^{(1)}(\boldsymbol{k})\rangle\langle\mathrm{D}_3^{(2)}| \\ |\mathrm{D}_3^{(1)}\rangle\langle\mathrm{D}_3^{(2)}(2\boldsymbol{k})| \\ |\mathrm{D}_3^{(1)}(2\boldsymbol{k})\rangle\langle\mathrm{D}_3^{(2)}| \\ |\mathrm{D}_3^{(1)}\rangle\langle\mathrm{D}_3^{(2)}| \end{pmatrix} \,, \tag{C.7a}$$

and the triangular matrix

$$\underline{\boldsymbol{A}}_2 = \begin{pmatrix} 2s_1 & 0 & 0 \\ 3\Sigma_{\boldsymbol{k}}(-s_0+s_1) & -3s_0+5s_1 & 0 \\ 3\Phi(-\boldsymbol{k})\Sigma_{\boldsymbol{k}}(s_1-s_2) & 0 & 5s_1-3s_2 \\ 3\Phi(\boldsymbol{k})(s_0-s_1) & 0 & 0 \\ 3\Phi(-\boldsymbol{k})(-s_1+s_2) & 0 & 0 \\ 0 & \Phi(-\boldsymbol{k})\Sigma_{\boldsymbol{k}}(s_1-s_2) & \Sigma_{\boldsymbol{k}}(-s_0+s_1) \end{pmatrix} \tag{C.7b}$$

$$\begin{pmatrix} 0 & 0 & 0 \\ 0 & 0 & 0 \\ 0 & 0 & 0 \\ -3s_0+5s_1 & 0 & 0 \\ 0 & 5s_1-3s_2 & 0 \\ \Phi(-2\boldsymbol{k})\Sigma_{2\boldsymbol{k}}(s_1-s_2) & \Sigma_{2\boldsymbol{k}}(-s_0+s_1) & -3s_0+8s_1-3s_2 \end{pmatrix}.$$

$\underline{\boldsymbol{A}}_2$'s eigenvalue spectrum is $\sigma(\underline{\boldsymbol{A}}_2) = \{2s_1, -3s_0+5s_1, 5s_1-3s_2, -3s_0+8s_1-3s_2\}$. The higher dimension of the matrix form represents the higher degeneracy of the considered transition $a=1 \leftrightarrow a=2$.

Reintroducing the site-dependent phases of the strong dressing field, we can merge the results of all three cases as

$$\begin{aligned}
&\widehat{\mathrm{U}}(\boldsymbol{k}_0)\mathrm{e}^{\mathrm{i}\widehat{\mathrm{H}}_3^{\mathrm{off}}t/\hbar}\,\widehat{\mathrm{U}}^\dagger(\boldsymbol{k}_0)\,\widehat{\mathrm{H}}_3^{\mathrm{ladder}}(\{\boldsymbol{k}_a\})\,\widehat{\mathrm{U}}(\boldsymbol{k}_0)\mathrm{e}^{-i\widehat{\mathrm{H}}_3^{\mathrm{off}}t/\hbar}\,\widehat{\mathrm{U}}^\dagger(\boldsymbol{k}_0) \\
&= \widehat{\mathrm{U}}(\boldsymbol{k}_0)\left[\sum_{a=1}^{N}\Omega_a^*\boldsymbol{v}_a\left(\mathrm{e}^{\mathrm{i}tA_a/\hbar}\boldsymbol{e}_a\right)+\mathrm{H.c.}\right]\widehat{\mathrm{U}}^\dagger(\boldsymbol{k}_0) \qquad \text{(C.8)} \\
&= \sqrt{3}\Omega_1^*\begin{pmatrix}|ggg\rangle\langle \mathrm{D}_3^{(1)}(\boldsymbol{k}_1)| \\ |ggg\rangle\langle \mathrm{D}_3^{(1)}(\boldsymbol{k}_0)|\end{pmatrix} \qquad \text{(C.8a)} \\
&\qquad\qquad \cdot\begin{pmatrix}\mathrm{e}^{\mathrm{i}t(3s_0-s_1)/\hbar} \\ (\mathrm{e}^{\mathrm{i}t(6s_0-4s_1)/\hbar}-\mathrm{e}^{\mathrm{i}t(3s_0-s_1)/\hbar})\Sigma_{\boldsymbol{k}_0-\boldsymbol{k}_1}/3\end{pmatrix}+\mathrm{H.c.} \\
&\quad+\sqrt{3}\Omega_3^*\begin{pmatrix}|\mathrm{D}_3^{(2)}(\boldsymbol{k}_3)\rangle\langle rrr|\Phi(-\boldsymbol{k}_0) \\ |\mathrm{D}_3^{(2)}(\boldsymbol{k}_0)\rangle\langle rrr|\Phi(-\boldsymbol{k}_0)\end{pmatrix} \\
&\qquad\qquad \cdot\begin{pmatrix}\mathrm{e}^{\mathrm{i}t(-s_1+3s_2)/\hbar} \\ \left(\mathrm{e}^{\mathrm{i}t(-4s_1+6s_2)/\hbar}-\mathrm{e}^{\mathrm{i}t(-s_1+3s_2)/\hbar}\right)\Sigma_{\boldsymbol{k}_0-\boldsymbol{k}_3}/3\end{pmatrix}+\mathrm{H.c.} \\
&\quad+\Omega_2^*\begin{pmatrix}3|\mathrm{D}_3^{(1)}(\boldsymbol{k}_2)\rangle\langle \mathrm{D}_3^{(2)}(\boldsymbol{k}_2)| \\ |\mathrm{D}_3^{(1)}(\boldsymbol{k}_0)\rangle\langle \mathrm{D}_3^{(2)}(\boldsymbol{k}_2)| \\ |\mathrm{D}_3^{(1)}(\boldsymbol{k}_2)\rangle\langle \mathrm{D}_3^{(2)}(\boldsymbol{k}_0)| \\ |\mathrm{D}_3^{(1)}(\boldsymbol{k}_0)\rangle\langle \mathrm{D}_3^{(2)}(2\boldsymbol{k}_2-\boldsymbol{k}_0)| \\ |\mathrm{D}_3^{(1)}(2\boldsymbol{k}_2-\boldsymbol{k}_0)\rangle\langle \mathrm{D}_3^{(2)}(\boldsymbol{k}_0)| \\ |\mathrm{D}_3^{(1)}(\boldsymbol{k}_0)\rangle\langle \mathrm{D}_3^{(2)}(\boldsymbol{k}_0)|\end{pmatrix}
\end{aligned}$$

$$\cdot \begin{pmatrix} e^{it2s_1/\hbar} \\ \left(e^{it(-3s_0+5s_1)/\hbar} - e^{it2s_1/\hbar}\right) \Sigma_{k_2-k_0} \\ \left(e^{it(5s_1-3s_2)/\hbar} - e^{it2s_1/\hbar}\right) \Sigma_{k_2-k_0} \Phi(k_0-k_2)) \\ \left(-e^{it(-3s_0+5s_1)/\hbar} + e^{it2s_1/\hbar}\right) \Phi(k_2-k_0) \\ \left(e^{it2s_1/\hbar} - e^{it(5s_1-3s_2)/\hbar}\right) \Phi(k_0-k_2) \\ \eta(k_2-k_0) \end{pmatrix} + \text{H.c.}$$

$$- \Omega_2^* e^{it2s_1/\hbar} \Phi(-k_2) \sum_{n=1}^{3} e^{i2k_2x_n} |gg\rangle|r\rangle_{nn}\langle g|\langle rr| + \text{H.c.}$$

with

$$\eta(k) = \frac{2\Sigma_{-k}}{3}\left(e^{it2s_1/\hbar} - e^{it(-3s_0+5s_1)/\hbar} - e^{it(5s_1-3s_2)/\hbar} + e^{it(-3s_0+8s_1-3s_2)/\hbar}\right). \tag{C.8b}$$

From the last equation, we can identify one relevant term per field ($j = a = 1,2,3$) and compensate for the exponential time dependence via fine detunings. Such fine detunings result in phase shifts of the respective Rabi frequencies (cf. eq. (5.71)). Choosing

$$\hbar\delta_1 = -6s_0 + 4s_1\,, \quad \hbar\delta_2 = 3s_0 - 8s_1 + 3s_2\,, \quad \hbar\delta_3 = 4s_1 - 6s_2\,, \tag{C.9}$$

and neglecting terms oscillating with non-vanishing residual frequencies results in the twisted ladder Hamiltonian in eq. (5.72). The remaining terms only include jump operators between twisted states $|D_3^{(a)}(k_0)\rangle$. The neglected terms oscillate with residual frequencies defined via

$$-3s_0 + s_1 - \hbar\delta_1 = 3s_0 - 3s_1\,, \qquad (a=1) \tag{C.10a}$$
$$-2s_1 - \hbar\delta_2 = -3s_0 + 6s_1 - 3s_2\,, \qquad (a=2) \tag{C.10b}$$
$$3s_0 - 5s_1 - \hbar\delta_2 = 3s_1 - 3s_2\,, \qquad (a=2) \tag{C.10c}$$
$$-5s_1 + 3s_2 - \hbar\delta_2 = -3s_0 + 3s_2\,, \qquad (a=2) \tag{C.10d}$$

and

$$s_1 - 3s_2 - \hbar\delta_3 = -3s_1 + 3s_2\,, \qquad (a=3) \tag{C.10e}$$

where each equation corresponds to one residual energy $\hbar\omega_R$, which we compile in the set $\{\omega_R\}$.

BIBLIOGRAPHY

1. Einstein, A., Podolsky, B. & Rosen, N. Can Quantum-Mechanical Description of Physical Reality Be Considered Complete? *Physical Review* **47,** 777–780. doi:10.1103/PhysRev.47.777 (1935) (cit. on pp. iii, 2).
2. Rau, A. R. P. *The Beauty of Physics: Patterns, Principles, and Perspectives* (Oxford University Press, Oxford, 2014) (cit. on pp. iii, 3, 33).
3. Kakalios, J. *The Amazing Story of Quantum Mechanics: A Maths-free Exploration of the Science that Made our World* (Duckworth Overlock, London, New York, 2010) (cit. on p. 1).
4. Acín, A. *et al.* The quantum technologies roadmap: a European community view. *New Journal of Physics* **20,** 080201. doi:10.1088/1367-2630/aad1ea (2018) (cit. on p. 1).
5. FAKSIMILE AUS DEN VERHANDLUNGEN DER DEUTSCHEN PHYSIKALISCHEN GESELLSCHAFT 2 (1900) S. 237: Zur Theorie des Gesetzes der Energieverteilung im Normalspectrum; von M. Planck. *Physik Journal* **4,** 146–151. doi:10.1002/phbl.19480040404 (1948) (cit. on p. 1).
6. Planck, M. Ueber das Gesetz der Energieverteilung im Normalspectrum. *Annalen der Physik* **309,** 553–563. doi:10.1002/andp.19013090310 (1901) (cit. on p. 1).
7. Einstein, A. Über einen die Erzeugung und Verwandlung des Lichtes betreffenden heuristischen Gesichtspunkt. *Annalen der Physik* **322,** 132–148. doi:10.1002/andp.19053220607 (1905) (cit. on p. 1).
8. Fraunhofer, J. Bestimmung des Brechungs- und des Farbenzerstreungsvermögens verschiedener Glasarten, in Bezug auf die Vervollkommnung achromatischer Fernröhre. *Annalen der Physik* **56,** 264–313. doi:10.1002/andp.18170560706 (1817) (cit. on p. 1).
9. Pauli, W. Über das Wasserstoffspektrum vom Standpunkt der neuen Quantenmechanik. *Zeitschrift für Physik* **36,** 336–363. doi:10.1007/BF01450175 (1926) (cit. on pp. 1, 4).
10. Mensing, L. Zur Störungsmechanik der Molekülmodelle. *Zeitschrift für Physik* **34,** 602–610. doi:10.1007/BF01328505 (1925) (cit. on p. 1).
11. Mensing, L. Die Rotations-Schwingungsbanden nach der Quantenmechanik. *Zeitschrift für Physik* **36,** 814–823. doi:10.1007/BF01400216 (1926) (cit. on pp. 1, 4).

12. Rutherford, E. VIII. Uranium radiation and the electrical conduction produced by it. *The London, Edinburgh, and Dublin Philosophical Magazine and Journal of Science* **47,** 109–163. doi:10.1080/14786449908621245 (1899) (cit. on p. 1).

13. Gamow, G. Zur Quantentheorie des Atomkernes. *Zeitschrift für Physik* **51,** 204–212. doi:10.1007/BF01343196 (1928) (cit. on pp. 1, 4).

14. Von Neumann, J. *Mathematische Grundlagen der Quantenmechanik* 2nd ed. doi:10.1007/978-3-642-61409-5 (Springer-Verlag, Berlin, Heidelberg, 1932) (cit. on p. 1).

15. Dirac, P. A. M. *The Principles of Quantum Mechanics* 4th ed. (1930) (cit. on p. 1).

16. Briggs, G. A. D., Butterfield, J. N. & Zeilinger, A. The Oxford questions on the foundations of quantum physics. *Proceedings of the Royal Society A: Mathematical, Physical and Engineering Sciences* **469,** 20130299. doi:10.1098/rspa.2013.0299 (2013) (cit. on p. 1).

17. Ares, N., Pearson, A. N. & Briggs, G. A. D. in *Do Wave Functions Jump?* (eds Allori, V., Bassi, A., Dürr, D. & Zanghi, N.) 361–384 (Springer, Cham, 2021). doi:10.1007/978-3-030-46777-7_25 (cit. on p. 1).

18. Feynman, R. P. Simulating physics with computers. *International Journal of Theoretical Physics* **21,** 467–488. doi:10.1007/BF02650179 (1982) (cit. on p. 1).

19. Nielsen, M. A. & Chuang, I. L. *Quantum Computation and Quantum Information* 10th ed. (Cambridge University Press, Delhi, 2000) (cit. on pp. 2, 4, 40, 44).

20. Dirac, P. A. M. A new notation for quantum mechanics. *Mathematical Proceedings of the Cambridge Philosophical Society* **35,** 416–418. doi:10.1017/S0305004100021162 (1939) (cit. on pp. 2, 137).

21. Shor, P. W. Polynomial-Time Algorithms for Prime Factorization and Discrete Logarithms on a Quantum Computer. *SIAM Journal on Computing* **26,** 1484–1509. doi:10.1137/S0097539795293172 (1997) (cit. on p. 2).

22. Horodecki, R., Horodecki, P., Horodecki, M. & Horodecki, K. Quantum entanglement. *Reviews of Modern Physics* **81,** 865–942. doi:10.1103/RevModPhys.81.865 (2009) (cit. on pp. 2–3).

23. Schrödinger, E. Die gegenwärtige Situation in der Quantenmechanik. *Die Naturwissenschaften* **23** (1935) (cit. on p. 2).

24. Bell, J. S. On the Einstein Podolsky Rosen paradox. *Physics Physique Fizika* **1,** 195–200. doi:10.1103/PhysicsPhysiqueFizika.1.195 (1964) (cit. on p. 2).

25. Aspect, A., Grangier, P. & Roger, G. Experimental Tests of Realistic Local Theories via Bell's Theorem. *Physical Review Letters* **47,** 460–463. doi:10.1103/PhysRevLett.47.460 (1981) (cit. on p. 3).

26. Ursin, R. *et al.* Entanglement-based quantum communication over 144 km. *Nature Physics* **3,** 481–486. doi:10.1038/nphys629 (2007) (cit. on p. 3).

27. Hensen, B. *et al.* Loophole-free Bell inequality violation using electron spins separated by 1.3 kilometres. *Nature* **526,** 682–686. doi:10.1038/nature15759 (2015) (cit. on p. 3).

28. Handsteiner, J. *et al.* Cosmic Bell Test: Measurement Settings from Milky Way Stars. *Physical Review Letters* **118,** 060401. doi:10.1103/PhysRevLett.118.060401 (2017) (cit. on p. 3).

29. Brunner, N., Gisin, N., Scarani, V. & Simon, C. Detection Loophole in Asymmetric Bell Experiments. *Physical Review Letters* **98,** 220403. doi:10.1103/PhysRevLett.98.220403 (2007) (cit. on p. 3).

30. Sauer, A. & Alber, G. Quantum Bounds on Detector Efficiencies for Violating Bell Inequalities Using Semidefinite Programming. *Cryptography* **4,** 2. doi:10.3390/cryptography4010002 (2020) (cit. on p. 3).

31. Sauer, A., Bernád, J. Z., Moreno, H. J. & Alber, G. Entanglement in bipartite quantum systems: Euclidean volume ratios and detectability by Bell inequalities. *Journal of Physics A: Mathematical and Theoretical* **54,** 495302. doi:10.1088/1751-8121/ac3469 (2021) (cit. on p. 3).

32. Bennett, C. H. & Brassard, G. Quantum cryptography: Public key distribution and coin tossing. *Theoretical Computer Science* **560,** 7–11. doi:10.1016/j.tcs.2014.05.025 (2014) (cit. on p. 3).

33. Fitzke, E., Krebs, R., Haase, T., Mengler, M., Alber, G. & Walther, T. Time-dependent POVM reconstruction for single-photon avalanche photo diodes using adaptive regularization. *New Journal of Physics* **24,** 023025. doi:10.1088/1367-2630/ac5004 (2022) (cit. on pp. 3, 12, 139).

34. Bennett, C. H., Brassard, G., Crépeau, C., Jozsa, R., Peres, A. & Wootters, W. K. Teleporting an unknown quantum state via dual classical and Einstein-Podolsky-Rosen channels. *Physical Review Letters* **70,** 1895–1899. doi:10.1103/PhysRevLett.70.1895 (1993) (cit. on p. 3).

35. Boschi, D., Branca, S., De Martini, F., Hardy, L. & Popescu, S. Experimental Realization of Teleporting an Unknown Pure Quantum State via Dual Classical and Einstein-Podolsky-Rosen Channels. *Physical Review Letters* **80,** 1121–1125. doi:10.1103/PhysRevLett.80.1121 (1998) (cit. on p. 3).

36. Bouwmeester, D., Pan, J.-W., Mattle, K., Eibl, M., Weinfurter, H. & Zeilinger, A. Experimental quantum teleportation. *Nature* **390** (eds Ekert, A., Jozsa, R. & Penrose, R.) 575–579. doi:10.1038/37539 (1997) (cit. on p. 3).

37. Nielsen, M. A. Conditions for a Class of Entanglement Transformations. *Physical Review Letters* **83,** 436–439. doi:10.1103/PhysRevLett.83.436 (1999) (cit. on p. 3).

38. Dür, W., Vidal, G. & Cirac, J. I. Three qubits can be entangled in two inequivalent ways. *Physical Review A* **62,** 062314. doi:10.1103/PhysRevA.62.062314 (2000) (cit. on p. 3).

39. Cabello, A. Bell's theorem with and without inequalities for the three-qubit Greenberger-Horne-Zeilinger and W states. *Physical Review A* **65,** 032108. doi:10.1103/PhysRevA.65.032108 (2002) (cit. on p. 3).

40. Koashi, M., Bužek, V. & Imoto, N. Entangled webs: Tight bound for symmetric sharing of entanglement. *Physical Review A* **62,** 050302. doi:10.1103/PhysRevA.62.050302 (2000) (cit. on p. 3).

41. Dür, W. Multipartite entanglement that is robust against disposal of particles. *Physical Review A* **63,** 020303. doi:10.1103/PhysRevA.63.020303 (2001) (cit. on p. 3).

42. Greenberger, D. M., Horne, M. A. & Zeilinger, A. in *Bell's Theorem, Quantum Theory and Conceptions of the Universe* (ed Kafatos, M.) 69–72 (Springer Netherlands, Dordrecht, 1989). doi:10.1007/978-94-017-0849-4 (cit. on p. 3).

43. Greenberger, D. M., Horne, M. A., Shimony, A. & Zeilinger, A. Bell's theorem without inequalities. *American Journal of Physics* **58,** 1131–1143. doi:10.1119/1.16243 (1990) (cit. on p. 3).

44. Bouwmeester, D., Pan, J. W., Bongaerts, M. & Zeilinger, A. Observation of three-photon greenberger-horne-zeilinger entanglement. *Physical Review Letters* **82,** 1345–1349. doi:10.1103/PhysRevLett.82.1345 (1999) (cit. on p. 3).

45. Pan, J.-W., Bouwmeester, D., Daniell, M., Weinfurter, H. & Zeilinger, A. Experimental test of quantum nonlocality in three-photon Greenberger–Horne–Zeilinger entanglement. *Nature* **403,** 515–519. doi:10.1038/35000514 (2000) (cit. on p. 3).

46. Gallagher, T. F. *Rydberg Atoms* doi:10.1017/CBO9780511524530 (Cambridge University Press, Cambridge, 1994) (cit. on pp. 3, 22, 63).

47. Adams, C. S., Pritchard, J. D. & Shaffer, J. P. Rydberg atom quantum technologies. *Journal of Physics B: Atomic, Molecular and Optical Physics* **53,** 012002. doi:10.1088/1361-6455/ab52ef (2020) (cit. on pp. 3, 63–64, 99–100).

48. Morgado, M. & Whitlock, S. Quantum simulation and computing with Rydberg-interacting qubits. *AVS Quantum Science* **3,** 023501. doi:10.1116/5.0036562 (2021) (cit. on pp. 3, 63).

49. Wineland, D. J., Drullinger, R. E. & Walls, F. L. Radiation-Pressure Cooling of Bound Resonant Absorbers. *Physical Review Letters* **40,** 1639–1642. doi:10.1103/PhysRevLett.40.1639 (1978) (cit. on p. 4).

50. Stenholm, S. The semiclassical theory of laser cooling. *Reviews of Modern Physics* **58,** 699–739. doi:10.1103/RevModPhys.58.699 (1986) (cit. on p. 4).

51. Fischer, M., Bader, M., Maiwald, R., Golla, A., Sondermann, M. & Leuchs, G. Efficient saturation of an ion in free space. *Applied Physics B: Lasers and Optics* **117,** 797–801. doi:10.1007/s00340-014-5817-y (2014) (cit. on p. 4).

52. Ohl de Mello, D., Schäffner, D., Werkmann, J., Preuschoff, T., Kohfahl, L., Schlosser, M. & Birkl, G. Defect-Free Assembly of 2D Clusters of More Than 100 Single-Atom Quantum Systems. *Physical Review Letters* **122,** 203601. doi:10.1103/PhysRevLett.122.203601 (2019) (cit. on pp. 4, 63).

53. Heisenberg, W. Über quantentheoretische Umdeutung kinematischer und mechanischer Beziehungen. *Zeitschrift für Physik* **33,** 879–893. doi:10.1007/BF01328377 (1925) (cit. on p. 4).

54. Born, M. & Jordan, P. Zur Quantenmechanik. *Zeitschrift für Physik* **34,** 858–888. doi:10.1007/BF01328531 (1925) (cit. on p. 4).

55. Born, M., Heisenberg, W. & Jordan, P. Zur Quantenmechanik. II. *Zeitschrift für Physik* **35,** 557–615. doi:10.1007/BF01379806 (1926) (cit. on p. 4).

56. Schrödinger, E. Quantisierung als Eigenwertproblem (Erste Mitteilung). *Annalen der Physik* **384,** 361–376. doi:10.1002/andp.19263840404 (1926) (cit. on p. 4).

57. Schrödinger, E. Quantisierung als Eigenwertproblem (Zweite Mitteilung). *Annalen der Physik* **384,** 489–527. doi:10.1002/andp.19263840602 (1926) (cit. on p. 4).

58. Schrödinger, E. Quantisierung als Eigenwertproblem (Dritte Mitteilung). *Annalen der Physik* **385,** 437–490. doi:10.1002/andp.19263851302 (1926) (cit. on p. 4).

59. Schrödinger, E. Quantisierung als Eigenwertproblem (Vierte Mitteilung). *Annalen der Physik* **386,** 109–139. doi:10.1002/andp.19263861802 (1926) (cit. on p. 4).

60. Schrödinger, E. Über das Verhältnis der Heisenberg-Born-Jordanschen Quantenmechanik zu der meinem. *Annalen der Physik* **384,** 734–756. doi:10.1002/andp.19263840804 (1926) (cit. on p. 4).

61. Dirac, P. A. M. The physical interpretation of the quantum dynamics. *Proceedings of the Royal Society of London. Series A, Containing Papers of a Mathematical and Physical Character* **113,** 621–641. doi:10.1098/rspa.1927.0012 (1927) (cit. on p. 4).

62. Ballentine, L. E. *Quantum mechanics: a modern development* (World Scientific Publishing, Singapore, 1998) (cit. on pp. 4, 13–14).

63. Haase, T., Alber, G. & Stojanović, V. M. Conversion from W to Greenberger-Horne-Zeilinger states in the Rydberg-blockade regime of neutral-atom systems: Dynamical-symmetry-based approach. *Physical Review A* **103,** 032427. doi:10.1103/PhysRevA.103.032427 (2021) (cit. on pp. 5, 31, 40, 61–62, 139).

64. Haase, T., Alber, G. & Stojanović, V. M. Dynamical generation of chiral *W* and Greenberger-Horne-Zeilinger states in laser-controlled Rydberg-atom trimers. *Physical Review Research* **4,** 033087. doi:10.1103/PhysRevResearch.4.033087 (2022) (cit. on pp. 6, 40, 64–65, 84, 102, 105, 139).

65. Fließbach, T. *Elektrodynamik* 7th ed. doi:10.1007/978-3-662-64889-6 (Springer, Berlin, Heidelberg, 2022) (cit. on pp. 9–10, 13).

66. Jackson, J. D. *Klassische Elektrodynamik* 4th ed. doi:10.1515/9783110200034 (Walter de Gruyter, Berlin, 2006) (cit. on pp. 9, 20).

67. Steck, D. A. *Classical and Modern Optics* (available online at http://steck.us/teaching (revision 1.7.6, 20 February 2020), 2006) (cit. on p. 9).

68. Born, M. & Wolf, E. *Principles of Optics: 60th Anniversary Edition* 7th ed. (Cambridge University Press, Cambridge, 2019) (cit. on p. 9).

69. Mandel, L. & Wolf, E. *Optical coherence and quantum optics* 10th ed. (Cambridge University Press, Cambridge, UK, 1995) (cit. on pp. 9, 15).

70. Loudon, R. *The Quantum Theory of Light* (Oxford University Press, 1973) (cit. on p. 9).

71. Cohen-Tannoudji, C., Dupont-Roc, J. & Grynberg, G. *Atom–Photon Interactions* doi:10.1002/9783527617197 (Wiley-VCH, 2004) (cit. on pp. 9, 21, 25).

72. Cohen-Tannoudji, C., Dupont-Roc, J. & Grynberg, G. *Photons and Atoms* 115–135. doi:10.1002/9783527618422 (Wiley-VCH, Weinheim, 2004) (cit. on p. 9).

73. Steck, D. A. *Quantum and Atom Optics* (available online at http://steck.us/teaching (revision 0.12.6, 23 April 2019), 2007) (cit. on pp. 9, 24–25, 27).

74. Agarwal, G. S. *Quantum Optics* doi:10.1017/CBO9781139035170 (Cambridge University Press, Cambridge, 2012) (cit. on p. 9).

75. Schleich, W. P. *Quantum Optics in Phase Space* (Wiley-VCH Verlag, Berlin, 2001) (cit. on pp. 9, 13, 15, 17–18, 21, 25).

76. Haase, T. *Laser Cooling in a Parabolic Mirror* Master's thesis (TU Darmstadt, 2017) (cit. on pp. 9, 13, 25).

77. Fabre, C. & Treps, N. Modes and states in quantum optics. *Reviews of Modern Physics* **92,** 035005. doi:10.1103/RevModPhys.92.035005 (2020) (cit. on pp. 12–13).

78. Trautmann, N. & Alber, G. Dissipation-enabled efficient excitation transfer from a single photon to a single quantum emitter. *Physical Review A* **93,** 053807. doi:10.1103/PhysRevA.93.053807 (2016) (cit. on pp. 12, 17).

79. Gajewski, M., Haase, T. & Alber, G. Dissipation-enabled resonant adiabatic quantum state transfer: Entanglement generation and quantum cloning. *Physical Review A* **104,** 052608. doi:10.1103/PhysRevA.104.052608 (2021) (cit. on pp. 12, 17, 139).

80. Gajewski, M. *Dissipation-enabled Entanglement Generation and Quantum Cloning* Master's thesis (TU Darmstadt, 2021) (cit. on pp. 12, 17, 139).

81. Brecht, B., Reddy, D. V., Silberhorn, C. & Raymer, M. G. Photon temporal modes: A complete framework for quantum information science. *Physical Review X* **5,** 1–17. doi:10.1103/PhysRevX.5.041017 (2015) (cit. on p. 12).

82. Raymer, M. G. & Walmsley, I. A. Temporal modes in quantum optics: then and now. *Physica Scripta* **95,** 064002. doi:10.1088/1402-4896/ab6153 (2020) (cit. on p. 12).

83. Fitzke, E., Bialowons, L., Dolejsky, T., Tippmann, M., Nikiforov, O., Walther, T., Wissel, F. & Gunkel, M. Scalable Network for Simultaneous Pairwise Quantum Key Distribution via Entanglement-Based Time-Bin Coding. *PRX Quantum* **3,** 020341. doi:10.1103/PRXQuantum.3.020341 (2022) (cit. on p. 12).

84. Krebs, R. *Time Resolved Quantum Detector Tomography* Bachelor's thesis (TU Darmstadt, 2020) (cit. on pp. 12, 139).

85. Biedenharn, L. C. & Louck, J. D. *Angular Momentum in Quantum Physics* (Addison-Wesley, Reading, 1981) (cit. on p. 13).

86. Alber, G. & Nikolopoulos, G. M. in *Lectures on Quantum Information* (eds Bruß, D. & Leuchs, G.) 555–571 (Wiley-VCH Verlag GmbH, Weinheim, Germany, 2007). doi:10.1002/9783527618637.ch29 (cit. on p. 13).

87. Gutiérrez-Jáuregui, R. & Jáuregui, R. Photons in the presence of parabolic mirrors. *Physical Review A* **98.** doi:10.1103/PhysRevA.98.043808 (2018) (cit. on p. 13).

88. Trautmann, N., Alber, G. & Leuchs, G. Efficient single-photon absorption by a trapped moving atom. *Physical Review A* **94,** 2–9. doi:10.1103/PhysRevA.94.033832 (2016) (cit. on p. 13).

89. Salakhutdinov, V., Sondermann, M., Carbone, L., Giacobino, E., Bramati, A. & Leuchs, G. Optical trapping of nanoparticles by full solid-angle focusing. *Optica* **3,** 1181. doi:10.1364/optica.3.001181 (2016) (cit. on p. 13).

90. Alber, L., Fischer, M., Bader, M., Mantel, K., Sondermann, M. & Leuchs, G. Focusing characteristics of a 4π parabolic mirror light-matter interface. *Journal of the European Optical Society* **13,** 14. doi:10.1186/s41476-017-0043-y (2017) (cit. on p. 13).

91. Schumacher, M. *Semiclassical laser cooling of multilevel atoms in a parabolic mirror* Master's thesis (TU Darmstadt, 2019) (cit. on pp. 13, 25, 139).

92. Casimir, H. *On the attraction between two perfectly conducting plates* in *Proc. Kon. Ned. Akademie van Wetenschappen* **51** (1948), 793–795 (cit. on p. 15).

93. Lamoreaux, S. K. Demonstration of the Casimir Force in the 0.6 to 6 μm Range. *Physical Review Letters* **78,** 5–8. doi:10.1103/PhysRevLett.78.5 (1997) (cit. on p. 15).

94. Undt, S. *Dissipation Enabled Quantum Information Storage* Master's thesis (TU Darmstadt, 2020) (cit. on pp. 17, 139).

95. Fock, V. Konfigurationsraum und zweite Quantelung. *Zeitschrift für Physik* **75,** 622–647. doi:10.1007/BF01344458 (1932) (cit. on p. 17).

96. Glauber, R. J. Coherent and Incoherent States of the Radiation Field. *Physical Review* **131,** 2766–2788. doi:10.1103/PhysRev.131.2766 (1963) (cit. on pp. 18, 72).

97. Fermi, E. Quantum Theory of Radiation. *Reviews of Modern Physics* **4,** 87–132. doi:10.1103/RevModPhys.4.87 (1932) (cit. on p. 19).

98. Trautmann, N. *Interfaces between light and matter for quantum information processing* PhD thesis (TU Darmstadt, 2017) (cit. on p. 19).

99. Göppert-Mayer, M. Über Elementarakte mit zwei Quantensprüngen. *Annalen der Physik* **401,** 273–294. doi:10.1002/andp.19314010303 (1931) (cit. on p. 21).

100. *The Nobel Prize in Physics 1944.* (NobelPrize.org. Nobel Prize Outreach AB 2022. Sat. 25 Jun 2022. https://www.nobelprize.org/prizes/physics/1944/summary) (cit. on p. 24).

101. Weisskopf, V. & Wigner, E. Berechnung der natürlichen Linienbreite auf Grund der Diracschen Lichttheorie. *Zeitschrift für Physik* **63,** 54–73. doi:10.1007/BF01336768 (1930) (cit. on p. 25).

102. Mollow, B. R. Pure-state analysis of resonant light scattering: Radiative damping, saturation, and multiphoton effects. *Physical Review A* **12,** 1919–1943. doi:10.1103/PhysRevA.12.1919 (1975) (cit. on p. 25).

103. Fladung, L. *Semiclassical Laser Cooling of Trapped Ions in a One-Dimensional Standing Wave* Bachelor's thesis (TU Darmstadt, 2017) (cit. on pp. 25, 139).

104. Galindo, A. & Pascual, P. *Quantum Mechanics II* (Springer-Verlag, Berlin, Heidelberg, 1991) (cit. on p. 27).

105. Richtmyer, R. D. *Principles of Advanced Mathematical Physics Volume I* (Springer-Verlag, New York Heidelberg Berlin, 1978) (cit. on p. 27).

106. Shirley, J. H. Solution of the Schrödinger Equation with a Hamiltonian Periodic in Time. *Physical Review* **138,** B979–B987. doi:10.1103/PhysRev.138.B979 (1965) (cit. on p. 28).

107. Ho, T. S., Chu, S. I. & Tietz, J. V. Semiclassical many-mode floquet theory. *Chemical Physics Letters* **96,** 464–471. doi:10.1016/0009-2614(83)80732-5 (1983) (cit. on p. 28).

108. DiVincenzo, D. P. Two-bit gates are universal for quantum computation. *Physical Review A* **51,** 1015–1022. doi:10.1103/PhysRevA.51.1015 (1995) (cit. on pp. 31, 61).

109. Zheng, R.-H., Kang, Y.-H., Ran, D., Shi, Z.-C. & Xia, Y. Deterministic interconversions between the Greenberger-Horne-Zeilinger states and the W states by invariant-based pulse design. *Physical Review A* **101,** 012345. doi:10.1103/PhysRevA.101.012345 (2020) (cit. on pp. 31, 33, 48, 56–59, 61–62, 76, 83, 87, 90, 103).

110. Lewis, H. R. & Riesenfeld, W. B. An exact quantum theory of the time-dependent harmonic oscillator and of a charged particle in a time-dependent electromagnetic field. *Journal of Mathematical Physics* **10,** 1458–1473. doi:10.1063/1.1664991 (1969) (cit. on pp. 33, 48, 56).

111. Torrontegui, E., Martínez-Garaot, S. & Muga, J. G. Hamiltonian engineering via invariants and dynamical algebra. *Physical Review A* **89,** 043408. doi:10.1103/PhysRevA.89.043408 (2014) (cit. on pp. 33, 56).

112. Barut, A. O. & Rączka, R. *Theory of Group Representations and Applications* 2nd ed. (World Scientific Publishing, Singapore, 1986) (cit. on p. 33).

113. Richtmyer, R. D. *Principles of Advanced Mathematical Physics Volume II* (Springer-Verlag, New York Heidelberg Berlin, 1981) (cit. on pp. 33, 37).

114. Hall, B. C. *Lie Groups, Lie Algebras, and Representations: An Elementary Introduction* 2nd ed., 516–554. doi:10.1007/978-3-319-13467-3 (Springer International Publishing, Cham, 2015) (cit. on pp. 33, 37–38, 119).

115. Rau, A. R. P., Selvaraj, G. & Uskov, D. Four-level and two-qubit systems, subalgebras, and unitary integration. *Physical Review A* **71,** 062316. doi:10.1103/PhysRevA.71.062316 (2005) (cit. on p. 33).

116. Rau, A. R. P. & Alber, G. Shared symmetries of the hydrogen atom and the two-bit system. *Journal of Physics B: Atomic, Molecular and Optical Physics* **50,** 242001. doi:10.1088/1361-6455/aa8e39 (2017) (cit. on p. 33).

117. Rau, A. R. P. Symmetries and Geometries of Qubits, and Their Uses. *Symmetry* **13,** 1732. doi:10.3390/sym13091732 (2021) (cit. on p. 33).

118. Kang, Y.-H., Shi, Z.-C., Huang, B.-H., Song, J. & Xia, Y. Deterministic conversions between Greenberger-Horne-Zeilinger states and W states of spin qubits via Lie-transform-based inverse Hamiltonian engineering. *Physical Review A* **100,** 012332. doi:10.1103/PhysRevA.100.012332 (2019) (cit. on pp. 48, 56, 59, 61).

119. Kang, Y.-H., Chen, Y.-H., Shi, Z.-C., Huang, B.-H., Song, J. & Xia, Y. Pulse design for multilevel systems by utilizing Lie transforms. *Physical Review A* **97,** 033407. doi:10.1103/PhysRevA.97.033407 (2018) (cit. on p. 56).

120. Nauth, J. K. & Stojanović, V. M. Quantum-brachistochrone approach to the conversion from *W* to Greenberger-Horne-Zeilinger states for Rydberg-atom qubits. *Physical Review A* **106,** 032605. doi:10.1103/PhysRevA.106.032605 (2022) (cit. on p. 61).

121. Carlini, A., Hosoya, A., Koike, T. & Okudaira, Y. Time-optimal quantum evolution. *Physical Review Letters* **96,** 1–4. doi:10.1103/PhysRevLett.96.060503 (2006) (cit. on p. 61).

122. Browaeys, A. & Lahaye, T. Many-body physics with individually controlled Rydberg atoms. *Nature Physics* **16,** 132–142. doi:10.1038/s41567-019-0733-z (2020) (cit. on p. 63).

123. Altman, E. *et al.* Quantum Simulators: Architectures and Opportunities. *PRX Quantum* **2,** 1–19. doi:10.1103/prxquantum.2.017003 (2021) (cit. on p. 63).

124. Kaufman, A. M. & Ni, K. K. Quantum science with optical tweezer arrays of ultracold atoms and molecules. *Nature Physics* **17,** 1324–1333. doi:10.1038/s41567-021-01357-2 (2021) (cit. on p. 63).

125. Shi, X.-F. Quantum logic and entanglement by neutral Rydberg atoms: methods and fidelity. *Quantum Science and Technology* **7,** 023002. doi:10.1088/2058-9565/ac18b8 (2022) (cit. on p. 63).

126. Ohl de Mello, D. *Rydberg interactions in a defect-free array of single-atom quantum systems* PhD thesis (TU Darmstadt, 2020) (cit. on pp. 63–64, 80).

127. Barredo, D., de Léséleuc, S., Lienhard, V., Lahaye, T. & Browaeys, A. An atom-by-atom assembler of defect-free arbitrary two-dimensional atomic arrays. *Science* **354,** 1021–1023. doi:10.1126/science.aah3778 (2016) (cit. on p. 63).

128. Schymik, K. N., Lienhard, V., Barredo, D., Scholl, P., Williams, H., Browaeys, A. & Lahaye, T. Enhanced atom-by-atom assembly of arbitrary tweezer arrays. *Physical Review A* **102,** 63107. doi:10.1103/PhysRevA.102.063107 (2020) (cit. on p. 63).

129. Norcia, M. A., Young, A. W. & Kaufman, A. M. Microscopic Control and Detection of Ultracold Strontium in Optical-Tweezer Arrays. *Physical Review X* **8,** 41054. doi:10.1103/PhysRevX.8.041054 (2018) (cit. on pp. 63, 85, 90, 100, 104).

130. Deist, E., Gerber, J. A., Lu, Y. H., Zeiher, J. & Stamper-Kurn, D. M. Superresolution Microscopy of Optical Fields Using Tweezer-Trapped Single Atoms. *Physical Review Letters* **128,** 83201. doi:10.1103/PhysRevLett.128.083201 (2022) (cit. on pp. 63, 85, 90, 100, 104).

131. Prevedel, R., Cronenberg, G., Tame, M. S., Paternostro, M., Walther, P., Kim, M. S. & Zeilinger, A. Experimental Realization of Dicke States of up to Six Qubits for Multiparty Quantum Networking. *Physical Review Letters* **103,** 020503. doi:10.1103/PhysRevLett.103.020503 (2009) (cit. on p. 69).

132. Bärtschi, A. & Eidenbenz, S. *Deterministic Preparation of Dicke States* in *Fundamentals of Computation Theory* (eds Gąsieniec, L. A., Jansson, J. & Levcopoulos, C.) (Springer International Publishing, Cham, 2019), 126–139 (cit. on p. 69).

133. Wieczorek, W., Krischek, R., Kiesel, N., Michelberger, P., Tóth, G. & Weinfurter, H. Experimental Entanglement of a Six-Photon Symmetric Dicke State. *Physical Review Letters* **103,** 020504. doi:10.1103/PhysRevLett.103.020504 (2009) (cit. on p. 69).

134. Dicke, R. H. Coherence in Spontaneous Radiation Processes. *Physical Review* **93,** 99–110. doi:10.1103/PhysRev.93.99 (1954) (cit. on p. 69).

135. Tóth, G. Multipartite entanglement and high-precision metrology. *Physical Review A* **85,** 022322. doi:10.1103/PhysRevA.85.022322 (2012) (cit. on p. 69).

136. Pezzè, L., Smerzi, A., Oberthaler, M. K., Schmied, R. & Treutlein, P. Quantum metrology with nonclassical states of atomic ensembles. *Reviews of Modern Physics* **90,** 035005. doi:10.1103/RevModPhys.90.035005 (2018) (cit. on p. 69).

137. Özdemir, S. K., Shimamura, J. & Imoto, N. A necessary and sufficient condition to play games in quantum mechanical settings. *New Journal of Physics* **9,** 43–43. doi:10.1088/1367-2630/9/2/043 (2007) (cit. on p. 69).

138. Kuramoto, Y. Cooperative Dynamics of Oscillator Community. *Progress of Theoretical Physics Supplement* **79,** 223–240. doi:10.1143/PTPS.79.223 (1984) (cit. on p. 70).

139. Wiley, D. A., Strogatz, S. H. & Girvan, M. The size of the sync basin. *Chaos* **16,** 015103. doi:10.1063/1.2165594 (2006) (cit. on p. 70).

140. Girnyk, T., Hasler, M. & Maistrenko, Y. Multistability of twisted states in non-locally coupled Kuramoto-type models. *Chaos* **22,** 013114. doi:10.1063/1.3677365 (2012) (cit. on p. 70).

141. Bolotov, D., Bolotov, M., Smirnov, L., Osipov, G. & Pikovsky, A. Twisted States in a System of Nonlinearly Coupled Phase Oscillators. *Regular and Chaotic Dynamics* **24,** 717–724. doi:10.1134/S1560354719060091 (2019) (cit. on p. 70).

142. Bloch, F. Über die Quantenmechanik der Elektronen in Kristallgittern. *Zeitschrift für Physik* **52,** 555–600. doi:10.1007/BF01339455 (1929) (cit. on p. 70).

143. Wen, X. G., Wilczek, F. & Zee, A. Chiral spin states and superconductivity. *Physical Review B* **39,** 11413. doi:10.1103/PhysRevB.39.11413 (1989) (cit. on p. 71).

144. Viola, L., Knill, E. & Laflamme, R. Constructing qubits in physical systems. *Journal of Physics A: Mathematical and General* **34,** 7067. doi:10.1088/0305-4470/34/35/331 (2001) (cit. on pp. 71, 85, 103).

145. Knill, E., Laflamme, R. & Viola, L. Theory of Quantum Error Correction for General Noise. *Physical Review Letters* **84,** 2525. doi:10.1103/PhysRevLett.84.2525 (2000) (cit. on pp. 71, 85, 103).

146. Lukin, M. D., Fleischhauer, M., Cote, R., Duan, L. M., Jaksch, D., Cirac, J. I. & Zoller, P. Dipole blockade and quantum information processing in mesoscopic atomic ensembles. *Physical Review Letters* **87,** 37901–1–37901–4. doi:10.1103/PhysRevLett.87.037901 (2001) (cit. on p. 80).

147. Heidemann, R., Raitzsch, U., Bendkowsky, V., Butscher, B., Löw, R., Santos, L. & Pfau, T. Evidence for Coherent Collective Rydberg Excitation in the Strong Blockade Regime. *Physical Review Letters* **99,** 163601. doi:10.1103/PhysRevLett.99.163601 (2007) (cit. on p. 80).

148. Dudin, Y. O., Li, L., Bariani, F. & Kuzmich, A. Observation of coherent many-body Rabi oscillations. *Nature Physics* **8,** 790–794. doi:10.1038/nphys2413 (2012) (cit. on p. 80).

149. Gaëtan, A., Miroshnychenko, Y., Wilk, T., Chotia, A., Viteau, M., Comparat, D., Pillet, P., Browaeys, A. & Grangier, P. Observation of collective excitation of two individual atoms in the Rydberg blockade regime. *Nature Physics* **5,** 115–118. doi:10.1038/nphys1183 (2009) (cit. on p. 80).

150. Schlosser, M., Ohl de Mello, D., Schäffner, D., Preuschoff, T., Kohfahl, L. & Birkl, G. Assembled arrays of Rydberg-interacting atoms. *Journal of Physics B: Atomic, Molecular and Optical Physics* **53,** 144001. doi:10.1088/1361-6455/ab8b46 (2020) (cit. on p. 80).

151. Tavis, M. & Cummings, F. W. Exact Solution for an N-Molecule — Radiation-Field Hamiltonian. *Physical Review* **170,** 379–384. doi:10.1103/PhysRev.170.379 (1968) (cit. on p. 80).

152. Jaynes, E. & Cummings, F. W. Comparison of quantum and semiclassical radiation theories with application to the beam maser. *Proceedings of the IEEE* **51,** 89–109. doi:10.1109/PROC.1963.1664 (1963) (cit. on p. 80).

153. Cummings, F. W. & Dorri, A. Exact solution for spontaneous emission in the presence of N atoms. *Physical Review A* **28,** 2282–2285. doi:10.1103/PhysRevA.28.2282 (1983) (cit. on p. 80).

154. Cole, D. C., Wu, J. J., Erickson, S. D., Hou, P.-Y., Wilson, A. C., Leibfried, D. & Reiter, F. Dissipative preparation of W states in trapped ion systems. *New Journal of Physics* **23,** 073001. doi:10.1088/1367-2630/ac09c8 (2021) (cit. on pp. 85, 103).

155. Browaeys, A. Alkaline Atoms Held with Optical Tweezers. *Physics* **11,** 135. doi:10.1103/Physics.11.135 (2018) (cit. on pp. 85, 90).

156. Cooper, A., Covey, J. P., Madjarov, I. S., Porsev, S. G., Safronova, M. S. & Endres, M. Alkaline-Earth Atoms in Optical Tweezers. *Physical Review X* **8,** 041055. doi:10.1103/PhysRevX.8.041055 (2018) (cit. on pp. 85, 90).

157. Gardiner, C. W. & Zoller, P. *Quantum Noise* 2nd ed. (Springer, Berlin, Heidelberg, 2000) (cit. on p. 94).

158. Breuer, H.-P. & Petruccione, F. *The Theory of Open Quantum Systems* doi:10.1093/acprof:oso/9780199213900.001.0001 (Oxford University Press, 2007) (cit. on p. 94).

159. Weimer, H., Kshetrimayum, A. & Orús, R. Simulation methods for open quantum many-body systems. *Reviews of Modern Physics* **93,** 015008. doi:10.1103/RevModPhys.93.015008 (2021) (cit. on p. 94).

160. Lindblad, G. On the generators of quantum dynamical semigroups. *Communications in Mathematical Physics* **48,** 119–130. doi:10.1007/BF01608499 (1976) (cit. on p. 95).

161. Johansson, J. R., Nation, P. D. & Nori, F. QuTiP: An open-source Python framework for the dynamics of open quantum systems. *Computer Physics Communications* **183,** 1760–1772. doi:10.1016/j.cpc.2012.02.021 (2012) (cit. on pp. 95, 102, 141).

162. Johansson, J. R., Nation, P. D. & Nori, F. QuTiP 2: A Python framework for the dynamics of open quantum systems. *Computer Physics Communications* **184,** 1234–1240. doi:10.1016/j.cpc.2012.11.019 (2013) (cit. on pp. 95, 102, 141).

163. Manzano, D. A short introduction to the Lindblad master equation. *AIP Advances* **10,** 025106. doi:10.1063/1.5115323 (2020) (cit. on p. 95).

164. Pachniak, E. & Malinovskaya, S. A. Creation of quantum entangled states of Rydberg atoms via chirped adiabatic passage. *Scientific Reports* **11,** 12980. doi:10.1038/s41598-021-92325-6 (2021) (cit. on p. 104).

165. Merzinger, G., Mühlbach, G., Wille, D. & Wirth, T. *Formeln + Hilfen Höhere Mathematik* 6th ed. (Binomi Verlag, Hannover, 2010) (cit. on p. 112).

166. Harris, C. R. *et al.* Array programming with NumPy. *Nature* **585,** 357–362. doi:10.1038/s41586-020-2649-2 (2020) (cit. on p. 141).

167. Hunter, J. D. Matplotlib: A 2D Graphics Environment. *Computing in Science & Engineering* **9,** 90–95. doi:10.1109/MCSE.2007.55 (2007) (cit. on p. 141).

Sets	
$\emptyset$	the empty set $\{\}$
$\{a_i\}$	set of elements $a_1, a_2, ..., a_n$
$\cup$; $\cap$; $\setminus$	union; intersection; complement
special sets/spaces	
$\mathbb{N}$; $\mathbb{N}_0$	set of natural numbers without zero; including zero
$\mathbb{Z}$	set of integers
$\mathbb{R}$	set of real numbers
$\mathbb{C}$	set of complex numbers
$\mathcal{H}$	Hilbert space (We use Dirac's Bra-Ket-notation [20])
Vectors, matrices and operators	
$\boldsymbol{a}$	vector $\boldsymbol{a}$ of components $a_1, a_2, ..., a_n$
$\underline{\boldsymbol{M}}$	matrix $\underline{\boldsymbol{M}}$ of matrix elements M_{ij}
$\widehat{\mathrm{O}}$	operator $\widehat{\mathrm{O}}$ acting on the corresponding Hilbert space
$\boldsymbol{\nabla}$	Nabla operator for derivatives in $\mathbb{R}^3$
Operations	
$\cdot$	standard scalar product in $\mathbb{R}^n/\mathbb{C}^n$
$\times$	cross product of vectors in $\mathbb{R}^3$
$\otimes$	tensor product or dyadic product
$\sum_{i=a}^{b} x_i$	sum over elements x_i from $i = a$ to $i = b$ (equivalent notation for products $\prod_{i=a}^{b} x_i$ and tensor products $\bigotimes_{i=a}^{b} x_i$)
c^*; c.c.	complex conjugate of the complex number c; the prior term
$\lvert c\rvert$; $\lvert\boldsymbol{a}\rvert$	absolute value (modulus) of the (complex) number c; the vector $\boldsymbol{a}$
$\mathbb{1}$	identity operator/matrix of the corresponding space
$\underline{\boldsymbol{M}}^{\mathrm{T}}$	transposition of a matrix $\underline{\boldsymbol{M}}$
$\widehat{\mathrm{A}}^{\dagger}$; H.c.	Hermitian conjugate of the operator $\widehat{\mathrm{A}}$; the prior term
$\overline{x}$	mean value $\sum_i x_i/N$ for N values x_i
$\binom{N}{a}$; $a!$	binomial coefficient binomial coefficient $N!/(a!(N-a)!)$; $a!$ describes a factorial
Physical constants	
c	speed of light in vacuum
ϵ_0	vacuum permittivity
$\hbar$	Reduced Planck's constant $h/(2\pi)$

LIST OF ACRONYMS

CNOT	Controlled NOT operation
EPR	Einstein-Podolsky-Rosen
4LS	four-level quantum system
GHZ	Greenberger-Horne-Zeilinger
Hd	Hamming distance
JC	Jaynes-Cummings
LOCC	local operations and classical communication
RWA	rotating wave approximation
QIP	quantum information processing
SPA	squared pulse area
TLS	two-level quantum system
TSPA	total squared pulse area

LIST OF PUBLICATIONS

The following list contains publications co-authored by the author.

- Haase, T., Alber, G. & Stojanović, V. M. Conversion from W to Greenberger-Horne-Zeilinger states in the Rydberg-blockade regime of neutral-atom systems: Dynamical-symmetry-based approach. *Physical Review A* **103,** 032427. doi:10.1103/PhysRevA.103.032427 (Mar. 2021), [63]

- Gajewski, M., Haase, T. & Alber, G. Dissipation-enabled resonant adiabatic quantum state transfer: Entanglement generation and quantum cloning. *Physical Review A* **104,** 052608. doi:10.1103/PhysRevA.104.052608 (Nov. 2021), [79]

- Fitzke, E., Krebs, R., Haase, T., Mengler, M., Alber, G. & Walther, T. Time-dependent POVM reconstruction for single-photon avalanche photo diodes using adaptive regularization. *New Journal of Physics* **24,** 023025. doi:10.1088/1367-2630/ac5004 (Feb. 2022), [33]

- Haase, T., Alber, G. & Stojanović, V. M. Dynamical generation of chiral *W* and Greenberger-Horne-Zeilinger states in laser-controlled Rydberg-atom trimers. *Physical Review Research* **4,** 033087. doi:10.1103/PhysRevResearch.4.033087 (July 2022), [64]

The following list contains (under)graduate projects in which the author actively co-supervised (under)graduate students. Projects which the author solely examined as second referee are not mentioned.

- Fladung, L. *Semiclassical Laser Cooling of Trapped Ions in a One-Dimensional Standing Wave* Bachelor's thesis (TU Darmstadt, 2017), [103]

- Schumacher, M. *Semiclassical laser cooling of multilevel atoms in a parabolic mirror* Master's thesis (TU Darmstadt, 2019), [91]

- Krebs, R. *Time Resolved Quantum Detector Tomography* Bachelor's thesis (TU Darmstadt, 2020), [84]

- Undt, S. *Dissipation Enabled Quantum Information Storage* Master's thesis (TU Darmstadt, 2020), [94]

- Gajewski, M. *Dissipation-enabled Entanglement Generation and Quantum Cloning* Master's thesis (TU Darmstadt, 2021), [80]

CURRICULUM VITAE

PERSONAL INFORMATION

Not included in the online version

PH.D. STUDIES AND EMPLOYMENT

2017-2022	Ph.D. studies and research assistant at Technische Universität Darmstadt (Germany) Institut für Angewandte Physik (supervised by Prof. Dr. Gernot Alber)

HIGHER EDUCATION

2014-2017	Master of Science in Physics Technische Universität Darmstadt (Germany)
2012-2013	Student exchange programme Universidad de Salamanca (Spain)
2010-2014	Bachelor of Science in Physics Technische Universität Darmstadt (Germany)

EDUCATION

2003-2010	Higher Education Entrance Qualification Tilman-Riemenschneider Gymnasium Osterode am Harz (Germany)
2001-2003	Middle school Orientierungsstufe Badenhausen (Germany)
1997-2001	Elementary school Grundschule Gittelde (Germany)

DECLARATIONS

The following tools have been used to produce parts of this dissertation and some of its results.

- To control many of the analytical results presented throughout this dissertation and to solve the specific numerical calculations described in chapter 4, we used *Wolfram Mathematica 12*: Version Number 12.0.0.0 for Linux x86 (64-bit) and 12.1.0.0 for Windows (64-bit). Licenses were provided by Technische Universität Darmstadt Fachbereich Physik.
- The numerical analysis in chapter 5 were conducted in *Python*. We especially relied on the packages *NumPy* (see numpy.org[2]; cf. [166]) and *QuTiP* (see qutip.org[2]; cf. [161, 162]).
- Most figures in this dissertation were designed using *Inkscape* (see inkscape.org[2]) and/or the python library *Matplotlib* (see matplotlib.org[2]; cf. [167]).

Although not used as a scientific source or reference in this dissertation, Wikipedia.org[2] offers information about almost all fields of interest and is often used for quick checks or overviews of specific topics. We acknowledge its importance for freely available information in science and society in general.

Since the author is not a native speaker, the online English grammar tool grammarly.com[2] was used for a basic check of grammar and spelling.

This document was typeset using the typographical look-and-feel `classicthesis` developed by André Miede and Ivo Pletikosić. The style was inspired by Robert Bringhurst's seminal book on typography "*The Elements of Typographic Style*". `classicthesis` is available for both LaTeX and LyX:

`https://bitbucket.org/amiede/classicthesis/`[2]

The author announces financial support from the Deutsche Forschungsgemeinschaft (DFG, German Research Foundation) – SFB 1119 – 236615297 within project P4.

2 All web pages mentioned on this page were assessed July 5, 2022.

ERKLÄRUNG LAUT PROMOTIONSORDNUNG

§8 Abs. 1 lit. c PromO
Ich versichere hiermit, dass die elektronische Version meiner Dissertation (mit Ausnahme der persönlichen Daten auf Seite 140)[3] mit der schriftlichen Version übereinstimmt.

§8 Abs. 1 lit. d PromO
Ich versichere hiermit, dass zu einem vorherigen Zeitpunkt noch keine Promotion versucht wurde. In diesem Fall sind nähere Angaben über Zeitpunkt, Hochschule, Dissertationsthema und Ergebnis dieses Versuchs mitzuteilen.

§9 Abs. 1 PromO
Ich versichere hiermit, dass die vorliegende Dissertation selbstständig und nur unter Verwendung der angegebenen Quellen verfasst wurde.

§9 Abs. 2 PromO
Die Arbeit hat bisher noch nicht zu Prüfungszwecken gedient.

§19 Abs. 1 PromO
Ich versichere hiermit, dass die elektronische Version meiner Dissertation mit der zur Veröffentlichung freigegebenen Fassung (mit Ausnahme der persönlichen Daten auf Seite 140)[3] identisch ist.

Darmstadt, den _____ _____
Thorsten Haase

3 Aus Datenschutzgründen sind die persönlichen Daten auf Seite 140 nicht in der elektronisch veröffentlichten Version enthalten.